Enclosure 8 to TN E-31647

Public Versions of Standardized Advanced NUHOMS® System UFSAR Pages and Drawings, Showing Proposed Amendment 3 Changes

PROPRIETARY AND SECURITY RELATED INFORMATION WITHHELD UNDER 10 CFR 2.390

REVISION	DESCRIPTION	DATE
0A	INITIAL ISSUE	12/13/11

ALL DIMENSIONS ARE NOMINAL UNLESS A SPECIFIC TOLERANCE IS INDICATED WITH THE DRAWING DIMENSION

DIMENSIONS ARE IN INCHES AND DEGREES UNLESS OTHERWISE SPECIFIED. DIMENSIONING IN ACCORDANCE WITH ASME Y14.5M.

INTERPRET WELD SYMBOLS PER ANSI / AWS 2.4

U.S. Patent No. 4,780,269

TRANSNUCLEAR
AN AREVA COMPANY

SAFETY ANALYSIS REPORT
NUHOMS® 32PTH2
TRANSPORTABLE CANISTER FOR PWR FUEL
MAIN ASSEMBLY

DRAWING NO.	SCALE	SHEET
ANUH-01-4002	NONE	1 OF 6

PROPRIETARY AND SECURITY RELATED INFORMATION WITHHELD UNDER 10 CFR 2.390

PROPRIETARY AND SECURITY RELATED INFORMATION WITHHELD UNDER 10 CFR 2.390

PROPRIETARY AND SECURITY RELATED INFORMATION WITHHELD UNDER 10 CFR 2.390

PROPRIETARY AND SECURITY RELATED INFORMATION WITHHELD UNDER 10 CFR 2.390

PROPRIETARY AND SECURITY RELATED INFORMATION WITHHELD UNDER 10 CFR 2.390

PROPRIETARY AND SECURITY RELATED INFORMATION WITHHELD UNDER 10 CFR 2.390

REVISION	DESCRIPTION	DATE
0A	INITIAL ISSUE	12/13/11

ALL DIMENSIONS ARE NOMINAL UNLESS A SPECIFIC TOLERANCE IS INDICATED WITH THE DRAWING DIMENSION

DIMENSIONS ARE IN INCHES AND DEGREES UNLESS OTHERWISE SPECIFIED. DIMENSIONING IN ACCORDANCE WITH ASME Y14.5M.

INTERPRET WELD SYMBOLS PER ANSI / AWS 2.4

U.S. Patent No. 4,780,269

TRANSNUCLEAR
AN AREVA COMPANY

SAFETY ANALYSIS REPORT
NUHOMS® 32PTH2
TRANSPORTABLE CANISTER FOR PWR FUEL
SHELL ASSEMBLY

DRAWING NO.	SCALE	SHEET
ANUH-01-4003	NONE	1 OF 3

PROPRIETARY AND SECURITY RELATED INFORMATION WITHHELD UNDER 10 CFR 2.390

PROPRIETARY AND SECURITY RELATED INFORMATION WITHHELD UNDER 10 CFR 2.390

PROPRIETARY AND SECURITY RELATED INFORMATION WITHHELD UNDER 10 CFR 2.390

REVISION	DESCRIPTION	DATE
0A	INITIAL ISSUE	12/13/11

ALL DIMENSIONS ARE NOMINAL UNLESS A SPECIFIC TOLERANCE IS INDICATED WITH THE DRAWING DIMENSION

DIMENSIONS ARE IN INCHES AND DEGREES UNLESS OTHERWISE SPECIFIED. DIMENSIONING IN ACCORDANCE WITH ASME Y14.5M.

INTERPRET WELD SYMBOLS PER ANSI / AWS 2.4

U.S. Patent No. 4,780,269

TRANSNUCLEAR
AN AREVA COMPANY

SAFETY ANALYSIS REPORT
NUHOMS® 32PTH2
TRANSPORTABLE CANISTER FOR PWR FUEL
BASKET ASSEMBLY

DRAWING NO.	SCALE	SHEET
ANUH-01-4004	NONE	1 OF 4

PROPRIETARY AND SECURITY RELATED INFORMATION WITHHELD UNDER 10 CFR 2.390

PROPRIETARY AND SECURITY RELATED INFORMATION WITHHELD UNDER 10 CFR 2.390

DRAWING NO.	SHEET	REVISION
ANUH-01-4004	3 OF 4	0A

PROPRIETARY AND SECURITY RELATED INFORMATION WITHHELD UNDER 10 CFR 2.390

PROPRIETARY AND SECURITY RELATED INFORMATION WITHHELD UNDER 10 CFR 2.390

REVISION	DESCRIPTION	DATE
0A	INITIAL ISSUE	12/13/11

ALL DIMENSIONS ARE NOMINAL UNLESS A SPECIFIC TOLERANCE IS INDICATED WITH THE DRAWING DIMENSION

DIMENSIONS ARE IN INCHES AND DEGREES UNLESS OTHERWISE SPECIFIED. DIMENSIONING IN ACCORDANCE WITH ASME Y14.5M.

INTERPRET WELD SYMBOLS PER AWS / AWS 2.4

U.S. Patent No. 4,780,269

TRANSNUCLEAR
AN AREVA COMPANY

SAFETY ANALYSIS REPORT
NUHOMS® 32PTH2
TRANSPORTABLE CANISTER FOR PWR FUEL
TRANSITION RAILS

DRAWING NO.	SCALE	SHEET
ANUH-01-4005	NONE	1 OF 4

PROPRIETARY AND SECURITY RELATED INFORMATION WITHHELD UNDER 10 CFR 2.390

PROPRIETARY AND SECURITY RELATED INFORMATION WITHHELD UNDER 10 CFR 2.390

PROPRIETARY AND SECURITY RELATED INFORMATION WITHHELD UNDER 10 CFR 2.390

DRAWING NO.	SHEET	REVISION
ANUH-01-4005	4 OF 4	0A

DRAWING NO. ANUH-01-4006 SHEET 1 OF 1

PROPRIETARY AND SECURITY RELATED INFORMATION WITHHELD UNDER 10 CFR 2.390

REVISION	DESCRIPTION	DATE
0A	INITIAL ISSUE	12/13/11

ALL DIMENSIONS ARE NOMINAL UNLESS A SPECIFIC TOLERANCE IS INDICATED WITH THE DRAWING DIMENSION

DIMENSIONS ARE IN INCHES AND DEGREES UNLESS OTHERWISE SPECIFIED. DIMENSIONING IN ACCORDANCE WITH ASME Y14.5M.

INTERPRET WELD SYMBOLS PER ANSI / AWS 2.4

U.S. Patent No. 4,780,269

TRANSNUCLEAR
AN AREVA COMPANY

SAFETY ANALYSIS REPORT
NUHOMS® 32PTH2
TRANSPORTABLE CANISTER FOR PWR FUEL
DAMAGED FUEL AND CAPS

DRAWING NO.	SCALE	SHEET
ANUH-01-4006	NONE	1 OF 1

PROPRIETARY AND SECURITY RELATED INFORMATION WITHHELD UNDER 10 CFR 2.390

REVISION	DESCRIPTION	DATE
0A	INITIAL ISSUE	12/13/11

ALL DIMENSIONS ARE NOMINAL UNLESS A SPECIFIC TOLERANCE IS INDICATED WITH THE DRAWING DIMENSION

DIMENSIONS ARE IN INCHES AND DEGREES UNLESS OTHERWISE SPECIFIED. DIMENSIONING IN ACCORDANCE WITH ASME Y14.5M.

INTERPRET WELD SYMBOLS PER ANSI / AWS 2.4

U.S. Patent No. 4,780,269

TRANSNUCLEAR
AN AREVA COMPANY

SAFETY ANALYSIS REPORT
STANDARDIZED ADVANCED NUHOMS®
ADVANCED HIGH SEISMIC HSM (AHSM-HS)
MAIN ASSEMBLY

DRAWING NO.	SCALE	SHEET
NUH-03-4012	NONE	1 OF 14

PROPRIETARY AND SECURITY RELATED INFORMATION WITHHELD UNDER 10 CFR 2.390

PROPRIETARY AND SECURITY RELATED INFORMATION WITHHELD UNDER 10 CFR 2.390

PROPRIETARY AND SECURITY RELATED INFORMATION WITHHELD UNDER 10 CFR 2.390

PROPRIETARY AND SECURITY RELATED INFORMATION WITHHELD UNDER 10 CFR 2.390

PROPRIETARY AND SECURITY RELATED INFORMATION WITHHELD UNDER 10 CFR 2.390

PROPRIETARY AND SECURITY RELATED INFORMATION WITHHELD UNDER 10 CFR 2.390

PROPRIETARY AND SECURITY RELATED INFORMATION WITHHELD UNDER 10 CFR 2.390

PROPRIETARY AND SECURITY RELATED INFORMATION WITHHELD UNDER 10 CFR 2.390

PROPRIETARY AND SECURITY RELATED INFORMATION WITHHELD UNDER 10 CFR 2.390

PROPRIETARY AND SECURITY RELATED INFORMATION WITHHELD UNDER 10 CFR 2.390

PROPRIETARY AND SECURITY RELATED INFORMATION WITHHELD UNDER 10 CFR 2.390

PROPRIETARY AND SECURITY RELATED INFORMATION WITHHELD UNDER 10 CFR 2.390

PROPRIETARY AND SECURITY RELATED INFORMATION WITHHELD UNDER 10 CFR 2.390

PROPRIETARY AND SECURITY RELATED INFORMATION WITHHELD UNDER 10 CFR 2.390

REVISION	DESCRIPTION	DATE
0A	INITIAL ISSUE	12/13/11

ALL DIMENSIONS ARE NOMINAL UNLESS A SPECIFIC TOLERANCE IS INDICATED WITH THE DRAWING DIMENSION

DIMENSIONS ARE IN INCHES AND DEGREES UNLESS OTHERWISE SPECIFIED. DIMENSIONING IN ACCORDANCE WITH ASME Y14.5M.

INTERPRET WELD SYMBOLS PER ANSI / AWS 2.4

U.S. Patent No. 4,780,269

TRANSNUCLEAR
AN AREVA COMPANY

SAFETY ANALYSIS REPORT
STANDARDIZED ADVANCED NUHOMS®
ADVANCED HIGH SEISMIC HSM (AHSM-HS)
TRANSITION ROOF AND TRANSITION WALLS ASSEMBLIES

DRAWING NO.	SCALE	SHEET
NUH-03-4013	NONE	1 OF 6

PROPRIETARY AND SECURITY RELATED INFORMATION WITHHELD UNDER 10 CFR 2.390

PROPRIETARY AND SECURITY RELATED INFORMATION WITHHELD UNDER 10 CFR 2.390

PROPRIETARY AND SECURITY RELATED INFORMATION WITHHELD UNDER 10 CFR 2.390

PROPRIETARY AND SECURITY RELATED INFORMATION WITHHELD UNDER 10 CFR 2.390

PROPRIETARY AND SECURITY RELATED INFORMATION WITHHELD UNDER 10 CFR 2.390

B.3.5 Fuel Rods General Standards for 32PTH2 DSC

This section provides the temperature criteria used in the 32PTH2 DSC thermal evaluation for the safe storage and handling of CE 16x16 class fuel assemblies in accordance with the requirements of 10 CFR Part 72 to ensure a very low probability of rod failure during long term storage, and to protect against gross failures during short term events. Short term events include transfer operations, off-normal conditions, accident conditions, and other short term operational events.

This section also contains the calculation of the thermal and irradiation growth of the fuel assemblies to demonstrate that adequate space exists within the 32PTH2 DSC cavity for the fuel assemblies to grow thermally under all conditions.

In addition, this section provides an evaluation of the fuel rod stresses and critical buckling loads due to accident drop loads. This section also contains the damaged fuel evaluation.

B.3.5.1 CE 16 x16 Class Fuel Rod Temperature Limits

B.3.5.1.1 Dry Storage

The maximum cladding temperature limit for the fuel rods at the beginning of the dry storage shall not exceed 400°C (752°F) for normal conditions of storage and for short-term operations, including canister drying and backfilling, according to NUREG-1536 [B3.8].

Repeated thermal cycling (more than 10 cycles) with temperature changes greater than 65°C (149°F) [B3.8] is not permitted.

B.3.5.1.2 Short Term Events

The fuel cladding (Zirconium based alloy) temperatures shall be maintained below 570°C (1058°F) [B3.8] for accident conditions involving fire, or off-normal thermal transients.

B.3.5.2 CE 16x16 Class Fuel Assembly Thermal and Irradiation Growth

The thermal and irradiation growth of the fuel assemblies are calculated in Section B.3.4.4.2.1. The evaluations performed show sufficient clearance exists within the 32PTH2 DSC cavity for free thermal expansion of the CE 16x16 class fuel assemblies.

Proprietary information withheld pursuant to 10 CFR 2.390

Proprietary information on pages B.3.5-2 through B.3.5-24
are withheld pursuant to 10 CFR 2.390
and the pages are deleted in their entirety.

B.4 THERMAL EVALUATION

This chapter presents the evaluations that demonstrate that the NUHOMS® 32PTH2 system meets the thermal requirements of 10 CFR Part 72 [B4.1]. Thermal analysis methodology for fuel cladding temperature limit criteria is consistent with the guidelines given in NUREG-1536 [B4.3] or Interim Staff Guidance (ISG) No. 11, Revision 3 [B4.4]. The NUHOMS® 32PTH2 DSC is designed for a maximum heat load of 37.2 kW. The analyses and results are presented herein.

B.4.1 Discussion

B.4.1.1 Overview and Purpose of Thermal Analysis

The NUHOMS® 32PTH2 system is designed to passively reject decay heat under normal and off-normal conditions of storage, and for accident and loading/unloading conditions while maintaining NUHOMS® 32PTH2 system component temperatures and pressures within specified limits.

To establish the heat removal capability, several thermal design criteria are established for the NUHOMS® 32PTH2 system. These are:

- Pressures within the 32PTH2 DSC cavity are within design values considered for structural and confinement analyses. The maximum DSC cavity internal design pressures for normal, off-normal and accident conditions are 15 psig, 20 psig and 140 psig, respectively.

- Maximum and minimum temperatures of the confinement structural components must not adversely affect the confinement function.

- Maximum fuel cladding temperature limit of 400°C (752°F) is applicable to normal conditions of storage, transfer operations from spent fuel pool to ISFSI pad, and all short term operations including vacuum drying and helium backfilling of the 32PTH2 DSC per NUREG-1536 [B4.3] or ISG-11 [B4.4]. In addition, NUREG-1536 or ISG-11 do not permit repeated thermal cycling of the fuel cladding with temperature differences greater than 65°C (117°F) during drying and backfilling operations.

- Maximum fuel cladding temperature limit of 570°C (1058°F) is applicable to storage or transfer accidents and off-normal storage conditions per [B4.3] or [B4.4].

- Thermal stresses for the 32PTH2 DSC, when appropriately combined with other loads, will be maintained at acceptable levels to ensure the confinement integrity of the NUHOMS® 32PTH2 system (see Chapters B.3 and B.7). Chapter B.2 presents the principal design bases for the NUHOMS® 32PTH2 system.

B.4.1.2 Thermal Load Specification/Ambient Temperature

The ambient temperature ranges and the hourly temperature variation for the extreme summer ambient conditions that are considered in the thermal analyses of the 32PTH2 DSC are the same as those given in Table 4.1-1 and Table 4.1-2. See Chapter 4, Section 4.1.2 for a discussion on the basis for these design temperatures.

The thermal evaluations presented herein include steady state and transient analyses of the thermal response of the NUHOMS® 32PTH2 system components to a defined set of thermal operating conditions. These operating conditions envelope the thermal conditions expected during all normal, off-normal, and postulated accident operations during loading, transfer, and storage for the design basis thermal conditions as defined in Chapter 4, Section 4.1.2. The

allowable temperatures are presented and comparisons are made with calculated temperatures as the basis for acceptance.

A total of four heat load zoning configurations (HLZCs) are allowed for the 32PTH2 DSCs as shown in Chapter B.2, Figure B.2.1-1. The total heat loads per DSC are 37.2 kW for HLZC # 1, 35.0 kW for HLZC # 2, 32.0 kW for HLZC # 3, and 31.2 kW for HLZC # 4.

ANSYS computer code, Version 10.0 [B4.26] is used for the thermal analyses of NUHOMS® 32PTH2 system. ANSYS is a comprehensive thermal, structural and fluid flow analysis package. It is a finite element analysis code capable of solving steady state and transient thermal analysis problems in one, two or three dimensions. Heat transfer via a combination of conduction, radiation and convection can be modeled by ANSYS.

The storage module AHSM-HS is used to store the 32PTH2 DSC. This module is thermally identical to the HSM-H module described in Appendix U, Section U.1.2.1.2 of the UFSAR for the Standardized NUHOMS® System [B4.22]. The thermal performance of the HSM-H was evaluated for a maximum decay heat load of 40.8 kW for 24PTH DSC and 32PTH1 DSC and a maximum heat load of 31.2 kW for 61BTH DSC as documented in Appendix P, Section P.4.4, Appendix T, Section T.4.4, and Appendix U, Section U.4.4, respectively, of the UFSAR for the Standardized NUHOMS® System [B4.22]. The same methodologies used for the thermal evaluation of the HSM-H in Appendix U, Section U.4.4 of the Standardized NUHOMS® System UFSAR [B4.22] are used in this chapter to evaluate the thermal performance of the AHSM-HS with the 32PTH2 DSC.

The thermal performance of the OS200FC Transfer Cask (TC) was previously evaluated for the 32PTH1 DSC with a maximum heat load of 40.8 kW as documented in Appendix U, Section U.4.5 of the UFSAR for the Standardized NUHOMS® System [B4.22]. The methodology used in Appendix U, Section U.4.5 of the Standardized NUHOMS® System UFSAR provides the basis for the thermal evaluation of the OS200FC TC with the 32PTH2 DSC in this chapter. It should be noted that computer codes Thermal Desktop and SINDA/FLUINT were used in Appendix U, Section U.4.5 of the Standardized NUHOMS® System UFSAR for the thermal evaluation of the OS200FC TC. However, ANSYS computer code is used in this chapter for the analysis of the OS200FC TC. The ANSYS model of the OS200FC TC was validated against the results presented in Appendix U, Section U.4.5 of the Standardized NUHOMS® System UFSAR [B4.22] and documented in the application for Amendment 13 to CoC 1004, Appendix T, Section T.4.5.6 [B4.23].

Analyses results for the AHSM-HS are provided in Section B.4.4, for the OS200FC TC in Section B.4.5, for the 32PTH2 DSC in Section B.4.6, and for loading/unloading conditions in Section B.4.8. A summary of the results from the analyses performed for normal, off-normal, and accident conditions, as well as maximum and minimum allowable temperatures, is provided in Table B.4.1-1, Table B.4.1-2, and Table B.4.1-3, respectively. The thermal evaluation concludes that with these heat loads, all design criteria for the NUHOMS® 32PTH2 system are satisfied for normal, off-normal, and accident conditions.

Table B.4.1-1
Component Maximum and Minimum Temperatures in NUHOMS® 32PTH2 System (Storage or Transfer) for Normal Conditions

Component	Storage[1] T_{max} (°F)	Transfer / Short-term[2] T_{max} (°F)	Storage / Transfer[3] T_{min} (°F)	Limit (°F)
AHSM-HS Concrete	<274	N/A	0	300 [B4.3]
AHSM-HS Heat Shield	<249	N/A	0	---
AHSM-HS Support Rail	<353	N/A	0	---
DSC Shell	<421	467	0	---
DSC Top Shield Plug	<282	456	0	---
DSC Bottom Shield Plug	<317	469	0	---
DSC Transition Rail	<493	529	0	---
Fuel Compartment	<704	702	0	---
Fuel Cladding	<727	725	0	752 [B4.3]

(1) The maximum component temperatures for normal storage conditions are bounded by the off-normal storage conditions. See Table B.4.1-2.

(2) The maximum component temperatures for normal transfer or short-term operation conditions are resulting for loading operation with TC inside fuel building, with 120°F ambient and no water in TC/DSC annulus.

(3) For the minimum normal ambient temperature of 0°F, the resulting component temperatures will approach 0°F if no credit is taken for the decay heat load.

Table B.4.1-2
Component Maximum and Minimum Temperatures in the NUHOMS® 32PTH2 System (Storage or Transfer) for Off-Normal Conditions

Component	Storage[1] T_{max} (°F)	Transfer[2] T_{max} (°F)	Storage / Transfer[3] T_{min} (°F)	Limit (°F)
AHSM-HS Concrete	276	N/A	-40 / 0	300 [B4.3]
AHSM-HS Heat Shield	257	N/A	-40 / 0	---
AHSM-HS Support Rail	356	N/A	-40 / 0	---
DSC Shell	425	473	-40 / 0	---
DSC Top Shield Plug	286	431	-40 / 0	---
DSC Bottom Shield Plug	320	441	-40 / 0	---
DSC Transition Rail	497	529	-40 / 0	---
Fuel Compartment	707	700	-40 / 0	---
Fuel Cladding	730	730	-40 / 0	1058 / 752[4] [B4.3]

(1) The maximum component temperatures for off-normal storage conditions are resulting for maximum ambient temperature of 117°F (daily average temperature of 107°F) with 50% blockage of the AHSM-HS inlet vents.

(2) The maximum component temperatures for off-normal transfer conditions are resulting for horizontal transfer with maximum ambient temperature of 117°F (daily average temperature of 107°F).

(3) For the minimum off-normal ambient temperature of -40°F for storage or 0°F for transfer, the resulting component temperatures will approach -40°F if no credit is taken for the decay heat load.

(4) The fuel cladding limit of 1058°F applies to the off-normal condition of storage and the fuel cladding limit of 752°F applies to the short term operations, including vacuum drying, helium backfilling and transfer operations from spent fuel pool to ISFSI pad.

Table B.4.1-3
Component Maximum Temperatures in the NUHOMS® 32PTH2 System (Storage and Transfer) for Accident Conditions

Component	Storage[1] T_{max} (°F)	Transfer[2] T_{max} (°F)	Limit (°F)
AHSM-HS Concrete [3]	408	N/A	350 [B4.28]
AHSM-HS Heat Shield	482	N/A	---
AHSM-HS Support Rail	553	N/A	---
DSC Shell	612	615	---
DSC Top Shield Plug	420	552	---
DSC Bottom Shield Plug	409	564	---
DSC Transition Rail	656	676	---
Fuel Compartment	839	869	---
Fuel Cladding	857	887	1058 [B4.3]

(1) The maximum component temperatures for accident storage conditions are resulting for complete blockage of inlet and outlet vents of AHSM-HS under maximum ambient temperature of 117°F (daily average temperature of 107°F) for a duration of 40 hours.

(2) The maximum component temperatures for accident transfer conditions are resulting for loss of liquid neutron shield combined with loss of air circulation, horizontal transfer under maximum ambient temperature of 117°F (daily average temperature of 107°F).

(3) The maximum concrete temperature for accident conditions is above the 350°F limit given in ACI-349 [B4.28]. Testing will be performed to demonstrate that the concrete compressive strength is greater than that assumed in structural analyses of Chapter B.2.

B.4.2 Summary of Thermal Properties of Materials

The thermal properties of materials used in the thermal analyses are reported below. The values are listed as given in the corresponding references. The following nomenclature is used in the tables of material properties.

T = temperature
k = thermal conductivity
C_p = specific heat
ρ = density

a. Effective Properties for CE 16×16 Class Fuel Assembly

In the thermal model, the fuel assembly is homogenized within the fuel compartment. For calculation of fuel assembly effective properties see Section B.4.9.

T (°F)	$k_{Transverse}$ (Btu/hr-in-°F)	T (°F)	k_{Axial} (Btu/hr-in-°F)	T (°F)	C_p (Btu/lb_m-°F)	ρ (lb_m/in^3)
165	0.0192	200	0.063	80	0.058	0.1268
256	0.0223	300	0.066	260	0.065	
348	0.0260	400	0.070	692	0.072	
441	0.0304	500	0.073	1502	0.078	
535	0.0354	600	0.076			
630	0.0411	800	0.082			
726	0.0474					
823	0.0544					
920	0.0623					
1018	0.0714					

b. Irradiated UO_2 (Fuel Pellet)

See Section B.4.9.1 for discussion of irradiated UO_2 thermal conductivity.

T (°F)	k (65 GWd/MTU) (Btu/hr-in-°F)	T (K)	C_p (J/kg-K) (Eq. 4.2 from [B4.32])	T (°F)	C_p (Btu/lb_m-°F)	ρ (lb_m/in^3) [B4.31]
80	0.186	300	235.4	80	0.056	0.396
260	0.172	400	265.8	260	0.063	
440	0.159	640	295.2	692	0.071	
620	0.146	1090	314.5	1502	0.075	
800	0.134					
980	0.125					
1160	0.116					
1340	0.109					

c. Zircaloy-4 (Fuel Cladding) [B4.5]

T (K)	k (W/m-K)	T (K)	C_p (J/kg-K)	T (°F)	k (Btu/hr-in-°F)	T (°F)	C_p (Btu/lb_m-°F)	ρ (lb_m/in^3)
366	13.600	300	281	200	0.655	80	0.067	
422	14.324	400	302	300	0.690	260	0.072	
478	15.020	640	331	400	0.723	692	0.079	
533	15.694	1090	375	500	0.756	1502	0.090	0.237
589	16.354			600	0.787			
700	17.664			800	0.851			
811	19.013			1000	0.916			
922	20.466			1200	0.985			

d. SA-240, Type 304, ASTM A240, Type 304, 18Cr-8Ni [B4.10]

T	ρ	k	C_p
(°F)	(lb/in^3)	(Btu/hr-in-°F)	(Btu/lb_m-°F)
70	0.290 [B4.13]	0.717	0.114
100		0.725	0.114
200		0.775	0.119
300		0.817	0.122
400		0.867	0.126
500		0.908	0.129
600		0.942	0.130

e. SA-240, Type 316, ASTM A240, Type 316, 16Cr-12Ni-2Mo [B4.10]

T	ρ	k	C_p
(°F)	(lb/in^3)	(Btu/hr-in-°F)	(Btu/lb_m-°F)
70	0.284 [B4.13]	0.683	0.120
100		0.692	0.121
200		0.733	0.124
300		0.775	0.126
400		0.817	0.129
500		0.850	0.130
600		0.892	0.132
700		0.933	0.134
800		0.967	0.135
900		1.008	0.137
1000		1.042	0.138

f. SA-240, Type XM19, ASTM A240, Type XM19, 22Cr-13Ni-5Mn [B4.10]

T	ρ	k	C_p
(°F)	(lb/in^3)	(Btu/hr-in-°F)	(Btu/lb$_m$-°F)
70	0.284(1) [B4.13]	0.533	0.113
100		0.550	0.116
150		0.575	0.119
200		0.592	0.120
300		0.642	0.125
400		0.684	0.127

(1) Density of carbon steel is considered for SA-240 XM-19.

g. A36 (Carbon Steel with C < 0.30%) [B4.10]

T	ρ	k	C_p
(°F)	(lb/in^3)	(Btu/hr-in-°F)	(Btu/lb$_m$-°F)
70	0.280 [B4.13]	2.908	0.103
100		2.892	0.106
200		2.808	0.114
300		2.692	0.119
400		2.575	0.124
500		2.450	0.128
600		2.333	0.134
700		2.217	0.140
800		2.108	0.147
900		1.983	0.155
1000		1.867	0.164

h. Aluminum 6061 [B4.10]

T	ρ	k	C_p
(°F)	(lb/in^3)	(Btu/hr-in-°F)	(Btu/lb$_m$-°F)
70	0.098	8.008	0.213
100		8.075	0.215
150		8.167	0.218
200		8.250	0.221
250		8.317	0.223
300		8.383	0.226
350		8.442	0.228
400		8.492	0.230

i. Aluminum 1100 [B4.10]

T	ρ	k	C_p
(°F)	(lb/in^3)	(Btu/hr-in-°F)	(Btu/lb$_m$-°F)
70	0.098	11.092	0.214
100		10.983	0.216
150		10.833	0.219
200		10.708	0.222
250		10.608	0.225
300		10.517	0.227
350		10.442	0.229
400		10.375	0.232

j. Neutron Absorber Thermal Conductivity (see Section B.4.3)

k. Lead [B4.12]

T	ρ	k	C_p
(°F)	(lb/in^3)	(Btu/hr-in-°F)	(Btu/lb$_m$-°F)
-100	0.413	1.767	0.030
-10	0.411	1.733	0.030
80	0.409	1.700	0.031
260	0.406	1.637	0.032
440	0.402	1.579	0.033
620	0.398	1.512	0.034

l. Neutron Shield Material NS-3 [B4.21]

T	ρ	k	C_p
(°F)	(lb/in^3)	(Btu/hr-in-°F)	(Btu/lb$_m$-°F)
--	0.0637	0.0407	0.145

m. Concrete (data from [B4.22], Appendix P, Section B.4.2)

T	ρ	K	C_p
(°F)	(lb/in^3)	(Btu/hr-in-°F)	(Btu/lb$_m$-°F)
70	0.084	0.0958	0.22
1382		0.0479	

n. Soil (data from [B4.22], Appendix P, Section P.4.2)

T	ρ	K	C_p
(°F)	(lb/in^3)	(Btu/hr-in-°F)	(Btu/lb_m-°F)
--	0.0578	0.0144	0.191

o. Water [B4.14]

T	ρ	k	C_p
(°F)	(lb/in^3)	(Btu/hr-in-°F)	(Btu/lb_m-°F)
44	0.033 (1)	0.0280	1.003
62		0.0288	0.999
80		0.0295	0.998
98		0.0302	0.998
116		0.0308	0.998
134		0.0313	0.999
152		0.0318	1.000
170		0.0322	1.002
188		0.0325	1.004
206		0.0327	1.006
224		0.0329	1.009
242		0.0330	1.012
260		0.0331	1.017
296		0.0331	1.028

(1) The water density is based on temperature of 296°F.

p. Helium Thermal Conductivity [B4.11]

T	k	T	k
(K)	(W/m-K)	(°F)	(Btu/hr-in-°F)
300	0.1499	80	0.0072
400	0.1795	260	0.0086
500	0.2115	440	0.0102
600	0.2466	620	0.0119
800	0.3073	980	0.0148
1000	0.3622	1340	0.0174
1050	0.3757	1430	0.0181

The above data are calculated based on the following polynomial function from [B4.11].

$k = \sum C_i T^i$ for conductivity in (W/m-K) and T in (K)

For 300 < T < 500 K		for 500< T < 1050 K	
C0	-7.761491E-03	C0	-9.0656E-02
C1	8.66192033E-04	C1	9.37593087E-04
C2	-1.5559338E-06	C2	-9.13347535E-07
C3	1.40150565E-09	C3	5.55037072E-10
C4	0.0E+00	C4	-1.26457196E-13

q. Air

Thermal conductivity of air is calculated based on the following polynomial function from [B4.11]:

$k = \sum C_i T^i$ for conductivity in (W/m-K) and T in (K)

For 250 < T < 1050 K	
C0	-2.2765010E-03
C1	1.2598485E-04
C2	-1.4815235E-07
C3	1.7355064E-10
C4	-1.0666570E-13
C5	2.4766304E-17

Prandtl number, specific heat, viscosity, and density of air are used to calculate heat transfer coefficients in AHSM-HS and OS200FC TC models based on the following data from [B4.11]:

$c_p = \sum A_i T^i$ for specific heat in (kJ/kg-K) and T in (K)

For 250 < T < 1050 K	
A0	0.103409E+1
A1	-0.2848870E-3
A2	0.7816818E-6
A3	-0.4970786E-9
A4	0.1077024E-12

$\mu = \sum B_i T^i$ for viscosity $(N/m^2)\times 10^6$ and T in (K)

For 250 < T < 600 K		For 600 < T < 1050 K	
B0	-9.8601E-1	B0	4.8856745
B1	9.080125E-2	B1	5.43232E-2
B2	-1.17635575E-4	B2	-2.4261775E-5
B3	1.2349703E-7	B3	7.9306E-9
B4	-5.7971299E-11	B4	-1.10398E-12

$\rho = P / RT$ for density (kg/m^3) with P=101.3 kPa; R = 0.287040 kJ/kg-K; T = air temp in (K)

$Pr = c_p \mu / k$ Prandtl number

r. Surface Properties

Material	Emissivity (ε)	Solar Absorptivity (α)	References
Zircaloy based Fuel Cladding	0.8	---	[B4.5]
Stainless steel	0.3 (1)	---	[B4.16]
	0.46 (2)	0.587	[B4.22], Appendix P, Section P.4.2
Rolled steel surfaces	0.587 (3)	0.587	[B4.8]
Concrete	0.9	1.0	[B4.15]

(1) For fuel compartments in calculation of effective fuel conductivity
(2) For machined or flat stainless steel surfaces
(3) For rolled surfaces of the transfer cask

Emissivity of rolled stainless steel plates is 0.587 as considered in [B4.8] consistent with data in Chapter 4, Section 4.2 (j) and Chapter A.4, Section A.4.2 (l). The emissivity for rolled steel sheets is 0.657 as reported in Table 10-17 of [B4.13]. An emissivity of 0.587 is assumed for the exterior surfaces of the 32PTH2 DSC, the inner shell of the OS200FC TC, the exterior surface of the liquid neutron shield, and the stainless steel skin enclosing the NS-3 material at the top and bottom of the TC.

For conservatism, an emissivity of 0.46 is assumed for the machined or flat stainless steel surfaces of the top and bottom forgings of the TC, support rail and top/side heat shields of the AHSM-HS identical to those used in [B4.22], Appendix U, Section U.4.2.

An emissivity of 0.3 is considered for the smooth surfaces of the fuel compartments in calculation of effective fuel conductivity based on data reported in [B4.16].

Solar absorptance values of 0.39 and 0.47 are given in [B4.17] for rolled and machined stainless steel plates, respectively. For conservatism, it is assumed that the absorptivity and the emissivity of stainless steel are equal in this evaluation. Solar absorptivity of 0.587 is used for the exposed stainless steel surfaces.

The solar absorptivity of the concrete surface is 0.73 - 0.91 at 300K [B4.15]. For conservatism a solar absorptivity of 1 is considered for the concrete surface.

B.4.3 Specifications for Neutron Absorber Thermal Conductivity

The 32PTH2 basket design allows for use of a neutron absorber plate (poison plate) with a thickness of 0.37 inches. The neutron absorber consists of one single poison sheet or a poison plate paired with an aluminum sheet. The thermal model of the 32PTH2 DSC considers a poison plate paired with an aluminum (Al 1100) sheet. The thickness of the poison plate and the paired aluminum sheets can be varied within the maximum neutron absorber thickness of 0.37 inches. To maintain the thermal performance of the basket assembly, the minimum thermal conductivity is taken so that the total thermal conductance (sum of conductivity × thickness) of the poison plate and aluminum sheet is equal to the conductance assumed in the thermal analysis.

The thermal analysis of the 32PTH2 DSC considers the following neutron absorber combination:

- A poison plate with a thickness 0.20 inches and a thermal conductivity of 130 W/m-K (6.3 Btu/hr-in-°F).
- An aluminum 1100 sheet with a thickness of 0.17 inches and a thermal conductivity of 230 W/m-K (11.1 Btu/hr-in-°F) at 70°F as specified per ASME Code, Section II, Part D [B4.10].

The minimum thermal conductivity of the neutron absorber used in the 32PTH2 DSC thermal analysis is calculated as follows:

$$\begin{aligned} k_{total,\,min} &= (k_{poison} \times t_{poison} + k_{Al1100} \times t_{Al1100}) / t_{total} \\ &= [(6.3\ \text{Btu/hr-in-°F} \times 0.2\ \text{in}) + (11.10\ \text{Btu/hr-in-°F} \times 0.17\ \text{in})] / 0.37\ \text{in.} \\ &= 8.5\ \text{Btu/hr-in-°F} \quad (177\ \ \text{W/m-K}) \end{aligned}$$

Where:

$k_{total,\,min}$ = Minimum thermal conductivity of neutron absorber within 32PTH2 DSC (Btu/hr-in-°F),

t_{total} = Total thickness of paired aluminum and poison plates = 0.37 in.
k_{poison} = Conductivity of poison plate = 6.3 Btu/hr-in-°F,
t_{poison} = Thickness of poison plate = 0.2 in,
k_{Al1100} = Conductivity of Al 1100 at 70°F = 11.1 Btu/hr-in-°F (see Section B.4.2(i)),
t_{Al1100} = Thickness of aluminum plate = 0.17 in.

If poison plate thicknesses other than those noted above are used for fabrication of the 32PTH2 basket assembly, the required minimum poison plate conductivity will be calculated by rearranging the above equation and solving for the k_{poison}. The k_{poison} resulting from this equation will be used as the minimum required conductivity to qualify the poison plate.

$$k_{poison} = \frac{k_{total,\,min} \times t_{total} - k_{Al} \times t_{Al}}{t_{poison}}$$

Where:

k_{poison} = Minimum required conductivity of poison plate at the corresponding temperature, Btu/hr-in-°F or W/m-K,

t_{poison} = Thickness of poison plate, in,

$k_{total,min}$ = Minimum thermal conductivity of neutron absorber within 32PTH2 DSC = 8.5 Btu/hr-in-°F or 177 W/m-K,

t_{total} = Total thickness of paired aluminum and poison plates = 0.37 in.,

k_{Al} = Conductivity of aluminum sheet / plate at the corresponding temperature, Btu/hr-in-°F or W/m-K,

t_{Al} = Thickness of the aluminum sheet / plate, in.

Since the conductivity of the poison plate generally increases at higher temperatures, testing at room temperature is adequate to qualify the poison plate.

B.4.4 Thermal Evaluation of AHSM-HS with 32PTH2 DSC

The AHSM-HS is used to store a loaded 32PTH2 DSC at the ISFSI. The form of the air channels, thermal features and thermal characteristics of the AHSM-HS are very similar to the HSM-H described in Appendix U, Section U.1.2.1.2 of [B4.22]. The design of the HSM-H was first described and evaluated in Appendix P, Section P.4.4 of [B4.22] for the 24PTH DSC with maximum heat load of 40.8 kW. The same design was also evaluated in Appendix U, Section U.4.4 of [B4.22] for the 32PTH1 DSC for heat loads of 40.8 kW and 31.2 kW. Due to similarities between the HSM-H and AHSM-HS designs, the AHSM-HS is evaluated in this section using the same methodologies used to evaluate the HSM-H in [B4.22].

B.4.4.1 Ambient Temperature Specification

As specified in Chapter 4, Section 4.1.2 and shown in Table 4.1-1 and Table 4.1-2, ambient temperatures in the range of 0°F to 104°F are considered as normal storage conditions. Off-normal ambient temperatures of -40°F to 117°F are considered as off-normal, cold and hot storage condition, respectively. Based on Chapter 4, Section 4.1.2, the daily average ambient temperatures of 97°F and 107°F correspond to the normal and off-normal hot storage ambient temperatures of 104°F and 117°F, respectively.

B.4.4.2 Description of Loading Cases for Storage of 32PTH2 DSC

The operating conditions listed in Table B.4.4-1 are used to determine the thermal performance of the AHSM-HS with 32PTH2 DSC for normal, off-normal and accident conditions.

The off-normal storage condition (Load Case S3) with a maximum heat load of 37.2 kW and maximum ambient temperature of 117°F is considered to bound the temperatures for the normal storage condition (Load Case S1) with a maximum ambient temperature of 104°F.

The off-normal storage conditions (Load Cases S3, S4, S5, and S5A) with various HLZCs are evaluated to demonstrate that the Load Case S3 with HLZC # 1 (37.2 kW) represents the bounding maximum temperatures for steady-state storage conditions.

The off-normal cold storage condition with a -40°F ambient temperature (Load Case S6) and maximum heat load of 37.2 kW is analyzed to provide the bounding thermal gradients.

Since the AHSM-HS is located outdoors, there is a remote probability that the air inlet or outlet openings will become blocked by debris from events such as flooding, high wind, and tornados. The perimeter security fence around the ISFSI and the location of the air inlet and outlet openings reduce the probability of such an accident. A complete blockage of all air inlets and outlets simultaneously is not a credible event. However to bound this scenario, analysis is carried out assuming complete blockage of the inlet and outlet vents as an accident case. For the blocked vent accident storage condition (Load Case S7), a transient model with a maximum ambient temperature of 117°F (daily average ambient temperature of 107°F) is analyzed. Initial temperatures are taken from steady-state results of the off-normal hot storage condition (Load Case S3). Blocked vent transient accident conditions are considered for up to 40 hours.

Although unlikely, an additional load case (Load Case S3A) is also considered with 50% blockage of the AHSM-HS inlet vents as an off-normal storage condition. For this load case, it is assumed that the blockage occurs over the bottom half of the 30″ high inlet vents reducing the area of both of the inlets by half. The 50% blockage of the AHSM-HS inlet vents is analyzed using a steady-state model.

B.4.4.3 Thermal Analysis of AHSM-HS with 32PTH2 DSC

The AHSM-HS is designed to provide an independent, passive system with substantial structural capacity to ensure safe storage of spent fuel assemblies in the 32PTH2 DSCs.

As noted previously, the methodology used to evaluate the HSM-H in Appendices P and U of [B4.22] is used in this section to evaluate the AHSM-HS with 32PTH2 DSC. This methodology consists of two steps. In the first step, an airflow analysis determines the air temperature exiting the outlet vents based on the geometry of the air channels inside of the AHSM-HS cavity and the amount of heat load in the 32PTH2 DSC. In the second step, an ANSYS model of the AHSM-HS determines the temperature distribution on the AHSM-HS walls and on the 32PTH2 DSC shell.

The DSC shell temperatures from the AHSM-HS model are then used to calculate the basket and peak fuel cladding temperature in a detailed model of the 32PTH2 DSC and basket described in Section B.4.6. For the analytical purpose of calculating the maximum temperatures, an AHSM-HS centered in an array of modules, each loaded with a 32PTH2 DSC with the maximum heat load of 37.2 kW, is considered for the analysis. Rows of modules are assumed to exist back-to-back for this model, which bounds the case of a single row array.

The methodology used to evaluate the HSM-H in Appendices P and U of [B4.22] was validated by thermal tests performed on a 1:1 scale of an HSM-H mockup structure for heat loads varying from 32 to 44 kW [B4.25]. The conservatism in this methodology is also confirmed by a confirmatory analysis documented in the SER for Amendment 10 to CoC 1004 [B4.27].

B.4.4.3.1 AHSM-HS Airflow Analysis (Stack Effect Calculations)

The methodology used in the HSM-H airflow analysis (stack effect calculations) is presented in [B4.22], Appendix P, Section P.4.4.3. Different equations for computing the total pressure loss due to flow losses, air mass flow rate, temperature rise from air inlet to outlet, and the stack average temperature are also provided in [B4.22], Appendix P, Section P.4.4.3. The inputs of these equations are changed based on the dimensions of the AHSM-HS and 32PTH2 DSC and the heat load of the 32PTH2 DSC to determine the exit air temperature for the AHSM-HS for various load cases described in Section B.4.4.2. For the AHSM-HS with 50% blocked inlet vents, the air flow analysis includes the additional resistance and loss coefficients due to the decrease in the inlet surface area.

A summary of the calculation results for mass flow rates, total loss coefficients, exit and mean air temperatures for normal and off-normal storage conditions is provided in Table B.4.4-2. These bulk air temperatures are used in the ANSYS model of the AHSM-HS to calculate the temperatures throughout the AHSM-HS and the 32PTH2 DSC shell.

The accident blocked vents condition conservatively assumes no closed cavity convection.

B.4.4.3.2 Description of the ANSYS Model of AHSM-HS with 32PTH2 DSC

A half symmetric, three dimensional, ANSYS [B4.26] finite element model of the AHSM-HS loaded with a 32PTH2 DSC is shown in Figure B.4.4-1. This model is essentially identical to the HSM-H model described in [B4.22], Appendix U, Section U.4.4.4 used for analysis of 32PTH1 DSC except that dimensions of the AHSM-HS and 32PTH2 DSC are considered in generation of the model geometry.

The AHSM-HS ANSYS model consists of SOLID70 conduction elements that represent concrete and steel support structures of the AHSM-HS, heat shields, DSC shell, and homogenized basket. SHELL57 elements superimposed on SOLID70 elements, as required, for generation of radiating surfaces for the MATRIX50 super elements. Radiation between the DSC shell, heat shields, and AHSM-HS walls is modeled using the ANSYS /AUX12 methodology. The SHELL57 elements used as radiation surfaces are unselected prior to solving the model. To reduce the number of nodes associated with the model's super-elements, the web of the supporting beam is modeled using only SHELL57 elements. As such, conservatively, radiation is not applied on the web of the supporting beam. This methodology is valid since the supporting beam's web is greatly shielded from the DSC radiation via its own flanges. The properties and dimensions of the support beam, such as the thickness of the web, are given as real constants to the appropriate SHELL57 elements.

During storage, the bottom portion of the 32PTH2 DSC resides within the door opening region of the front wall. Convection is conservatively omitted in the space between the bottom portion of the DSC and the concrete module in this region.

The boundary conditions for the AHSM-HS model are applied using the same methodology described in [B4.22], Appendix P, Section P.4.4.4. Ambient, exit and mean bulk air temperatures listed in Table B.4.4-2 are used to determine the boundary conditions.

The correlation for convection coefficients over the AHSM-HS surfaces, including the AHSM-HS vertical flat surfaces, horizontal surfaces, the side heat shield, the top heat shield and the horizontal DSC cylinder surface are discussed in detail in [B4.22], Appendix P, Section P.4.9. Convection and radiation from the HSM-H roof and the front wall to the ambient are combined as a total effective heat transfer coefficient as discussed in [B4.22], Appendix P, Section P.4.9. Figure B.4.4-2 shows the convection boundary conditions applied to the AHSM-HS model. Presence of DSC support structure restricts air flow over certain portions of the DSC shell. The region with restricted airflow is called the "dead zone." No convection is considered in this region for conservatism. The no convection zone at the DSC shell-support structure interface is 16.5°, as shown in Figure B.4.4-4.

A soil temperature of 70°F is assumed at a depth of 10 feet below the ISFSI pad for hot conditions. The soil temperature for the cold condition (0°F or -40°F) is assumed to be 45°F. These assumptions are consistent with the assumptions used in the Chapter 4, Section 4.4.2.2 and Appendix A, Section A.4.10.

The modeling of insolation on the surfaces of the AHSM-HS roof and front wall, which are exposed to ambient is identical to that described in [B4.22], Appendix P, Section P.4.4.4. The methodology to apply solar heat flux is also identical to that described in [B4.22], Appendix P, Section P.4.4.4. The values of the applied solar heat fluxes are listed below:

AHSM-HS Surface	Insolation (gcal/cm^2)	Averaged over 24 hr (Btu/hr-in^2)
AHSM-HS roof	800	0.8537
AHSM-HS front wall	200	0.2134

Insolation is conservatively neglected for the ambient temperatures of 0° and -40°F.

The DSC basket, including fuel assemblies, is modeled as a homogenized material with effective properties as discussed in Section B.4.6.6. The heat generation rate in the AHSM-HS thermal model is determined using the same method as [B4.22], Appendix P, Section P.4.4.5. Heat generating boundary conditions are applied uniformly on the elements representing the homogenized DSC basket. The amount of generated heat per unit volume of the DSC contents for a heat load of 37.2 kW is calculated as follows:

$$\text{Heat generation rate} = \frac{Q}{\left(\pi / 4\, D_i^{\,2} L_b\right)} = 0.196 \text{ Btu/hr-in}^3$$

Where:

Q = decay heat load =37.2 kW (to convert from kW to Btu/hr multiply by 3412.3)

D_i = inner DSC diameter = 68.5″

L_b= basket assembly length = 177.15″

The thermal analysis of a typical AHSM-HS is performed for a loaded 32PTH2 DSC located in the interior of a multiple module array with a 32PTH2 DSC present in the two adjacent AHSM-HSs. The AHSM-HS top and front surfaces are modeled as exposed to the prevailing ambient conditions in this model. The side and back surfaces are modeled as being adiabatic in order to simulate the adjacent modules. Figure B.4.4-3 shows the heat generation rate, solar heat load, and fixed temperature boundary conditions applied in the AHSM-HS model.

B.4.4.3.3 Description of the AHSM-HS Blocked Vent Model

To determine the maximum temperatures of the AHSM-HS and the 32PTH2 DSC shell for the blocked vent accident case, the finite element model of the AHSM-HS described in Section B.4.4.3.2 is modified to a transient model with no convection in the AHSM-HS cavity. The modeling approach is similar to one described in [B4.22], Appendix U, Section P.4.4.5.

During the blockage of the air inlet and outlet vents in the AHSM-HS, free convection between the 32PTH2 DSC and AHSM-HS walls is present within the closed AHSM-HS cavity. However, no convection is considered within the AHSM-HS cavity during the blocked vent condition for

conservatism. The analysis considers only the thermal conductivity of air within the AHSM-HS cavity.

The initial temperatures for the blocked vent accident case are identical to those resulting from the off-normal storage condition (Load Case S3) with a maximum ambient temperature of 117°F (average ambient temperature of 107°F) and heat load of 37.2 kW.

B.4.4.4 AHSM-HS Thermal Analysis Results

A summary of the airflow analysis results is provided in Table B.4.4-2. Table B.4.4-2 also shows the maximum expected air temperature rises for the maximum heat loads of 37.2 kW, 35.2 kW, 32.0 kW and 31.2 kW for the maximum ambient temperature of 117°F. The maximum AHSM-HS component temperatures for the normal, off-normal, and accident cases are listed in Table B.4.4-3. Temperature distributions for the hot and cold off-normal cases are shown in Figure B.4.4-5 and Figure B.4.4-6, respectively.

Temperature distributions for the blocked vent accident case with 37.2 kW decay heat load at 40 hours after blockage of the vents are shown in Figure B.4.4-7. The time-temperature histories of AHSM-HS components for this transient model are shown in Figure B.4.4-8.

B.4.4.5 Evaluation of AHSM-HS Performance

The thermal performance of the AHSM-HS has been evaluated under normal, off-normal, and accident conditions of operation as described above and is shown to satisfy all the temperature limits and criteria. The 32PTH2 DSC shell temperatures calculated here are used in the 32PTH2 DSC model as a boundary condition in Section B.4.6. The results presented in Section B.4.6 show that all the basket and fuel cladding material temperature limits are also satisfied.

The results of the blocked vent accident condition show that the maximum concrete temperature at the end of 40 hours is 408°F. This is above the 350°F limit given in Section A.4 of ACI-349 [B4.28] for accident conditions. To account for the effect of higher concrete temperature on the concrete compressive strengths, the structural analysis of AHSM-HS concrete components in Section B.3 is based on 10% reduction in concrete material properties. Testing will be performed to document that concrete compressive strength will be greater than that used in the structural analysis documented in Chapter B.3.

B.4.4.5.1 Monitoring of AHSM-HS Concrete Temperature

AHSM-HS temperature monitoring is provided to alert operators to a possible blocked vent condition. The location and coordinates of the temperature sensor in the AHSM-HS half-symmetry ANSYS model is illustrated in Figure B.4.4-9. The reference origin at point "P" shown in Figure B.4.4-9 of the coordinate system (X′, Y′, Z′) corresponds to the ANSYS model coordinates of x=0″, y=178″, and z=206″. The temperature sensor location at point "S" in Figure B.4.4-9 has coordinates of X′=-24″, Y′=3″, and Z′=-48″. This corresponds to the ANSYS model coordinates of x=-24″, y=181″, z=158″.

The temperatures at the location of the sensor at point "s" are retrieved from the transient ANSYS model of the ASHM-HS during blocked vent accident condition. These temperatures,

along with the corresponding maximum concrete temperature, are listed in Table B.4.4-4 to provide the basis for the monitoring system. As shown in Table B.4.4-4 for the 37.2 kW heat load, the sensor temperature at point "s" at the beginning of the blocked vent for 117°F ambient conditions ($T_{sensor\ @\ 0hr}$) is 219°F and the sensor temperature after 40 hours of blocked vent accident conditions ($T_{sensor\ @\ 40\ hrs}$) is 303°F. These temperatures correspond to maximum AHSM-HS concrete temperatures of 274°F at 0 hour and 408°F at 40 hours, respectively.

Table B.4.4-4 also lists the sensor temperature rise at point "s" during blocked vent accident conditions (ΔT_{sensor}) as calculated below:

$$\Delta T_{sensor} = T_{sensor} - T_{sensor\ @\ 0hr}$$

Where

T_{sensor} = Transient sensor temperature after blocked vent accident conditions, °F,
$T_{sensor\ @\ 0hr}$ = 219°F listed in Table B.4.4-4.

The maximum sensor temperature at point "s" after 24 hours of vent blockage is 272°F and the sensor temperature rise at point "s" is 52°F per 24 hours. These values can be used as an early warning to correct a possible blocked vent condition before the maximum concrete temperature is exceeded.

It should be noted that typically, there are redundant temperature sensors embedded in the AHSM-HS. The locations of the redundant temperature sensors are symmetric such that the above results are applicable at either location. Concrete temperature does not vary significantly for small changes in the location of the sensor.

Table B.4.4-1
Design Load Cases for 32PTH2 DSC in AHSM-HS

Operation	Load Case No.	Condition	Model	Heat Load[1] (kW)	T_{amb}[2] (°F)	Insolation
Storage	S1	Normal, Hot	Steady-State	37.2 (HLZC#1)	104	Yes
	S2	Normal, Cold		37.2 (HLZC#1)	0	No
	S3	Off-Normal, Hot		37.2 (HLZC#1)	117	Yes
	S3A[3]			37.2 (HLZC#1)	117	Yes
	S4			35.2 (HLZC#2)	117	Yes
	S5			32.0 (HLZC#3)	117	Yes
	S5A			31.2 (HLZC#4)	117	Yes
	S6	Off-Normal, Cold		37.2 (HLZC#1)	-40	No
	S7	Accident[4]	Transient for 40 hr	37.2 (HLZC#1)	117	Yes

(1) The four heat load zone configurations (HLZCs) are described in Chapter B.2, Figures B.2.1-1.

(2) The maximum daily temperature of 104°F correspond to daily average temperature of 97°F and the maximum daily temperature of 117°F correspond to daily average temperature of 107°F.

(3) This load case considers a 50% blockage of the AHSM-HS inlet vents.

(4) This load case considers a complete blockage of the AHSM-HS inlet and outlet vents.

Table B.4.4-2
Summary of Air-Flow Calculation Results

Load Case No.[1]	T_{amb} (°F)	Heat load (kW)	Mass Flow Rate (lb_m/s)	Total Loss Coefficient (ft^{-4})	T_{mean} (°F)	T_{exit} (°F)	$\Delta T_{AHSM-HS}$, (°F)
S1	104	37.2	1.623	0.1017	142	187	90
S2	0	37.2	2.000	0.0997	37	73	73
S3	117	37.2	1.595	0.1019	153	199	92
S3A	117	37.2	1.431	0.1381	158	209	102
S4	117	35.2	1.569	0.1020	151	195	88
S5	117	32.0	1.525	0.1021	148	190	82
S5A	117	31.2	1.514	0.1022	148	188	81
S6	-40	37.2	2.213	0.0988	-7	26	66

(1) See Table B.4.4-1 for description of the load cases.

Table B.4.4-3
AHSM-HS Thermal Analysis Results Summary

Load Case #	S1/S2	S3A [3]	S3	S6	S7
Components	**Normal Hot/ Normal Cold T_{max} (°F)**	**Off-Normal Hot[1] T_{max} (°F)**	**Off-Normal Hot T_{max} (°F)**	**Off-Normal Cold T_{max} (°F)**	**Blocked Vent @ 40 Hours T_{max} (°F)**
Concrete [1]	<274	276	274	117	408 [2]
DSC shell	<421	425	421	292	612
Side heat shield	<246	251	246	60	482
Top heat shield	<249	257	249	61	418
Support rail	<353	356	353	213	553

(1) The maximum allowable concrete temperature is 300°F for normal/off-normal conditions [B4.3].

(2) The maximum concrete temperature for accident conditions is above the 350°F limit given in ACI-349 [B4.28]. Testing will be performed to demonstrate that the concrete compressive strength is greater than that assumed in structural analyses.

(3) This load case considers a 50% blockage of the AHSM-HS inlet vents.

Table B.4.4-4
Concrete Temperature at the Temperature Sensor
Blocked Vent Accident Condition for 37.2 kW Heat Load

Time (hr)	$T_{concrete\ max}$ (°F)	T_{sensor} (2) (°F)	ΔT_{sensor} (1) (°F)
0	274	219	0
2	283	223	4
4	293	228	8
6	302	233	13
8	311	237	18
10	319	242	22
12	326	246	27
14	333	251	31
16	339	255	36
18	345	259	40
20	350	264	44
22	356	268	48
24	361	272	52
26	366	276	56
28	371	280	60
30	376	284	64
32	380	287	68
34	385	291	72
36	393	295	76
38	400	299	80
40	408	303	83

(1) ΔT_{sensor} is the sensor temperature rise during blocked vent at point "s" shown in Figure B.4.4-9 for accident conditions and is calculated as $\Delta T_{sensor} = T_{sensor} - T_{sensor\ @\ 0hr}$.

(2) T_{sensor} is the sensor temperature at point "s" shown in Figure B.4.4-9. The T_{sensor} data can be linearly interpolated between time intervals.

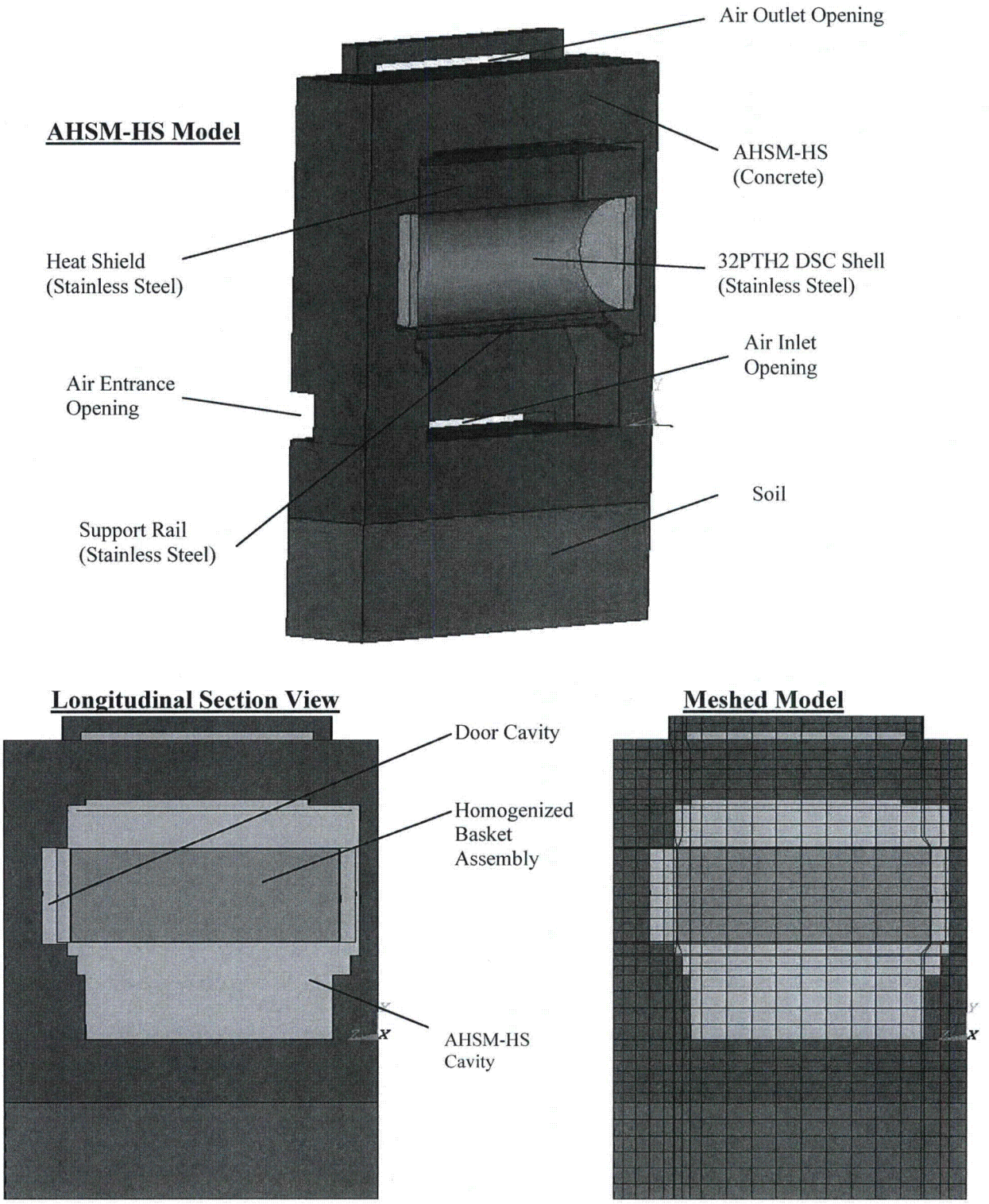

Figure B.4.4-1
AHSM-HS Model

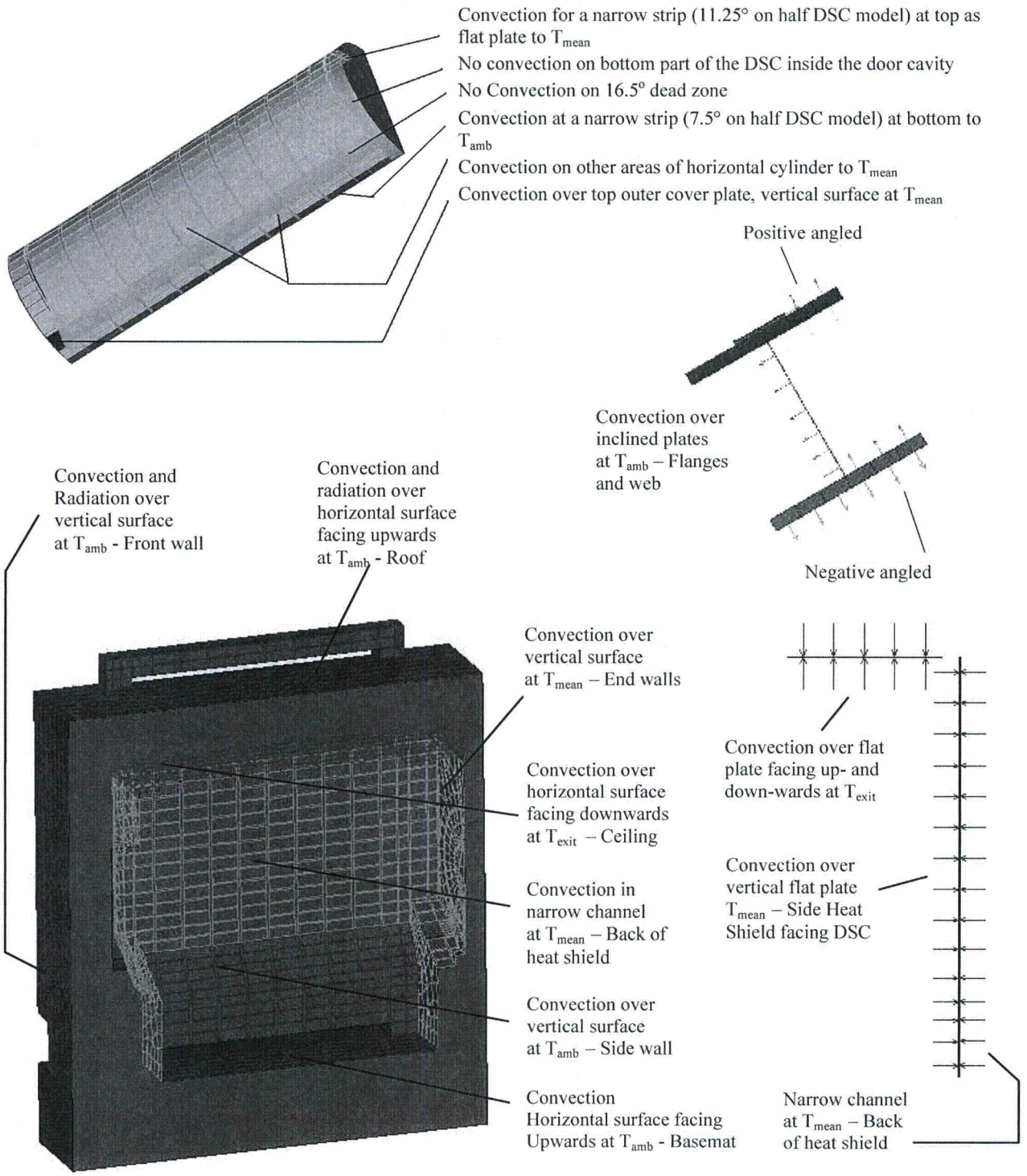

Figure B.4.4-2
Convection Boundary Conditions in AHSM-HS Model

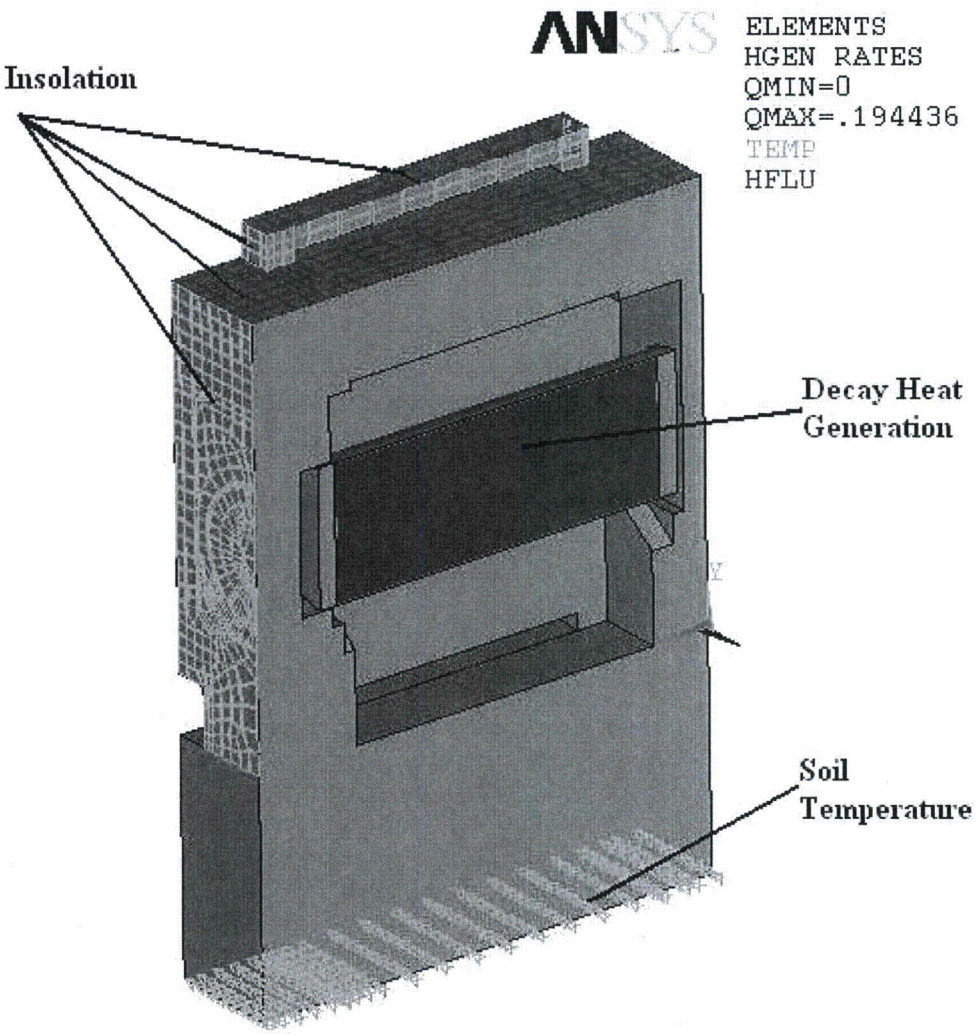

Figure B.4.4-3
Heat Load, Insolation, and Fixed Temperature Boundary Conditions in AHSM-HS Model

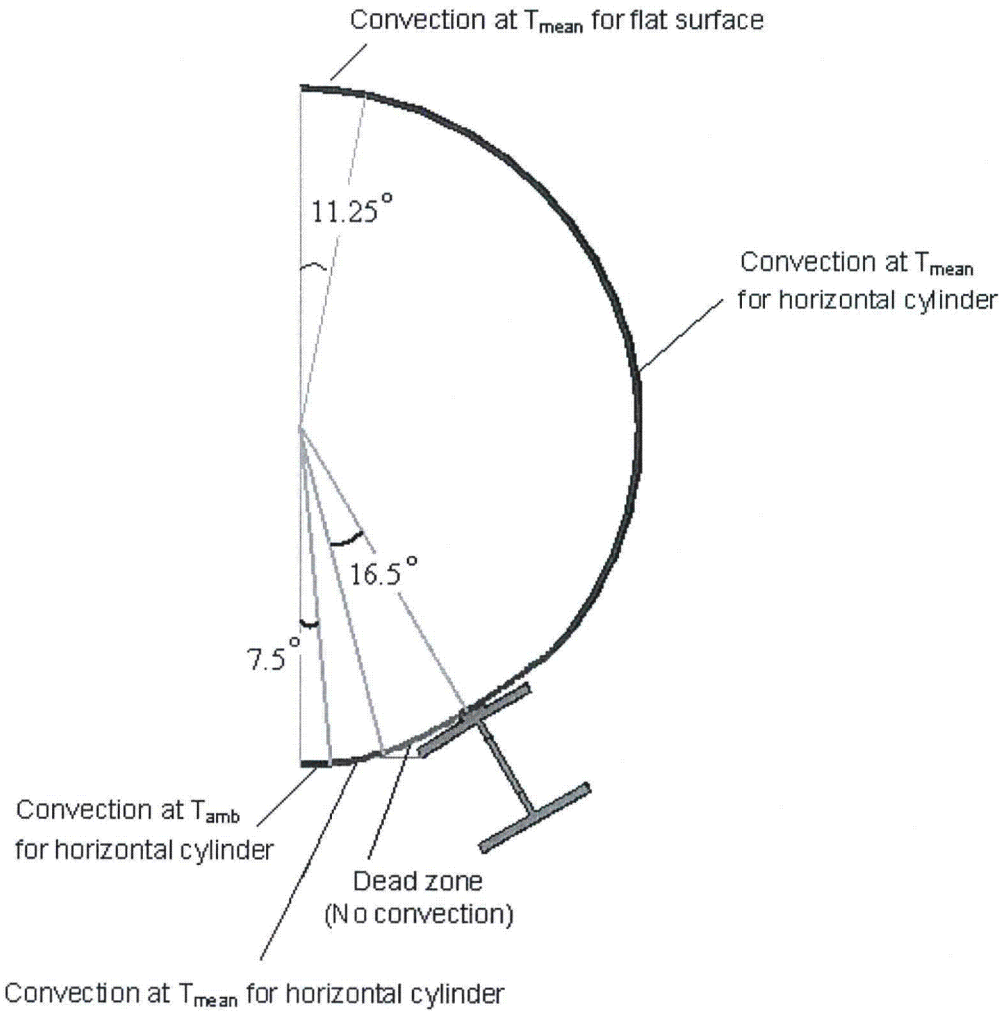

Figure B.4.4-4
Convection Regions around 32PTH2 DSC in AHSM-HS Model

Figure B.4.4-5
AHSM-HS with 32PTH2 DSC, Temperature Profiles for Off-Normal Hot Condition, 37.2 kW (Load Case S3)

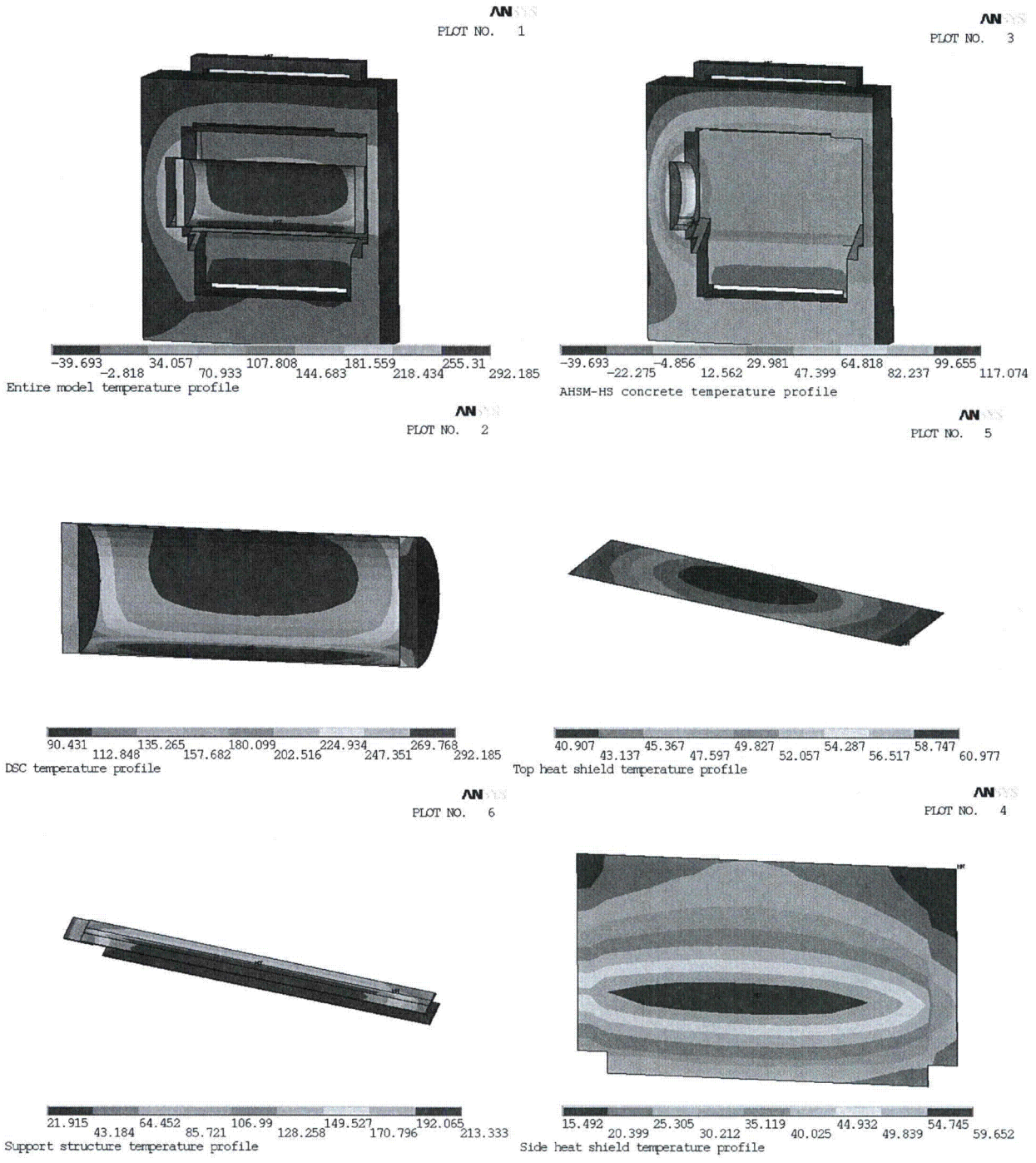

Figure B.4.4-6
AHSM-HS with 32PTH2 DSC, Temperature Profiles for Off-Normal Cold Condition, 37.2 kW (Load Case S6)

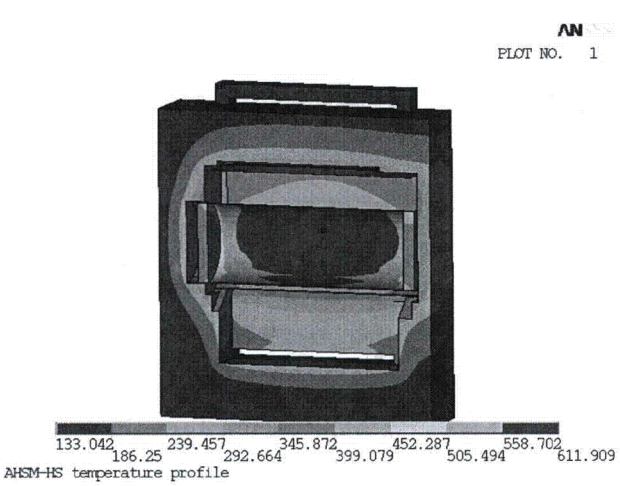

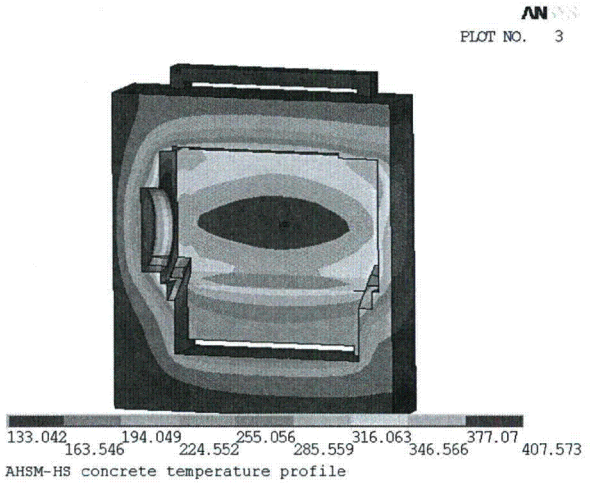

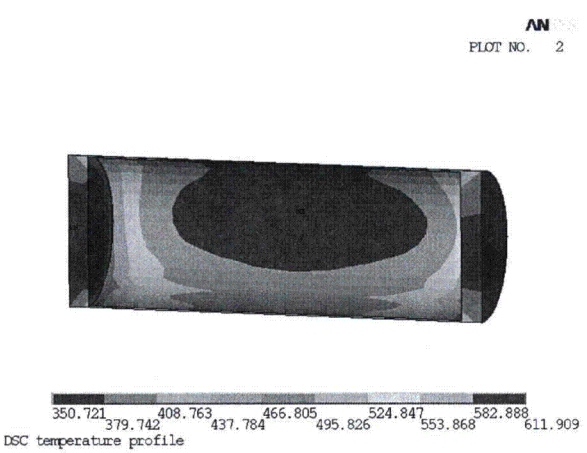

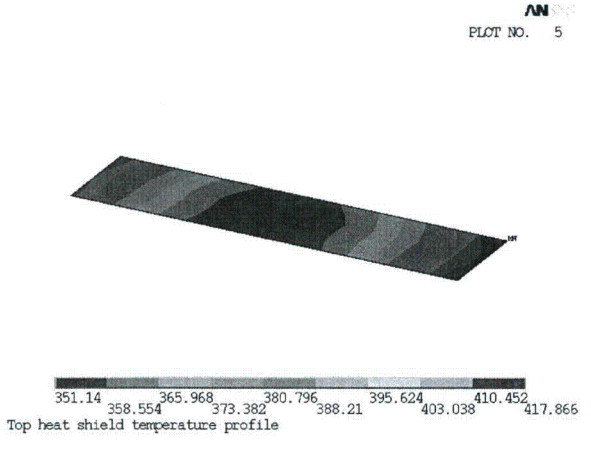

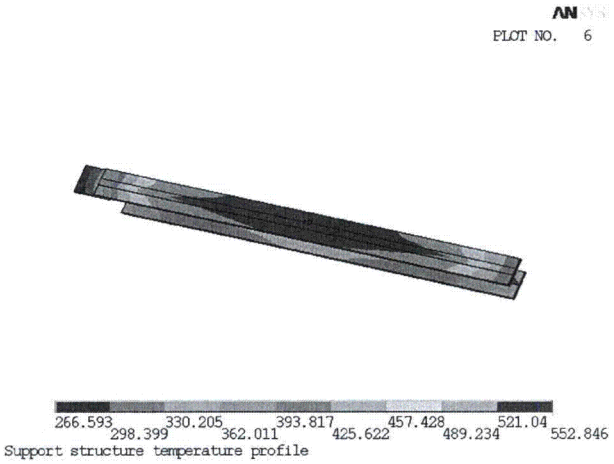

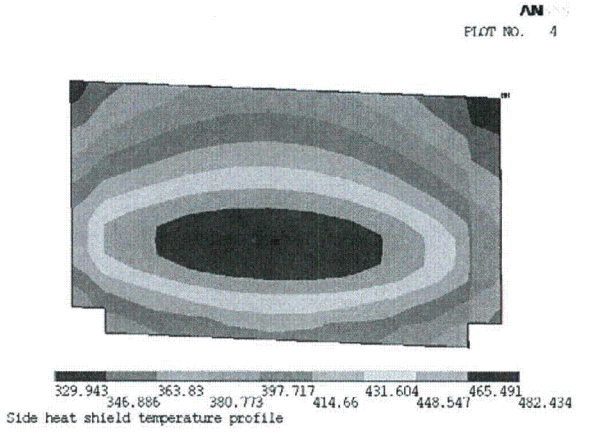

Figure B.4.4-7
AHSM-HS with 32PTH2 DSC, Temperature Profiles for Blocked Vent @ 40 Hour Accident Condition, 37.2 kW (Load Case S7)

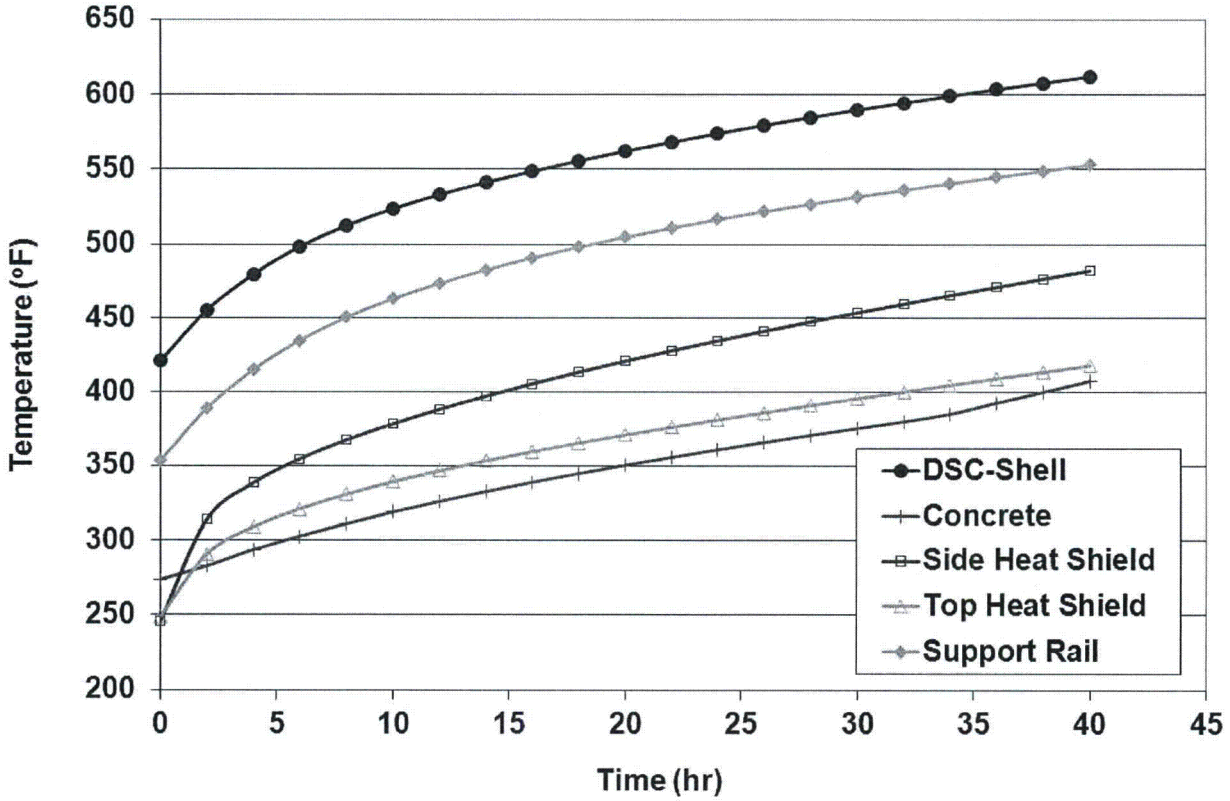

Figure B.4.4-8
AHSM-HS with 32PTH2 DSC, Component Temperature History for Accident Blocked Vent Condition, 37.2 kW

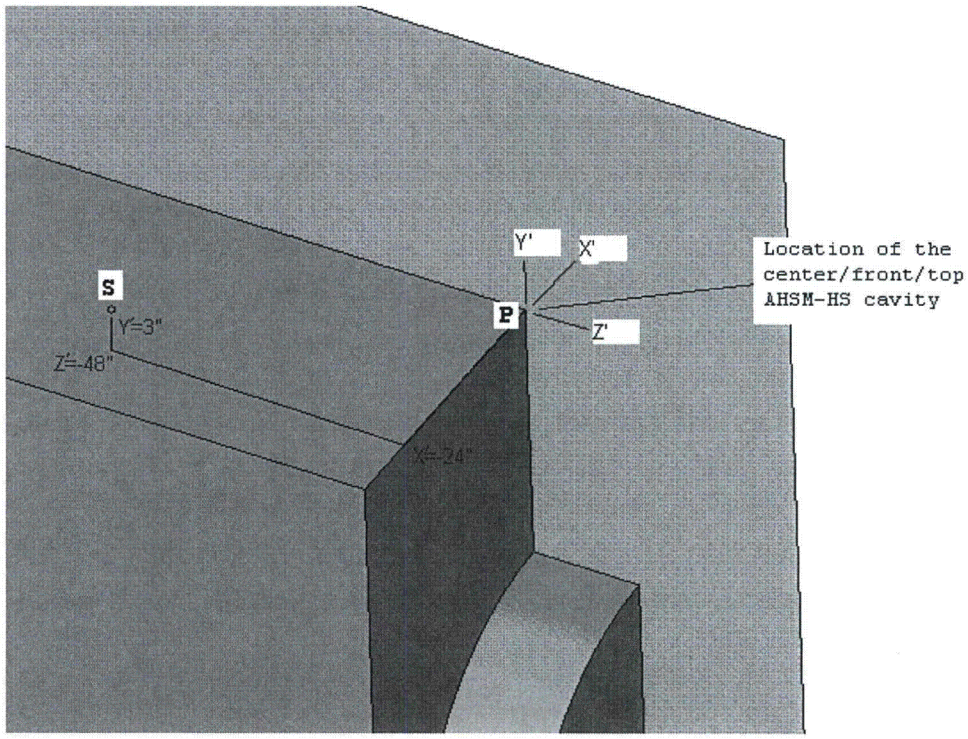

Figure B.4.4-9
Temperature Sensor Location in AHSM-HS Model

B.4.5 Thermal Evaluation of OS200FC TC with 32PTH2 DSC

The OS200FC TC is used to transfer a loaded 32PTH2 DSC between the fuel building and the AHSM-HS at the ISFSI site. The OS200FC TC is designed to passively remove the decay heat load from the DSC under normal, off-normal, and accident conditions while maintaining fuel cladding temperatures and DSC internal pressures within specified regulatory and design limits. The design of the OS200FC TC includes optional features such as a slotted cask lid and a cask bottom spacer to allow air circulation through the TC/DSC annulus as a recovery option when the time limit for transfer operation exceeds or is anticipated to exceed. For 32PTH2 DSCs with HLZCs 1 through 3 (decay heat load over 31.2 kW), administrative measures ensure that the transfer operation is completed within the allotted time or some form of recovery operation such as air circulation is initiated. Transfer operation for 32PTH2 DSC with HLZC 4 (heat load $\leq$ 31.2 kW) does not require a time limit.

In addition to the applicable thermal design criteria listed in Section B.4.1, the following thermal limits are considered for the temperature sensitive components of the OS200FC TC. These components are the lead in the gamma shield, the water in the neutron shield, and the NS-3 solid neutron shielding material.

The ASTM B29 lead used in the gamma shield has a melting point of approximately 620°F [B4.13]. The maximum temperature of the gamma shield is limited to the melting point of lead.

The temperature of the water in the neutron shield is limited by the rating (i.e., 45 psig) of the pressure relief valves on the shield. The temperature of the water cannot rise above the equivalent steam saturation temperature at this pressure (i.e., approximately 290°F) without risk of activating the relief valves and losing some of the water in the neutron shield.

NS-3 is a solid, cementious material that sets within 24 hours and cures in 28 days. NS-3 responds to heat input in a manner similar to that of concrete, remaining a non-combustible solid even when subjected to temperatures as high as 1,300 °F [B4.21]. The thermal properties for this material are insensitive to temperature. The long term operating temperature limit for NS-3 is limited by the need to prevent the outgassing of its water content and, for NS-3 material enclosed in sealed cavities, to control the potential pressure increase associated with the loss of water. By testing [B4.29] in an open (non-sealed) system, the NS-3 material is shown to experience a weight loss of 4.16% (in the form of water vapor) after 2 hours at a constant temperature of 340°F. The effect is significantly reduced at lower temperatures, with a weight loss of 2.15% after 100 hours at 150°F. By sealing the enclosure surrounding the NS-3 material and maintaining the maximum bulk average temperature of the material to 250°F or less, no reduction in water content is expected to occur during extended normal operating conditions. For design purposes of this application, the long-term, bulk average temperature of the NS-3 material is set to 250°F or less, short-term limits for normal operations should be 300°F or less, and short-term limits for accident conditions should be 1,300°F or less.

B.4.5.1 Ambient Temperature Specification

Operations involving the OS200FC TC will occur within the fuel handling facility and outdoors. Ambient temperatures in the range of 0 to 120°F are considered for operations within the fuel handling facility.

Ambient temperatures in the range of 0 to 104°F are considered as normal, outdoor transfer conditions, while an ambient temperature of 117°F is considered for the off-normal, hot transfer condition and for transfer accident conditions. As noted previously in Chapter 4, Section 4.1.2 and shown in Table 4.1-1 and Table 4.1-2, the daily average ambient temperatures of 97°F and 107°F correspond to the normal and off-normal hot storage ambient temperatures of 104°F and 117°F, respectively. No averaging is considered for the ambient temperature inside the fuel building. Instead, the maximum temperature of 120°F is considered for the analysis.

B.4.5.2 Description of Loading Cases for Transfer of 32PTH2 DSC

The loading cases considered for transfer of the 32PTH2 DSC include the vertical loading condition inside of the fuel handling facility, normal and off-normal horizontal transfer conditions with and without air circulation, and two accident scenarios. The first accident scenario involves the potential loss of both the air circulation system and the water in the neutron shield. This case includes a transient heat up trend, which achieves the ultimate temperatures under steady-state conditions. The second accident scenario involves a 15-minute hypothetical fire. The maximum duration of the fire event will be controlled under actual operations by administratively limiting the available fuel sources within the vicinity of the OS200FC TC. An additional condition is considered which involves the potential interruption of the air circulation system, if used, and determines the time available to re-establish the air circulation, complete the transfer operation, or initiate some other recovery mode.

The operating conditions listed in Table B.4.5-1 are analyzed in this section to determine the thermal performance of OS200FC TC with 32PTH2 DSC. The following naming convention is used to abbreviate the description of the loading cases listed in Table B.4.5-1:

- Hot refers to the highest ambient temperature with insolation
- Cold refers to lowest ambient temperature without insolation
- Horizontal refers to transfer operation outside of the fuel building
- Vertical refers to operations occurring within the fuel building
- Steady-state refers to modeling mode for conditions without a time limit
- Transient refers to modeling mode for conditions with a time limit

Load Case T3 (Off-Normal Hot, Horizontal, Steady-State) is used to determine the bounding maximum temperatures for normal and off-normal conditions with heat loads less than or equal to 32 kW (Load Cases T1, T2, and T4). This approach is acceptable since the ambient

temperature for Load Case T3 represents the highest ambient temperature for all these load cases.

Load Case T5A (Normal Hot, Vertical, Steady-State) is used to determine the bounding maximum temperatures for normal loading conditions when the OS200FC TC is inside the fuel building and the TC/DSC annulus is drained. This load case demonstrates that no time limit is required for operations within fuel building for 32PTH2 DSC with HLZC # 4 (31.2 kW heat load).

Load Cases T5, T6, and T7 are used to determine the time limits for the loading operations inside the fuel building or transfer operations outside the fuel building for HLZCs # 1 through # 3 (heat loads > 31.2 kW and $\leq$ 37.2 kW). In this evaluation, the maximum component temperatures and time limits for the OS200FC TC loaded with 32PTH2 DSC and HLZC # 1 (37.2 kW heat load) are considered to bound the corresponding values for 32PTH2 DSC with HLZC # 2 (35.0 kW heat load). The transient analyses for both the horizontal transfer operations and vertical loading operations in these load cases begin with initial conditions established from steady-state thermal analyses with the 32PTH2 DSC centered in the OS200FC TC in vertical orientation, with water in the TC/DSC annulus and a 120°F ambient temperature within the fuel building. The initial conditions are determined using Load Case T11 with 37.2 kW decay heat load and Load Case T12 with 32.0 kW decay heat load.

Load Case T8 (Off-Normal Hot, Horizontal, Steady-State, Air Circulation) is performed to demonstrate that the maximum component temperatures for the OS200FC TC and 32PTH2 DSC remain below the allowable limits if the air circulation as the recovery operation is initiated. This load case bounds the maximum temperatures for heat loads less than or equal to 37.2 kW when the air circulation is activated.

Load Case T9 considers the accident case of the loss of neutron shield, wherein the liquid neutron absorber is replaced with air, combined with the loss of air circulation in a steady-state analysis. Off-normal ambient temperature of 117°F (daily average ambient temperature of 107°F) is considered for this load case.

Due to large thermal inertia of the OS200FC TC and the relative short period of 15 minute fire, the effect of heat input from the fire on the 32PTH2 DSC shell and basket assembly is minimal. The maximum DSC shell temperature is achieved at the post-fire steady-state conditions. The conditions and material properties during the post-fire period are the same as those for the accident case of loss of neutron shield and loss of air circulation, except for the TC outer surface emissivity. As discussed in [B4.22], Appendix U, Section U.4.5.4.2, the sooting and oxidation of the exterior TC surfaces for the fire event raises the surface emissivity, thus improving the heat transfer between the TC and the ambient. As shown in [B4.22], Appendix U, Table U.4-10, and discussed in [B4.22], Appendix U, Section U.4.5.5, other than certain components at the top and bottom ends of the OS200FC TC, which are exposed to fire, there are no adverse effects on the performance of the OS200FC TC due to fire accident. Therefore, maximum DSC shell temperature for fire accident transfer case is bounded by the loss of neutron shield, loss of air circulation accident case and no further analysis is required for fire accident transfer case.

Load Case T10 is applicable to two conditions. The first condition applies for an OS200FC TC with 32PTH2 DSC with a heat load greater than 31.2 kW. If the air circulation is activated as a recovery operation during transfer, the air circulation needs to be turned off before transferring the 32PTH2 DSC into the AHSM-HS storage module. This condition presents a routine transfer operation.

The second condition occurs in a postulated scenario wherein steady-state conditions are established with the air circulation in operation and, subsequently the air circulation is lost during transfer operation. To minimize the occurrence of this condition, the OS200FC TC skid is equipped with redundant industrial grade blowers and each one of these blowers is capable of supplying the required minimum air flow rate. These blowers are also powered with a redundant power supply.

Both the above scenarios i.e. turning off air circulation to offload the 32PTH2 DSC to AHSM-HS or failure of the air circulation will decrease the heat dissipation and will result in a gradual increase of the maximum temperatures of the OS200FC TC and 32PTH2 DSC components. Therefore, for these conditions, an additional time limit is calculated to complete the transfer of the 32PTH2 DSC from the OS200FC TC to the AHSM-HS or to restart the air circulation or initiate other recovery operations to ensure that the peak fuel cladding temperature remains below the temperature limit of 752°F established in [B4.3].

As described above, Load Case T10 starts from a steady state condition with air circulation in operation. In order to estimate the duration needed for the 32PTH2 DSC to reach steady-state conditions, a transient thermal analysis is performed. For this analysis, the worst case hottest initial condition is considered, which corresponds to Load Case T7 at the end of the time limit for the transfer operation. The analysis applies the boundary conditions from Load Case T8 with air circulation in operation through the transient phase and considers the DSC shell temperature as criteria to reach the steady state condition.

For all the normal, off-normal hot conditions and accident design load cases considered in Table B.4.5-1, insolation is considered per 10 CFR 71.71 [B4.2].

B.4.5.3 Thermal Analysis of OS200FC TC with 32PTH2 DSC

The purpose of the TC thermal analysis is to determine the maximum component temperatures including the 32PTH2 DSC shell temperatures, and to establish the time limits for completion of transfer operations during normal and off-normal conditions. The 32PTH2 DSC shell temperatures determined in the TC thermal analysis are then used as boundary conditions in a subsequent 32PTH2 DSC basket thermal analysis described in Section B.4.6.

The design of the OS200FC TC was described in [B4.22], Appendix U for transfer of the 32PTH1 DSC with a maximum heat load of 40.8 kW. The same TC is used for transfer of the 32PTH2 DSC without any modifications. The thermal analysis and the thermal model of the OS200FC TC loaded with the 32PTH1 DSC were presented in [B4.22], Appendix U, Section U.4.5 and [B4.23], Appendix T, Section T.4.5.6 using Thermal Desktop, SINDA/FLUINT and ANSYS computer codes, respectively. The ANSYS model of the OS200FC TC is used in this section to evaluate the thermal performance.

Based on the methodology described in [B4.23], Appendix T, Section T.4.5.6, two finite element models are developed using ANSYS [B4.26] to analyze the thermal performance of the OS200FC TC with the 32PTH2 DSC.

- For the OS200FC TC model without air circulation, which includes the accident conditions, a half-symmetric 3D thermal model is used to analyze the thermal performance for steady-state and transient operations. This model is described in Section B.4.5.3.2.

- For the OS200FC TC model with air circulation, a steady state thermal evaluation is performed using two sequential models. First a flow rate model is used to determine the air mass flow rate through the TC/DSC annulus and then a half-symmetric 3D model of the TC is used to determine the maximum component temperatures. These models are described in Section B.4.5.3.1 and B.4.5.3.2, respectively.

The OS200FC TC model with air circulation is used for Load Case T8 (Off-Normal Hot, Steady-State, Air Circulation) with the maximum heat load of 37.2 kW as listed in Table B.4.5-1.

The following steps are taken to determine the maximum steady state temperatures of the 32PTH2 DSC and OS200FC TC components with the air circulation using ANSYS:

1. Assume a temperature difference (ΔT_{air}) between the air temperature entering the cooling system (T_{amb}) and the air temperature exiting the slotted cask lid (T_{exit}) for initial run, Calculate T_{exit} and T_{avg} based on the initial guess and the air properties based on T_{avg}.

   Where,
   $T_{exit} = T_{amb} + \Delta T_{air}$
   $T_{avg} = (T_{amb} + T_{exit})/2$

2. Run Flow Rate Model described in Section B.4.5.3.1 iteratively based on average properties of air calculated in Step 1 to compute the air mass flow rate in each TC/DSC annulus segment.

3. Determine the heat transfer coefficients within the annulus based on the mass flow rates computed in Step 2 for the 37.2 kW load case. The equations to calculate these heat transfer coefficients are described in Section B.4.5.3.2.1.

4. Run OS200FC TC Thermal Model for 37.2 kW based on mass flow rates and heat transfer coefficients calculated in Step 2 and Step 3.

5. Calculate T_{exit}, T_{avg}, and ΔT_{air} based on results from OS200FC TC Thermal Model in Step 4.

6. If difference between assumed ΔT_{air} in Step 1 and calculated ΔT_{air} in Step 5 is less than 1°F, stop iterations, otherwise proceed to Step 7.

7. Rerun the Flow Rate Model described in Section B.4.5.3.1 with air properties based on T_{avg} from Step 5.

8. If differences between air mass flow rates in each TC/DSC annulus segment from Step 7 and Step 2 are less than 0.1 lbm/hr, stop iterations, otherwise proceed to Step 9.

9. Repeat Steps 4 to 9 until the solution converges.

B.4.5.3.1 Flow Rate Model Description

The flow rate model is used only for Load Case T8 (Off-Normal Hot, Steady-State, Air Circulation) listed in Table B.4.5-1 as noted in Section B.4.5.3.

The air from the blowers enters the TC from the ram access opening and the airflow turns and enters the ten (10) flow paths formed by the 1.0" thick wedge segments welded to the OS200FC TC's bottom. After the air exits from the flow paths formed by the wedge segments, the airflow turns and flows in the annulus between the 32PTH2 DSC and the OS200FC TC's inner liner. Given that the gap between the 32PTH2 DSC and OS200FC TC varies with circumferential position, plus variances in the heating of the air, the airflow will distribute itself around the circumference of the TC/DSC inner liner, until an equal pressure drop is achieved everywhere.

For the purposes of this calculation, each half of the annulus is divided into 19 angular segments with 0° at the top of the normally horizontal OS200FC TC and 180° at the bottom. The mass flow rate along each of the 19 angular segments is calculated using the Flow Rate Model. The mass flow rates obtained from this model are used as input to the thermal model of the TC/DSC described in Section B.4.5.3.2.

Since the outer diameter of the 32PTH2 DSC (69.75") is the same as the outer diameter of the 32PTH1 DSC evaluated in [B4.23], Appendix T, Section T.4.5.6.2 and since the OS200FC TC remains the same, flow area and hydraulic diameters calculated for the 32PTH1 DSC in OS200FC TC remain valid for the current calculation and the same values are used. The flow area, and hydraulic diameter, and friction factors for the 19 angular segments are shown in [B4.23], Appendix T, Section T.4.5.6.2.

The flow rate model consists of ANSYS FLUID116 elements each representing one of the angular segments of the TC/DSC annulus region. The flow areas, hydraulic diameters, and friction factors calculated for the 19 annular segments are applied using the same methodology as described in [B4.23], Appendix T, Section T.4.5.6.2. The final air exit temperature is determined iteratively through the steps described in Section B.4.5.3.

The air introduced into the annular gap between the 32PTH2 DSC and the OS200FC TC distributes itself based upon the flow area and hydraulic diameter. The Flow Rate Model computes the air flow rate in each annular segment based on achieving an equal pressure drop over any segments of the annulus. The Flow Rate Model for determining the mass flow rates is shown in Figure B.4.5-1.

The mass flow rates obtained for each of the 19 annular segments for use in the OS200FC TC thermal model along with the hydraulic diameters and flow areas are presented in Table B.4.5-2 for the 37.2 kW load case.

B.4.5.3.2 OS200FC TC Model Description

The half-symmetric, three-dimensional finite element model of OS200FC TC loaded with 32PTH1 DSC simulating air circulation described in [B4.23], Appendix T, Section T.4.5.6 is modified to consider the dimensions of the 32PTH2 DSC in the OS200FC TC. The model contains the cask shells, cask bottom plate, cask lid, DSC shell, and DSC end plates with a homogenized basket assembly. The OS200FC TC model with 32PTH2 DSC is shown in Figure B.4.5-2 and Figure B.4.5-3.

SOLID70 elements are used to model the components, including the gaseous gaps. SURF152 surface elements are used for applying the insolation boundary conditions. Radiation along the gap between the DSC and TC inner liner is modeled using the AUX12 processor with SHELL57 elements used to compute the form factors.

Decay heat load is applied as a uniform volumetric heat generated throughout the homogenized region of the basket assembly. The homogenized basket assembly is centered axially in the 32PTH2 DSC. A uniform gap of 0.75" is considered between the homogenized basket assembly and the top/bottom ends of the 32PTH2 DSC. This assumption reduces the axial heat transfer and maximizes the DSC shell temperature, which in turn results in higher fuel cladding temperature. The volumetric heat generation rate is calculated as:

$$q''' = \frac{Q}{\pi (D_i / 2)^2 L_b}$$

q''' = Volumetric heat generation rate (Btu/hr-in^3)
Q = decay heat load (Btu/hr) (to convert from kW multiply by 3412.3)
D_i = 32PTH2 DSC inner diameter (in)
L_b = Length of basket assembly (in)

The applied decay heat values in the model are listed below.

Heat Load (kW)	Heat Load (Btu/hr)	D_i (in)	L_b (in)	Volumetric Heat Generation (Btu/hr-in^3)
37.2	126938	68.5	177.15	0.1944
32.0	109194			0.1673
31.2	106464			0.1631

The insolation is applied as a heat flux over the OS200FC TC outer surfaces using average insolation values from 10 CFR 71.71 [B4.2]. The insolation values are averaged over 24 hours and multiplied by the surface absorptivity factor to calculate the solar heat flux. The solar heat flux values used in the OS200FC TC model are summarized below.

Surface Material	Shape	Insolance over 12 hrs [B4.2] (gcal/cm^2)	Solar Absorptivity(1)	Total solar heat flux averaged over 24 hrs (Btu/hr-in^2)
Stainless Steel	Curved	400	0.587 (2)	0.250
	Flat vertical	200	0.587 (2)	0.125

(1) See Section B.4.2(r) for surface properties.
(2) Solar absorptivity of stainless steel is taken equal to its emissivity.

Convection and radiation heat transfer from the OS200FC TC outer surfaces are combined together as total heat transfer coefficients. The total heat transfer coefficients are calculated using free convection correlations from Rohsenow Handbook [B4.11] and are incorporated in the model using ANSYS macros.

The typical boundary conditions applied on the OS200FC TC model are shown in Figure B.4.5-4.

During transfer, when the OS200FC TC is in a horizontal orientation, the 32PTH2 DSC shell rests on two rails in the OS200FC TC. These rails are flat stainless steel plates welded to the inner shell of the TC. The thickness of the rail is 0.12". Considering an angle of 12° between the lower and vertical plane, the dimensions of the rail, the 32PTH2 DSC and inner OS200FC TC diameter, the center line of the 32PTH2 DSC is shifted down within the OS200FC TC cavity by 0.26". The eccentric location of the 32PTH2 DSC within the TC cavity is accounted for in the model considering the above shift. The thermal resistance between the 32PTH2 DSC and the OS200FC TC rails is assumed to be approximately 2.7 Btu/hr-in^2-°F identical to that used in the TC model described in [B4.22], Appendix U, Section U.4.5.2.

During loading operations, the water level in the TC/DSC annulus is maintained 12" below the 32PTH2 DSC top and is open to atmospheric pressure until the 32PTH2 DSC is sealed. The water level in the annulus will be observed and replenished. These operational requirements prevent annulus water from approaching boiling temperature and assure that the DSC shell temperature does not exceed the boiling temperature of water. Therefore, a conservative DSC shell temperature of 212°F is used for establishing the initial conditions for the transient analyses in the OS200FC TC when the TC is in the vertical orientation and the TC/DSC annulus is filled with water (see Load Cases T11 and T12 listed in Table B.4.5-1) for initial conditions with 37.2 and 32.0 kW decay heat loads.

Due to differences between the heat loads considered for 32PTH1 DSC and 32PTH2 DSC, the effective properties for the neutron shield segments are modified iteratively to accurately capture the temperature gradients across each of the 19 neutron shield segments in the axial direction. Calculation of the effective properties for the neutron shield segments is described in Section B.4.5.3.3.

B.4.5.3.2.1 OS200FC TC Model with Air Circulation

Air circulation through the annulus of the TC/DSC is modeled using the FLUID116 and LINK34 elements. The FLUID116 elements model the air flow along the axial length of the TC/DSC annulus by conducting heat and transmitting the fluid between its nodes, whereas the LINK34 elements model the convection from the TC/DSC surfaces due to the air flow. The FLUID116 elements are modeled such that they are connected to the LINK34 convection elements.

Air circulation is conservatively omitted and air conduction only is assumed in the region between the TC support rails (i.e., approximately 150° to 180°) due to the narrowness of the gap between the 32PTH2 DSC and the TC inner liner. The mass flow rates obtained from the Flow Rate Model described in Section B.4.5.3.1 for each of the annular segments from 0° to 150° are applied to the FLUID116 elements using the "SFE,,,hflux" command.

Based on the mass flow rates obtained for each of the annular segments from 0° to 150°, the convection heat transfer coefficients for the TC/DSC annulus are computed using the correlations for flow within ducts and pipes. The convection heat transfer coefficients are computed as a function of the local hydraulic diameter, the Reynolds number, and the thermophysical properties of air. These convection heat transfer coefficients are applied to the LINK34 elements using the mpdata,hf/mp,hf commands.

The correlations for the convection coefficients are identical to those used in the thermal analysis of the OS200FC TC with a 32PTH1 DSC in [B4.22], Appendix U, Section U.4.5 and [B4.23], Appendix T, Section T.4.5.6 and are taken from equations 7, 43, 44, 45, 57, and 57a in Chapter 7 of [B4.12].

Based on the above correlations and the mass flow rates shown in Table B.4.5-2, the heat transfer coefficients for the annular segments from 0° to 150° are calculated and are presented in Table B.4.5-3 considering 37.2 kW heat load for Load Case T8. As noted before, the convection through air circulation is omitted conservatively for the annular segments from approximately 150° to 180°, which are located between the TC support rails.

The ANSYS model of the OS200FC TC with air circulation is used only for Load Case T8 as listed in Table B.4.5-1.

B.4.5.3.2.2 OS200FC TC Model without Air Circulation

For the thermal analysis of the OS200FC TC with 32PTH2 DSC and without air circulation, the LINK34 and FLUID 116 elements are removed from the model described in Section B.4.5.3.2.1 for both the steady-state and transient analyses. This ANSYS model is used for all load cases listed in Table B.4.5-1 except Load Case T8.

B.4.5.3.3 Effective Neutron Shield Properties

The neutron shield panel consists of a cylindrical shell welded to the TC structural shell and supported by 18 rings. Each of the 16 inner supporting rings has seven holes to allow filling and draining of water in or out of the panel. The water in the neutron shield panel is modeled as 17 individual, cylindrical segments using SOLID70 elements as shown in Figure B.4.5-2.

Effective conductivities are calculated for individual segments based on the methodology described in [B4.30], Chapter 4, Section 4.9.1 to model the combination of the conduction and convection heat transfer through the water contained in the shielding panel for normal/off-normal transfer operations for radial direction. The conductivity of water is considered for the neutron shield panels in the axial direction.

The radial effective conductivity in each segment depends primarily on the temperature gradient across the panel between the structural shell and the neutron shield shell. An average temperature gradient is assumed to calculate the effective conductivity for the water contained in each segment. The assumed average temperature gradient is verified iteratively by computing the temperature difference across each segment of the neutron shield based on the results of the analysis model. Considering that the average temperature gradient across one panel segment is limited to less than 10°F, based on the discussion in [B4.22], Appendix U, Section U.4.5.4.3, the angular variation of the Nusselt number inside the panel does not have a significant effect on the maximum TC component temperatures.

Similarly for accident conditions, effective conductivities are also calculated based on the methodology described in [B4.30], Chapter 4, Section 4.9.1 to model the combination of the conduction, convection and radiation heat transfer through the air contained in the shielding panel.

The neutron shielding effective conductivities are calculated for a heat load of 32 kW and are used for thermal evaluations with higher heat loads. The temperature differences across the neutron shield will increase with higher heat loads, thereby increasing the effective thermal conductivity. Therefore, ignoring these higher effective conductivity values is conservative when determining the thermal performance of the OS200FC TC at heat loads greater than 32 kW. The neutron shielding effective conductivities determined for a heat load of 32 kW are used for the lower heat load of 31.2 kW. The small difference between the heat loads is considered to have an insignificant effect on the maximum temperatures of the OS200FC TC components and DSC shell temperature distributions.

For the OS200FC TC with 32PTH2 DSC and with air circulation, the heat dissipated from the 32PTH2 DSC is removed primarily via air circulation, thereby decreasing the temperature gradient and hence effective conductivities across the neutron shield. Since a large amount of the heat load is removed via air circulation, the decline in neutron shield effective conductivity is considered to have an insignificant effect on the maximum fuel cladding temperature for this condition.

B.4.5.4 OS200FC TC Thermal Analysis Results

Due to the high decay heat loads considered for the NUHOMS® 32PTH2 system, certain time limits are applicable to the transfer operations under normal and off-normal conditions. The time limits are established in conjunction with the thermal analysis of the 32PTH2 DSC described in Section B.4.6 to maintain the fuel cladding temperature and the OS200FC TC components below the allowable limits. An overview of these time limits is provided in Figure B.4.5-10.

The results of the thermal analyses for OS200FC TC under normal, off-normal, and accident conditions are presented in Sections B.4.5.4.1 through B.4.5.4.4. For each condition, the DSC shell temperature profile resulting from the corresponding load case is used to determine the peak fuel cladding and basket assembly component temperatures based on the 32PTH2 DSC thermal model described in Section B.4.6.

B.4.5.4.1 Normal / Off-Normal Transfer Conditions without Air Circulation for Heat Loads ≤ 32.0 kW

The analyses results for vertical loading operations within the fuel building for heat loads ≤ 31.2 kW (HLZC #4) assigned as Load Case T5A and for off-normal transfer conditions for heat loads ≤ 32.0 kW (HLZCs #3 and #4) assigned as Load Case T3 are summarized in Table B.4.5-4. As seen, the maximum temperatures of the OS200FC TC components for these two cases are below the allowable limits.

Figure B.4.5-5 shows the temperature distribution of the OS200FC TC and 32PTH2 DSC shell for steady-state, normal, vertical loading operations within the fuel building with 31.2 kW heat load (Load Case # T5A).

For heat loads > 31.2 and ≤ 32.0 kW (HLZC #3), based on the transient thermal analysis a maximum duration of 75 hours is allowed for the vertical loading operations (Load Case T5) once the water in TC/DSC annulus is drained. Table B.4.5-4 summarizes the maximum temperatures for the OS200FC TC components and shows that the maximum TC component temperatures are below the allowable limits for the duration of 75 hours.

Based on analysis results shown in Table B.4.5-4 for Load Case T3, no time limit is required for the horizontal transfer operation for heat loads > 31.2 kW and ≤ 32.0 kW (HLZC #3). For conservatism, the time limit of 75 hours used for the vertical loading operation is also used for the horizontal transfer operation with heat loads > 31.2 kW and ≤ 32.0 kW (HLZC #3). This conservatism does not apply to horizontal transfer operation for heat loads ≤ 31.2 kW (HLZC #4). Therefore, the transfer operations for heat loads ≤ 31.2 kW (HLZC #4) require no time limit.

B.4.5.4.2 Normal / Off-Normal Transfer Conditions without Air Circulation for Heat Loads > 32.0 kW and ≤ 37.2 kW

For both the normal, hot, vertical transient condition (Load Case T6) and off-normal, hot, transient condition (Load Case # T7), the initial conditions are determined from a steady state analysis of the OS200FC TC with 32PTH2 DSC with 212°F water in the TC/DSC annulus and the TC is in vertical orientation.

For the normal, hot, vertical transient condition (Load Case T6), at time t= 0, the water in the TC/DSC annulus is assumed to be drained, and the TC closure is completed. The TC is assumed to be left inside the fuel building in the vertical position.

For the off-normal, hot transient condition (Load Case T7), at time = 0, the TC/DSC annulus is assumed to be drained, and the TC closure is completed, TC is assumed to be rotated to a horizontal orientation and moved outdoors.

For practical purposes, the time limits for vertical or horizontal transfer operations should be considered after sealing the 32PTH2 DSC when the water in the TC/DSC annulus starts to drain.

Based on the transient thermal analyses a maximum duration of 36 hours is allowed for both the normal, hot, vertical loading operations (Load Case T6) and the off-normal, hot, horizontal transfer operations (Load Case T7). Table B.4.5-5 summarizes the maximum temperatures for the OS200FC TC components and shows that the maximum TC component temperatures are below the allowable limits for duration of 36 hours for these two load cases.

Figure B.4.5-6 shows the temperature distribution of the OS200FC TC and 32PTH2 DSC for transient, off-normal, hot, horizontal transfer conditions (Load Case T7) at 36 hours.

B.4.5.4.3 Normal / Off-Normal Transfer Conditions with Air Circulation for Heat Loads > 32.0 kW and ≤ 37.2 kW

Steady state thermal analysis is performed for the OS200FC TC with 32PTH2 DSC and 37.2 kW heat load with air circulation for off-normal, hot, horizontal transfer conditions (Load Case T8) to demonstrate that the maximum TC component temperatures remain below the allowable limits once the air circulation is activated. Table B.4.5-6 summarizes the maximum temperatures for this load case. The temperature profiles for Load Case T8 are presented in Figure B.4.5-7. The DSC shell temperature profiles resulting from this load case are used to determine the peak fuel cladding and basket assembly component temperatures in a steady-state model of the 32PTH2 DSC described in Section B.4.6.

A transient thermal analysis is performed for the OS200FC TC with 32PTH2 DSC and 37.2 kW heat load without air circulation to analyze the thermal performance of the system if the air circulation is turned off or lost (Load Case T10) to determine the DSC shell temperature profile and the maximum TC component temperatures. This analysis assumes that the transient begins with TC and DSC at steady-state conditions from Load Case T8. At time = 0, the fan airflow is turned off or lost and the system starts to heat up.

Based on the transient thermal analysis a maximum duration of 12 hours is available to complete the transfer of the DSC to the AHSM-HS or to re-establish the air circulation.

Table B.4.5-7 summarizes the maximum temperatures for the OS200FC TC with 32PTH2 DSC and 37.2 kW heat load and shows that the maximum TC component temperatures are below the allowable limits.

As described in Section B.4.5.2, an additional transient analysis is performed to estimate the duration needed for the 32PTH2 DSC to reach the steady-state conditions when the air circulation starts at the end of the time limit for transfer operation. The initial condition for this analysis corresponds to Load Case T7 at 36 hours to bound the hottest expected temperatures during transfer operation before air circulation starts. The amount of time needed to use the air circulation is determined by comparison of the maximum DSC shell from this transient analysis to the maximum DSC shell temperature of 406°F calculated for Load Case T8 (see Table B.4.5-6). Figure B.4.5-8 presents the maximum temperature history of the DSC shell once the air circulation is started at the end of Load Case T7. As seen from Figure B.4.5-8, the maximum DSC shell temperature decreases instantly once the air circulation is started and the maximum

temperature decrease is observed within the first 6 hours after the start of air circulation. After 6 hours, the temperature decrease in the DSC shell temperature due to air circulation is approximately 1°F/hr until 8 hours. The total temperature decrease of the DSC shell from 8 hours to 38 hours is approximately 3°F (0.1°F/hr). Due to small changes after 8 hours, it can be reasonably considered that using air circulation for 8 hours after achieving the time limit of 36 hours will decrease the DSC shell temperature from the hottest condition to the steady state level for the maximum heat load of 37.2 kW and maximum ambient temperature of 117°F.

B.4.5.4.4 Accident Conditions

As noted in Section B.4.5.2, the loss of neutron shield and loss of air circulation is bounding for the fire accident case. The maximum temperatures for the bounding loss of neutron shield and loss of air circulation steady-state accident condition (Load Case T9) are presented in Table B.4.5-8. As seen from Table B.4.5-8, maximum component temperatures are below the allowable limits. Figure B.4.5-9 presents the temperature profiles for the loss of neutron shield and loss of air circulation accident condition for the OS200FC TC with 32PTH2 DSC and 37.2 kW heat load.

B.4.5.5 Evaluation of OS200FC TC Performance

The thermal performance of the OS200FC TC is evaluated under normal, off-normal, and accident conditions of operation as described above and is shown to satisfy all the temperature limits and criteria. The DSC shell temperatures calculated here are used in the DSC basket and fuel cladding models as a boundary condition in Section B.4.6. The results show that all the basket and fuel cladding material temperature limits are also satisfied.

Based on the discussions presented in Sections B.4.5.2 and B.4.5.4, time limits for transfer operations are necessary to maintain the fuel cladding temperature and the OS200FC TC components temperatures below the allowable limits. Figure B.4.5-10 presents an overview of the transfer operations for OS200FC TC with 32PTH2 DSC.

Table B.4.5-1
Design Load Cases for 32PTH2 DSC in OS200FC TC

Operation	Load Case No.	Condition	Orientation	Model	Heat Load [1] (kW)	T_{amb} [2] (°F)	Airflow (cfm)	Insolation
Transfer	T1 [3]	Normal, Hot	Horizontal	Steady-State	32.0 (HLZC#3)	104	0	Yes
	T2 [3]	Normal, Cold				0		No
	T3	Off-Normal, Hot				117		Yes
	T4 [3]	Off-Normal, Cold				0		No
	T5A	Normal, Hot	Vertical	Steady-State	31.2 (HLZC#4)	120	0	No
	T5			Transient	32.0 (HLZC#3)			
	T6			Transient	37.2 (HLZC#1)			
	T7	Off-Normal, Hot	Horizontal	Transient	37.2 (HLZC#1)	117	0	Yes
	T8	Off-Normal, Hot		Steady-State			450	
	T9	Accident		Steady-State			0	
	T10 [4]	Off-Normal, Hot		Transient			0	
	T11	Normal, Hot	Vertical	Steady-State (Initial Conditions)[5]	37.2 (HLZC#1)	120	0	No
	T12				32.0 (HLZC#3)			

(1) The four heat load zone configurations (HLZCs) are described in Chapter B.2, Figures B.2.1-1.

(2) The maximum ambient temperature of 104°F corresponds to a daily average temperature of 97°F and the maximum ambient temperature of 117°F corresponds to a daily average temperature of 107°F, as shown in Chapter 4, Section 4.1.2 and shown in Table 4.1-1 and Table 4.1-2. No averaging is considered for the ambient temperature of 120°F inside the fuel building.

(3) Load cases T1, T2 and T4 are bounded by Load Case T3 (see Section B.4.5.2 for justification).

(4) Initial temperatures for this load case are taken from steady-state results of Load Case T8. At time t=0, the air circulation is assumed to be turned off or lost and the system begins to heat up.

(5) Initial steady-state conditions are determined assuming water in the TC/DSC annulus and a 120°F ambient temperature within the fuel building. The initial conditions determined from Load Case T11 are used for transient operations with 37.2 kW decay heat load (Load Cases T6 and T7) and initial conditions determined from Load Case T12 are used for transient operations with 32.0 kW decay heat load (Load Case T5). At time t=0 for the transient runs (Load Cases T5, T6, and T7), the water in the TC/DSC annulus is assumed to be immediately drained and the system begins to heat up. Time limits are considered for Load Cases T5, T6 and T7 to maintain the fuel cladding temperature below the allowable limit in [B4.3].

Table B.4.5-2
Mass Flow Rates Along Each Annular Segment

Section	Mass flow (lb_m/hr)	Hydraulic Diameter (in)	Flow Area (in^2)
1	99.00	1.27	3.84
2	98.00	1.26	3.82
3	95.02	1.24	3.75
4	90.17	1.20	3.63
5	83.20	1.15	3.48
6	75.09	1.09	3.29
7	66.27	1.01	3.07
8	57.07	0.93	2.82
9	48.13	0.84	2.56
10	39.72	0.75	2.28
11	31.40	0.66	2.01
12	24.30	0.57	1.74
13	18.33	0.49	1.49
14	13.67	0.41	1.27
15	10.02	0.35	1.07
16	7.45	0.30	0.91
17	5.74	0.26	0.80
18	4.78	0.24	0.72
19	4.48	0.23	0.70

Table B.4.5-3
Heat Transfer Coefficients in the TC/DSC Annulus for Air Circulation
(37.2 kW Load Case)

Heat Transfer Coefficients (Btu/hr-in^2-°F)						
Temperature (°F)	**Wedge[1]**	**Section 1**	**Section 2**	**Section 3**	**Section 4**	**Section 5**
111	0.004	0.027	0.027	0.027	0.026	0.026
211		0.028	0.028	0.028	0.027	0.027
311		0.029	0.029	0.028	0.028	0.027
411		0.029	0.029	0.029	0.029	0.028
511		0.030	0.030	0.030	0.029	0.028

Heat Transfer Coefficients (Btu/hr-in^2-°F)						
Temperature (°F)	**Section 6**	**Section 7**	**Section 8**	**Section 9**	**Section 10**	**Section 11**
111	0.025	0.024	0.023	0.022	0.020	0.009
211	0.026	0.025	0.023	0.022	0.009	0.010
311	0.026	0.025	0.024	0.022	0.010	0.011
411	0.027	0.026	0.024	0.010	0.011	0.012
511	0.027	0.026	0.024	0.011	0.011	0.012

Heat Transfer Coefficients (Btu/hr-in^2-°F)					
Temperature (°F)	**Section 12**	**Section 13**	**Section 14**	**Section 15**	**Exit at Top Lid [1]**
111	0.009	0.011	0.012	0.014	0.016
211	0.011	0.012	0.014	0.016	
311	0.012	0.013	0.015	0.018	
411	0.013	0.015	0.017	0.020	
511	0.014	0.016	0.018	0.021	

(1) The lowest heat transfer coefficient is used for the wedge and exit at top for conservatism.

Table B.4.5-4
Maximum Temperatures of OS200FC TC with 32PTH2 DSC ≤ 32.0 kW, Without Air Circulation

	Normal Hot, Vertical Steady-State Load Case T5A	Normal Hot, Vertical Transient Load Case T5	Off-Normal Hot, Horizontal Steady-State Load Case T3	Max. Allowable (°F)
Heat Load	31.2 kW	32.0 kW	32.0 kW	
Time	No time limit	75 hrs	No time limit[3]	
Component	**T_{max} (°F)**	**T_{max} (°F)**	**T_{max} (°F)**	
DSC Shell	466	448	473	---
Inner Liner	314	297	336	---
Gamma Shield	312	295	330	620 [B4.13]
Structural Shell	273	258	278	---
Neutron Shield, Max. / Avg.	269/258	254 / 242	273 / 251	-- / 290 [2]
Neutron Shield Outer Skin	259	245	261	---
Bulk Average NS-3	277	251	200	250 / 300 [1]
Closure Lid	293	253	237	---
Top Forging	277	255	292	---
Bottom Forging	296	263	252	---

(1) For NS-3, 250°F is the temperature limit for long-term operations and 300°F is the temperature limit for short-term normal operations like vertical loading.

(2) Bulk average temperature of water in the neutron shield is limited by the 45 psig pressure relief valves on the shield. The equivalent steam saturation temperature at this pressure is approximately 290°F.

(3) Although Load Case T3 is analyzed for steady-state conditions, a time limit of 75 hours is selected for transfer operations of the 32PTH2 DSC in the OS200FC TC with heat loads > 31.2 kW and ≤ 32.0 kW (HLZC #3) for conservatism.

Table B.4.5-5
Maximum Temperatures of OS200FC TC with 32PTH2 DSC @ 37.2 kW, Without Air Circulation

	Normal Hot, Vertical Transient Load Case T6	Off-Normal Hot, Horizontal Transient Load Case T7	Max. Allowable (°F)
Time	36 hrs	36 hrs	
Component	T_{max} (°F)	T_{max} (°F)	
DSC Shell	440	448	---
Inner Liner	283	312	---
Gamma Shield	281	305	620 [B4.13]
Structural Shell	243	254	---
Neutron Shield, Max. / Avg.	240 / 227	249 / 226	-- / 290 (2)
Neutron Shield Outer Skin	231	239	---
Bulk Average NS-3	226	181	250 / 300 (1)
Closure Lid	223	212	---
Top Forging	236	259	---
Bottom Forging	233	225	---

(1) For NS-3, 250°F is the temperature limit for long-term operations and 300°F is the temperature limit for short-term normal operations like vertical loading.

(2) Bulk average temperature of water in the neutron shield is limited by the 45 psig pressure relief valves on the shield. The equivalent steam saturation temperature at this pressure is approximately 290°F.

Table B.4.5-6
Maximum Temperatures of OS200FC TC with 32PTH2 DSC @ 37.2 kW, With Air Circulation

	Off-Normal Hot, Horizontal, Steady-State with Air Circulation Load Case T8	Max. Allowable (°F)
Time	No time limit	
Component	**T_{max} (°F)**	
DSC Shell	406	---
Inner Liner	330	---
Gamma Shield	324	620 [B4.13]
Structural Shell	273	---
Neutron Shield, Max. / Avg.	268 / 227	-- / 290 (2)
Neutron Shield Outer Skin	257	---
Air, Inlet / Exit	107 / 293	---
Bulk Average NS-3	192	250 / 300 (1)
Closure Lid	252	---
Top Forging	288	---
Bottom Forging	215	---

(1) For NS-3, 250°F is the temperature limit for long-term operations and 300°F is the temperature limit for short-term normal operations like vertical loading.

(2) Bulk average temperature of water in the neutron shield is limited by the 45 psig pressure relief valves on the shield. The equivalent steam saturation temperature at this pressure is approximately 290°F.

Table B.4.5-7
Maximum Temperatures of OS200FC TC with 32PTH2 DSC @ 37.2 kW,
Air Circulation Turned Off / Air Circulation Failure during Transfer Operations

	Air Circulation turned-off or Air Circulation failure during transfer operation Load Case T10	Max. Allowable (°F)
Time	12 hrs	
Component	**T_{max} (°F)**	
DSC Shell	444	---
Inner Liner	331	---
Gamma Shield	325	620 [B4.13]
Structural Shell	273	---
Neutron Shield, Max. / Avg.	268 / 231	-- / 290 (2)
Neutron Shield Outer Skin	257	---
Bulk Average NS-3	185	250 / 300 (1)
Closure Lid	234	---
Top Forging	287	---
Bottom Forging	220	---

(1) For NS-3, 250°F is the temperature limit for long-term operations and 300°F is the temperature limit for short-term normal operations like vertical loading.

(2) Bulk average temperature of water in the neutron shield is limited by the 45 psig pressure relief valves on the shield. The equivalent steam saturation temperature at this pressure is approximately 290°F.

Table B.4.5-8
Maximum Temperatures of OS200FC TC with 32PTH2 DSC @ 37.2 kW, Accident Loss of Neutron Shield with Loss of Air Circulation Accident Conditions

	Accident Loss of Neutron Shield with Loss of Air Circulation Load Case T9	Max. Allowable (°F)
Time	No time limit	
Component	**T_{max} (°F)**	
DSC Shell	615	---
Inner Liner	524	---
Gamma Shield	519	620 [B4.13]
Structural Shell	494	---
Neutron Shield, Max. / Avg.	---	---
Neutron Shield Outer Skin	310	---
Bulk Average NS-3	255	1,300 (1)
Closure Lid	320	---
Top Forging	407	---
Bottom Forging	346	---

(1) For NS-3, 1,300°F is the temperature limit for accident conditions as noted in Section B.4.5.

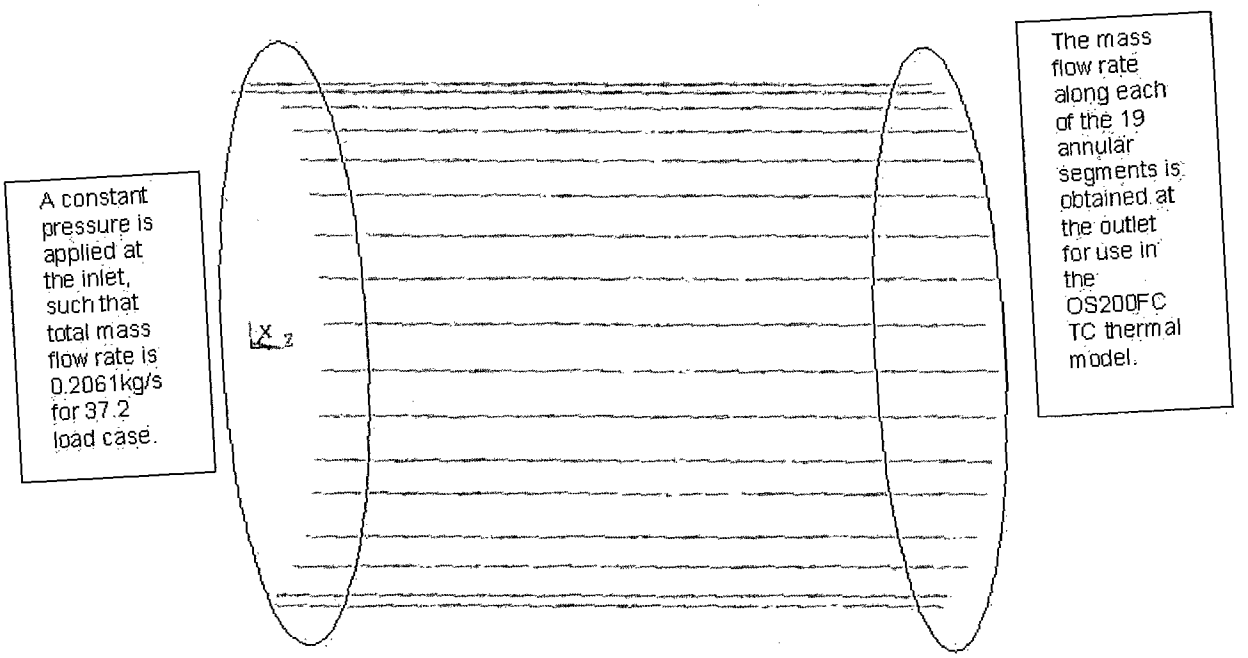

Figure B.4.5-1
Finite Element Mesh of Flow Rate Model with FLUID116 Elements

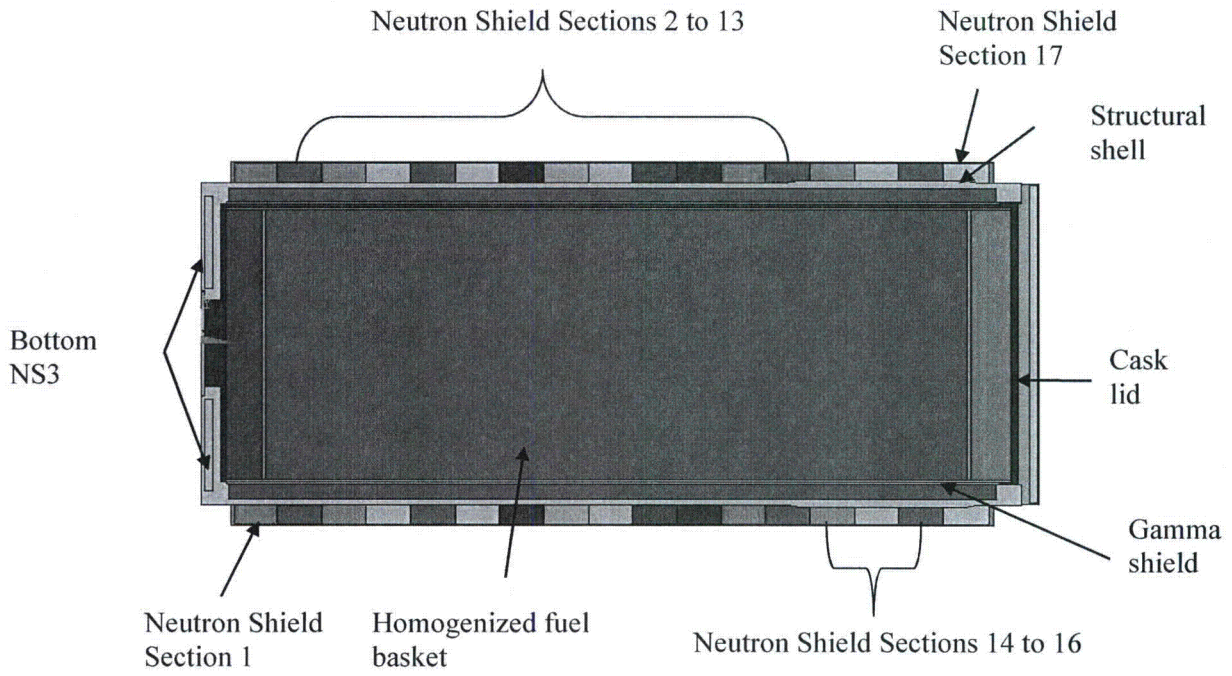

Figure B.4.5-2
Finite Element Model of the OS200FC TC with the 32PTH2 DSC

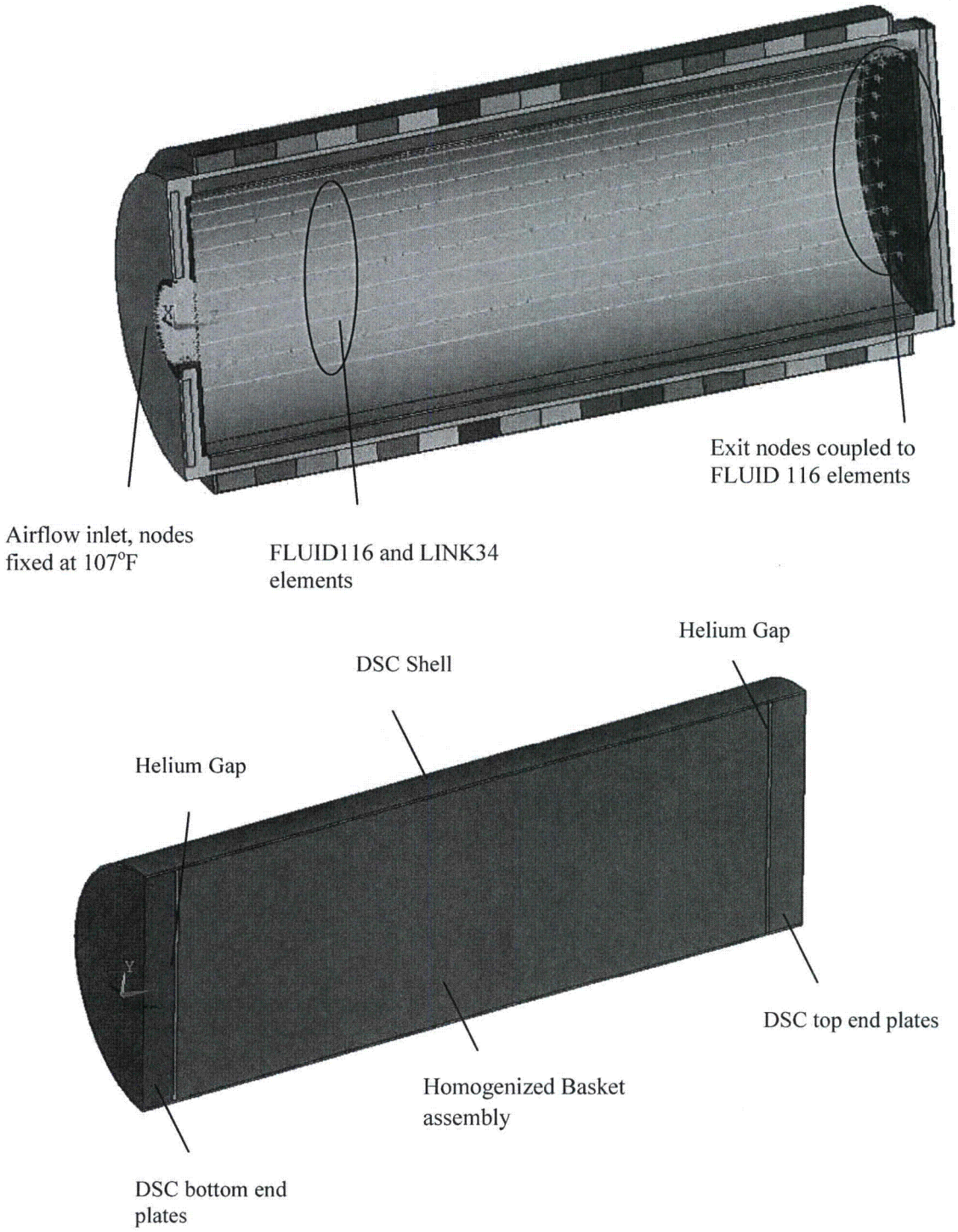

Figure B.4.5-3
OS200FC TC Finite Element Model, Components

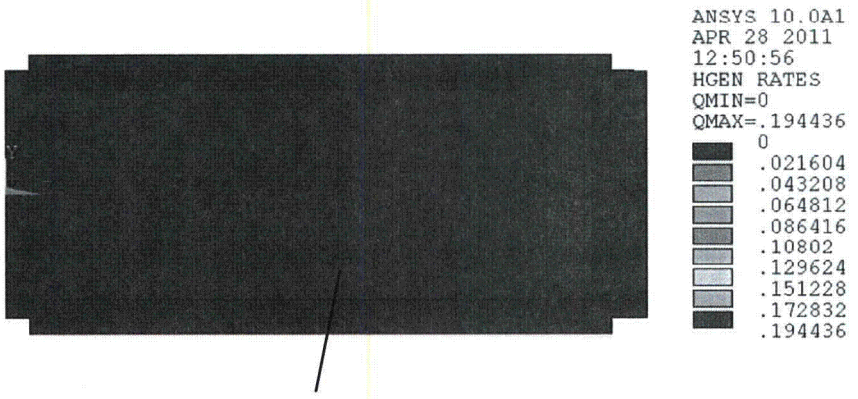

Uniform Volumetric Heat Generation Applied
Throughout Homogenized Basket Region

Insolance boundary
conditions

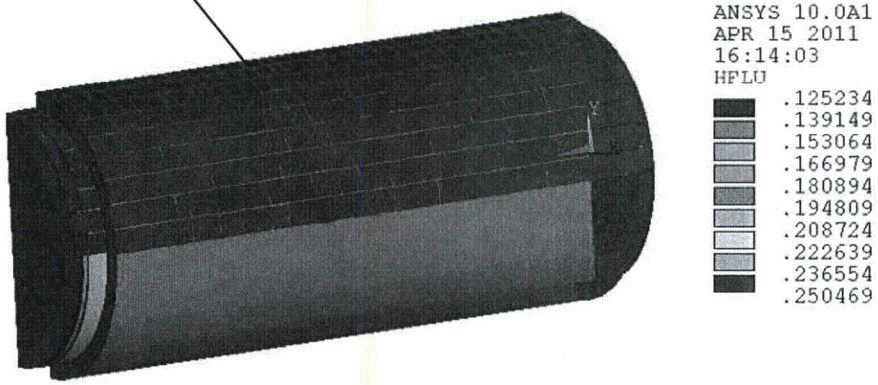

Radiation and convection
boundary conditions

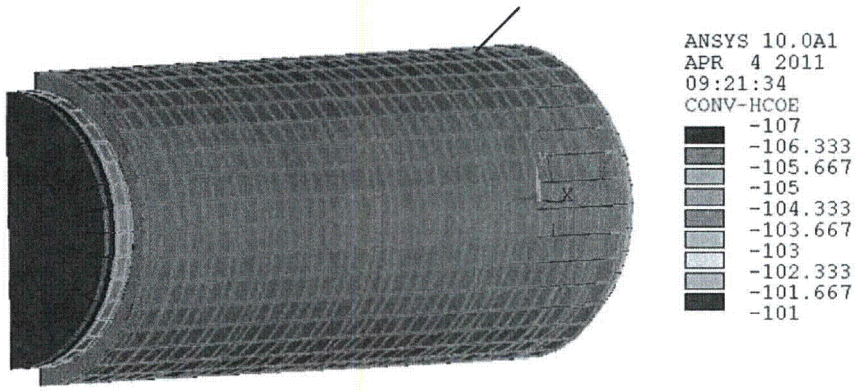

Figure B.4.5-4
OS200FC TC Boundary Conditions

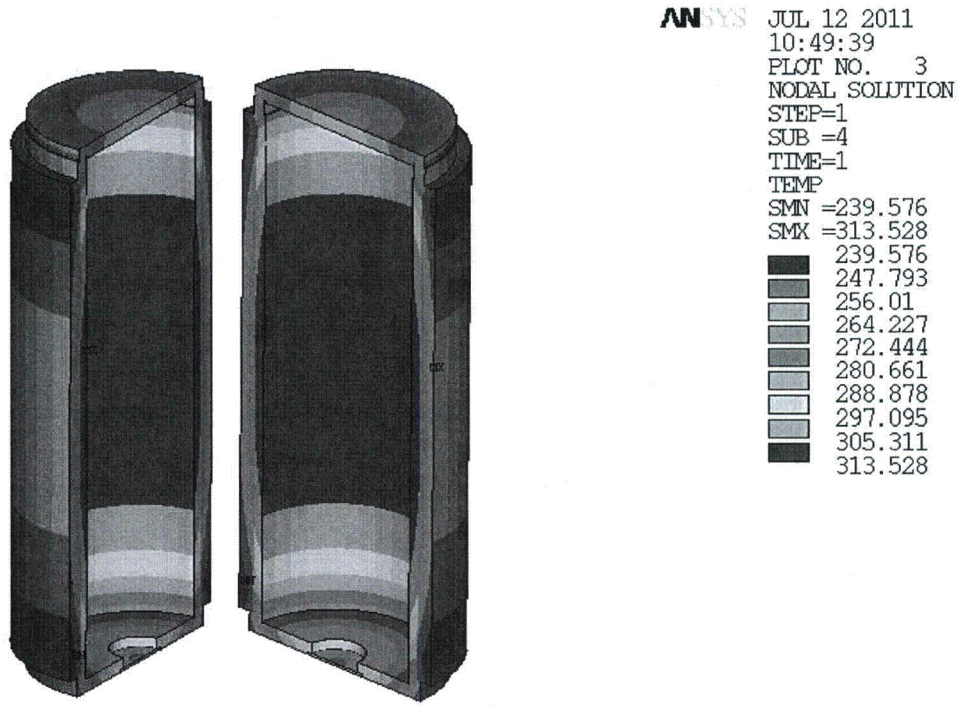

OS200FC TC

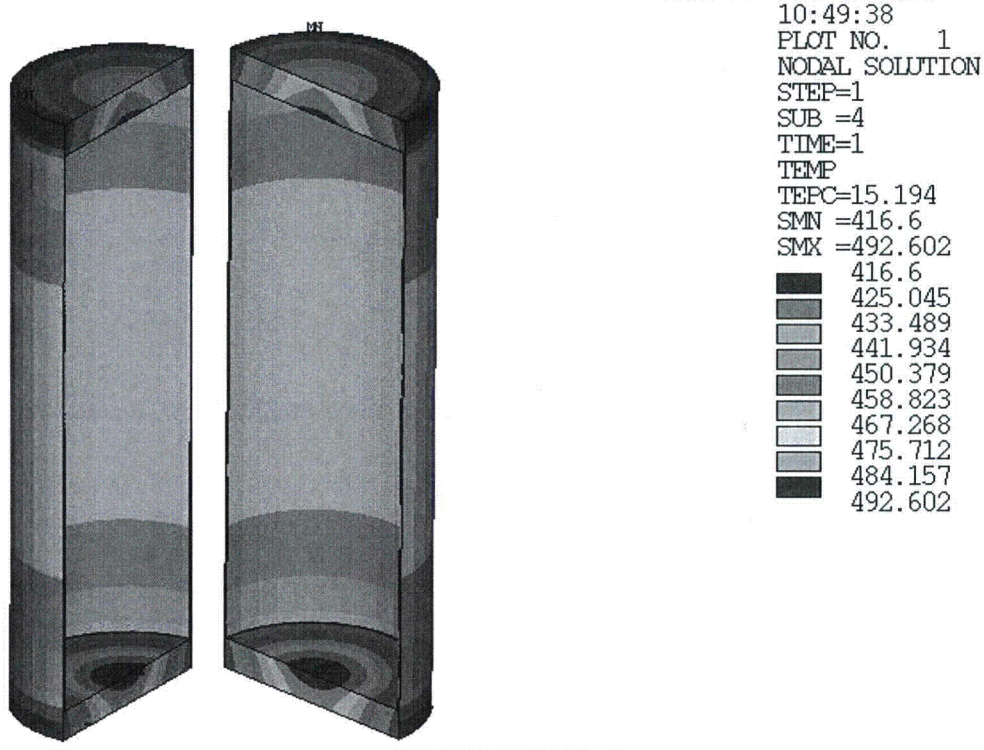

32PTH2 DSC Shell

Figure B.4.5-5
Temperature Distribution for OS200FC TC with 32PTH2 DSC @ 31.2 kW, Normal Hot, Vertical Steady-State (Load Case T5A)

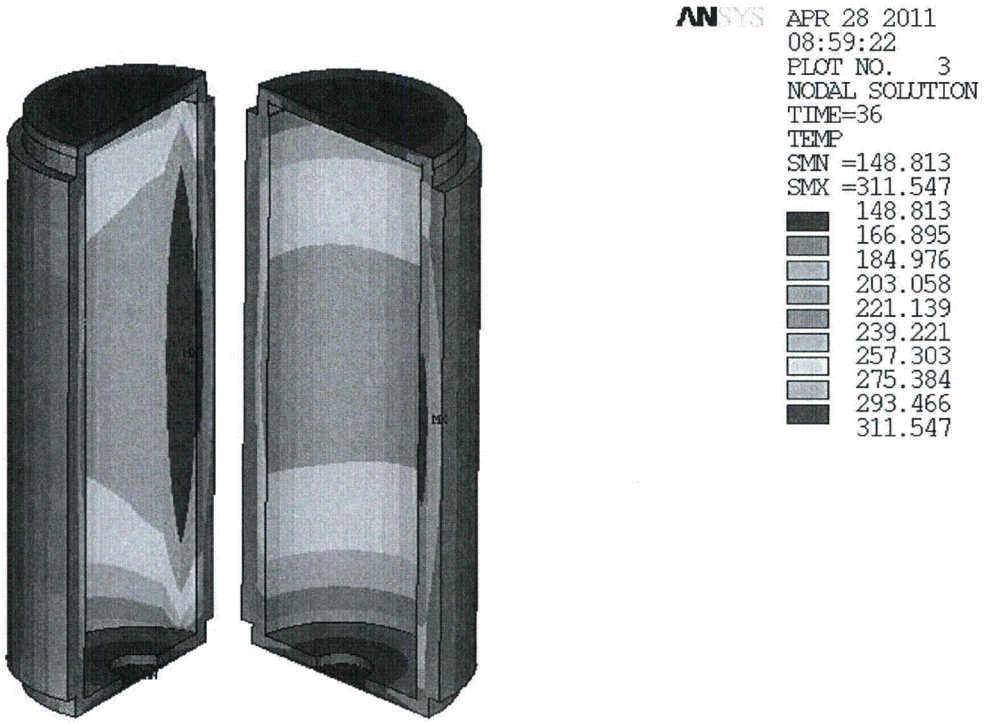

OS200FC TC

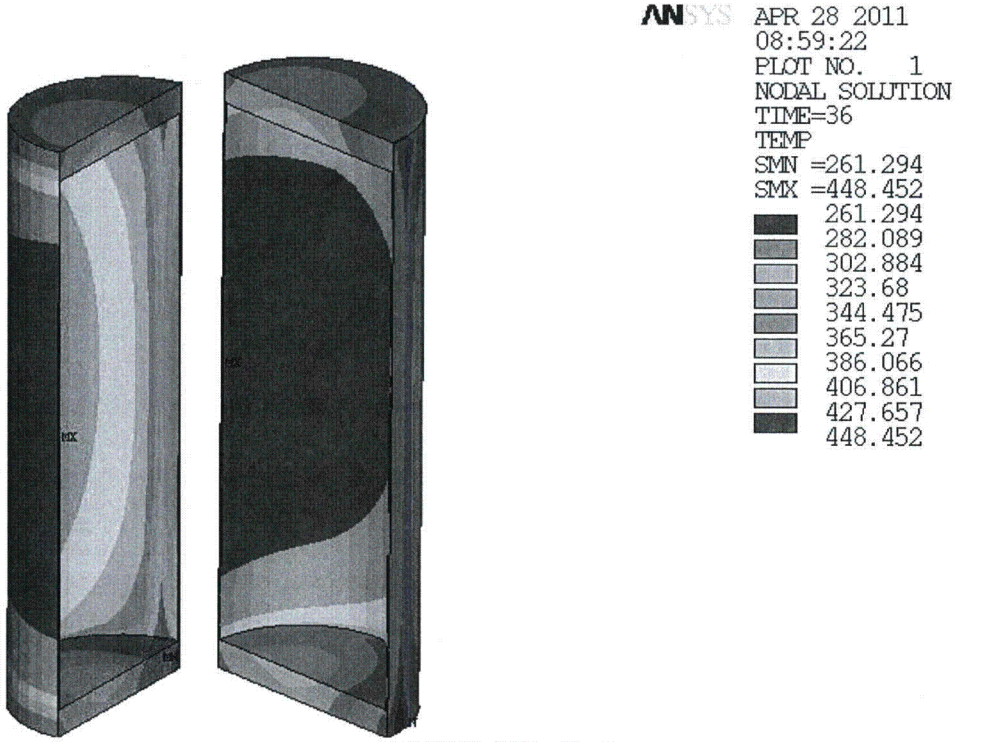

32PTH2 DSC Shell

Figure B.4.5-6
Temperature Distribution for OS200FC TC with 32PTH2 DSC @ 37.2 kW, Without Air Circulation, Off-Normal Hot, Horizontal Transient Operations at 36 hrs (Load Case T7)

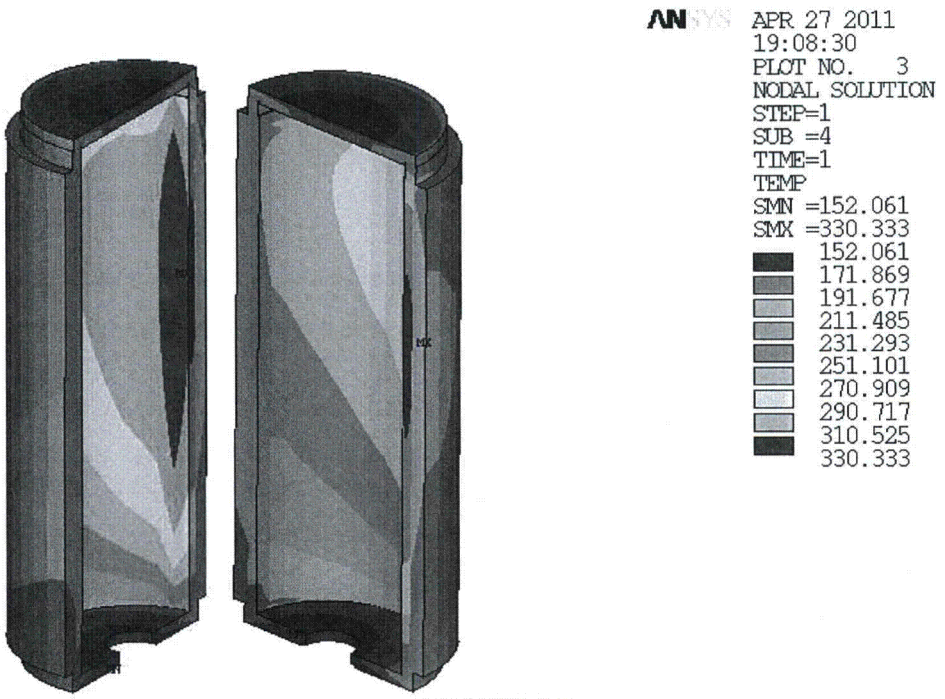

OS200FC TC

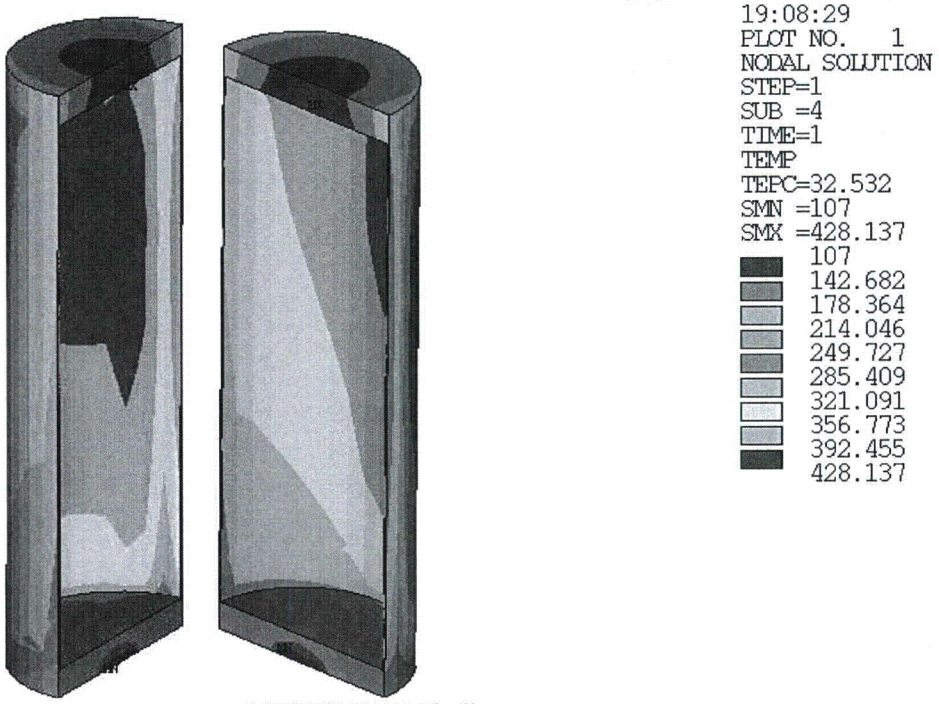

32PTH2 DSC Shell

Figure B.4.5-7
Temperature Distribution for OS200FC TC with 32PTH2 DSC @ 37.2 kW, With Air Circulation, Off-Normal Hot, Horizontal Steady-State Operations (Load Case T8)

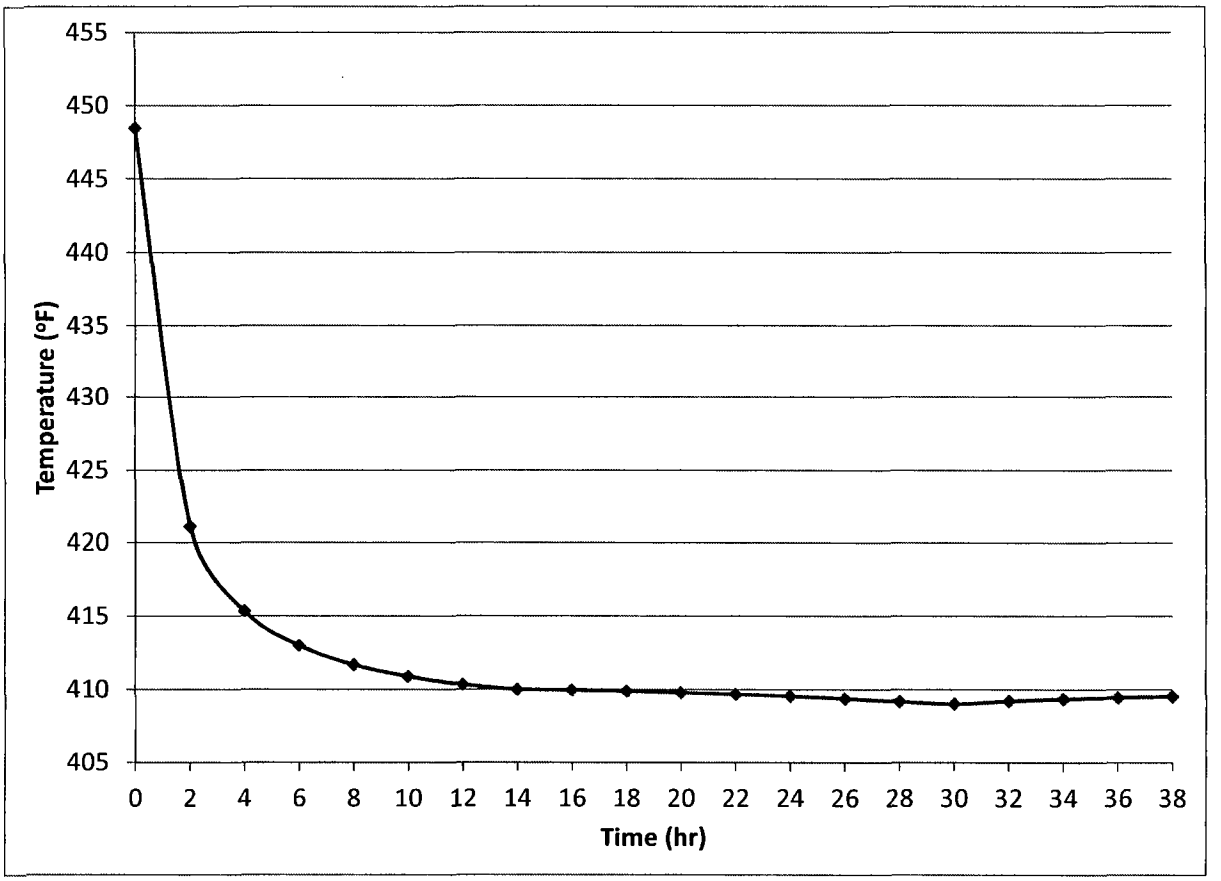

Figure B.4.5-8
Maximum DSC Shell Temperature versus Time with Air Circulation starting at End of Time limit for Load Case T7 with 37.2 kW and 117°F Ambient

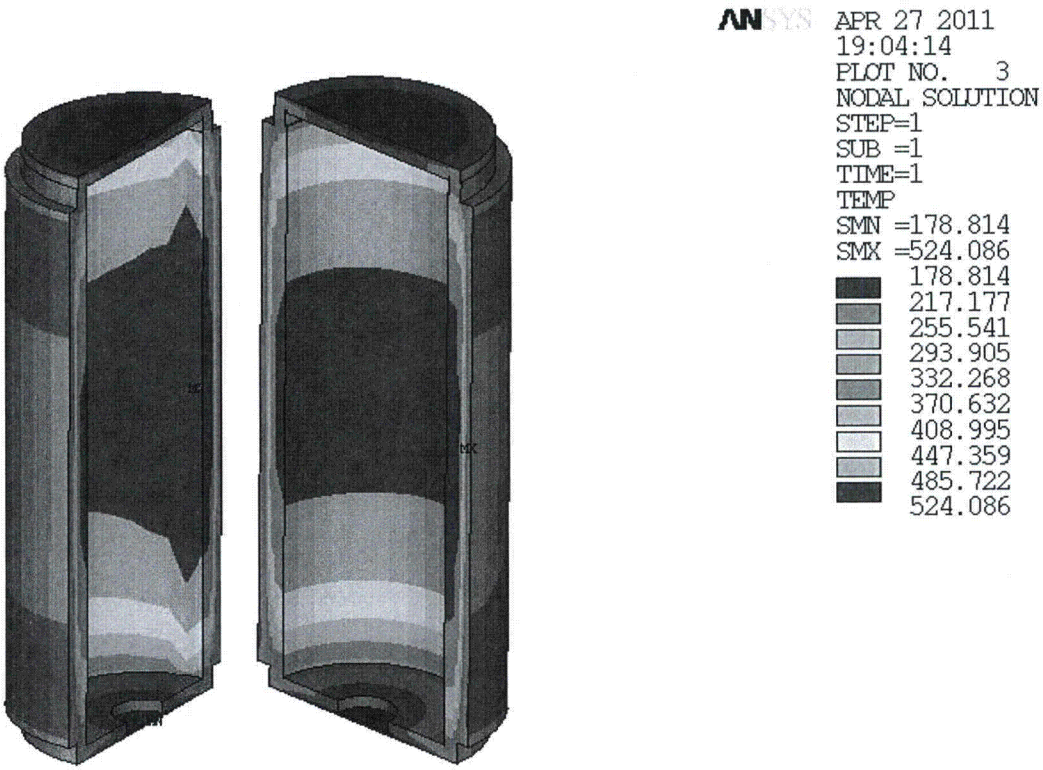

OS200FC TC

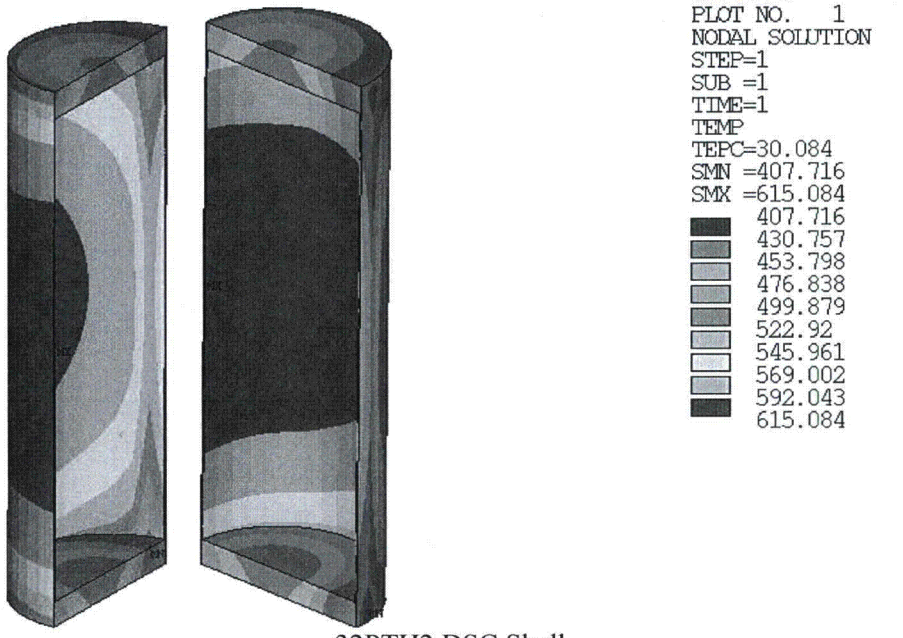

32PTH2 DSC Shell

Figure B.4.5-9
Temperature Distribution for OS200FC TC with 32PTH2 DSC @ 37.2 kW, Accident Loss of Neutron Shield with Loss of Air Circulation Accident Condition, Horizontal (Load Case T9)

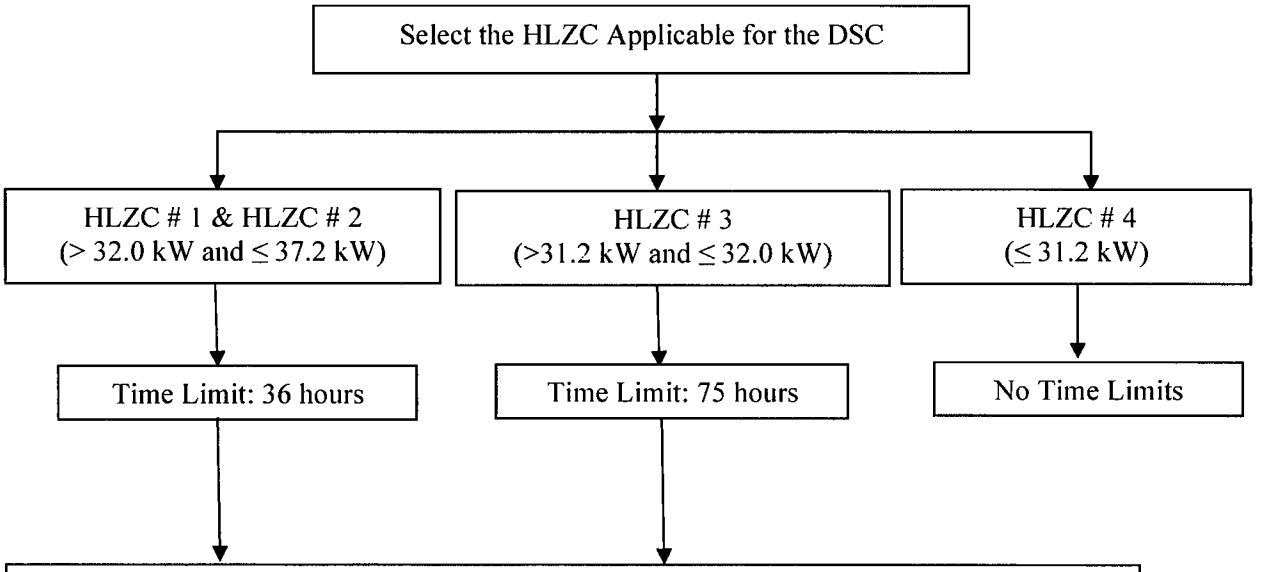

For All Transfer Operations with Time limits

Start of Time Limit: Initiation of Drainage of the TC/DSC Annulus.

End of Time Limit: Complete Insertion of the DSC from the TC to the AHSM-HS.

Corrective Action
If the operation cannot be completed within the time limit noted above, the following corrective actions can be performed:

a. Fill the TC/DSC annulus with water if the TC is in a vertical orientation or
b. Initiate air circulation system if the TC is in a horizontal orientation.

- The time limit specified above can be restarted if the corrective action in Step "a" is completed.
- If the corrective action in Step "b" is performed, a time limit of 12 hours is available once the air circulation system is turned off to complete the insertion of the DSC from the TC to the AHSM-HS.

Figure B.4.5-10
Time Limits for Transfer of 32PTH2 DSC in OS200FC TC

B.4.6 Thermal Evaluation of 32PTH2 DSC

The 32PTH2 DSC is designed to store 32 intact (or up to 16 damaged and remaining intact) fuel assemblies. Up to 16 damaged fuel assemblies (DFA) can be placed in cells located at the outer edge of the 32PTH2 basket assembly (Zone 3) as shown in Chapter B.2, Figures B.2.1-1.

The design of the 32PTH2 DSC is very similar to the 32PTH1 DSC described in [B4.22], Appendix U. The 32PTH1 DSC was evaluated based on a finite element model described in [B4.22], Appendix U, Section U.4.6. Due to similarities between the 32PTH1 and 32PTH2 DSCs, the 32PTH2 DSC is evaluated in this section using the same methodologies used to evaluate the 32PTH1 DSC in [B4.22].

B.4.6.1 Ambient Temperature Specification and Load Cases

The ambient temperatures for storage and transfer conditions are specified in Sections B.4.4.1 and B.4.5.1, respectively.

The load cases considered for evaluation of the NUHOMS® 32PTH2 system for storage and transfer conditions are described in Sections B.4.4.2 and B.4.5.2, respectively.

B.4.6.2 Thermal Analysis of 32PTH2 DSC

The purpose of the 32PTH2 DSC thermal analysis is to determine the maximum temperatures of the fuel cladding and the basket components. As noted in Section B.4.4.3 and B.4.5.3, the DSC shell temperatures determined in the AHSM-HS and OS200FC TC thermal analyses are used as boundary conditions in the 32PTH2 DSC model to evaluate the maximum temperature under normal, off-normal, and accident conditions.

The thermal analysis of the NUHOMS® 32PTH2 DSC is based on a finite element model developed using the ANSYS computer code [B4.26]. The methodology used is identical to that used for the 32PTH1 DSC model described in Appendix U, Section U.4.6.

B.4.6.2.1 Description of the ANSYS Model of 32PTH2 DSC

A three-dimensional model representing the 32PTH2 DSC and basket is developed using ANSYS computer code [B4.26]. This model represents a longitudinally full-length, one-half (180°) cross section of the 32PTH2 DSC as shown in Figure B.4.6-1 through Figure B.4.6-4. The 32PTH2 DSC model comprises the shell assembly (including the shell, top/bottom cover plates, and shield plug plates), the basket assembly (including fuel compartments, aluminum and neutron absorber basket plates, and transition rails) and the homogenized fuel assemblies. All of these DSC components are modeled using SOLID70 elements. The following assumptions are considered for the 32PTH2 DSC model:

- The fuel assemblies contained in the DSC basket are intact fuel assemblies. Since the damaged fuel assemblies are loaded in the outermost fuel compartment cells, they do not affect the maximum temperatures or the maximum temperature gradients in this evaluation. A sensitivity analysis is conducted to capture the effects of the damaged fuel assemblies on

the thermal performance of the 32PTH2 DSC, in which the damaged fuel assemblies become rubble. This sensitivity analysis is discussed in Section B.4.6.8.

- No convection is considered within the canister cavity.

- Only helium conduction is considered from the basket upper surface to the canister top shield plug.

- Radiation is considered only implicitly between the fuel rods and the fuel compartment walls in the calculation of effective fuel conductivity. No other radiation heat exchange is considered within the DSC model.

- Based on fuel assembly characteristics provided in Chapter A.3, Table A.3.5-2, an active fuel length of 150.0 inches is considered for CE 16x16 class fuel assemblies in 32PTH2 DSC. The position of the active fuel in the 32PTH2 DSC model is assumed to begin 4.0 inches from the bottom end of the 32PTH2 DSC cavity. The fuel assembly beyond the active fuel region is modeled as helium. Lower conductivity at fuel assembly ends results in higher maximum fuel cladding temperature and is therefore conservative.

The following gaps are considered in the 32PTH2 DSC model at thermal equilibrium:

Radial Gaps

- A diametrical hot gap of 0.30″ is considered between the basket assembly outer surface and the 32PTH2 DSC shell inner surface (see Figure B.4.6-3). This assumption is justified in Section B.4.6.3.1.

- A diametrical hot gap of 0.30″ is considered between the shield plugs and the 32PTH2 DSC inner surface (see Figure B.4.6-4). The assumed gap is larger than the fabrication cold gap considered between these components and is therefore conservative.

- A total gap of 0.01″ is considered between the stainless steel basket support plates and the fuel compartments in the cross section of the basket assembly. This gap is used in the calculation of the effective thermal conductivity as described in Section B.4.6.5. The basket support plates are welded to the compartment plates. For conservatism, no credit is taken for the weld spots. Instead a uniform gap of 0.01″ is considered between these components, which is similar to a gap between adjacent plates without welds. The gap between adjacent plates is justified in Section B.4.6.3.2.

- A total gap of 0.01″ is considered between the fuel compartment and paired poison/center basket plates. This gap is used in the calculation of the effective thermal conductivity as described in Section B.4.6.5. This gap is larger than the cold gap of 0.005″ in the 32PTH2 basket assembly and is therefore conservative.

- A contact gap of 0.005″ is considered between the fuel compartment and the outer basket support plates / outer basket plates. This gap is used in calculation of the effective thermal conductivity as described in B.4.6.5. The outer basket support plates are welded to the

compartment plates. For conservatism, no credit is taken for the weld spots. Instead a uniform gap of 0.01″ is considered between these components, which is similar to a gap between adjacent plates without welds. The gap between adjacent plates is justified in Section B.4.6.3.2.

- A contact gap of 0.01″ is considered between the outer support basket/outer basket plates and the transition rails (see Figure B.4.6-3). The rails are bolted to the outer basket support plates at multiple locations. For conservatism, no credit is taken for the bolted joints. Instead, a uniform gap of 0.01″ is considered between the rails and the adjacent basket components, which is similar to a gap between adjacent plates without bolts. The gap between adjacent plates is justified in Section B.4.6.3.2.

- A uniform gap of 0.125″ is considered between the various segments of the R90 transition rails in the cross section of the basket assembly (see Figure B.4.6-3). This gap is larger than the fabrication gap and is therefore conservative.

Axial Gaps

- A nominal cold gap of 0.07″ is considered between the support basket plates and the paired poison/center basket plates. In the 32PTH2 DSC ANSYS model, a 0.01″ gap is assumed on the bottom and 0.06″ gap is assumed on the top (see Figure B.4.6-4). These gaps together are equal to the total cold gap and are therefore conservative.

- An axial air gap of 0.01″ representing contact gap is considered between shield plugs and 32PTH2 DSC top/bottom cover plates (see Figure B.4.6-4). This assumption is justified in Section B.4.6.3.2.

- A gap of 0.130″ is considered between the paired poison/center basket plates within the intersecting slots (see Figure B.4.6-4). These gaps are equal to the cold gaps and are therefore conservative.

- An axial gap of 0.49″ between the bottom of the basket assembly and the 32PTH2 DSC inner bottom cover plate, and a gap of 1.01″ between the top of the basket assembly and the 32PTH2 DSC top shield plug plate are considered (see Figure B.4.6-4). Since gaseous conduction is the only heat transfer mechanism considered, these gaps reduce the heat dissipation in the axial direction and increase the heat dissipation in the radial direction. This maximizes the fuel cladding temperature and is therefore conservative.

- The width of the intersection slot within the 32PTH2 outer/center basket plates is 0.75″. However, a width of 1.0″ is assumed in the 32PTH2 DSC model (see Figure B.4.6-4). This is larger than the cold gap and is therefore conservative.

The major component dimensions in the 32PTH2 DSC model are based on nominal sizes of the 32PTH2 DSC and basket assembly. Due to the above conservative assumptions, small dimension differences between the modeling and nominal sizes have an insignificant effect on thermal analysis results.

Decay heat load is applied as heat generation over the elements representing homogenized fuel assemblies.

The heat generation rate used in this analysis is calculated as follows.

$$\dot{q}''' = \left(\frac{q}{a^2 L_a} \times PF \right) \times CF$$

Where,

q = Decay heat load per fuel assembly, kW (Multiply by 3412.3 to convert to Btu/hr),

a = Width of the fuel compartment = 8.65″,

L_a =Active fuel length = 150″,

PF = Peaking Factor (see Section B.4.6.4 for distribution of peaking factor),

CF = correction factor = 1.016 assumed for 32PTH2 DSC (see Section B.4.6.4).

The base heat generation rates used in 32PTH2 DSC model are listed below.

Heat Load in the Model (kW)	$\dot{q}'''$ value without PF (Btu/hr-in^3)
0.8	0.243
0.9	0.274
1.0	0.304
1.3	0.395
1.5	0.456

The base heat generation rate is multiplied by peaking factors along the axial fuel length to represent the axial decay heat profile. The peaking factors for burnup higher than 30 GWd/MTU from Table 3 of [B4.6] are converted to match the regions defined for the fuel assembly in the finite element model. Section B.4.6.4 describes the conversion method and lists the peaking factors used in the 32PTH2 DSC model.

The heat generating rates for the elements representing the active fuel are calculated based on the HLZC for the 32PTH2 DSC as shown in Chapter B.2, Figure B.2.1-1.

The DSC shell temperatures determined in the AHSM-HS and OS200FC TC thermal analyses for various load cases are used as boundary conditions in the 32PTH2 DSC model.

Typical boundary conditions used in the 32PTH2 DSC model are shown in Figure B.4.6-5. The effective thermal conductivities for the basket plates are calculated in Section B.4.6.5. The other material properties used in the 32PTH2 DSC model are listed in Section B.4.2.

The effective properties for the homogenized 32PTH2 basket used in AHSM-HS and OS200FC TC models are calculated in Section B.4.6.6. Mesh sensitivity of the model is discussed in Section B.4.6.7.

B.4.6.3 Justification of Gaps Assumed in 32PTH2 DSC Model

B.4.6.3.1 Hot Gap Between Basket Assembly and 32PTH2 DSC Shell

A nominal diametrical cold (fabrication) gap of 0.375″ is considered between the basket assembly and the 32PTH2 DSC shell. The nominal 32PTH2 DSC inner diameter (ID) is 68.5″. The nominal basket assembly outer diameter (OD) is then 68.125″.

The average temperatures for the basket assembly, transition rails, and shell at the hottest cross section are retrieved from the 32PTH2 DSC model to calculate the nominal hot gap size at thermal equilibrium. The hot dimensions of the basket assembly OD and 32PTH2 DSC ID are calculated as follows.

The outer diameter of the hot basket assembly is:

$$OD_{B,hot} = OD_B + [L_{SS,B} \times \alpha_{SS,B} (T_{avg,B} - T_{ref})] + L_{Rail} \times [\alpha_{Al,0} (T_{avg,R0} - T_{ref}) + \alpha_{Al,180} (T_{avg,R180} - T_{ref})]$$

Where:

$OD_{B,hot}$ = Hot OD of the basket assembly,
OD_B = Nominal cold OD of the basket assembly
= 68.5″ – 0.375″ = 68.125″,
$L_{SS,B}$ = width of basket assembly at 0-180 direction
= 12 × fuel compartment thickness (0.187″) +
6 × compartment width (8.65″) +
5 × center basket plate thickness (3/8″) +
2 × outer basket plate thickness (5/16″)
= 12*0.187+6*8.65+5*3/8+2*5/16 ≈ 56.644″,
L_{Rail} = Width of transition rail = $(OD_B - L_{SS,B})/2 \approx 5.741$″,
$\alpha_{SS,B}$ = Average coefficient of thermal expansion for SA-240 Type 304 steel, in/in-°F, interpolated using data in [B4.10]),
α_{Al} = Average aluminum coefficient of thermal expansion, in/in-°F (interpolated using data in [B4.10],
$T_{avg,B}$ = Average basket assembly temperature at the hottest cross section, °F,
$T_{avg,R0}$ = Average transition rail temperature at the hottest cross section at 0 degree orientation, °F,
$T_{avg,R180}$ = Average transition rail temperature at the hottest cross section at 180 degree orientation, °F,
T_{ref} = Reference temperature = 70°F [B4.10].

The inner diameter of the hot 32PTH2 DSC shell is:

$ID_{CAN, hot} = ID_{CAN} [1 + \alpha_{SS, CAN} (T_{avg, CAN} - T_{ref})]$

Where:

$ID_{CAN, hot}$ = Hot ID of 32PTH2 DSC shell,
ID_{CAN} = Cold ID of 32PTH2 DSC shell = 68.5″,
$\alpha_{SS, CAN}$ = Average coefficient of thermal expansion for SA-240 Type 316 steel, in/in-°F (interpolated using data in [B4.10],
$T_{avg, CAN}$ = Average 32PTH2 DSC shell temperature at hottest cross section, °F,
T_{ref} = Reference temperature = 70°F [B4.10].

The diametrical hot gap between the basket assembly and 32PTH2 DSC inner shell (G_{hot}) is:

$G_{hot} = ID_{CAN, hot} - OD_{B,hot}$.

The hot gap between the 32PTH2 DSC shell and basket assembly is calculated for the maximum heat load of 37.2 kW and listed in the following table.

Diametrical Hot Gaps in 32PTH2 DSC

37.2 kW (HLZC#1) Heat Load, Off-Normal Storage @ 117°F Ambient (Load Case S3)					
Component	**Cold dimension**	**Temp**	**$\alpha x10^{-6}$**	**ΔL**	**Hot dimension**
	(in)	(°F)	(in/in/°F)	(in)	(in)
Basket assembly width	56.644	593	9.886	0.293	56.937
Transition rail @ 0°	5.7405	471	13.842	0.032	5.772
Transition rail @ 180°	5.7405	462	13.824	0.031	5.772
Basket OD	68.125	---	---	---	68.481
DSC shell ID	68.50	409	9.518	0. 221	68.721
Gap	0.375	---	---	---	0.240

Since the above calculated hot gap of 0.240″ is smaller than the uniform diametrical gap of 0.30″ assumed in the 32PTH2 DSC model, the assumed gap is conservative.

B.4.6.3.2 Gaps Between Adjacent Plates

The gaps between two adjacent plates are related to the flatness and roughness tolerances of the plates, the contact pressure, and the conductivity of the interface gas. The micro gaps related to these tolerances are non-uniform and provide interference contact at some areas and gaps on the other areas. The calculation of the theoretical thermal contact resistance (R_j) between two adjacent plates is described in Appendix A, Section A.3.6.7.2 of [B4.24]. A very small contact pressure of 10^{-6} psi is assumed to give a negligible contact conductance and thereby theoretical thermal contact resistance (R_j) is mainly determined by gap conductance. The values of thermal contact resistance for air and helium contact gaps are estimated in Appendix A, Section A.3.6.7.2 and Section A.3.6.7.4 of [B4.24], respectively.

The equivalent thermal resistance ($R_{j, model}$) for a gap size (G) between the two adjacent plates is:

$R_{j,\ model} = G / k_g$

Where

k_g= Thermal conductivity of the interface gas, W/m-K,

G= The gap size between two adjacent plates, m.

Thermal contact resistances of R_j and $R_{j,\ model}$ between two adjacent plates are calculated for 32PTH2 DSC components and summarized in the following table:

Thermal Contact Resistances between Adjacent Plates

Contact Gap Assumed in the DSC Model	k_g (1) (W/m-K)	R_j (2) (m^2-k/W)	$R_{j,\ model}$ (m^2-k/W)	$R_{j,\ model}$ /R_j
0.01″ air gap for DSC top/bottom cover plates	0.031	2.7E-3	8.2E-3	3.0
0.005″ helium gap for stainless steel basket support plates	0.204	4.2E-4	6.2E-4	1.5
0.01″ helium gap between outer basket plate and transition rail			1.2E-3	3.0

(1) The thermal conductivity values of air at 200°F and helium at 400°F are considered.

(2) The thermal contact resistance values calculated in Appendix A, Section A.3.6.7.2 and Section A.3.6.7.4 of [B4.24] are considered.

As shown in the above table, the calculated thermal contact resistances ($R_{j,\ model}$) for the 32PTH2 DSC model are higher than the corresponding theoretical thermal contact resistance (R_j). Further, it should be noted that no contact pressure was considered between the adjacent plates in determining R_j. This assumption implies that no friction exists between the adjacent plates within the basket assembly, which adds to the conservatism considered in the 32PTH2 DSC model. Therefore, the assumed sizes of the gaps used in the 32PTH2 DSC model are conservative.

In addition a sensitivity analysis is performed in which the gap sizes between the adjacent plates in the basket are doubled from 0.005″ to 0.01″. The result of this analysis shows that the maximum fuel cladding temperature increases only by 8°F and remains below the allowable limits. Considering the margins to the limits, it shows that adequate conservatism is considered for the gap sizes between the plates in the basket. It should be noted that the presence of large gaps between the basket plates is unrealistic as would result in an oversized basket that exceeds the size of the DSC shell.

B.4.6.4 Axial Decay Heat Profile for Fuel Assemblies

The axial decay heat profile for fuel assemblies considered in the 32PTH2 DSC is based on a typical axial burnup distribution of PWR fuel assemblies with burnup range higher than 30 GWd/MTU as listed in Table 3 of [B4.6] and is shown in Table B.4.6-1 for reference. The maximum fuel assembly average burnup allowed in the 32PTH2 DSC is 62.5 GWd/MTU, which is considerably higher than 30 GWd/MTU considered in [B4.6]. The discussion in [B4.6] shows that at a higher burnup, the heat flux shape tends to flatten with a reduction in the maximum

axial peaking factor in the middle region, and the flux shape becomes more pronounced in the fuel end regions. Therefore, the application of a decay heat profile resulting for a lower burnup (30 GWd/MTU) spent fuel assembly to a higher burnup spent fuel assembly (up to 62.5 GWd/MTU for fuel assemblies in 32PTH2 DSC) is conservative.

The active fuel length of the homogenized fuel assemblies in the 32PTH2 DSC model is divided into 20 sections. The peaking factors from Table 3 of [B4.6] are converted as follows to match the 20 regions defined for the active fuel length.

- An average height is calculated for each peaking factor section of defined in Table 3 of [B4.6].
- An average height is calculated for each section of active fuel length defined in the model of 32PTH2 DSC.
- The peaking factor for each section in the DSC model is calculated by interpolation between the peaking factors in Table 3 of [B4.6] using the average heights.

The peaking factors for fuel assemblies in the 32PTH2 DSC model are listed in Table B.4.6-2 and illustrated in Figure B.4.6-6.

As seen in Table B.4.6-2, the normalized area under peaking factor curve is smaller than 1.0. To avoid any degradation of decay heat load, a correction factor of 1.016 calculated as follows is used when applying the peaking factors.

$$\text{Nomalized Area under Curve} = \frac{\text{Area under Axial Heat Profile}}{\text{Active Fuel Length}} = 0.984,$$

Active fuel length = 150″,

$$\text{Correction Factor} = \frac{1}{\text{Normalized Area under Curve}} = 1.016$$

B.4.6.5 Effective Thermal Conductivity for Plates and Gaps within 32PTH2 DSC Basket Assembly

To simplify the 32PTH2 DSC model, various plates and the associated gaps are homogenized as one material using effective conductivities. The following plates along with the gaps are considered as homogenized materials in the 32PTH2 DSC model:

a) 0.37″ (3/8″) thick paired aluminum center basket plates and poison plates along with two 0.005″ gaps. The gaps account for the contact resistance between the fuel compartments and the paired aluminum poison plates on either side.

b) 0.37″ (3/8″) thick center basket support plate with two 0.005″ gaps. The gaps account for the contact resistance between the fuel compartments and center basket support plates on either side.

c) 0.3125″ (5/16″) thick outer basket support plate with 0.005″ gap. The gap accounts for the contact resistance between the fuel compartments and outer basket support plates.

d) 0.30″ thick outer basket plate with 0.005″ gap. The gap accounts for the contact resistance between the fuel compartments and outer basket plates. Further, this is conservative since the 0.3125″ (5/16″) thick outer basket plates are modeled with 0.30″ thickness.

The paired plates build up parallel thermal resistances along their length and serial thermal resistances across their thickness. The gaps considered between the paired plates and their adjacent basket plates at the cross-section account for the contact resistance between the plates.

For plates oriented in the 0°-180°, the effective conductivities calculated across the plates in the ANSYS model are applied in the x direction ($k_{across} = k_{xx}$) and the effective conductivities calculated along the plates are applied in the y and z direction ($k_{along} = k_{yy}$ and k_{zz}).

For plates oriented in the 90°-270°, the effective conductivities calculated across the plates in the ANSYS model are applied in the y direction ($k_{across} = k_{yy}$) and the effective conductivities calculated along the plates are applied in the x and z direction ($k_{along} = k_{xx}$ and k_{zz}).

The effective conductivities calculated are based on the total thickness of the model (t_{model}) for each homogenized region and account for either an increase or decrease in the total thicknesses of various individual plates and gaps that make up the homogenized region.

The effective conductivities of the paired plates are calculated as follows:

$$k_{along} = \frac{\sum k_{plate} \cdot t_{plate} + n \cdot k_{gap} \cdot t_{gap}}{t_{model}}$$ along the length (parallel resistances)

$$k_{across} = \frac{t_{model}}{\sum \frac{k_{plate}}{t_{plate}} + \frac{n \cdot k_{gap}}{t_{gap}}}$$ across the thickness (serial resistances)

where,
k_{plate} = conductivity of poison plate or basket plates or basket support plates (Btu/hr-in-°F),
t_{plate} = thickness of poison plate or basket plates or basket support plates (in),
k_{gap} = conductivity of helium gap (Btu/hr-in-°F),
t_{gap} = thickness of the helium gap (in),
n = number of gaps.

The calculated effective conductivity values for the various combinations listed from a through d above are shown in Table B.4.6-3 through Table B.4.6-6.

B.4.6.6 Effective Basket Assembly Thermal Properties for 32PTH2 DSC

The 32PTH2 basket assembly effective density, specific heat and thermal conductivity are calculated for use in the various thermal analyses of the 32PTH2 DSC. The calculation of these effective thermal properties is based on the DSC components' weight data provided in Chapter B.3, Section B.3.2 and nominal dimensions of the 32PTH2 DSC provided on drawings shown in Chapter B.1, Section B.1.5.2.

B.4.6.6.1 Effective Density and Specific Heat

The basket assembly effective density $\rho_{eff\ basket}$, and specific heat $c_{p\ eff\ basket}$ are calculated as weight average, using the equations listed below:

$$\rho_{eff\ basket} = 0.95 \cdot \frac{\sum W_i}{V_{basket}} = 0.95 \cdot \frac{W_{steel} + W_{Al} + W_{poison} + W_{fuel}}{L_{basket} \cdot \pi \cdot D_{basket}^{\ 2} / 4}$$

$$c_{p\ eff\ basket} = 0.95 \cdot \frac{\sum W_i \cdot c_{pi}}{\sum W_i} = 0.95 \cdot \frac{W_{steel} \cdot c_{p\ steel} + W_{Al} \cdot c_{p\ Al} + W_{poison} \cdot c_{p\ poison} + W_{fuel} \cdot c_{pfuel}}{W_{steel} + W_{Al} + W_{poison} + W_{fuel}}$$

Where

W_i = weight of the basket assembly components,

V_{basket} = total volume of the basket in the model = $\pi / 4 \cdot D_{basket}^{\ 2} \cdot L_{basket}$

L_{basket} = basket assembly length (177.15″),

D_{basket} = basket assembly OD (68.125″),

$c_{p\ i}$ = specific heat of the basket assembly components.

The specific heat and density values for various materials used are listed in Section B.4.2. The following assumptions are used in the calculation of the basket assembly effective density and specific heat:

- Specific heat of SA 240, Type 304 and Aluminum 6061 are considered for stainless steel and aluminum components, respectively.
- For poison material C_p and ρ values are conservatively assumed equal to those for Aluminum 6061.
- For aluminum at T > 400°F, specific heat (cp) value is conservatively assumed equal to value at 400°F.
- Helium is conservatively not included in density and specific heat calculations.

Based on Table B.3.2-1 in Section B.3.2, the total weights of the stainless steel components (fuel compartments, center/outer basket support plates) and aluminum components (center/outer basket plates, poison plates and transition rails) within the 32PTH2 DSC are 12,700 lbs and 17,000 lbs, respectively. However, for conservatism, the total weights of the stainless steel plates and aluminum/poison plates/ aluminum transition rails within the 32PTH2 DSC assumed in this calculation are 12,500 lbs and 16,500 lbs. This is conservative since assuming lower weights reduces the effective density and specific heat of the 32PTH2 DSC basket assembly.

The effective density for the 32PTH2 DSC basket assembly is summarized in Table B.4.6-7. The effective specific heats for 32PTH2 DSC basket assembly are summarized in Table B.4.6-8.

B.4.6.6.2 Effective Thermal Conductivity

To determine the effective thermal conductivity a slice of the 32PTH2 DSC model is used without the DSC shell. The length of the slice model is twice the length of the paired poison plate and center basket plates, center basket support plates and the axial gaps between them.

B.4.6.6.2.1 Axial Effective Thermal Conductivity

To calculate the axial effective conductivity of the basket assembly, constant temperature boundary conditions are applied at the top and bottom of the slice models. No heat generation is considered for the homogenized fuel assembly in these cases. The axial effective conductivity is calculated using the equation listed below.

$$k_{basket,axl} = \frac{Q_{axl} \cdot L}{A_{slice} \cdot \Delta T} \cdot 0.95$$

Where: Q_{axl} = Amount of heat leaving the upper face of the slice model – reaction solution of the uppermost nodes (Btu/hr),

L = Length of the model = 30″,

A_{slice} = Surface area of the upper (or bottom) face of the basket assembly slice model = 1822 in^2 ($=\pi/8 \times D_{basket}^2$),

$\Delta T = (T_2 - T_1)$ =Temperature difference between upper and lower faces of the model (°F),

T_2 = Constant temperature applied on the upper face of the model (°F),

T_1 = Constant temperature applied on the lower face of the model (°F).

Only 95% of the estimated axial effective conductivity is considered for conservatism.

In determining the temperature dependent axial effective conductivities an average temperature $T_{avg} = (T_1 + T_2)/2$, is used for the basket assembly temperature. The axial effective conductivities for 32PTH2 DSC basket assembly are listed in Table B.4.6-9.

B.4.6.6.2.2 Radial Effective Thermal Conductivity

The basket assembly slice model is also used to calculate the transverse effective conductivity of the basket. For this purpose, constant temperature boundary conditions are applied on the outermost radial nodes of the slice model and heat generating conditions are applied over the fuel elements.

The heat generation rates for the slice model of the 32PTH2 basket are calculated based on the HLZC # 3 shown in Chapter B.2, Figure B.2.1-1 with a total heat load of 32 kW and a peaking factor of 1.2 for PWR assemblies. The heat generation boundary conditions are applied using the same methodology as described in Section B.4.6.2.1.

The following equation is given in [B4.18] for long solid cylinders with uniformly distributed heat sources.

$$T = T_o + \frac{\dot{q}\, r_o^2}{4k}\left[1 - \left(\frac{r}{r_o}\right)^2\right]$$

Where: T_o= Temperature at the outer surface of the cylinder (°F),

T = Maximum temperature of cylinder (°F),

$\dot{q}$ = Heat generation rate (Btu/hr-in^3),

r_o = Outer radius = D_{basket} /2 = 34.0625″,

r = Inner radius = 0 for slice model,

k = Thermal Conductivity (Btu/hr-in-°F).

The above equation is rearranged to calculate the transverse effective conductivity of the basket assembly as follows.

$$\dot{q} = \frac{Q_{rad}}{V},$$

$$k_{basket,rad} = \frac{Q_{rad} \cdot r_0^2}{4 \cdot V \cdot \Delta T} \cdot 0.95 = \frac{0.95 \cdot Q_{rad}}{2\pi \cdot L \cdot \Delta T}$$

With Q_{rad} = Amount of heat leaving the periphery of the slice model – reaction solution of the outermost nodes (Btu/hr),

L = Length of the slice model = 30″,

V = Volume of the slice model = $(\pi r_0^2 L)/2$,

$\Delta T = (T_{max} - T_o)$ = Difference between maximum and the outer surface temperatures (°F).

Since the surface area of the fuel assemblies at the basket cross section is much larger than the other components, assuming a uniform heat generation is a reasonable approximation to calculate the radial effective conductivity.

Only 95% of the estimated radial effective conductivity is considered for conservatism.

In determining the temperature dependent transverse effective conductivities an average temperature $T_{avg} = (T_{max} + T_o)/2$, is used for the basket assembly temperature.

The transverse effective conductivities of 32PTH2 DSC basket assembly are listed in Table B.4.6-10.

B.4.6.7 Mesh Sensitivity of 32PTH2 DSC Model

In general, the resultant temperature from a finite element model might vary when the mesh density is increased or decreased. On the other hand, increasing the mesh density requires more computer memory and consumes more computation time, particularly for various thermal

evaluations, whereas using a lower mesh density might not adequately capture the temperature contours and the maximum temperatures.

To determine the appropriate mesh density for the full 32PTH2 DSC model, a 30″ slice three-dimensional finite element model of the 32PTH2 DSC is developed using ANSYS version 10.0 [B4.26]. The length of the slice model is twice the length of the paired poison plate and center basket plates, center basket support plates and the axial gaps between those plates. The dimensions used for the 32PTH2 DSC slice model are the same as those used in the 32PTH2 DSC model described in Section B.4.6.2.1.

The 32PTH2 DSC slice model is modified to create various mesh densities in both the axial and radial directions to determine the appropriate mesh density. A mesh density is considered acceptable for use in thermal analyses when the resultant temperature changes are insignificant (≤1°F) with changes in mesh sizing in both radial and axial directions.

The slice model contains the DSC shell, aluminum transition rails, outer basket plates, center/outer basket support plates, paired poison plate / center basket plates and homogenized fuel assemblies. Only SOLID70 elements are used in the 32PTH2 DSC slice model.

For the mesh sensitivity analysis of 32PTH2 DSC model, a fixed temperature of 400°F on the outer surface of the DSC shell and a decay heat of 32 kW with HLZC # 3 are selected as boundary conditions. A peaking factor of 1.2 is considered to apply the heat generation rate on the homogenized fuel assemblies. Decay heat load is applied as heat generation boundary condition over the elements representing the homogenized fuel assemblies in the mesh sensitivity analysis. The heat generation rate used in this analysis is calculated as follows.

$$\dot{q}''' = \left(\frac{q}{a^2 L_a} \times PF \right) = 0.3648 \text{ Btu/hr} - \text{in}^3$$

Where,

$\dot{q}'''$ = Heat generation rate (Btu/hr-in^3)
q = Decay heat load per FA = 1 kW
(Multiply by 3412.3 to convert to Btu/hr),
a = Width of the homogenized fuel assembly = 8.65″,
L_a = Length of active fuel region = 150″,
PF = Peaking Factor = 1.2.

The material properties used in the 32PTH2 DSC slice model are the same as those for the 32PTH2 DSC model.

A two-step evaluation is performed to determine the proper mesh density. In the first step, the mesh density of the model is increased gradually in the radial direction (cross section of the 32PTH2 DSC) until the changes of the maximum component temperatures were limited to ±1°F. Three models (see Table B.4.6-11) were developed for the mesh density analysis in the radial

direction. The lowest mesh density at which the changes of the maximum component temperatures are limited to ±1°F is considered as the threshold mesh density.

The threshold mesh density from the first step is chosen to increase the mesh density in the axial direction in the second step. The mesh density in the axial direction is considered sufficient when the changes of the maximum component temperatures were limited to ±1°F. Three additional models (see Table B.4.6-11) were developed for the mesh density analysis in the axial direction.

Figure B.4.6-7 and Figure B.4.6-8 illustrate the mesh density of various models developed for this calculation in the radial and axial directions, respectively. The numbers of the elements for the models used in the mesh density analysis are summarized in Table B.4.6-11 for radial and axial directions.

The maximum 32PTH2 DSC component temperatures resulting from the models are summarized in Table B.4.6-12 for mesh sensitivity analysis in the radial direction. As seen in Table B.4.6-12, the changes in the maximum component temperatures are within ±1°F for model "32PTH2_Sens_Medium" when the mesh density is further increased. The maximum fuel cladding temperature change due to increased radial mesh density (Model "32PTH2_Sens_Fine") is about +0.77°F and is less that the criteria of ±1°F. Therefore, in the radial direction, the mesh density of the model "32PTH2_Sens_Medium" is considered adequate for the thermal analysis.

Model "32PTH2_Sens_Medium" is selected for the mesh sensitivity analysis in the axial direction. The resultant maximum 32PTH2 DSC component temperatures and the differences for various mesh densities are presented in Table B.4.6-12 for axial mesh sensitivity analysis.

Since the changes between the maximum 32PTH2 DSC components temperatures do not exceed ±1°F for model "32PTH2_Sens_Medium" when compared to the axially refined models listed in Table B.4.6-12, the mesh density of this model is considered appropriate for thermal analysis and used to develop the full-length model of the 32PTH2 DSC described in Section B.4.6.2.1.

B.4.6.8 Sensitivity Study for Effects of Damaged Fuel Assemblies

The 32PTH2 DSC is designed to store 32 intact or up to 16 damaged and remaining intact fuel assemblies. Up to 16 damaged fuel assemblies can place in cells located at the outer edge of the 32PTH2 basket as shown in Chapter B.2, Figure B.2.1-1.

The cladding of damaged fuel assemblies can experience further damages due to a postulated drop accident considered during transfer operations in an OS200FC TC. To bound the effect of these damages, a sensitivity analysis is conducted considering the worst case condition, in which the damaged fuel assemblies become rubble. Following the rationale in NUREG/CR-6835 [B4.7], it is assumed that the fuel rods do not shatter into very small pieces and the fuel rubble is not in a tightly compacted mass. Instead, the fuel rubble is assumed to be 50% void by volume. To provide the maximum heat generation, the fuel rubble is assumed to be contained within the original active fuel volume, albeit in the lower portion of the original volume. Consistent with NUREG/CR-6835, the axial-burnup variation in the rubble is also assumed to be uniform. The heat generation rate used for the fuel rubble is calculated as:

$$\dot{q}''' = \left(\frac{q}{a^2 L_a} \right)$$

Where,

$\dot{q}'''$ = Heat generation rate (Btu/hr-in^3)
q = Decay heat load per fuel assembly in Zone 3 of HLZC # 1 = 1.0 kW,
(Multiply by 3412.3 to convert kW to Btu/hr),
a = Width of the homogenized fuel assembly = 8.65″,
L_a =Active fuel length = 150″.

The height of the fuel rubble with the assumption of 50% void by volume is determined based on the volume of fuel rods. The fuel rubble height (H_{Rubble}) is calculated as follows:

$V_{UO2,\ Compact} = (OD_{Fuel\ Rod})^2 \times (n) \times (L_a) = 0.382^2 \times 236 \times 150 = 5166\ in^3$,
$V_{Rubble} = V_{UO2,\ Compact} / 0.5 = 5166/0.5 = 10331\ in^3$,
$H_{Rubble} = V_{Rubble} / a^2 = 10331/8.65^2 = 138$ in,

Where

$OD_{Fuel\ Rod}$ = Outer diameter of fuel rods = 0.382 in,
n = Number of fuel rods = 236,
$V_{UO2,\ Compact}$ = Volume of the fuel rods (in^3),
V_{Rubble} = Volume of the fuel rubble with 50% void volume (in^3).

For the fuel assemblies considered within the 32PTH2 DSC, the fuel rubble height is calculated as 138″ and is summarized in Table B.4.6-13. However, for conservatism, a fuel rubble height of 136.75″ is considered in the model.

The bounding accident condition i.e. loss of neutron shield with loss of air circulation (Load Case T9, see Table B.4.5-1) is considered for this evaluation to determine the bounding temperature. In the sensitivity run, the heat generation rate corresponding to the damaged fuel assemblies is applied uniformly over the fuel rubble height of 136.75″ concentrated at the bottom axial portion of the original active fuel volume with a peaking factor of one. The DSC shell temperature profile retrieved from the OS200FC TC model for Load Case T9 is applied as boundary conditions for the 32PTH2 DSC model.

To bound the uncertainty of effective thermal conductivity for the fuel rubble region, helium conductivity is selected for the elements within the outer 16 fuel compartments that are loaded with damaged fuel assemblies. The results of the sensitivity study are discussed in Section B.4.6.9.

B.4.6.9 32PTH2 DSC Thermal Analysis Results

The 32PTH2 DSC components are evaluated herein for normal, off-normal, and accident conditions of storage and transfer over a range of design basis ambient temperatures. Ambient

temperatures for normal and off-normal storage conditions are assumed to occur for a sufficient duration such that a steady-state temperature distribution exists within the components.

The maximum fuel cladding temperatures during normal, off-normal, and accident conditions of storage and transfer are listed in Table B.4.6-14 and Table B.4.6-15, respectively. The maximum temperatures of the basket assembly components are listed in Table B.4.6-16 and Table B.4.6-17 for storage and transfer conditions, respectively.

Figure B.4.6-9 and Figure B.4.6-10 present the typical 32PTH2 DSC temperature distributions for storage conditions. The time-temperature histories for 32PTH2 DSC components during transient blocked vent accident conditions are shown in Figure B.4.6-11.

Figure B.4.6-12 through Figure B.4.6-15 present the typical 32PTH2 DSC temperature distributions for various transfer conditions. The time-temperature histories for 32PTH2 DSC components during transient transfer conditions are shown in Figure B.4.6-16 through Figure B.4.6-18.

The average temperatures for the fuel assemblies and the assembly components are listed in Table B.4.6-18. The average temperatures are used for thermal expansion and DSC internal pressure calculations.

The maximum component temperatures for a 32PTH2 DSC loaded with damaged fuel assemblies resulting from the sensitivity analysis described in Section B.4.6.8 for the loss of neutron shield with loss of air circulation accident condition (Load Case T9 with 16 damaged fuel assemblies) are compared to the corresponding values for the 32PTH2 DSC with intact only fuel assemblies in Table B.4.6-19.

As seen in Table B.4.6-19, the maximum fuel cladding temperature is 900°F for a 32PTH2 DSC loaded with damaged fuel assemblies wherein thermal conductivity of rubble is conservatively considered as helium conductivity. This corresponds to a temperature increase of 13°F when compared to the maximum fuel cladding temperature for the 32PTH2 DSC loaded with intact fuel for Load Case T9. Therefore, considering the large margin of 158°F for the maximum fuel cladding temperature to the accident limit of 1058°F [B4.3], this change does not affect the thermal performance of the 32PTH2 DSC.

Typical component temperature plots for a 32PTH2 DSC with 16 damaged fuel assemblies for the loss of neutron shield with loss of air circulation accident condition are shown in Figure B.4.6-19.

B.4.6.10 Maximum Internal Pressures for the 32PTH2 DSC

Maximum internal pressure within the 32PTH2 DSC is calculated in Section B.4.7. A summary of the maximum operating pressures for the 32PTH2 DSC is presented in Table B.4.7-1.

B.4.6.11 Evaluation of 32PTH2 DSC Thermal Performance

As presented in Table B.4.6-14 and Table B.4.6-15, the maximum fuel cladding temperatures are below the allowable fuel temperature limit of 752°F (400°C) [B4.3] for normal storage and

normal/off-normal transfer conditions. The 50% blockage of the ASHM-HS inlet vents are considered as an off-normal condition.

The complete blockage of the AHSM-HS inlet and outlet vents during storage and the loss of liquid neutron shield in combination with failure of the air circulation during transfer are considered as accident conditions. As shown in Table B.4.6-14 and Table B.4.6-15, the maximum fuel cladding temperatures remain well below the allowable fuel temperature limit of 1058°F (570°C) [B4.3] for off-normal storage and accident conditions.

The time limits required for transfer operation to maintain the fuel cladding temperature below the allowable limits are discussed in Section B.4.5 and summarized in Figure B.4.5-10.

As presented in Table B.4.7-1, the maximum 32PTH2 DSC internal pressures for normal, off-normal, and accident conditions are 9.4 psig, 18.2 psig, and 124 psig, respectively. These values are calculated based on bounding transfer and storage conditions as documented in Section B.4.7. The calculated DSC internal pressures are lower than the design pressure limits of 15 psig for normal, 20 psig for off-normal, and 140 psig for accident storage and transfer conditions. Hence, the NUHOMS® 32PTH2 DSC design meets all applicable thermal requirements for normal, off-normal, and accident conditions.

Table B.4.6-1
Peaking Factors for a Typical PWR Fuel Assemblies

% of Core Height [B4.6]	Length (in)	Peaking Factor [B4.6]
0.00	0.00	0.000
2.78	4.17	0.652
8.33	12.50	0.967
13.89	20.84	1.074
19.44	29.16	1.103
25.00	37.50	1.108
30.56	45.84	1.106
36.11	54.17	1.102
41.67	62.51	1.097
47.22	70.83	1.094
52.78	79.17	1.094
58.33	87.50	1.095
63.89	95.84	1.096
69.44	104.16	1.095
75.00	112.50	1.086
80.56	120.84	1.059
86.11	129.17	0.971
91.67	137.51	0.738
97.22	145.83	0.462
100.00	150.00	0.000

Table B.4.6-2
Peaking Factors for Fuel Assemblies in the 32PTH2 DSC Model

Proprietary information withheld pursuant to 10 CFR 2.390

Table B.4.6-3
Effective Thermal Conductivity for Paired Poison Plate/Aluminum Center Basket Plates/ Helium Gaps in 32PTH2 Basket

Proprietary information withheld pursuant to 10 CFR 2.390

Table B.4.6-4
Effective Thermal Conductivity for 3/8″ Stainless Steel Center Basket Support Plates/Helium Gaps in 32PTH2 Basket

Proprietary information withheld pursuant to 10 CFR 2.390

Table B.4.6-5
Effective Thermal Conductivity for 5/16″ Stainless Steel Outer Basket Support Plates/Helium Gap in 32PTH2 Basket

Proprietary information withheld pursuant to 10 CFR 2.390

Table B.4.6-6
Effective Thermal Conductivity for Aluminum Outer Basket Plates/ Helium Gap in 32PTH2 Basket

Proprietary information withheld pursuant to 10 CFR 2.390

Table B.4.6-7
Effective Density for 32PTH2 DSC Basket Assembly

Components	Material	Total Weight (lb_m)
Fuel Assembly	---	49600
Stainless Steel Components (Fuel Compartments, Center/Outer Basket Support Plates)	SS304	12500
Aluminum Components (Center/Outer Basket Plates, Poison Plates and Transition Rails)	Aluminum	16500
Total		
	Dimension	
D_{basket}	68.125	in
L_{basket}	177.15	in
V_{basket}	645720	in^3
$\rho_{eff\ basket}$	0.116	lb_m/in^3

Table B.4.6-8
Effective Specific Heat for 32PTH2 DSC Basket Assembly

Components	Fuel Assembly	Fuel Compartments, Center/Outer Basket Support Plates	Center/Outer Basket Plates, Poison Plates and Transition Rails	Total	
Material	---	Stainless Steel(1)	Aluminum(1)	---	
Weight (lb_m)	49600	12500	16500	78600	
T	$m.C_p$	$m.C_p$	$m.C_p$	$\Sigma\ m.C_p$	$C_{p\ eff\ basket}$
(°F)	(Btu/°F)	(Btu/°F)	(Btu/°F)	(Btu/°F)	(Btu/lb_m-°F)
70	2858	1425	3531	7814	0.094
100	2915	1425	3564	7904	0.096
200	3108	1488	3663	8259	0.100
300	3256	1525	3746	8527	0.103
400	3337	1575	3828	8740	0.106
500	3417	1613	3828	8857	0.107
600	3497	1625	3828	8950	0.108
700	3574	1650	3828	9052	0.109
800	3611	1663	3828	9101	0.110
900	3648	1675	3828	9151	0.111
1000	3684	1688	3828	9200	0.111

(1) Specific heat values for stainless steel and aluminum are listed in Section B.4.2.

Table B.4.6-9
Effective Axial Conductivity for 32PTH2 DSC Basket Assembly

T_1	T_2	T_{avg}	Q_{axl}	$k_{basket,axl}$
(°F)	(°F)	(°F)	(Btu/hr)	(Btu/hr-in-°F)
50	150	100	13405	2.097
150	250	200	13658	2.136
250	350	300	13872	2.170
350	450	400	14052	2.198
450	550	500	14119	2.208
550	650	600	14166	2.216
650	750	700	14215	2.223
750	850	800	14261	2.230
850	950	900	14292	2.235
950	1050	1000	14318	2.239

Table B.4.6-10
Effective Radial Conductivity for 32PTH2 DSC Basket Assembly

T_O	T_{MAX}	T_{avg}	Q_{rad}	$k_{basket,rad}$
(°F)	(°F)	(°F)	(Btu/hr)	(Btu/hr-in-°F)
0	406	203	13099	0.163
100	485	293	13099	0.172
200	563	382	13099	0.182
300	643	471	13099	0.193
400	725	562	13099	0.203
500	808	654	13099	0.214
600	893	747	13099	0.225
700	980	840	13099	0.236
800	1069	934	13099	0.246
900	1162	1031	13099	0.252
1000	1259	1129	13099	0.255
1100	1357	1228	13099	0.257

Table B.4.6-11
Mesh Density in the Radial and Axial Directions

Radial Direction

From Z=0 to Z=1.75" Segment	Number of Elements in Cross Section		
Model Name (ID)	**32PTH2_Sens_Coarse**	**32PTH2_Sens_Medium**	**32PTH2_Sens_Fine**
Fuel Assembly	3520	5696	8384
Basket Assembly Components	1484	1786	2086
Transition Rails and DSC Shell	540	542	654
For the entire 30" Slice Model	---	---	---
Total No of Elements	127512	184552	255852

Axial Direction

Model Name (ID)	No. of Segments in Axial Direction	Total No. of Elements
32PTH2_Sens_Medium	23	184552
32PTH2_Sens_CoarseA	33	264792
32PTH2_Sens_MediumA	47	377128
32PTH2_Sens_FineA	61	489464

Table B.4.6-12
Maximum Component Temperatures for Different Mesh Density in Radial and Axial Directions

Radial Direction

Model Name (ID)	32PTH2_Sens_Coarse	32PTH2_Sens_Medium	32PTH2_Sens_Fine
Component	**Maximum Temperature (°F)**		
Fuel Cladding	726.18	727.55	728.32
Fuel Compartment	697.86	699.46	700.39
Poison/ Center Basket Plates	695.94	697.40	698.40
Transition Rail	484.16	484.37	484.55
DSC Shell	403.74	403.75	403.75

Component	ΔT (°F) $T_{32PTH2\_Sens\_Medium} - T_{32PTH2\_Sens\_Coarse}$	ΔT (°F) $T_{32PTH2\_Sens\_Fine} - T_{32PTH2\_Sens\_Medium}$
Fuel Cladding	1.37	0.77
Fuel Compartment	1.60	0.93
Poison/ Center Basket Plates	1.46	1.00
Transition Rail	0.21	0.18
DSC Shell	0.01	0.00

Axial Direction

Model Name (ID)	32PTH2_Sens_Medium	32PTH2_Sens_CoarseA	32PTH2_Sens_MediumA	32PTH2_Sens_FineA
Component	**Maximum Temperature (°F)**			
Fuel Cladding	727.55	728.29	728.62	728.76
Fuel Compartment	699.46	700.14	700.53	700.70
Poison/ Center Basket Plates	697.40	698.18	698.54	698.69
Transition Rail	484.37	484.33	484.34	484.34
DSC Shell	403.75	403.75	403.74	403.74

Component	ΔT (°F) $T_{32PTH2\_Sens\_CoarseA} - T_{32PTH2\_Sens\_Medium}$	ΔT (°F) $T_{32PTH2\_Sens\_MediumA} - T_{32PTH2\_Sens\_CoarseA}$	ΔT (°F) $T_{32PTH2\_Sens\_FineA} - T_{32PTH2\_Sens\_MediumA}$
Fuel Cladding	0.74	0.33	0.14
Fuel Compartment	0.68	0.39	0.17
Poison/ Center Basket Plates	0.78	0.36	0.15
Transition Rail	-0.04	0.01	0.00
DSC Shell	0.00	0.01	0.00

Table B.4.6-13
Fuel Assembly Rubble Height in a Fuel Compartment for 32PTH2 DSC

No. Fuel Rods	236
Active Fuel Length, in	150
Fuel Rod OD, in	0.382
$V_{UO2,\ Compact,}$ in^3	5166
$V_{Rubble,}$ in^3 (50% Void Volume)	10331
Fuel Assembly Rubble Length, in	138

Table B.4.6-14
Maximum Fuel Cladding Temperatures for Storage Conditions

Load Case No.[1]	Load Case Description	Time (hr)[3]	Fuel Cladding (°F)	Limit (°F) [B4.3]
S1[2]	Normal Hot Storage, 37.2 kW (HLZC#1)	∞	<727	752
S2[2]	Normal Cold Storage, 37.2 kW (HLZC#1)	∞	<727	
S3	Off-normal Hot storage, 37.2 kW (HLZC#1)	∞	727	
S3A	Off-normal Hot Storage, 37.2 kW (HLZC#1) and 50% AHSM-HS Inlet Vent Blockage.	∞	730	
S4	Off-normal Hot Storage, 35.2 kW (HLZC#2)	∞	707	
S5	Off-normal Hot Storage, 32.0 kW (HLZC#3)	∞	670	1058
S5A	Off-normal Hot Storage, 31.2 kW (HLZC#4)	∞	643	
S6	Off-normal Cold Storage, 37.2 kW (HLZC#1)	∞	613	
S7	Accident storage, 37.2 kW (HLZC#1), Blocked Vents, Transient	40	857	

(1) See Table B.4.4-1 for detail descriptions of load cases.

(2) The results for hot and cold normal storage conditions (Load Cases S1 and S2) are bounded by the results for hot off-normal storage condition (Load Case S3).

(3) Symbol of "∞" indicates a steady-state analysis.

Table B.4.6-15
Maximum Fuel Cladding Temperatures for Transfer Conditions

Load Case No.[1]	Load Case Description	Time (hr)[3]	Fuel Cladding (°F)	Limit (°F) [B4.3]
T1[2]	Normal Hot Transfer, Horizontal, 32.0 kW (HLZC#3)	∞	<730	752
T2[2]	Normal Cold Transfer, Horizontal, 32.0 kW (HLZC#3)	∞	<730	
T3	Off-Normal Hot Transfer, Horizontal, 32.0 kW (HLZC#3)	∞[4]	730	
T4[2]	Off-Normal Cold Transfer, Horizontal, 32.0 kW (HLZC#3)	∞	<730	
T5A	Normal Hot Transfer, Vertical, 31.2 kW (HLZC#4)	∞	725	
T5	Normal Hot Transfer, Vertical Transient, 32.0 kW (HLZC#3)	75	718	
T6	Normal Hot Transfer, Vertical Transient, 37.2 kW (HLZC#1)	36	715	
T7	Off-Normal Hot Transfer, Horizontal Transient, 37.2 kW (HLZC#1)	36	711	
T8	Off-Normal Hot Transfer, Horizontal, Air Circulation, 37.2 kW (HLZC#1)	∞	693	
T9	Accident, Loss of Neutron Shield with Loss of Air Circulation, 37.2 kW (HLZC#1)	∞	887	1058
T10	Off-Normal, Air Circulation turned-off for off-loading DSC to AHSM-HS or Air Circulation Failure during Transfer Operation, 37.2 kW (HLZC#1)	12	709	752
T11	Normal Hot, Vertical, Initial Conditions, 37.2 kW (HLZC#1)	∞	572	
T12	Normal Hot, Vertical Steady-State, Initial Conditions, 32.0 kW (HLZC#3)	∞	540	

(1) See Table B.4.5-1 for detail descriptions of load cases.

(2) The results for normal hot, cold and off-normal cold transfer conditions (Load Cases T1, T2 and T4) are bounded by the results for hot off-normal storage condition (Load Case T3).

(3) Symbol of "∞" indicates a steady-state analysis.

(4) Although Load Case T3 is analyzed for steady-state conditions, a time limit of 75 hours is selected for transfer operations of the 32PTH2 DSC in the OS200FC TC with heat loads > 31.2 kW and ≤ 32.0 kW (HLZC #3) for conservatism.

Table B.4.6-16
Maximum 32PTH2 DSC Component Temperatures for Storage Conditions

Load Case No.[1]	Time (hr)[3]	Fuel Compartment (°F)	Transition Rails (°F)	Top Shield Plug (°F)	Bottom Shield Plug (°F)	DSC Shell (°F)
S1[2]	<704	<704	<493	<282	<317	<420
S2[2]	<704	<704	<493	<282	<317	<420
S3	704	704	493	282	317	420
S3A	707	707	497	286	320	425
S4	680	679	477	275	309	408
S5	637	637	451	264	295	388
S5A	616	616	444	261	292	382
S6	584	584	363	126	178	292
S7 [3]	839	839	656	420	409	612

(1) See Table B.4.4-1 for detail descriptions of load cases.

(2) The results for hot and cold normal storage conditions (Load Cases S1 and S2) are bounded by the results for hot off-normal storage condition (Load Case S3).

(3) The temperatures for Load Case S7 are calculated at 40 hours for blocked vent accident condition.

Table B.4.6-17
Maximum 32PTH2 DSC Component Temperatures for Transfer Conditions

Load Case No.[1]	Time (hr)[3]	Fuel Compartment (°F)	Transition Rails (°F)	Top Shield Plug (°F)	Bottom Shield Plug (°F)	DSC Shell (°F)
T1[2]	∞	<700	<529	<431	<441	<473
T2[2]	∞	<700	<529	<431	<441	<473
T3	∞[4]	700	529	431	441	473
T4[2]	∞	<700	<529	<431	<441	<473
T5A	∞	702	529	456	469	467
T5	75	691	509	416	429	449
T6	36	694	504	377	387	441
T7	36	683	506	367	375	449
T8	∞	668	467	390	273	404
T9	∞	869	676	552	564	615
T10	12	687	500	400	321	443
T11	∞	540	311	282	264	262
T12	∞	498	296	272	256	254

(1) See Table B.4.5-1 for detail descriptions of load cases.

(2) The results for normal hot, cold and off-normal cold transfer conditions (Load Case T1, T2 and T4,) are bounded by the results for hot off-normal storage condition (Load Case T3).

(3) Symbol of "∞" indicates a steady-state analysis.

(4) Although Load Case T3 is analyzed for steady-state conditions, a time limit of 75 hours is selected for transfer operations of the 32PTH2 DSC in the OS200FC TC with heat loads > 31.2 kW and ≤ 32.0 kW (HLZC #3) for conservatism.

Table B.4.6-18
Average Temperatures of 32PTH2 DSC Components for Storage and Transfer Conditions

Component					Hottest DSC Section [5]			
Load Case No.[1]	Time (hr)[4]	Fuel Assembly (°F)	Cavity Gas (°F)	DSC Shell (°F)	Fuel Compartment (°F)	R90 Transition Rail @ 180° (°F)	R90 Transition Rail @ 0° (°F)	DSC Shell (°F)
S1 [2]	∞	<586	<426	<387	<593	<462	<471	<409
S2 [2]	∞	<586	<426	<387	<593	<462	<471	<409
S3	∞	586	426	387	593	462	471	409
S3A	∞	590	430	390	597	464	475	412
S4	∞	565	413	376	571	448	456	397
S5	∞	531	392	357	535	424	432	377
S5A	∞	521	386	353	524	418	426	372
S6	∞	467	294	249	470	339	337	273
S7	40	726	571	552	742	612	638	589
T1[3]	∞	<594	<474	<430	<598	<448	<515	<443
T2[3]	∞	<594	<474	<430	<598	<448	<515	<443
T3	∞	594	474	430	598	448	515	443
T4[3]	∞	<594	<474	<430	<598	<448	<515	<443
T5A	∞	609	496	454	612	512	512	465
T5	75	590	471	433	594	492	492	446
T6	36	591	454	421	597	484	484	438
T7	36	577	438	402	583	423	489	419
T8	∞	551	419	354	555	433	397	366
T9	∞	751	613	571	764	616	658	597
T10	12	580	450	405	587	441	479	423
T11	∞	429	286	215	423	286	286	213
T12	∞	397	275	215	391	276	276	213

(1) See Table B.4.4-1 and Table B.4.5-1 for a description of the load cases.

(2) The results for hot and cold normal storage conditions (Load Cases S1 and S2) are bounded by the results for hot off-normal storage condition (Load Case S3).

(3) The results for hot and cold normal storage conditions (Load Cases S1 and S2) are bounded by the results for hot off-normal storage condition (Load Case S3).

(4) Symbol of "∞" indicates a steady-state analysis.

(5) Average values are based on the hottest 32PTH2 DSC cross section at the maximum fuel cladding temperature.

Table B.4.6-19
Maximum Temperatures for 32PTH2 DSC with Damaged Fuel Assemblies

	Fuel Cladding (°F)	Fuel Compartment (°F)	Transition Rails (°F)
32PTH2, 37.2 kW, Load Case T9, Intact Fuel (see Table B.4.6-15 and Table B.4.6-17)	887	869	676
32PTH2, 37.2 kW, Load Case T9, (16 Intact FAs and 16 Damaged FAs as Rubble with Helium Conductivity)	900	883	679
Maximum Difference	+13	+14	+3

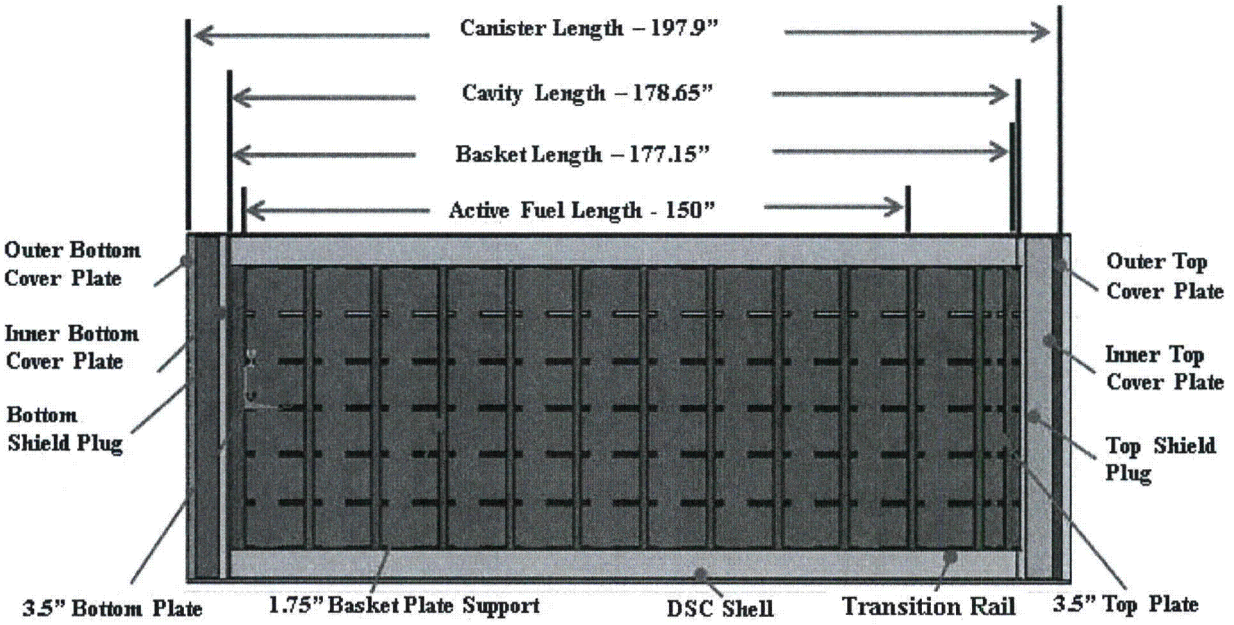

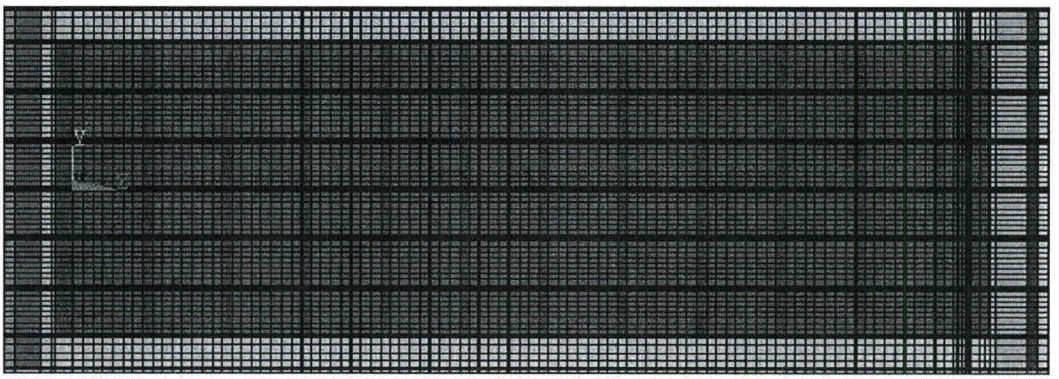

Mesh Density

Figure B.4.6-1
Finite Element Model of 32PTH2 DSC – Longitudinal Section

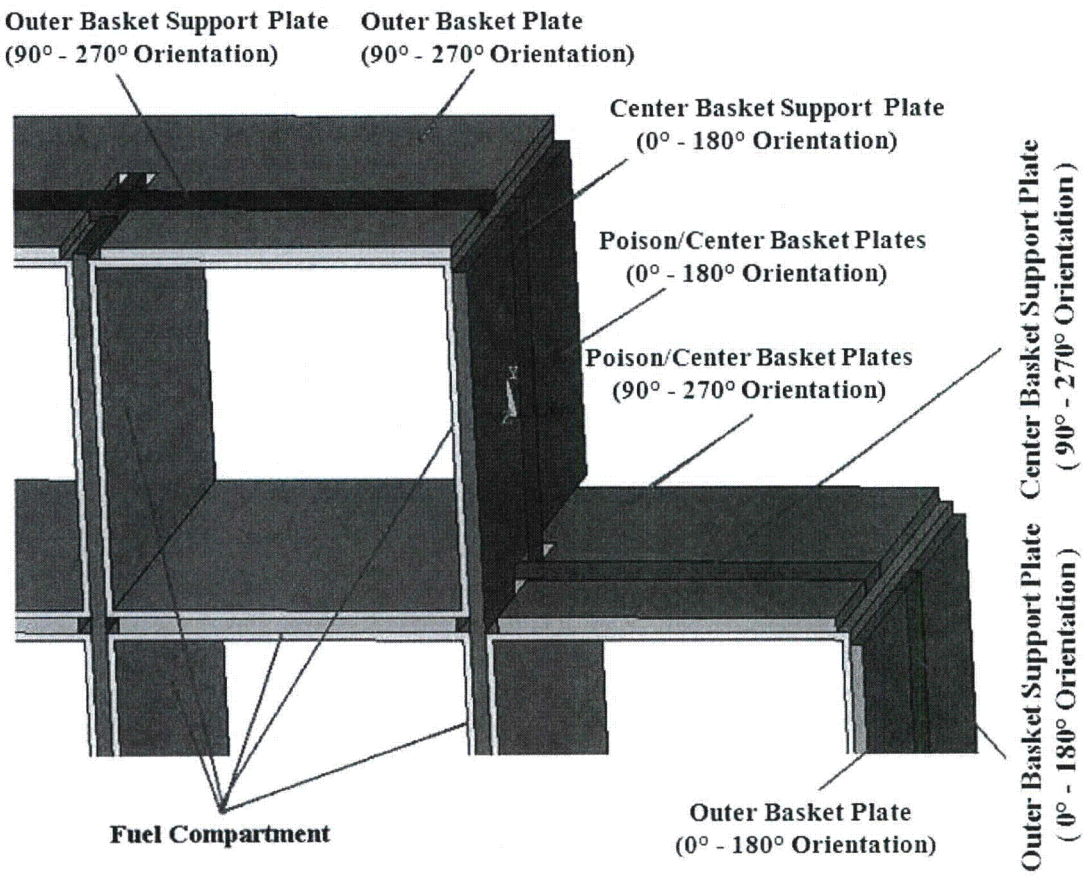

Basket Plate Locations

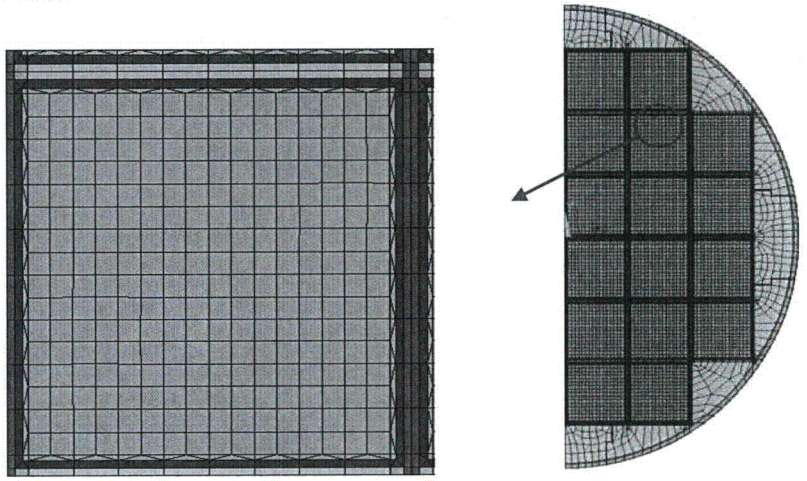

Mesh Density

Figure B.4.6-2
32PTH2 DSC Model – Cross Section

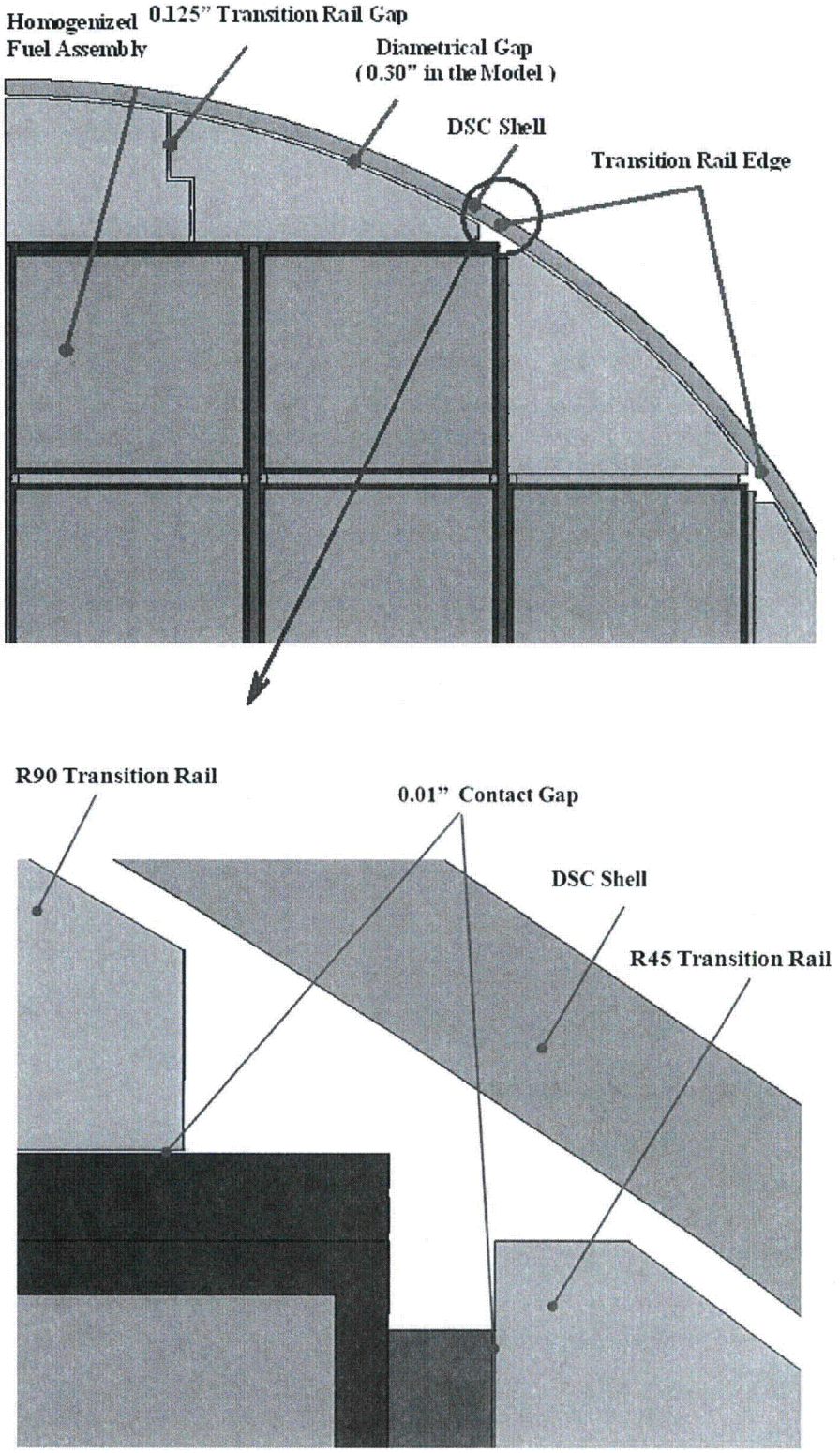

Figure B.4.6-3
32PTH2 DSC Model – Gaps in the Basket Assembly

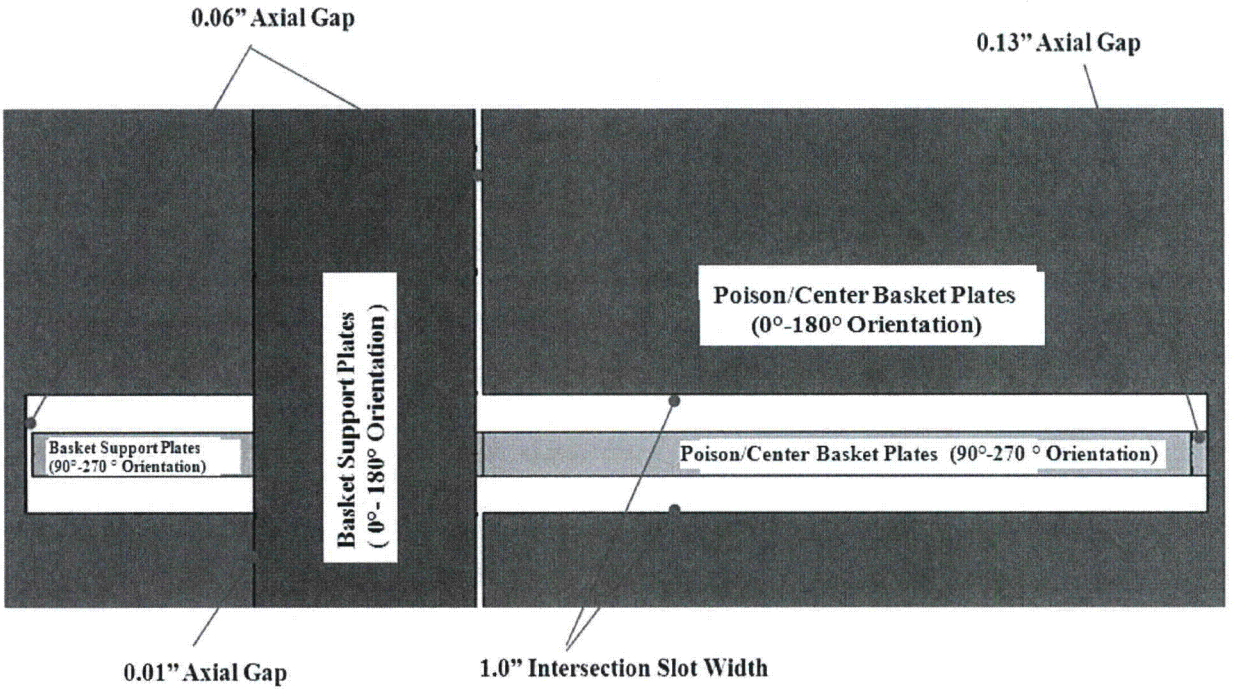

Basket Support Plate and Paired Poison/Center Basket Plates

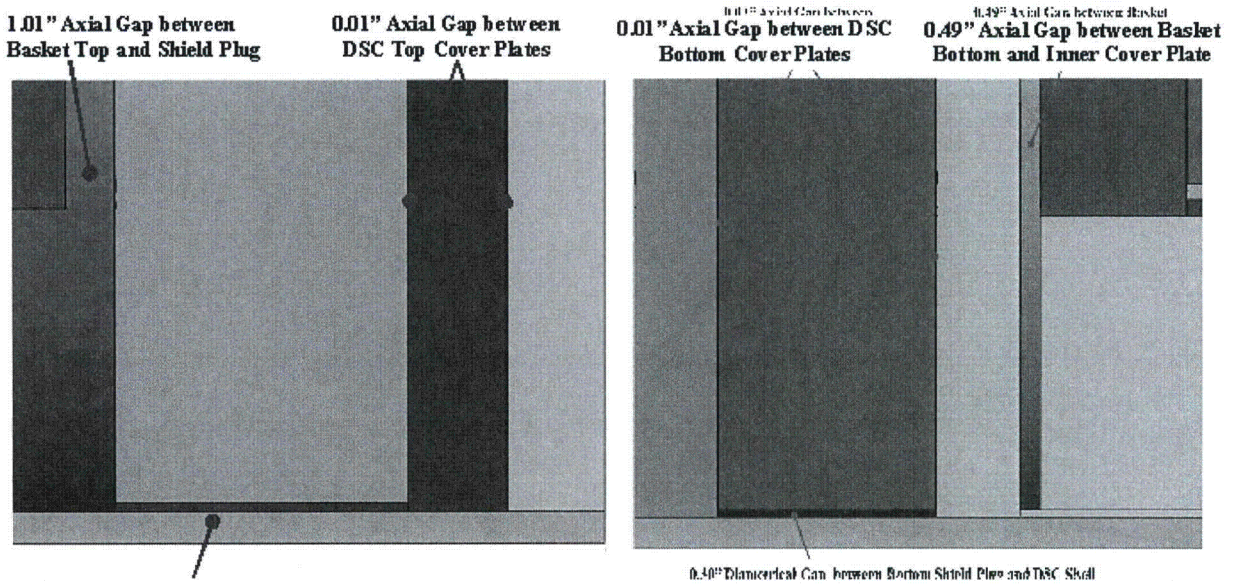

DSC Top End Plates

DSC Bottom End Plates

Figure B.4.6-4
32PTH2 DSC Model – Axial Gaps at DSC Ends

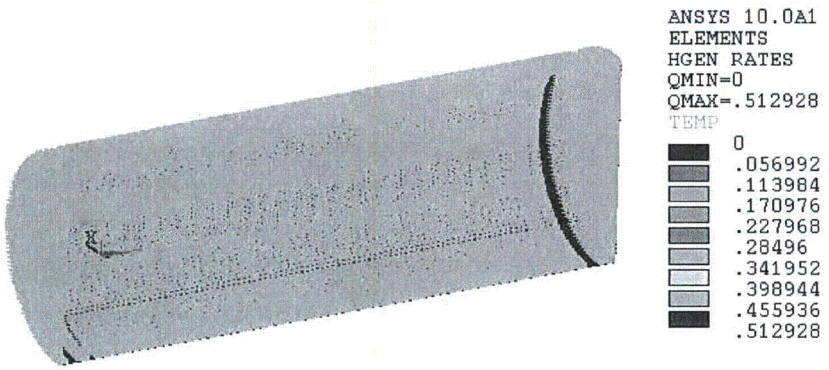

Temperature Boundary Condition and Heat Generation Rate

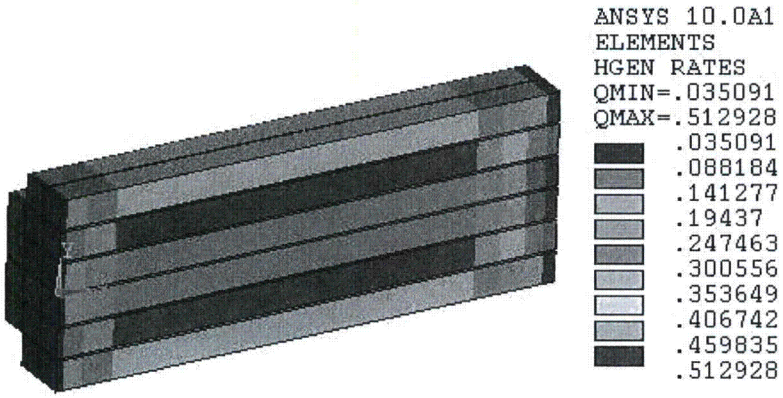

37.2 kW Heat Load (HLZC#1)

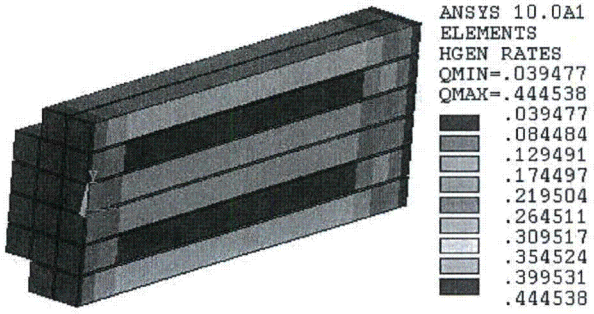

35.2 kW Heat Load (HLZC#2)

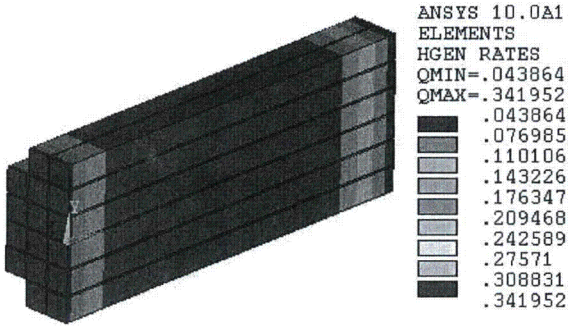

32.0 kW Heat Load (HLZC#3)

Figure B.4.6-5
Typical Boundary Conditions for 32PTH2 DSC Model

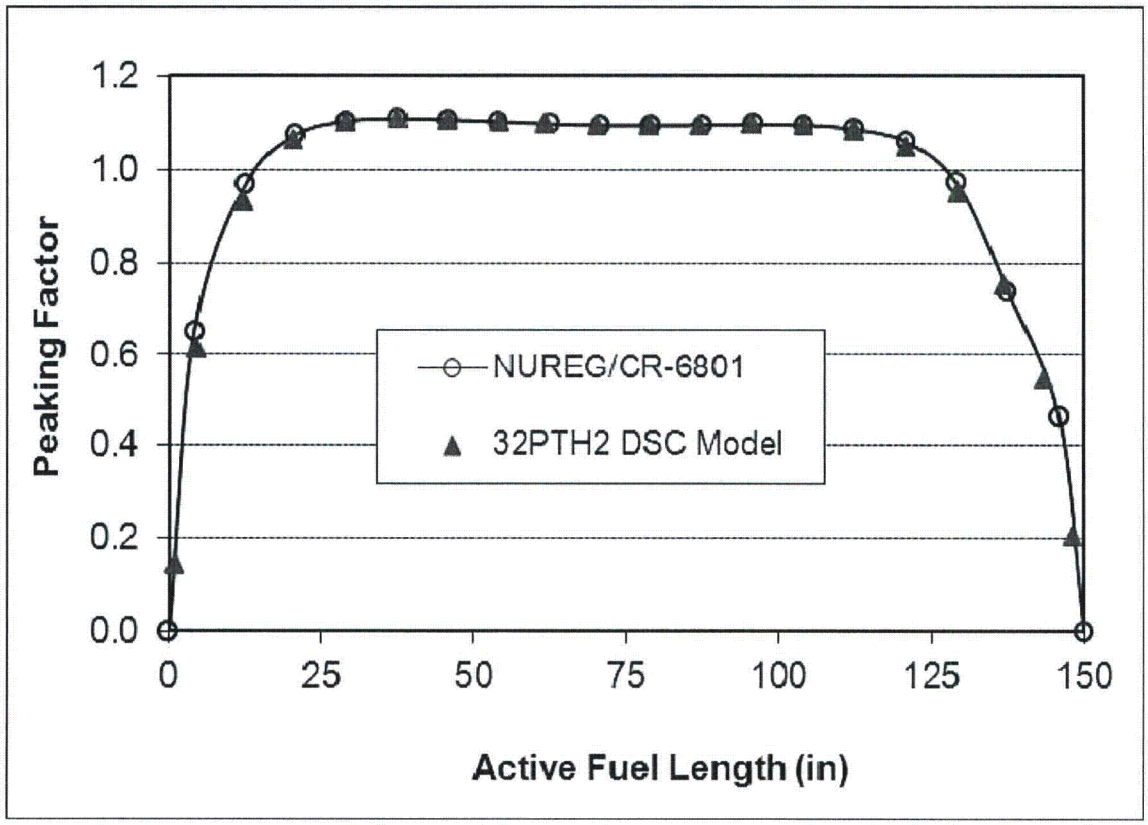

Figure B.4.6-6
Peaking Factor Curve for PWR Fuel Assemblies

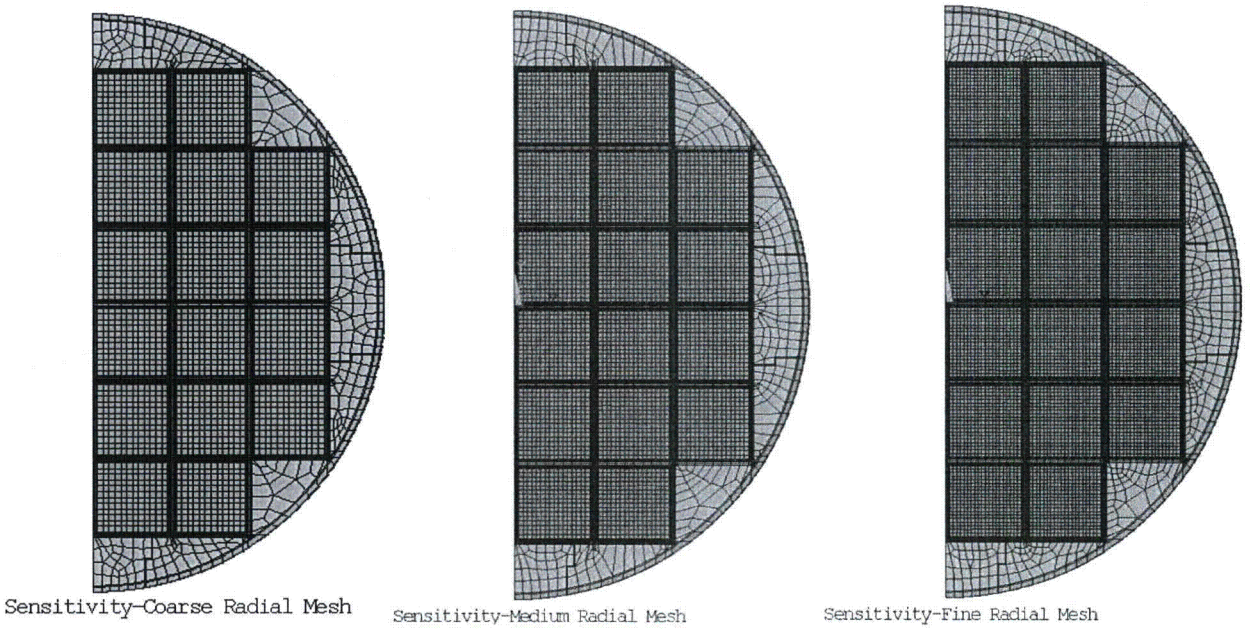

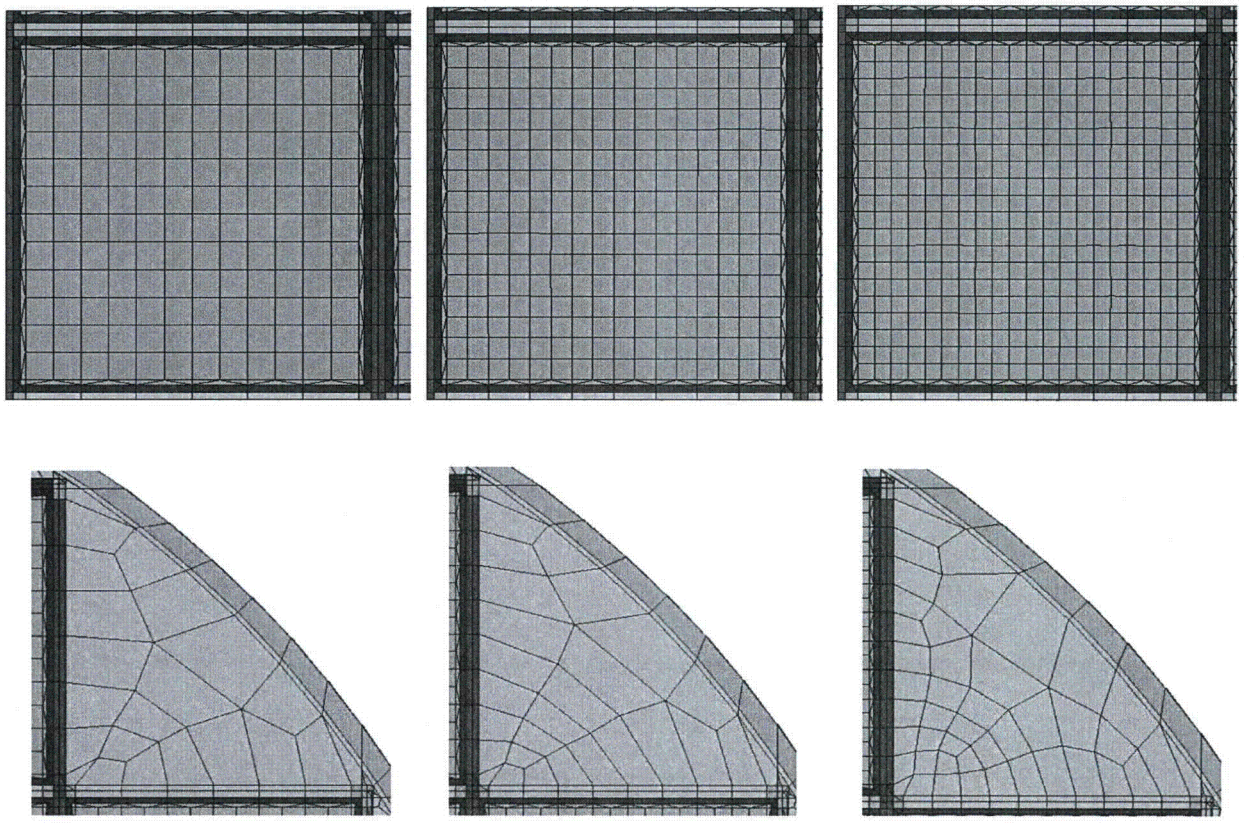

Figure B.4.6-7
Mesh Densities of 32PTHT2 DSC Model in Radial Direction

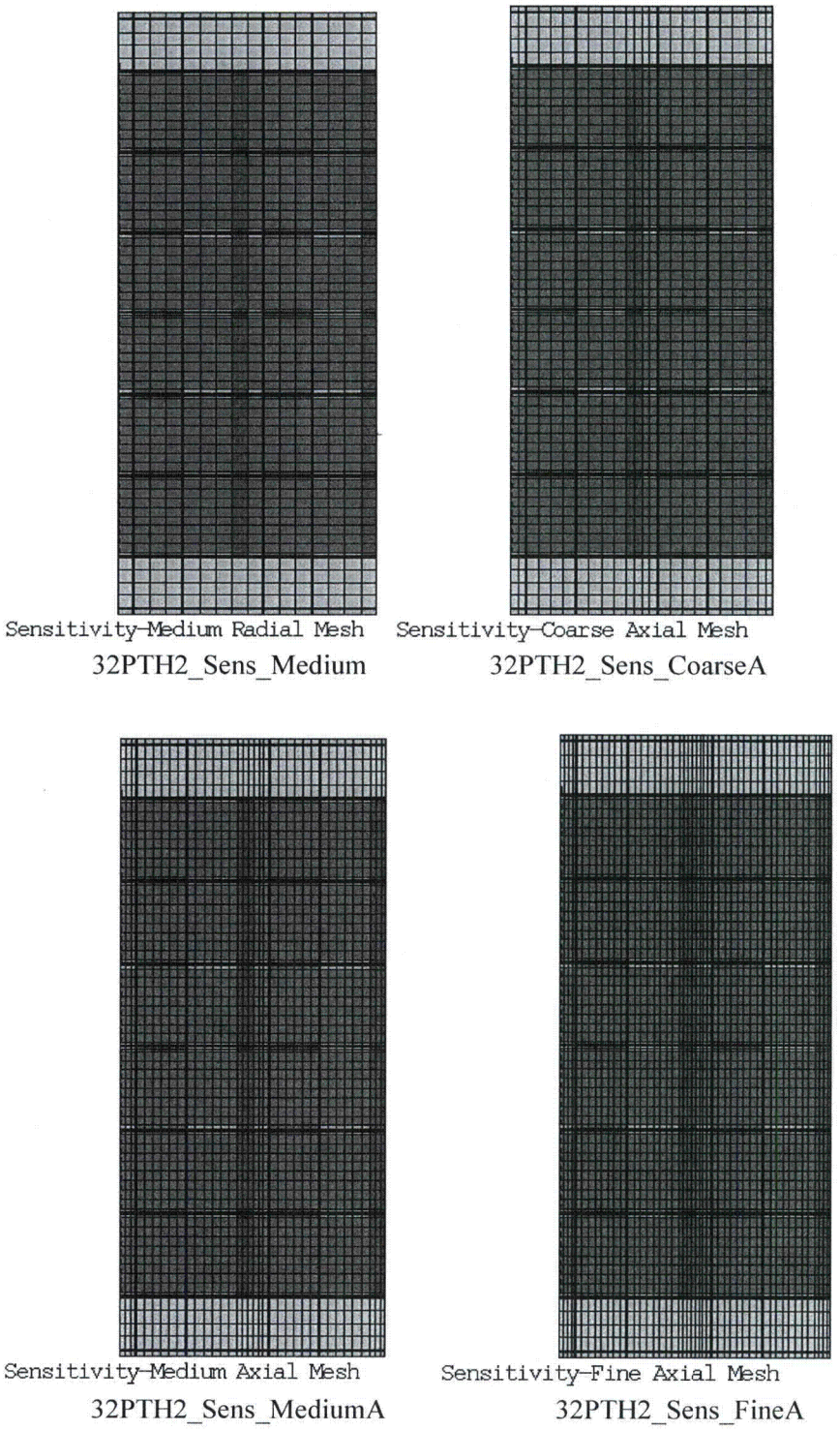

Figure B.4.6-8
Mesh Densities of 32PTH2 DSC Model in Axial Direction

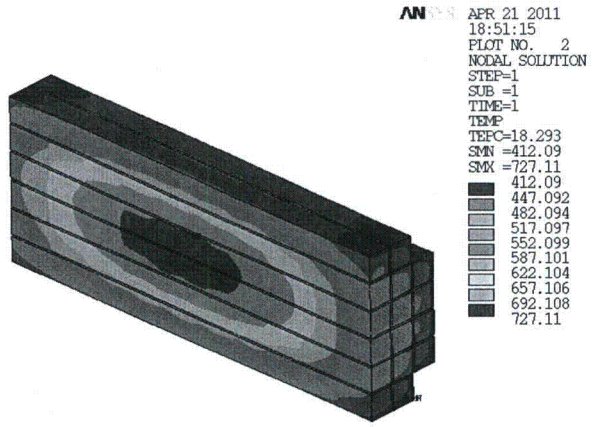

Off-Normal 107F, 32PTH2 DSC in AHSM-HS - HLZC#1 (32PTH2_S3 Load No.1)

Fuel Cladding

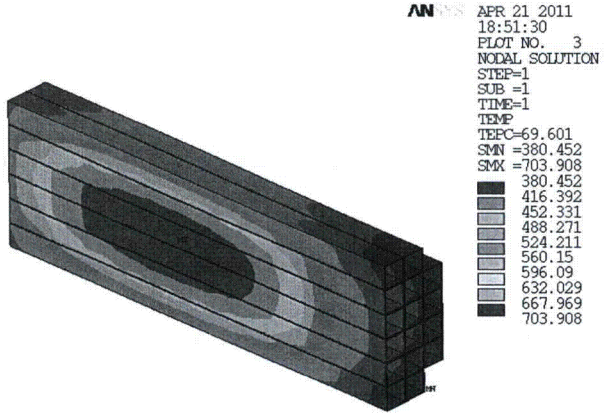

Off-Normal 107F, 32PTH2 DSC in AHSM-HS - HLZC#1 (32PTH2_S3 Load No.1)

Fuel Compartment

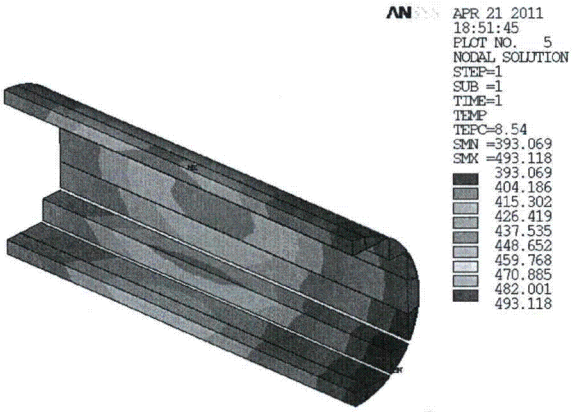

Off-Normal 107F, 32PTH2 DSC in AHSM-HS - HLZC#1 (32PTH2_S3 Load No.1)

Transition Rail

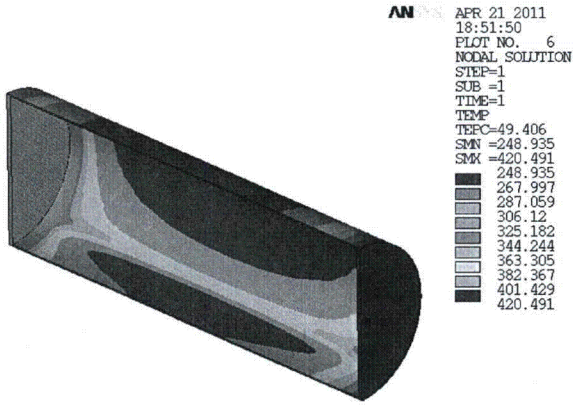

Off-Normal 107F, 32PTH2 DSC in AHSM-HS - HLZC#1 (32PTH2_S3 Load No.1)

32PTH2 DSC Shell

Figure B.4.6-9
Temperature Plots for 32PTH2 DSC
Off-Normal Storage @ 117°F, 37.2 kW/HLZC#1 (Load Case S3)

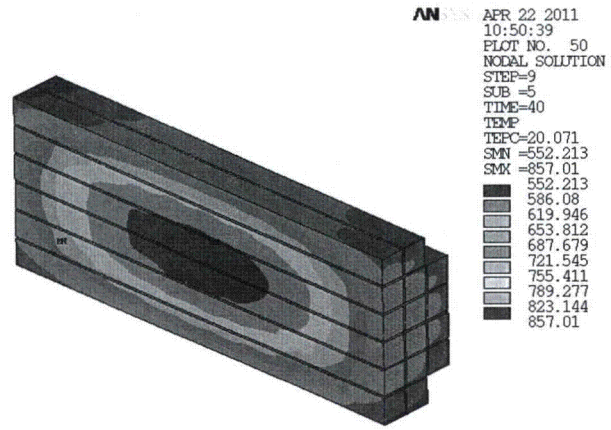

Blocked Vent @ 107F, 32PTH2 DSC in AHSM-HS - HLZC#1 (32PTH2_S7)

Fuel Cladding

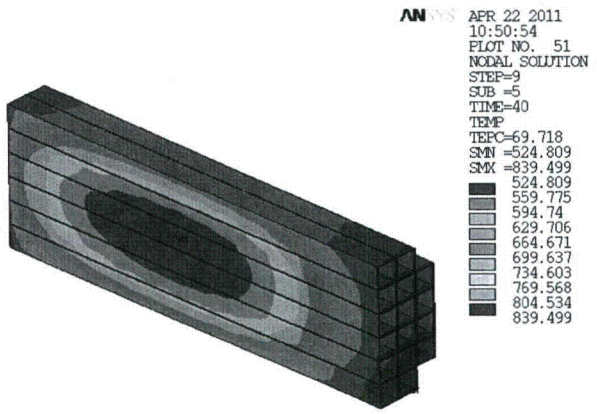

Blocked Vent @ 107F, 32PTH2 DSC in AHSM-HS - HLZC#1 (32PTH2_S7)

Fuel Compartment

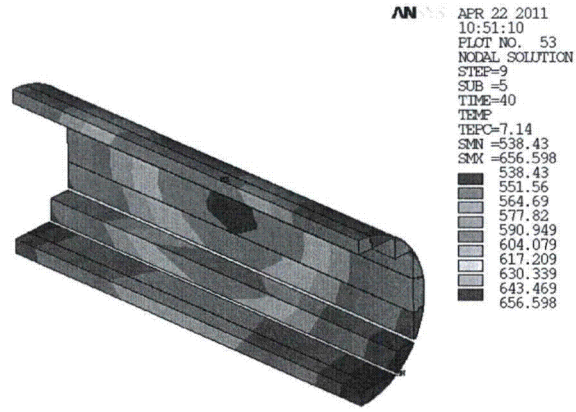

Blocked Vent @ 107F, 32PTH2 DSC in AHSM-HS - HLZC#1 (32PTH2_S7)

Transition Rail

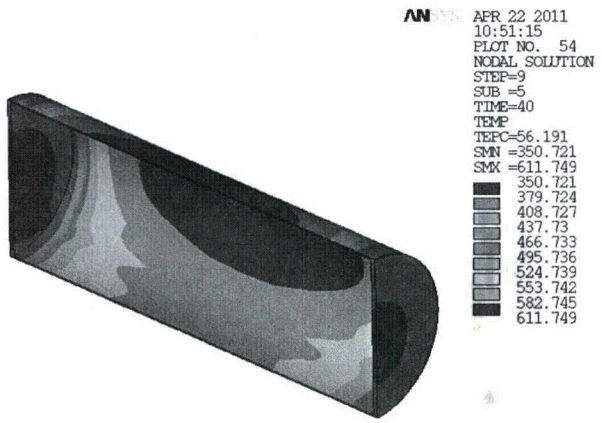

Blocked Vent @ 107F, 32PTH2 DSC in AHSM-HS - HLZC#1 (32PTH2_S7)

32PTH2 DSC Shell

Figure B.4.6-10
Temperature Plots for 32PTH2 DSC
Blocked Vent @ 40 Hour, 117°F, 37.2 kW/HLZC#1 (Load Case S7)

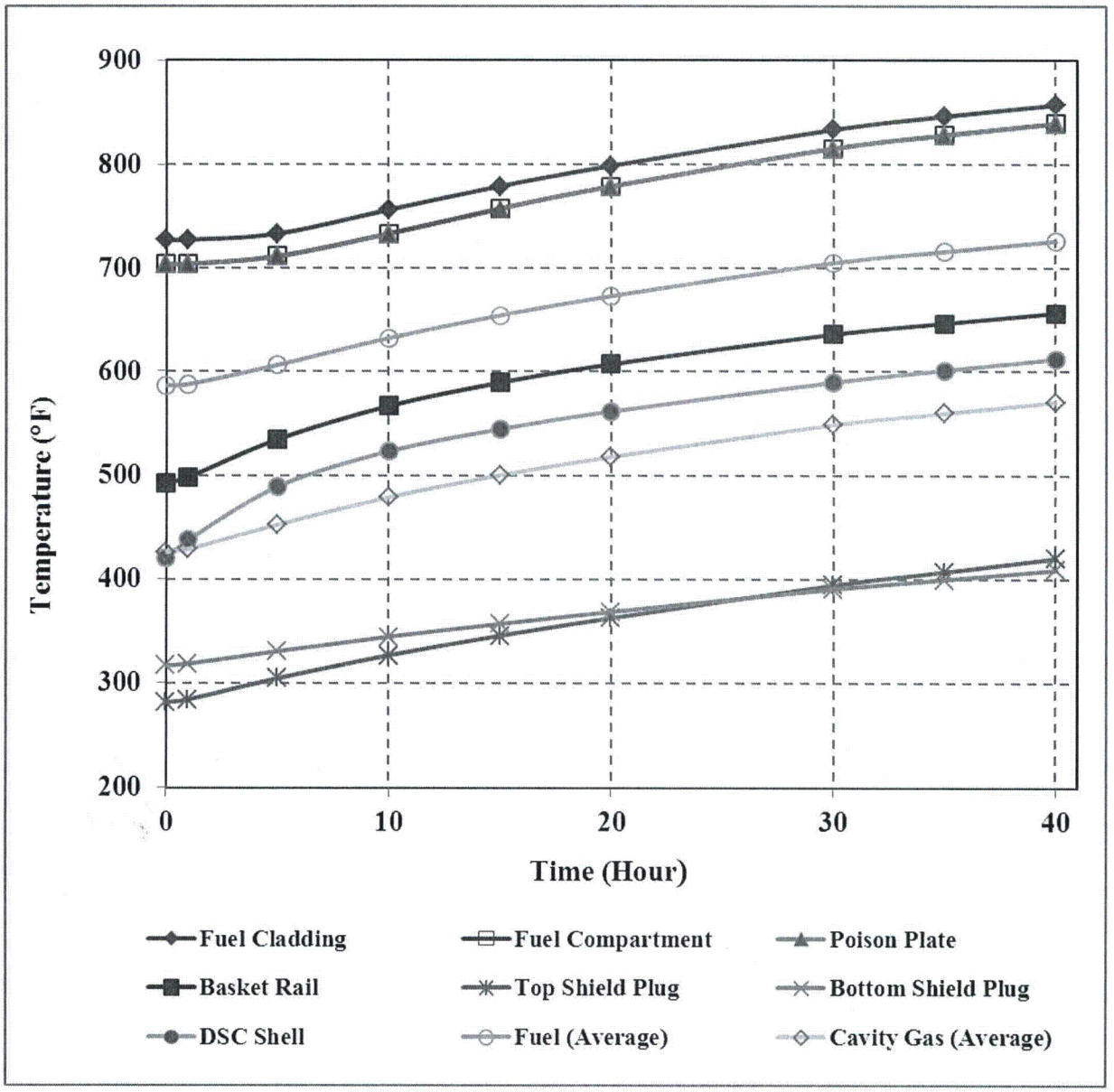

Figure B.4.6-11
Time-Temperature Histories for 32PTH2 DSC, Blocked Vent, 37.2 kW/HLZC#1 (Load Case S7)

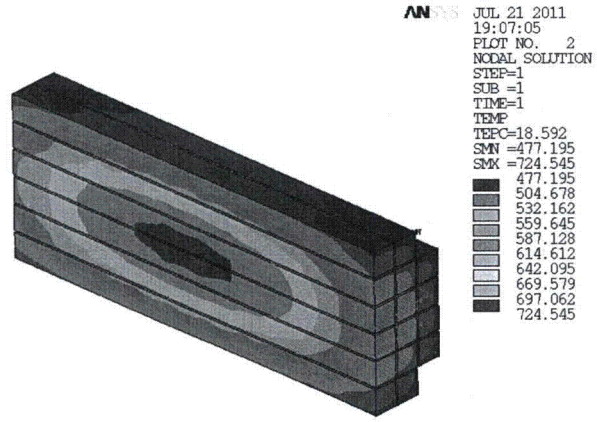

32PTH2 DSC in TC Vertical-Normal-Steady-State,120F,31 kW(HL2C#4)

Fuel Cladding

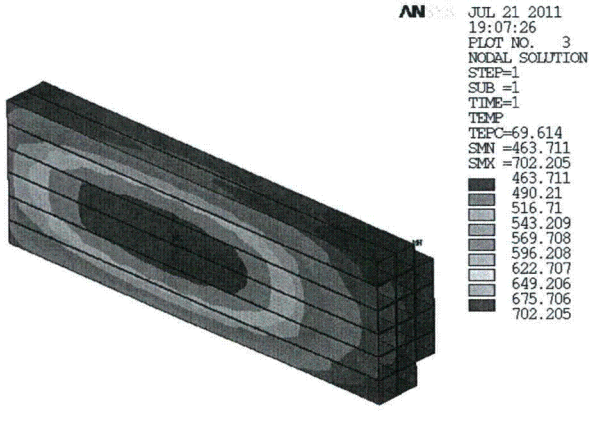

32PTH2 DSC in TC Vertical-Normal-Steady-State,120F,31 kW(HL2C#4)

Fuel Compartments

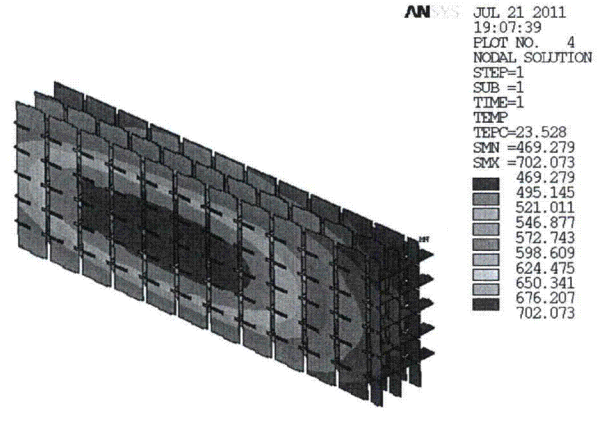

32PTH2 DSC in TC Vertical-Normal-Steady-State,120F,31 kW(HL2C#4)

Paired Poison Plates/Center Basket Plates

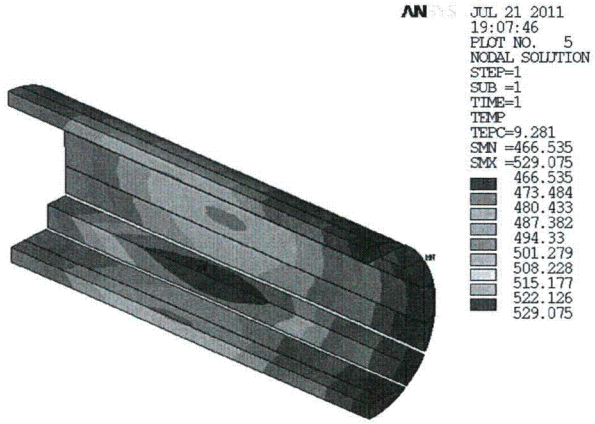

32PTH2 DSC in TC Vertical-Normal-Steady-State,120F,31 kW(HL2C#4)

Transition Rails

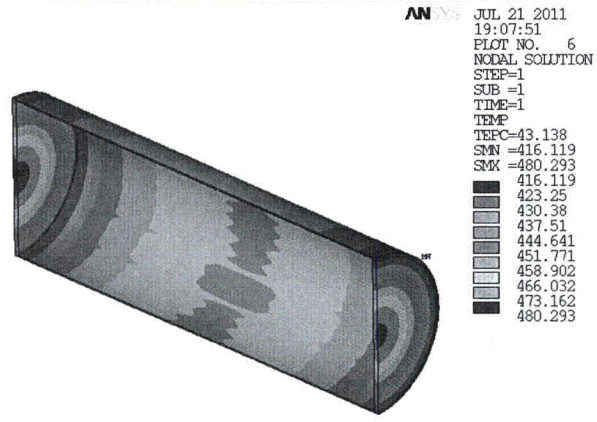

32PTH2 DSC in TC Vertical-Normal-Steady-State,120F,31 kW(HL2C#4)

DSC Shell

Figure B.4.6-12
Temperature Distribution for 32PTH2 DSC with 31.2 kW in OS200FC TC , without Air Circulation, Normal Hot, Vertical Steady-State Operations (Load Case T5A)

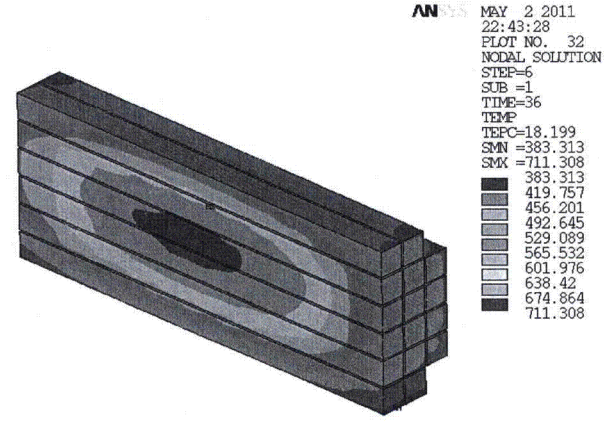

32PTH2 DSC in TC Off-Normal-Transient,107F, 37.2 kW (HL2C#1)

Fuel Cladding

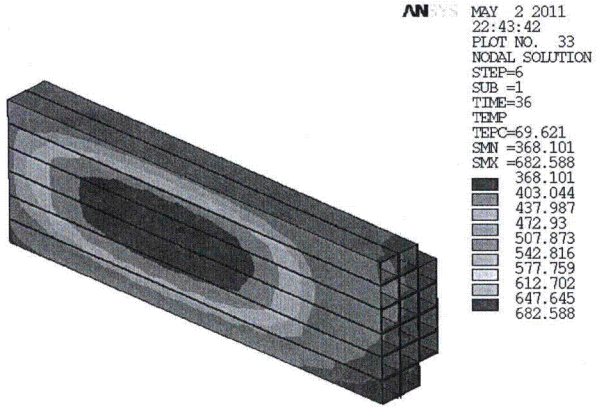

32PTH2 DSC in TC Off-Normal-Transient,107F, 37.2 kW (HL2C#1)

Fuel Compartments

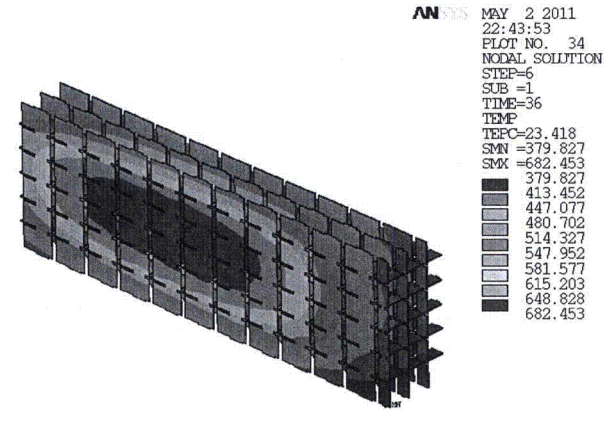

32PTH2 DSC in TC Off-Normal-Transient,107F, 37.2 kW (HL2C#1)

Paired Poison Plates/Center Basket Plates

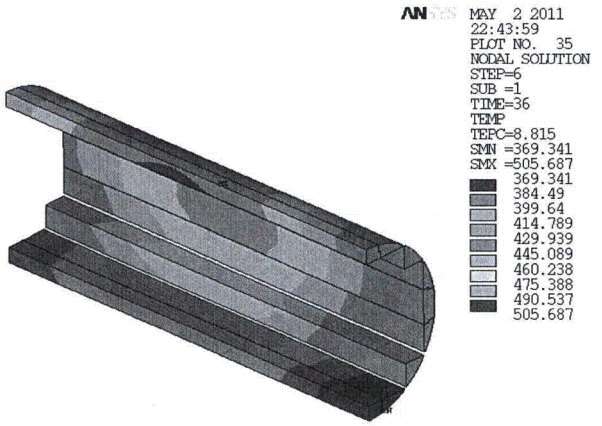

32PTH2 DSC in TC Off-Normal-Transient,107F, 37.2 kW (HL2C#1)

Transition Rails

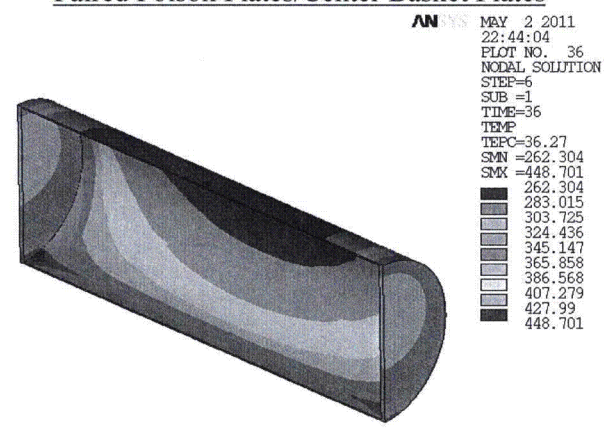

32PTH2 DSC in TC Off-Normal-Transient,107F, 37.2 kW (HL2C#1)

DSC Shell

Figure B.4.6-13
Temperature Distribution for 32PTH2 DSC with 37.2 kW in OS200FC TC, without Air Circulation, Off-Normal Hot, Horizontal Transient Operations at 36 hrs (Load Case T7)

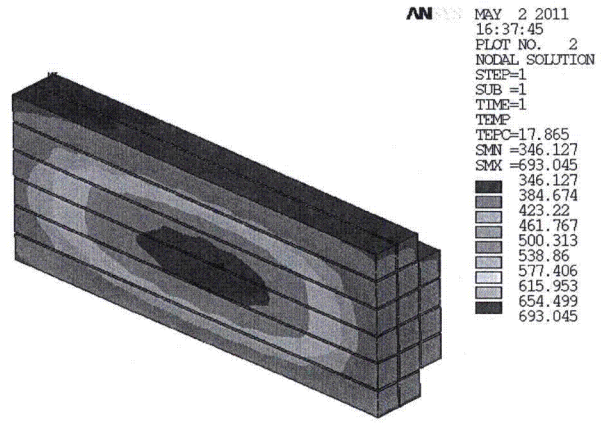

Fuel Cladding

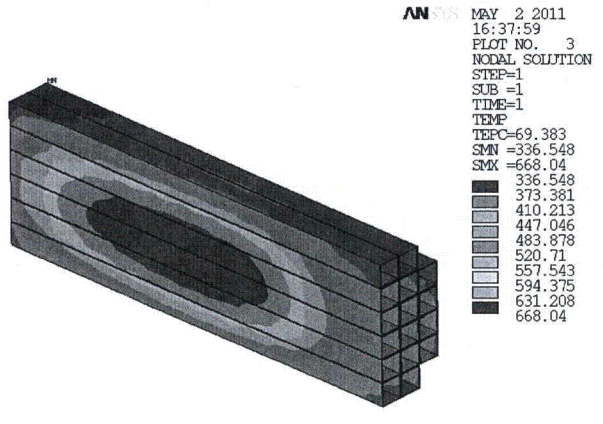

Fuel Compartments

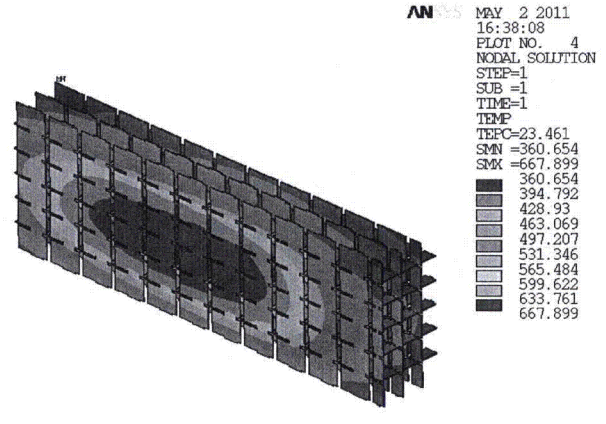

Paired Poison Plates/Center Basket Plates

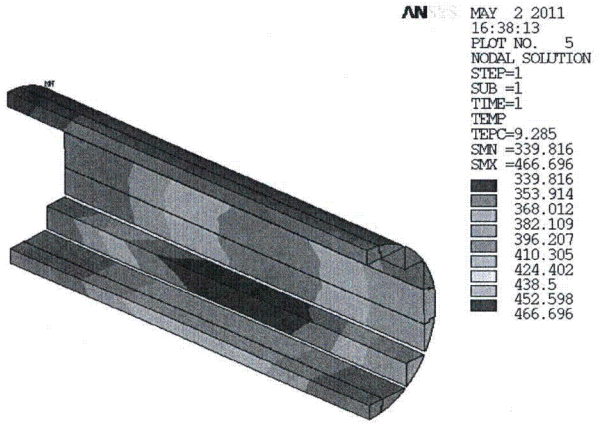

Transition Rails

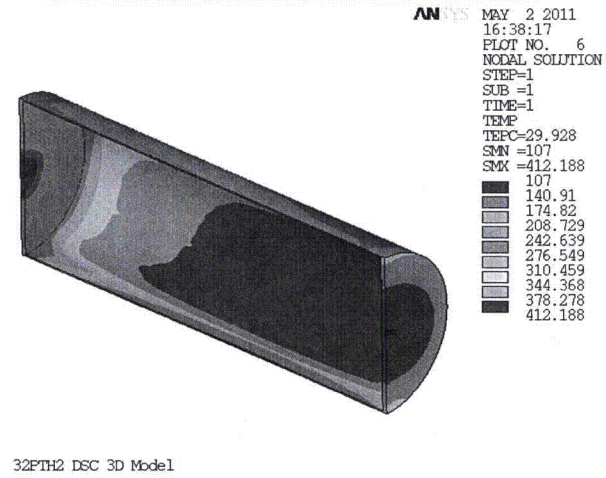

DSC Shell

Figure B.4.6-14
Temperature Distribution for 32PTH2 DSC with 37.2 kW in OS200FC TC, with Air Circulation, Off-Normal Hot, Horizontal Steady-State Operations (Load Case T8)

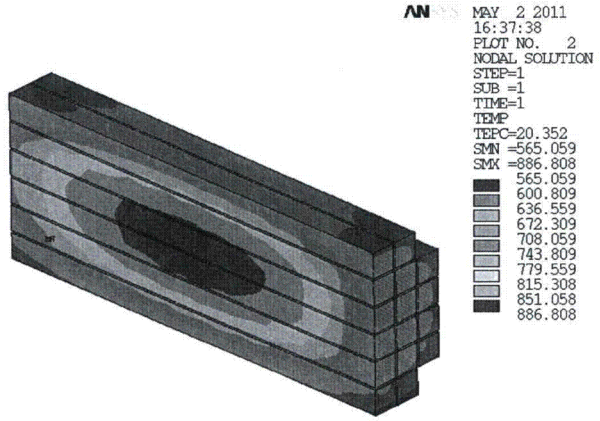

32PTH2 DSC 3D Model

Fuel Cladding

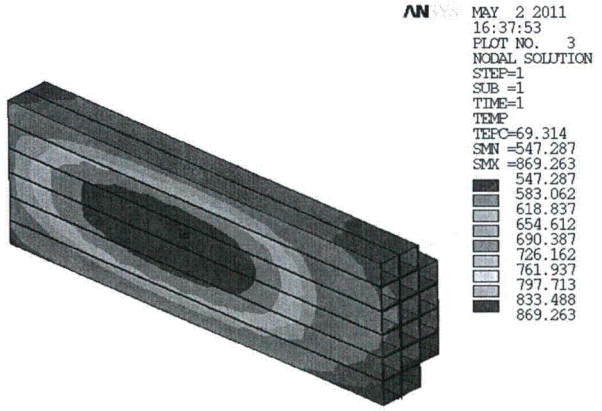

32PTH2 DSC 3D Model

Fuel Compartments

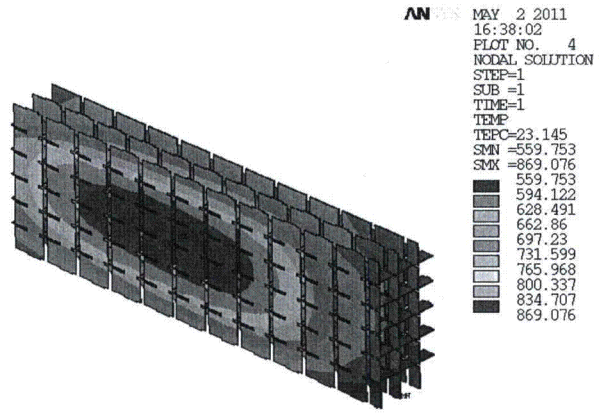

32PTH2 DSC 3D Model

Paired Poison Plates/Center Basket Plates

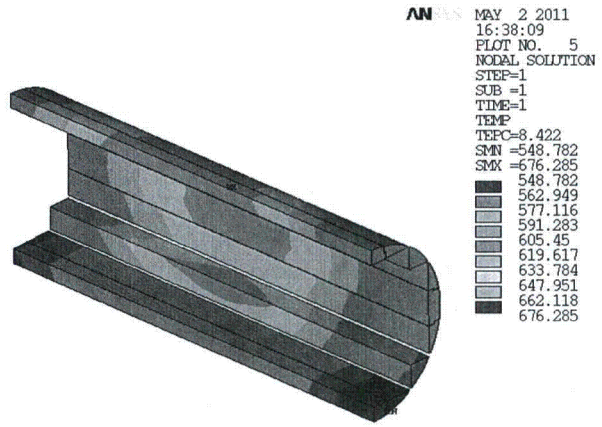

32PTH2 DSC 3D Model

Transition Rails

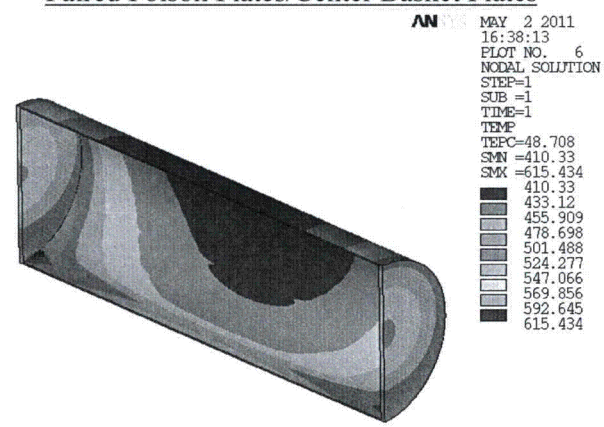

32PTH2 DSC 3D Model

DSC Shell

Figure B.4.6-15
Temperature Distribution for 32PTH2 DSC with 37.2 kW in OS200FC TC, Accident, Loss of Neutron Shield with Loss of Air Circulation Accident Condition (Load Case T9)

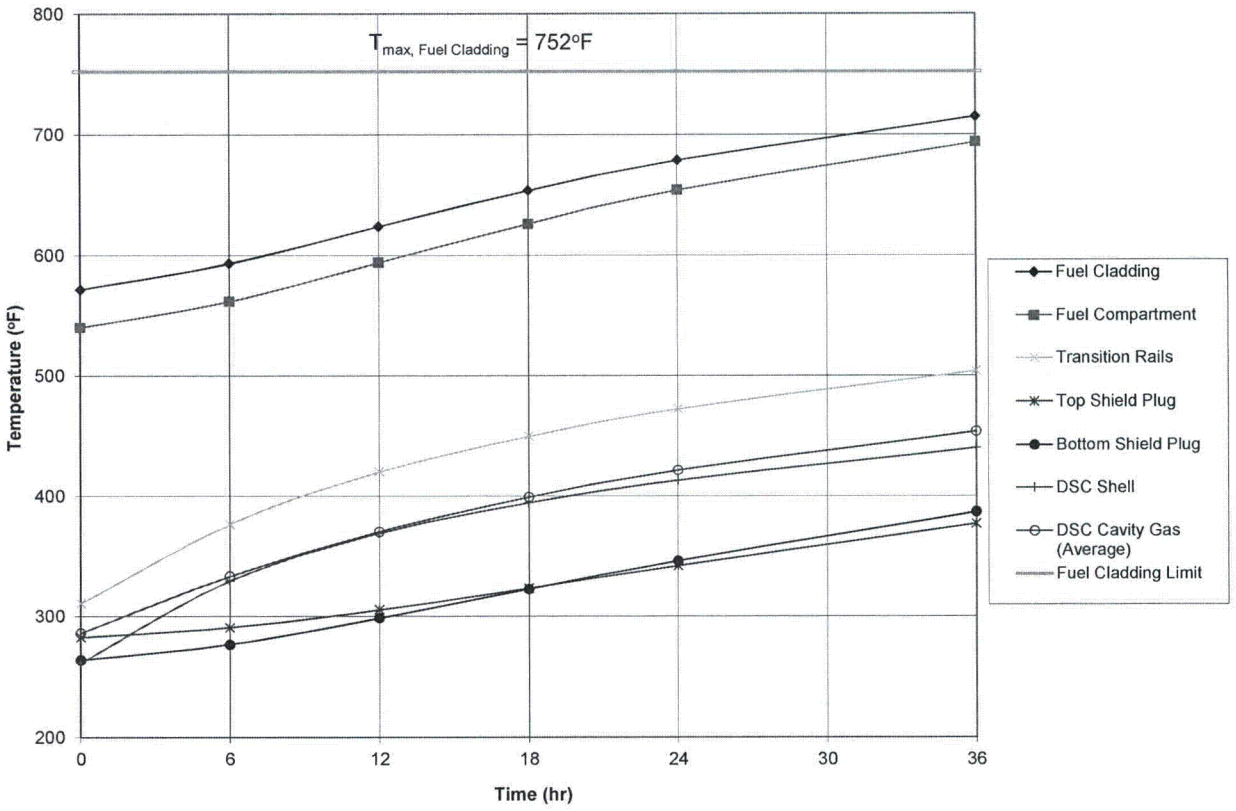

Figure B.4.6-16
Temperature Time History for 32PTH2 DSC with 37.2 kW in OS200FC TC, without Air Circulation, Normal Hot, Vertical Transient Operations (Load Case T6)

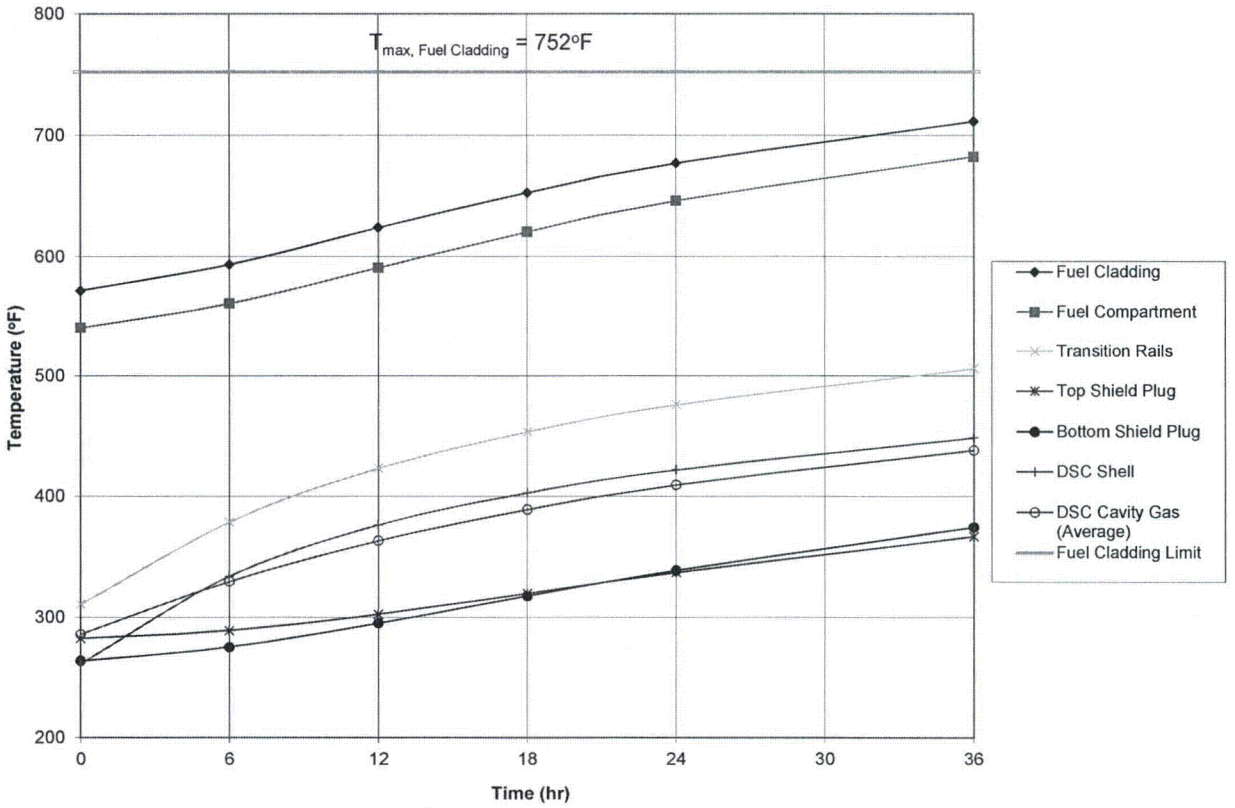

Figure B.4.6-17
Temperature Time History for 32PTH2 DSC with 37.2 kW in OS200FC TC, without Air Circulation, Off-Normal Hot, Horizontal, Transient Operations (Load Case T7)

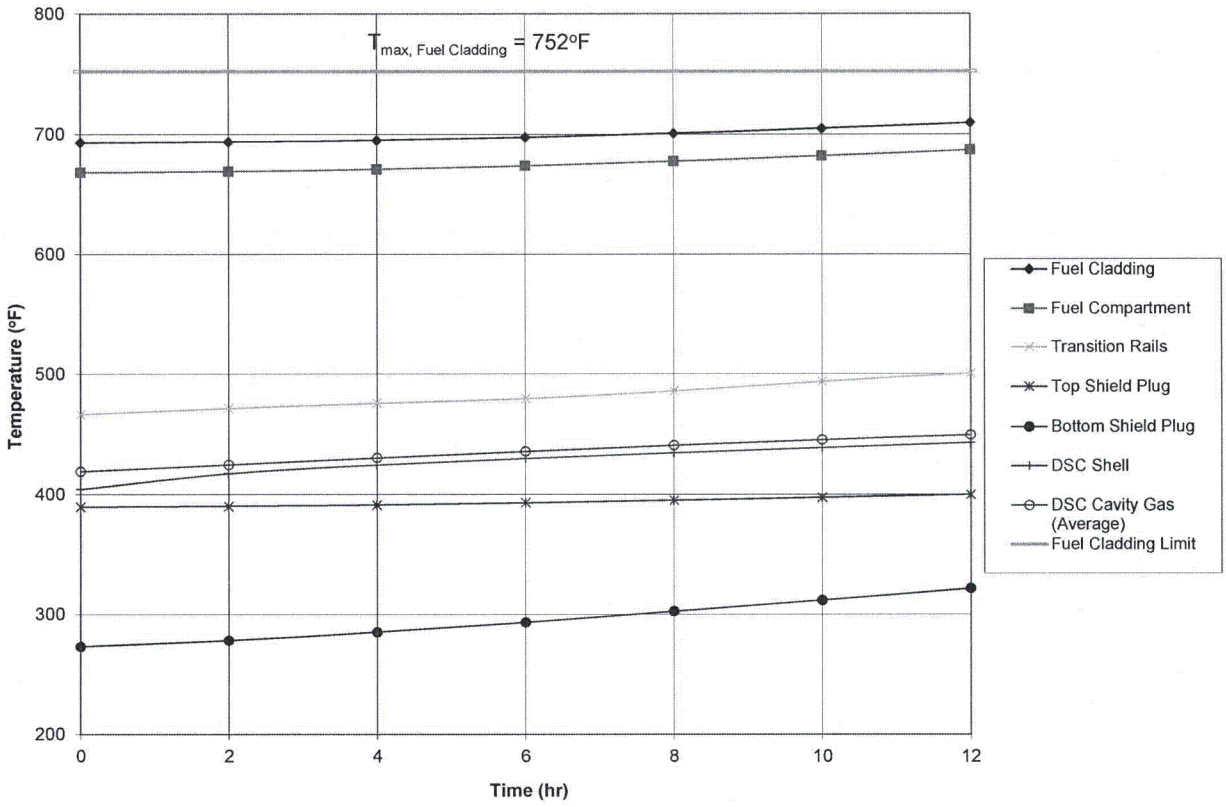

Figure B.4.6-18
Temperature Time History for 32PTH2 DSC with 37.2 kW in OS200FC TC, Air Circulation turned off/ Air Circulation Failure during Transfer Operations (Load Case # T10)

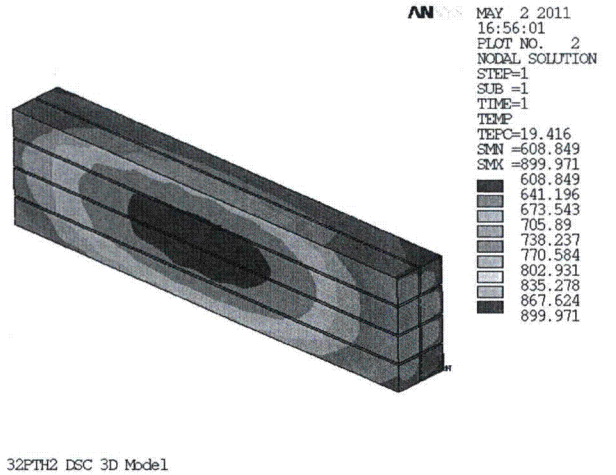

Fuel Cladding

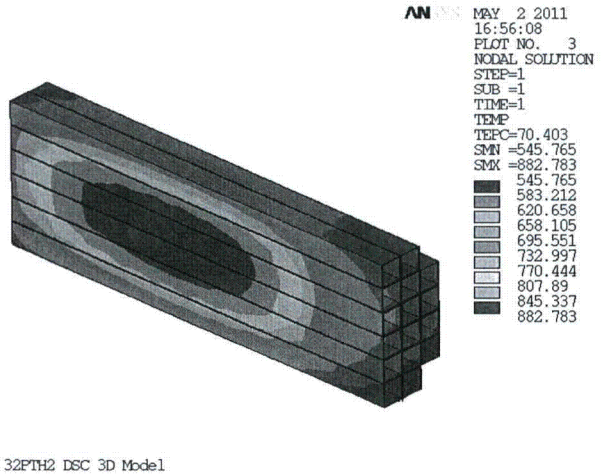

Fuel Compartments

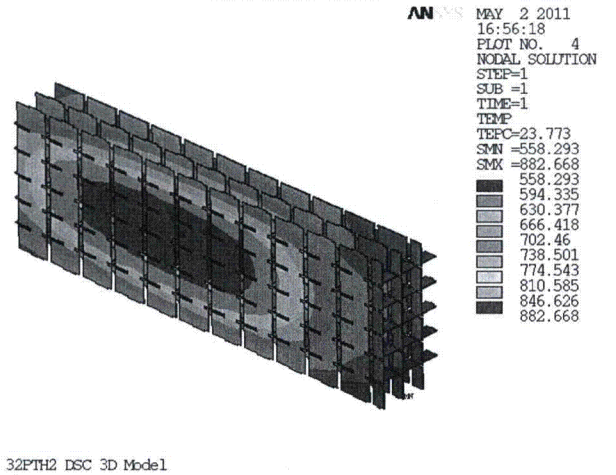

Paired Poison Plates/Center Basket Plates

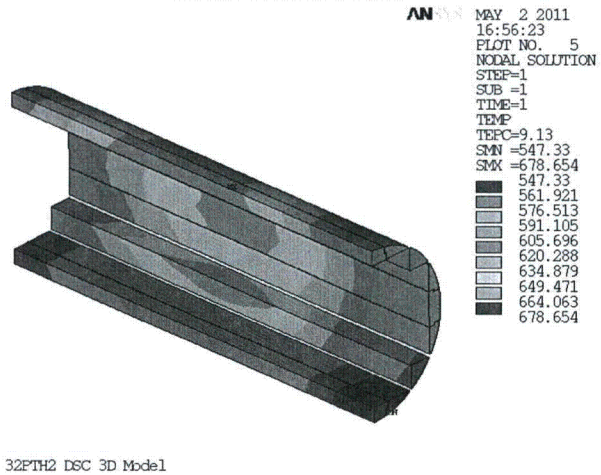

Transition Rails

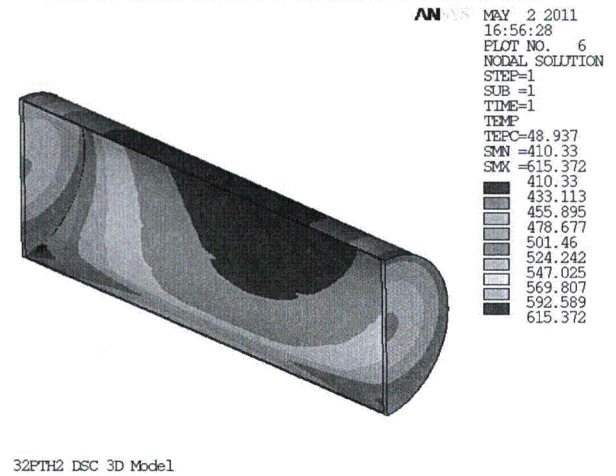

DSC Shell

Figure B.4.6-19
Temperature Distribution for 32PTH2 DSC with 37.2 kW with Damaged FAs in OS200FC TC, Accident, Loss of Neutron Shield with Loss of Air Circulation Accident Condition

B.4.7 Maximum Internal Pressures

The calculation of the maximum internal pressures for the 32PTH2 DSC is described in this section for normal, off-normal, and accident conditions. The calculations account for the 32PTH2 DSC free volume, the quantities of DSC backfill gas, fuel rod fill gas, and fission products and the average DSC cavity gas temperature. The internal DSC pressures are then calculated using ideal gas law (PV=nRT).

$$P_{DSC} = \frac{\left(1.4504 * 10^{-4} \frac{psia}{Pa}\right) * (n_{total}) * R * T_{cavity,avg} * (5/9K/^{\circ}R)}{V_{free\_in\_cavity} * (1.6387 * 10^{-5} m^3/in^3)}$$

Where:
n_{total} = Total number of moles of gases within 32PTH2 DSC cavity (g-moles),
R = Universal gas constant (8.314 J/g-moles-K),
$T_{cavity,avg}$ = Average cavity gas temperature in the 32PTH2 DSC cavity (°R),
$V_{free\_in\_cavity}$ = Free volume in the cavity (in^3),
P_{DSC} = 32PTH2 DSC internal pressure (psia).

The following assumptions are considered in calculating the maximum internal pressures within the 32PTH2 DSC:

- Based on the evaluation presented in Section B.4.8, the bounding initial thermal condition during and after vacuum drying operations is established with helium in the 32PTH2 DSC and 212°F water in the TC/DSC annulus. This helium temperature is used to determine the initial amount of helium within the 32PTH2 DSC cavity. For conservatism, the lower initial helium backfill temperature is considered based on thermal analysis results for heat load of 31.2 kW as discussed in Section B.4.7.3.

- The average temperature of homogenized fuel assemblies within the active fuel region are considered as the average helium temperature within the active fuel region in the fuel compartments ($T_{free\_in\_FAs}$).

- A review of the average fuel cladding temperature ($T_{free\_in\_FAs}$) and average helium temperature ($T_{free\_out\_FAs}$) for helium outside of the active fuel region computed for normal storage and transfer operations in Table B.4.6-18 shows that the normal hot, vertical steady-state transfer operations (Load Case T5A) result in the bounding temperatures. Therefore, bounding average temperatures from Load Case T5A are used to compute the bounding average cavity gas temperature for all normal transfer/storage operations.

- A review of the average fuel cladding temperature ($T_{free\_in\_FAs}$) and average helium temperature ($T_{free\_out\_FAs}$) for helium outside of the active fuel region computed for off-normal storage and transfer operations in Table B.4.6-18 shows that the off-normal hot, horizontal steady-state transfer operations (Load Case T3) results in the bounding temperatures. Therefore, bounding average temperatures from Load Case T3 are used to compute the bounding average cavity gas temperature for all off-normal transfer/storage operations.

- A review of the average fuel cladding temperature ($T_{free\_in\_FAs}$) and average helium temperature ($T_{free\_out\_FAs}$) for helium outside of the active fuel region computed for accident storage and transfer operations in Table B.4.6-18 shows that the loss of neutron shield with loss of air circulation accident condition (Load Case T9) results in the bounding temperatures. Therefore, bounding average temperatures from Load Case T9 are considered to compute the bounding average cavity gas temperature for all accident conditions during transfer/storage operations.

- The pressure calculation for intact fuel bounds the damaged fuel since the fuel rod fill gas and fission gases have already escaped through the damaged fuel assembly cladding in the pool and will not contribute to the total amount of gases in the 32PTH2 DSC. Further, the effect of damaged fuel assemblies on thermal performance of the 32PTH2 DSC is insignificant as justified in Section B.4.6.9.

B.4.7.1 Free DSC Cavity Volume

The volume of helium in the 32PTH2 DSC cavity ($V_{free\_in\_cavity}$) is equal to volume of water with loaded fuel assemblies in the 32PTH2 DSC. The weight of water in the 32PTH2 DSC cavity, loaded with 32 fuel assemblies, is 10,400 lbs and the water density is 0.0361, as provided in Table B.3.2-1 in Chapter B.3, Section B.3.2.

$V_{free\_in\_cavity} = 10,400 / 0.0361 \text{ in}^3 \approx 288,000 \text{ in}^3$.

The volume of helium within the active fuel region of the fuel assemblies in the fuel compartment ($V_{free\_in\_FAs}$) is calculated as,

$V_{free\_in\_FAs} = (n \times a_{comp}^2 \times La) - V_{FAs} = 32 \times 8.65^2 \times 150 - 152,000 \approx 207,000 \text{ in}^3$.

Where
n = Number of fuel assemblies = 32,
a_{comp} = Fuel compartment width = 8.65 in,
La = Active fuel length = 150 in, and
V_{FAs} = Total volume of fuel assemblies (in^3).

The total volume of fuel assemblies in the 32PTH2 DSC cavity is calculated based on the difference of water weights in the DSC cavity for loaded and unloaded conditions as provided in Table B.3.2-1 in Chapter B.3, Section B.3.2.

$V_{free\_out\_FAs} = (W_{no\_FAs} - W_{FAs}) / \rho_{water} = (15,900-10,400)/0.0361 \approx 152,000 \text{ in}^3$.

With

W_{no_FAs} = Weight of water without fuel assemblies in the 32PTH2 DSC cavity = 15,900 lbs,
W_{no_FAs} = Weight of water with 32 fuel assemblies in the 32PTH2 DSC cavity = 10,400 lbs.

The volume of helium outside the active fuel region of the FAs ($V_{free\_out\_FAs}$) is calculated as:

$V_{free\_out\_FAs} = V_{free\_in\_cavity} - V_{free\_in\_FAs} = 228,000 - 207,000 = 81,000 \text{ in}^3$.

B.4.7.2 Average Cavity Gas Temperatures

Based on the discussion presented in Section B.4.7, the bounding average cavity gas temperatures ($T_{cavity,avg}$) for normal, off-normal, and accident cases occur for transfer operations. Therefore, transfer operations are considered as bounding events to determine the maximum 32PTH2 DSC internal pressures. The bounding average temperatures for normal, off-normal and accident operations as noted in Section B.4.7 are selected to calculate the average cavity gas temperature in the 32PTH2 DSC cavity ($T_{cavity,avg}$) as follows:

$$T_{cavity,avg} = (T_{free\_in\_FAs} \times V_{free\_in\_FAs} + T_{free\_out\_FAs} \times V_{free\_out\_FAs}) / V_{free\_in\_cavity}$$
$$= (T_{free\_in\_FAs} \times 207{,}000 + T_{free\_out\_FAs} \times 81{,}000) / 288{,}000$$

Where

$T_{cavity,avg}$ = Average cavity gas temperature (°F),
$T_{free\_in\_FAs}$= Average helium temperature within the active fuel region in the fuel compartments (°F),
T_{free,out_FAs}= Average helium temperature excluding active fuel region in the fuel compartments (°F).

The volumes of helium in the above equation, $V_{free\_in\_cavity}$, $V_{free\_in\_FAs}$ and $V_{free\_out\_FAs}$ are calculated in Section B.4.7.1.

Based on the above equation, the bounding average cavity gas temperatures to calculate maximum internal pressures are listed below.

Bounding Average Cavity Gas Temperatures for Storage and Transfer Conditions

Operation Conditions	Bounding Load Case	$T_{free\_in\_FAs}$ (°F)	$T_{free\_out\_FAs}$ (°F)	$T_{cavity,avg}$ (°F)
Normal Transfer	T5A	609	496	577
Off-Normal Transfer	T3	594	474	560
Accident Transfer	T9	751	613	712
Helium Backfill	(1)	391	273	358

(1) Bounding average cavity gas temperature for helium backfill operation is based on thermal analysis results for the heat load of 31.2 kW (HLZC#4) as discussed in Section B.4.7.3.

B.4.7.3 Quantity of Helium Backfill Gas in 32PTH2 DSC

The final backfill pressure for the 32PTH2 DSC is 2.5 ±1.0 psig after vacuum drying. The free volume of 32PTH2 DSC cavity is assumed to be filled with helium up to a maximum pressure of 3.5 psig (18.2 psia) to maximize the DSC internal pressure.

An analysis is performed using the 32PTH2 DSC model in an OS200FC TC in the vertical orientation with 31.2 kW and water in the TC/DSC annulus to determine the average fuel assembly and cavity gas temperatures. For this analysis, a DSC shell temperature of 212°F is

used. The lower bound of maximum heat load (31.2 kW) is considered to maximize the amount of helium in the DSC cavity during the backfill operation.

The resulting temperatures from the above analysis provide the necessary inputs to determine the quantity of helium backfilled into the 32PTH2 DSC cavity in Section B.4.7.2. The average temperature of the fuel assemblies is 391°F and the average temperature of the cavity gas outside the fuel assemblies is 273°F. Based on the data presented in Section B.4.7.2, an average helium temperature of 358°F (818°R) is used for the 32PTH2 DSC cavity for the backfilling operation. The average helium temperature is used to determine the quantity of helium backfill gas in the 32PTH2 DSC cavity in accordance with the ideal gas law.

$$PV = nRT,$$

$$n = PV / RT,$$

$$R = 8.314\ J/(mol - K).$$

Where

P = Internal pressure (Pa),
R = Universal gas constant = 8.314 J/(mol-K),
n = Number of moles of gases (g-moles),
T = Gas temperature (K),
V = Gas volume (m^3).

The quantity of helium in the 32PTH2 DSC cavity ($n_{he,cavity}$) is:

$$n_{he,cavity} = \frac{(18.2\,psia)(6894.8\,Pa/psi)(288000\,in^3)(1.6387\times10^{-5}\,m^3/in^3)}{(8.314\,J/(mol-K)(818°R)(5/9\,K/°R)},$$

$$n_{he,cavity} = 157\ g-moles.$$

B.4.7.4 Quantity of Fill Gas in Fuel Rods of CE16x16 Class Fuel Assembly

As shown in Chapter A.4, Table A.4.4-9, the maximum volume of the helium fill gas in a fuel rod of CE16x16 class fuel assembly at cold and unirradiated condition is 1.53 in^3 and there are 236 fuel rods in a CE16x16 class fuel assembly with a maximum fill pressure of 395 psig (≈ 410 psia).

The fill gas is assumed to be at room temperature (68°F or 527.67°R). Per the ideal gas law, the quantity of fuel rod fill gas in 32 assemblies ($n_{he,rod}$) is:

$$n_{he,rod} = \frac{(410\,psia)(6894.8\,Pa/psi)(32\times236\times1.53\,in^3)(1.6387\times10^{-5}\,m^3/in^3)}{(8.314\,J/(mol\cdot K)(527.67°R)(5/9\,K/°R)},$$

$$n_{he,rod} = 219\ g-moles.$$

Ruptured fuel rods will vent fill gas into the 32PTH2 DSC cavity until they come into equilibrium with the 32PTH2 DSC pressure. Therefore, the plenum volume within the ruptured

rods can be included in the total 32PTH2 DSC internal volume. For 100% ruptured fuel rods, the additional plenum volume (V_{plenum}) for 32PTH2 DSC is calculated below:

$$V_{plenum} = 236\,\text{rods/assembly} \times 1.53\ \text{in}^3/\text{rod} \times 32\,\text{assembly/basket} = 11600\ \text{in}^3.$$

Based on NUREG-1536 [B4.3], the maximum fraction of the fuel rods that are assumed to rupture and release their charge gases for normal, off-normal, and accident operations is 1%, 10%, and 100%, respectively. Table B.4.7-1 summarizes the plenum volume and the amount of helium gas released from ruptured fuel rods for the 32PTH2 DSC for normal, off-normal, and accident operations.

B.4.7.5 Total Amount of Fission Gases Released as a Result of Irradiation

The amount of fission gases released into the 24PT4-DSC cavity based on 30% of the total fission gases for 24 CE16×16 class fuel assemblies at 60,000 MWd/MTU burnup as a result of irradiation (including additional gases released from burnable poison rods) is 351.3 g-moles as listed in Chapter A.4, Table A.4.4-10.

Therefore, the total amount of fission gases ($n_{fission}$) released into the 32PTH2 DSC cavity based on 30% of the total fission gases for 32 CE16×16 class fuel assemblies as a result of irradiation up to 62,500 MWd/MTU burnup is as follows:

$$n_{fission} = 351.3\ \text{g-moles} / 24 \times 32 \times 62{,}500 / 60{,}000 = 488\ \text{g-moles}.$$

B.4.7.6 Total Amount of Gases within the 32PTH2 DSC Cavity

The maximum pressure in the 32PTH2 DSC cavity is calculated based on the total amount of gases within the cavity. The total amount of gas in the 32PTH2 DSC cavity is determined as follows for normal, off-normal, and accident operations.

$$n_{total} = n_{he,cavity} + (n_{he,rod} + n_{fission}) \times f$$

Where

n_{total} = Total amount of gases within the 32PTH2 DSC cavity (g-moles),
$n_{he,cavity}$ = Total amount of helium within the 32PTH2 DSC cavity =157 g-moles listed in Section B.4.7.3,
$n_{he,rod}$ = Total amount of helium fill gas in fuel rods = 219 g-moles listed in Section B.4.7.4,
$n_{fission}$ = Total amount of fission gases in fuel rods released into the 32PTH2 DSC cavity = 488 g-moles listed in Section B.4.7.5,
f = Fraction of assumed ruptured rods (1% for normal, 10% for off-normal, and 100% for accident operations)

The total amount of gases within the 32PTH2 DSC cavity for normal, off-normal, and accident operations are summarized below.

Total Amount of Gases in the 32PTH2 DSC Cavity

Operating Conditions	Fraction of Ruptured Rods (f)	Helium Backfill ($n_{he,cavity}$)	Fuel Rod Fill Gas ($n_{he,rod}$)	Fission Products ($n_{fission}$)	Total Gas (n_{total})
	(%)	(g-moles)	(g-moles)	(g-moles)	(g-moles)
Normal	1	157	2.19	4.88	164
Off-normal	10	157	21.9	48.8	228
Accident	100	157	219	488	864

B.4.7.7 Maximum 32PTH2 DSC Internal Pressure Calculation

The maximum internal pressures for the 32PTH2 DSC for normal, off-normal, and accident operations are calculated using the methodology as described in Section B.4.7. The average cavity gas temperatures are calculated in Section B.4.7.2. The total amounts of gases within the 32PTH2 DSC cavity are obtained from Section B.4.7.6.

The maximum internal pressure for normal operation is calculated as:

$$P_{nor} = \frac{(1.4504 \cdot 10^{-4} \frac{psia}{Pa})(164\,mol)(8.314\,J/mol \cdot K)(577^{\circ}F + 460^{\circ}R)}{(288000\,in^3 + 116\,in^3)(1.6387 \cdot 10^{-5}\,m^3/in^3)(1.8^{\circ}R/K)}$$

$$P_{nor} = 24.1\,psia\,(9.4psig)$$

The maximum internal pressure for off-normal operation is calculated as:

$$P_{off-nor} = \frac{(1.4504 \cdot 10^{-4} \frac{psia}{Pa})(228\,mol)(8.314\,J/mol \cdot K)(560^{\circ}F + 460^{\circ}R)}{(288000 + 1160\,in^3)(1.6387 \cdot 10^{-5}\,m^3/in^3)(1.8^{\circ}R/K)}$$

$$P_{off-nor} = 32.9\,psia\,(18.2\,psig)$$

The maximum internal pressure for accident operation is calculated as:

$$P_{acc} = \frac{(1.4504 \cdot 10^{-4} \frac{psia}{Pa})(864\,mol)(8.314\,J/mol \cdot K)(712^{\circ}F + 460^{\circ}R)}{(288000\,in^3 + 11600\,in^3)(1.6387 \cdot 10^{-5}\,m^3/in^3)(1.8^{\circ}R/K)}$$

$$P_{acc} = 138.2\,psia\,(124\,psig)$$

The calculated maximum DSC internal pressures for normal, off-normal, and accident conditions during transfer/storage operations are summarized in Table B.4.7-1 for 32PTH2 DSC. As seen, the maximum internal DSC pressures remain below the design pressures considered for the 32PTH2 DSC for all conditions.

Table B.4.7-1
Maximum Internal Pressures of 32PTH2 DSC for Transfer/ Storage Operations

Operating Operations	DSC Cavity Volume (in^3)	Helium Backfill Amount (g-moles)	Plenum Volume (in^3)	Fuel Rod Fill Gas Amount (g-moles)	Fission Products Amount (g-moles)	Total Gas Amount (g-moles)	Average Cavity Gas (°F)
Normal	288000	157	116	2.19	4.88	164	577
Off-normal	288000	157	1160	21.9	48.8	228	560
Accident	288000	157	11600	219	488	864	712

Operating Operations	Calculated Pressure (psig)	Design Pressure (psig)
Normal	9.4	15
Off-normal	18.2	20
Accident	124	140

B.4.8 Thermal Evaluation for Loading/Unloading Conditions

All fuel loading operations occur when the 32PTH2 DSC and OS200FC TC are in the spent fuel pool. The fuel is always submerged in free-flowing pool water permitting heat dissipation. After completion of the fuel loading, the TC and DSC are removed from the pool and the DSC is drained, dried, sealed, and backfilled with helium. These operations occur when the annulus between the TC and DSC remains filled with water.

The water in the annulus is replenished with fresh water to prevent boiling and maintain the water level if excessive evaporation occurs. Presence of water within the annulus maintains the maximum DSC shell temperature below the boiling temperature of water in open atmosphere (212°F).

Water in the DSC cavity is forced out of the cavity (blowdown operation) before the start of vacuum drying. Helium is used as the medium to remove water and subsequent vacuum drying occurs with a helium environment in the DSC cavity. The vacuum drying operation does not reduce the pressure sufficiently to reduce the thermal conductivity of the helium in the DSC cavity as discussed in Appendix U, Section U.4.7.1 of the UFSAR for the Standardized NUHOMS® System [B4.22].

With helium being present during vacuum drying operations and a DSC shell temperature equal to water boiling temperature of 212°F, the 32PTH2 DSC model described in Section B.4.6.2.1 is used in a steady-state analysis to determine the maximum fuel cladding temperature for vacuum drying operations. The maximum fuel cladding temperature for vacuum drying operations in the 32PTH2 DSC is 572°F and 540°F for 37.2 kW and 32.0 kW decay heat loads, respectively.

The presence of helium during blowdown and vacuum drying operations eliminates the thermal cycling of fuel cladding during helium backfilling of the DSCs subsequent to vacuum drying. Therefore, the thermal cycling limit of 65°C (117°F) for short-term operations set by NUREG-1536 [B4.3] is satisfied for vacuum drying operation.

The bounding unloading operation considered is the reflood of the 32PTH2 DSCs with water. For unloading operations, the DSC is filled with the spent fuel pool water through its siphon port. During this filling operation, the 32PTH2 DSC vent port remains open with effluents routed to the plant's off-gas monitoring system.

The maximum fuel cladding temperature during the reflooding event is significantly less than the vacuum drying condition owing to the presence of water/steam in the DSC cavity. Based on the above rationale, the maximum cladding temperature during unloading operation is bounded by the maximum fuel cladding temperature for vacuum drying operation.

Initially, when spent fuel pool water is added to the 32PTH2 DSC cavity containing hot fuel and basket components, some water will flash to steam causing the internal DSC pressure to rise. This steam pressure is released through the vent port. The procedures in Chapter B.8, Section B.8.2 specify that the flow rate of the reflood water will be controlled such that the internal pressure in the DSC cavity does not exceed the maximum pressure of 20 psig considered for reflooding operations. This is assured by monitoring the maximum internal pressure in the

32PTH2 DSC cavity during the reflood event. The reflood for the 32PTH2 DSC is considered as a Service Level D event with a design pressure of 140 psig. The design pressure for the 32PTH2 DSC for this condition is well above the pressure limit of 20 psig. Therefore, there is sufficient margin in the DSC internal pressure during the reflooding event to assure that the DSC will not be over pressurized.

The effects of the thermal loads on the fuel cladding during reflooding operations are evaluated in Appendix U, Section U.4.7.3 of the UFSAR for the Standardized NUHOMS® System [B4.22] for PWR fuel assemblies. Since the fuel assemblies that are allowed in the 32PTH2 DSC are the same as those allowed within 32PTH1 DSC, these evaluations remain valid for 32PTH2 DSC.

B.4.8.1 Heatup Analysis

Heatup of the water within the 32PTH2 DSC cavity prior to blowdown and backfilling with helium occurs as operations are performed to load fuel, decontaminate the cask and drain and dry the 32PTH2 DSC.

Based on discussions in Chapter 4, Section 4.7.3 for 24PT1-DSC and Chapter A.4, Section A.4.7.3 for the 24PT4-DSC, prevention of boiling in the DSC is not required due to consideration of low moderator density (boiling water) in the criticality evaluation, continuous venting of the DSC cavity prior to blowdown, and welding procedures. The only potential concern associated with steam generation is the unexpected loss of water within the DSC cavity, which could result in decreased shielding and hence increased occupational exposure.

Similar to the 24PT1 and 24PT4-DSCs, the criticality analysis of 32PTH2 DSC considers a wide range of moderator densities to demonstrate that the 32PTH2 DSC meets the criticality limits for low moderator density. The 32PTH2 DSC cavity remains vented during loading operation and the welding operations for the 32PTH2 DSC are conducted in the same way as was considered for the 24PT1 and 24PT4-DSCs.

The potential increase of occupational exposure during loading operation for the 32PTH2 DSC operation is eliminated since the shielding analysis for the 32PTH2 DSC does not take credit for the water within the DSC cavity during loading activities such as welding. Therefore, the calculated occupational dose rates are bounding and the calculation of the time to boil to address ALARA concerns for the 32PTH2 DSC is not required.

B.4.9 Fuel Assembly Effective Properties for CE 16×16 Class Fuel Assemblies

The thermal analysis of the 32PTH2 DSC presented in Section B.4.6 models the fuel assemblies in the 32PTH2 DSC as homogeneous solid regions. To accurately predict the fuel cladding temperature within each fuel assembly using this type of modeling, the effective thermal properties of the homogeneous solid region must be determined. The effective thermal conductivity calculation accounts for the actual geometry of the fuel assembly and the fact that the heat generation occurs only within the fuel rods. A CE 16×16 spent fuel assembly is selected as the design basis assembly to calculate the effective thermal properties for fuel assemblies in 32PTH2 DSC. Since the cladding material of CE 16×16 fuel assembly, Zicaloy-4, has a lower conductivity than other cladding materials (Zirlo^{TM} , M5^{TM} , etc.), this selection is conservative.

The following assumptions are considered in the calculation of the CE 16x16 fuel assembly effective properties.

- Irradiated UO_2 thermal conductivity is considered for fuel pellets.
- No convection heat transfer is considered within the fuel compartment.
- The fuel assemblies are centered within a fuel compartment.
- The axial effective thermal conductivity of the fuel assembly is calculated only based on fuel cladding material.
- The helium backfill gas is not included in the effective density and specific heat of the fuel assembly.

The material properties used for calculation of the fuel assembly effective properties are listed in Section B.4.2. The methodologies used in this section to evaluate the effective properties of fuel assemblies are the same as those described in Appendix U, Section U.4.8 of [B4.22].

B.4.9.1 Thermal Conductivity of Irradiated Fuel Pellet

The thermal conductivity data given in [B4.19] and [B4.20] indicates changes in the thermal conductivity of irradiated UO_2 that potentially affects the heat transfer in the CE16×16 class fuel assembly.

The average irradiation temperature (T_{irr}) for a typical fuel pellet is approximately 1300K during irradiation as shown in [B4.19]. This high temperature changes the characteristics of the UO_2 pellets so that the thermal conductivity of the pellet decreases after irradiation.

The irradiated UO_2 conductivity is evaluated in [B4.20] for various irradiation temperatures from 680 to 1490K and various burnups from 34 to 94 GWd/MTU. A maximum design basis burnup of 62.5 GWd/MTU is allowed for fuel assemblies to be stored in the 32PTH2 DSC. A review of [B4.20] shows that the thermal conductivity of irradiated UO_2 with 62.5 GWd/MTU and irradiation temperature of $T_{irr} \geq 1300K$ decreases significantly (more that 50%) compared to un-irradiated UO_2.

The thermal conductivity values of irradiated UO_2 are inter/extrapolated based on the data in [B4.20] for a conservative burnup of 65 GWd/MTU and listed below.

Thermal Conductivity of Irradiated UO2

Burnup (GWd/MTU)	51	92	65	Interpolated values for 65 GWd/MTU	
T (K)	k_{UO2} (W/m-K)	k_{UO2} (W/m-K)	k_{UO2} (W/m-K)	T (°F)	k_{UO2} (Btu/hr-in-°F)
300	4.33 (1)	2.95 (1)	3.86	80	0.186
400	3.99 (1)	2.79 (1)	3.58	260	0.172
500	3.65	2.63	3.30	440	0.159
600	3.31	2.47	3.02	620	0.146
700	3.03	2.33	2.79	800	0.134
800	2.79	2.2	2.59	980	0.125
900	2.59	2.08	2.42	1160	0.116
1000	2.42	1.98	2.27	1340	0.109

(1) Extrapolated based on data from [B4.20].

Using irradiated UO_2 thermal conductivity decreases the fuel assembly effective conductivity in the radial direction. The axial effective thermal conductivity is calculated based on the fuel cladding material only and does not include the UO_2 fuel pellet thermal conductivity. Therefore, the axial effective conductivity of the fuel assembly is not impacted by UO_2 properties.

B.4.9.2 Axial Fuel Assembly Effective Conductivity

The axial fuel assembly effective conductivity, $k_{eff\,axial}$, is limited to the cladding conductivity weighted by its fractional area as required in Section 4.5.4.2 of NUREG 1536 [B4.3].

$$k_{eff\,axial} = (k_{zirc})(A_{zirc}/A_{eff})$$

Where
k_{zirc} = Thermal conductivity of Zircaloy-4,
A_{eff} = Cross section area of fuel compartment $8.65'' \times 8.65'' = 74.8225\ in^2$,
A_{zirc} = Cross section area of fuel cladding (in^2),
A_{zirc} = Number of fuel rods × cross sectional area of fuel rod cladding +
Number of guide tubes × cross sectional area Zircaloy-4 in guide tube.

The resulting axial fuel assembly effective conductivity values are listed in Section B.4.2(a).

B.4.9.3 Transverse (Radial) Fuel Assembly Effective Conductivity

The transverse (radial) fuel assembly effective conductivity is determined by creating a two-dimensional finite element model of the fuel assembly centered within a fuel compartment. The outer surfaces, representing the fuel compartment walls, are held at a constant temperature, and heat generating boundary condition is applied to the fuel pellets within the model. The maximum fuel assembly temperature is then determined. The isotropic effective thermal conductivity of a heat generating square, such as the fuel assembly, is calculated as described in [B4.9]:

$$k_{eff,radial} = 0.29468 \times \frac{Q''' a'^2}{(T_c - T_o)}$$

Where
Q''' = heat generation per unit volume of fuel assembly, (Btu/hr·in^3),
a' = half width of fuel compartment opening = 8.65″ / 2 = 4.325″,
T_c = Maximum temperature of fuel assembly, (°F),
T_o = Compartment wall temperature, (°F).

With

$$Q''' = \frac{Q}{4 a'^2 L_a}$$

Q = decay heat load per fuel assembly, (Btu/hr),
L_a = active fuel length, (in),
Q_{react} = Reaction solution retrieved from the fuel assembly model, (Btu/hr),

$$Q_{react} = \frac{Q}{L_a}$$

Rearranging the above equation based on Q_{react} gives:

$$k_{eff,radial} = 0.29468 \times \frac{Q_{react}}{4 \cdot (T_c - T_o)}$$

In determining the temperature dependent transverse fuel assembly effective conductivities, an average temperature, equal to $(T_c + T_o)/2$, is used for the fuel assembly temperature. The resulting effect transverse effective fuel conductivity values are listed in Section B.4.2(a).

B.4.9.3.1 Finite Element Model of Fuel Assembly

A two-dimensional, finite element model of a CE 16×16 fuel assembly is modeled using the ANSYS computer code [B4.26]. PLANE55 elements were used to model components such as the fuel pellets, fuel cladding, and the helium back fill gas. The gap between the fuel cladding and the fuel pellets is included in the model. The cross section of the CE16×16 fuel assembly is shown in Figure B.4.9-1.

Heat generated in the fuel pellets dissipates by conduction and radiation to the fuel compartment walls. Convection is not considered in the model. Radiation between the fuel rods, guide tubes, and fuel compartment walls is simulated using the radiation super-element processor (AUX12). LINK32 elements were used for modeling of radiating surfaces in creating the radiation super-element and were unselected prior to the solution of the model. The fuel compartment walls are not modeled as a solid entity but using LINK32 elements. These elements, which are aligned with the outermost nodes of the model, are given an emissivity of 0.3 for the fuel compartment walls.

The heat generation applied to the fuel pellets in the model is calculated as follows.

$$dhl = \frac{Q/N}{n\left(\frac{\pi}{4}d_p^{\ 2}\right)L_a}$$

Where:

dhl = heat generation rate (Btu/hr-in^3),
Q = total decay heat load (Btu/hr),
N = number of assemblies =32,
n = number of fuel rods = 236,
d_p = pellet outer diameter = 0.382 in,
L_a = active fuel length =150 in.

The models were run with a series of isothermal boundary conditions applied to the nodes representing the fuel compartment walls. Typical boundary conditions used in the finite element model of the fuel assembly are shown in Figure B.4.9-2.

B.4.9.4 Fuel Assembly Effective Density and Specific Heat

Volume average density and weight average specific heat are calculated to determine the effective density and specific heat for the fuel assembly. The equations to determine the effective density ρ_{eff} and specific heat $C_{p\,eff}$ are shown below.

$$\rho_{eff} = \frac{\sum \rho_i V_i}{V_{assembly}} = \frac{\rho_{UO2}\ V_{UO2} + \rho_{Zr4}\ V_{Zr4}}{4a'^2 L_a}$$

$$C_{P\,eff} = \frac{\sum \rho_i\ V_i\ C_{Pi}}{\sum \rho_i\ V_i} = \frac{\rho_{UO2}\ V_{UO2}\ C_{P\,UO2} + \rho_{Zr4}\ V_{Zr4}\ C_{P\,Zr4}}{\rho_{UO2}\ V_{UO2} + \rho_{Zr4}\ V_{Zr4}}$$

Where:

ρ_{UO2} , ρ_{Zr4} – density of fuel pellets and cladding,

V_{UO2} , V_{Zr4} – volume of fuel pellets and cladding (calculated using geometry data from Chapter A.2, Table A.2.1-3),

$C_{P\,UO2}$, $C_{P\,Zr4}$ – specific heats of fuel pellet and cladding.

The resulting effective density and specific heat values for a fuel assembly in 32PTH2 DSC are listed in Section B.4.2(a).

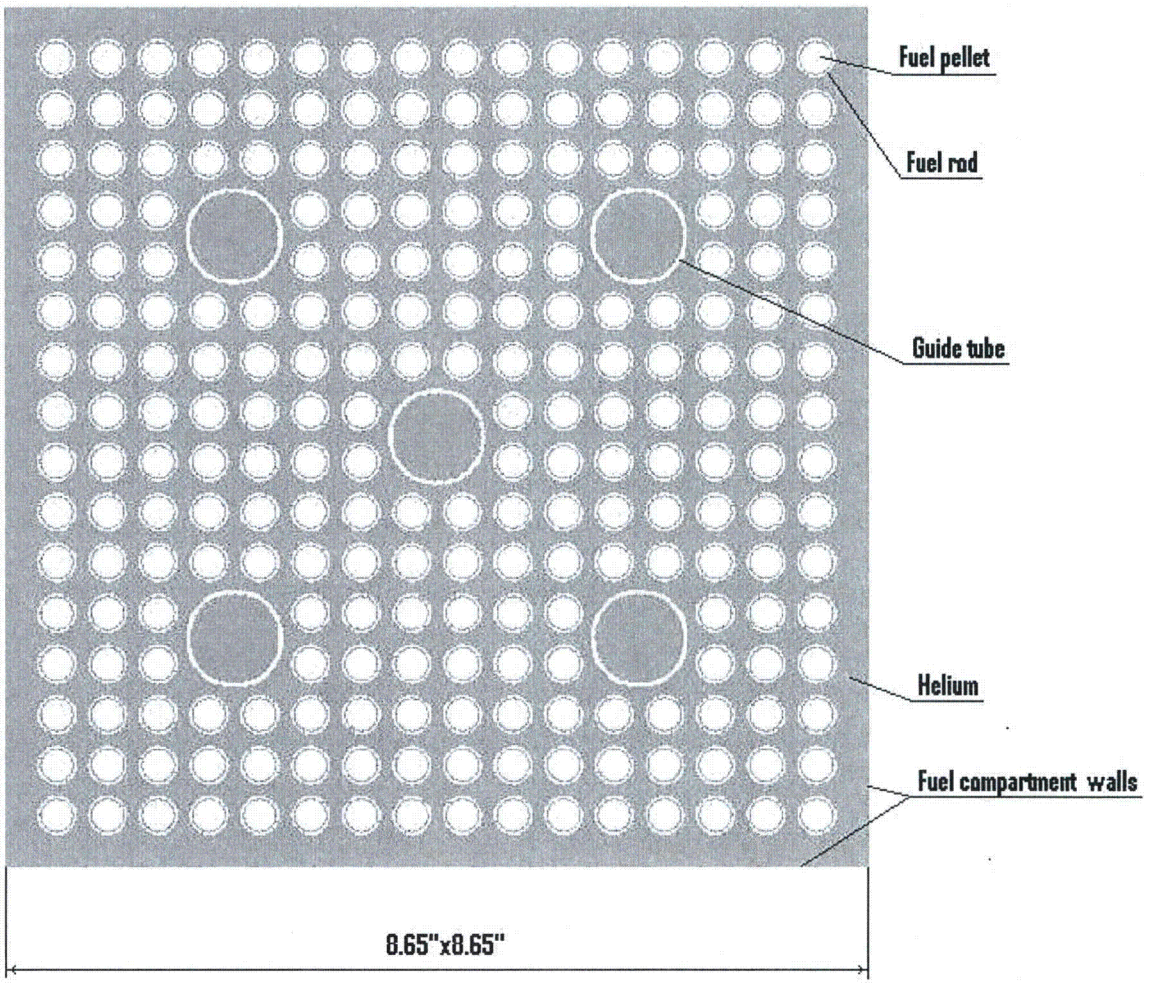

Figure B.4.9-1
Cross-section of CE 16×16 Class Fuel Assembly in a Fuel Compartment

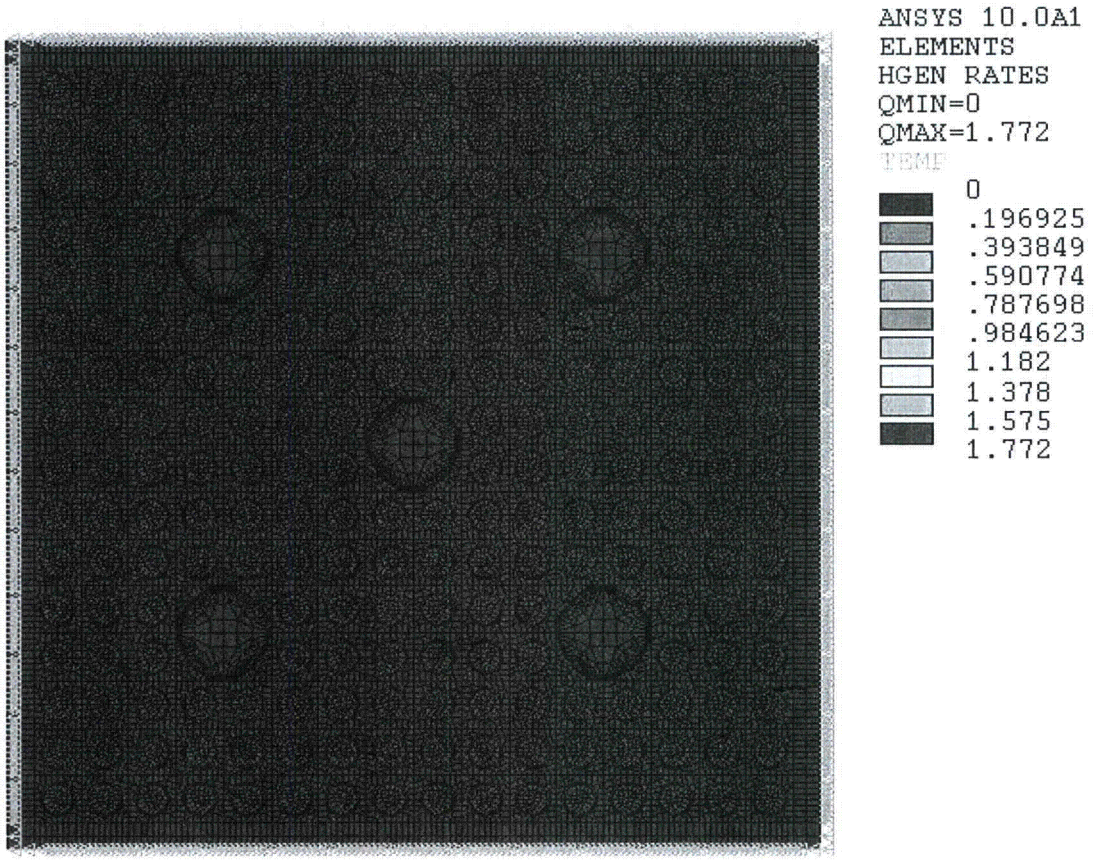

Figure B.4.9-2
Typical Boundary Condition and Heat Generation in Finite Element Model of Fuel Assembly

B.4.10 References

[B4.1] U.S. Nuclear Regulatory Commission, Title 10, Code of Federal Regulations, Part 72, Licensing Requirements for the Independent Storage of Spent Nuclear Fuel and High-Level Radioactive Waste.

[B4.2] U.S. Nuclear Regulatory Commission, Title 10, Code of Federal Regulations, Part 71, Packaging and Transportation of Radioactive Materials, U.S. Nuclear Regulatory Commission.

[B4.3] U.S. Nuclear Regulatory Commission, Standard Review Plan for Dry Cask Storage Systems, NUREG-1536, Revision 1, July 2010.

[B4.4] U.S. Nuclear Regulatory Commission, Interim Staff Guidance No. 11, ISG-11, Revision 3, Cladding Considerations for the Transportation and Storage of Spent Fuel, November 2003.

[B4.5] U.S. Nuclear Regulatory Commission, A Handbook of Materials Properties for Use in the Analysis of Light Water Reactor Fuel Rod Behavior, MATPRO - Version 11 (Revision 2), EG&G Idaho, Inc., TREE-1280, NUREG/CR-0497, September 1981.

[B4.6] Oak Ridge National Laboratory, Recommendations for Addressing Axial Burnup in PWR Burnup Credit Analyses, by J.C. Wagner, M. D. DeHart, and C.V. Parks, NUREG/CR-6801, Revision 0, (ORNL/TM-2001/273) March 2003.

[B4.7] Oak Ridge National Laboratory, Effect of Fuel Failure on Criticality Safety and Radiation Dose for Spent Fuel Casks, by K.R. Elam, J.C. Wagner and C.V. Parks, NUREG/CR-6835 (ORNL/TM-2002/255), September 2003.

[B4.8] Oak Ridge National Laboratory, Scoping Design Analysis for Optimized Shipping Casks Containing 1-, 2-, 3-, 5-, 7-, or 10-Year old PWR Spent Fuel, by J. A. Bucholz, ORNL/CSD/TM-149, January 1983.

[B4.9] Sandia National Laboratories, A Method for Determining the Spent-Fuel Contribution to Transport Cask Containment Requirements, by Sanders, T. L., et al., SAND90-2406, TTC-1019, UC-820, November 1992.

[B4.10] American Society of Mechanical Engineers, Boiler and Pressure Vessel Code, Section II, Part D, Materials Properties, 2010 Edition.

[B4.11] Rohsenow, Hartnett, and Cho, Handbook of Heat Transfer, 3rd Edition, 1998.

[B4.12] Rohsenow, Hartnett, and Ganic, Handbook of Heat Transfer Fundamentals, 2nd Edition, 1985.

[B4.13] Perry, Chilton, Chemical Engineers' Handbook, 5th Edition, 1973.

[B4.14] Incropera, DeWitt, Fundamentals of Heat and Mass Transfer, 4th Edition, 1996.

[B4.15] Siegel and Howell, Thermal Radiation Heat Transfer, 4th Edition, 2002.

[B4.16] Paloposki and Leidquist, Steel Emissivity for Higher Temperatures, Nordic Innovation Centre, NT Technical Report #570, 2006.

[B4.17] Henninger, J. H., "Solar Absorptance and Thermal Emittance of Some Common Spacecraft Thermal-Control Coatings," NASA Scientific and Technical Information Branch, NASA Reference Publication 1121, 1984.

[B4.18] Kreith, Frank, Principles of Heat Transfer, 3rd Edition, 1973.

[B4.19] Amaya, M. et al., Thermal Conductivities of Irradiated UO2 and (U,Gd)O2, Journal of Nuclear Materials 300 (2002) 57–64.

[B4.20] Ronchi, et. al., Effect of Burn-up on the Thermal Conductivity of Uranium Dioxide up to 100,000 MWd/t, Journal of Nuclear Materials, 327 (2004) 58-76.

[B4.21] GESC, NAC International, Atlanta Corporate Headquarters, 655 Engineering Drive, Norcross, Georgia, (Engineering Report #NS3-020, Effects of 1300°F on Unfilled NS-3, while Bisco Products, Inc., 11/84).

[B4.22] Transnuclear, Inc., Updated Final Safety Analysis Report for the Standardized NUHOMS® Horizontal Modular Storage System for Irradiated Nuclear Fuel, Revision 11, USNRC Docket No. 72-1004.

[B4.23] Transnuclear, Inc., E-29954, Application for Amendment 13 to Standardized NUHOMS® Certificate of Compliance No. 1004 for Spent Fuel Storage Casks, February, 2011, Revision 0 (ML110460525), Enclosure 7, supplemented by E-31217 (ML11217A043), Enclosure 7, 22 July, 2011.

[B4.24] Transnuclear, Inc., Safety Analysis Report for the NUHOMS®-MP197 Transport Packaging, Chapter A.3, USNRC Docket No. 71-9302, Revision 10, ML11238A106.

[B4.25] Transnuclear, Inc., Report, Thermal Testing of the NUHOMS® Horizontal Storage Module, Model HSM-H, Report No. E-21625, Revision 1, ML050680050.

[B4.26] ANSYS computer code and On-Line User's Manuals, Version 10.0.

[B4.27] U.S. Nuclear Regulatory Commission, Final Safety Evaluation Report, Transnuclear, Inc., Standardized NUHOMS® Horizontal Modular Storage System for Irradiated Nuclear Fuel, Docket No. 72-1004, Amendment No. 10, ML092290329.

[B4.28] American Concrete Institute, Code Requirements for Nuclear Safety Related Concrete Structures (ACI 349-97) and Commentary (ACI 349R-97), 1997.

[B4.29] GESC NS-3, NAC International, Atlanta Corporate Headquarters, 655 Engineering Drive, Norcross, Georgia (Test Report NS-3-001, while Bisco Products, Inc.).

[B4.30] Transnuclear, Inc., Updated Final Safety Analysis Report for NUHOMS® HD Horizontal Modular Storage System for Irradiated Nuclear Fuel, Revision 2.

[B4.31] Oak Ridge National Laboratory, RSIC Computer Code Collection, "SCALE, A Modular Code System for Performing Standardized Computer Analyses for Licensing Evaluation", NUREG/CR-0200, Revision 1, ORNL/NUREG/CSD-2/V3/R6, May 2010.

[B4.32] Oak Ridge National Laboratory, Thermo-physical Properties of MOX and UO2 Fuels Including the Effect of Irradiation, by S.G. Popov, J.J. Carbajo, V. K. Ivanov, G.L. Yoder, ORNL/TM-2000-351, November 2000.

B.5 SHIELDING EVALUATION

The shielding evaluation presented for the NUHOMS® 32PTH2 system demonstrates adequacy of the shielding design for the authorized contents described in Chapter B.2. The geometry of the NUHOMS® 32PTH2 system is described in Chapter B.1. The heavy concrete walls and roof of the Advanced Horizontal Storage Module (AHSM-HS) provide the bulk of the shielding for the 32PTH2 DSC and the authorized contents in the storage condition. The 32PTH2 DSC configuration in the AHSM-HS is further detailed in a series of sketches in Figure B.5.5-1 through Figure B.5.5-5. The AHSM-HS has the same basic geometry as the HSM-HS and the following shielding evaluation is performed using the same techniques and models as described in Appendix U, Chapter U.5 of the Standardized NUHOMS® System UFSAR [B5.6].

During fuel loading and transfer operations, the combination of thick steel and lead shield plugs at the ends of the 32PTH2 DSC and heavy steel/lead/neutron shield material of the OS200FC Transfer Cask (TC) provide shielding for personnel loading and transferring the 32PTH2 DSC for storage in the AHSM-HS.

Table B.5.5-1 provides the general configuration and nominal material thicknesses of the important components utilized in the shielding models of the NUHOMS® 32PTH2 system.

The design basis PWR fuel source terms are derived for the Combustion Engineering 16x16 (CE 16x16) assembly design as described in Section B.5.2, for the authorized PWR fuel assemblies as described in Chapter B.2.

The 32PTH2 DSC is designed to store intact and damaged PWR fuel assemblies with the specifications described in Chapter B.2, Tables B.2.1-1 through B.2.1-3. The 32PTH2 DSC may store PWR fuel assemblies arranged in any one of the four alternate heat zoning configurations shown in Figure B.2.1-1, with a maximum decay heat of 1.5 kW per assembly and a maximum heat load of 37.2 kW per canister. Qualification of reconstituted fuel is also discussed in Section B.5.2. The limiting spent fuel parameters are burnup, initial enrichment, cooling time, fissile material type, number of fuel rods, number of guide/instrument tubes and initial heavy metal content.

The design-basis fuel source terms employed in the shielding evaluations bound the source term from all authorized fuel assemblies with the burnup/enrichment/cooling time (BECT) combinations given in Chapter B.2, Table B.2.1-6 and positioned in the basket per Figure B.2.1-1.

The design basis radiological source terms for the shielding analysis for loading and transfer are determined to obtain the bounding total dose rates near the OS200FC TC. They correspond to the design basis fuel assembly with a burnup of 33 GWd/MTU, an enrichment of 1.7 wt. % U-235, and a cooling time of 5.2 years in Zones 1 and 3 and a burnup of 33 GWd/MTU, an enrichment of 1.7 wt. % U-235, and a cooling time of 5.0 years in Zone 2.

The design basis source terms for the shielding analysis for storage in the AHSM-HS are based on bounding gamma and bounding neutron radiation sources which occur at different BECT combinations and results in conservative calculation of dose rates. The design basis gamma

radiation source terms used in the AHSM-HS shielding evaluation are based on fuel assemblies with a burnup of 31 GWd/MTU, an enrichment of 1.7 wt. % U-235 and a cooling time of 5 years. The design basis neutron radiation source for the AHSM-HS shielding evaluation are based on fuel assemblies with a burnup of 57 GWd/MTU, an enrichment of 3.6 wt. % U-235 and a cooling time of 13.2 years. As detailed above, no single fuel assembly qualified per Table B.2.1-2 can simultaneously contain the bounding neutron and bounding gamma source terms.

These gamma and neutron source terms result in bounding dose rates on the surface of the AHSM-HS and OS200FC TC under all conditions of loading, transfer, and storage. The bounding shielding evaluation presented herein assumes a fully loaded 32PTH2 DSC.

The fuel enrichment described throughout this chapter corresponds to assembly average enrichment. The burnup described throughout this chapter corresponds to assembly average burnup.

The methodology, assumptions, and criteria used in this evaluation are summarized in the following sections.

B.5.1 Discussion and Results

The dose rates for 32 design basis CE 16x16 class PWR fuel assemblies in the NUHOMS® 32PTH2 system are summarized in Table B.5.5-2 through Table B.5.5-8. These dose rates are calculated using MCNP5, a three-dimensional Monte Carlo transport code [B5.8]. Table B.5.5-2 and Table B.5.5-3 provide the dose rates on the surface of the AHSM-HS, while Table B.5.5-4 through Table B.5.5-8 provide the dose rates on and around the OS200FC TC during transfer (normal), decontamination, welding, accident conditions, respectively.

The source term calculations presented in Section B.5.2, are developed for the design basis fuel. The design basis source terms for the shielding analysis for storage in the AHSM-HS are based on the use of bounding gamma and bounding neutron radiation sources as discussed previously. The design basis gamma radiation source terms correspond to fuel assemblies with a burnup of 31 GWD/MTU, an enrichment of 1.7 wt. % U-235, and cooling time of 5.0 years. The design basis neutron radiation source terms are due to fuel assemblies with a burnup of 57 GWd/MTU, an enrichment of 3.6 wt. % U-235 and a cooling time 13.2 years. For the OS200FC TC shielding evaluations, the design basis source terms correspond to fuel assemblies with a burnup of 33 GWD/MTU, an enrichment of 1.7 wt. % U-235, and a cooling time of 5.2 years in radial Zones 1 and 3 and with a burnup of 33 GWD/MTU, an enrichment of 1.7 wt. % U-235, and a cooling time of 5.0 years in Zone 2. The arrangement of DSC fuel compartments within the zones is illustrated in Figure B.2.1-1.

A discussion of the method used to determine the design basis source terms is included in Section B.5.2. The shielding model specification and shielding material densities are provided in Section B.5.3. Radiological source terms employed for the determination of BECT combinations resulting in the bounding dose rates and decay heat utilized in the determination of the decay heat equation (DHE) are calculated with the SAS2H/ORIGEN-S modules of SCALE 4.4 [B5.1]. The design basis radiological sources in the four axial exposure regions of the fuel assembly and the design basis radiological sources due to control components are calculated with the TRITON\T-DEPL module of SCALE 6.0 [B5.17]. The method used to determine the dose rates due to 32 design basis fuel assemblies in the NUHOMS® 32PTH2 system is provided in Section B.5.4.

Loading and transfer configurations are modeled with the NUHOMS® 32PTH2 system intact, including the filled neutron shield in the OS200FC TC. The shielding calculations are performed using the MCNP5 three-dimensional Monte Carlo transport code [B5.8]. Average and peak dose rates on the front, side, top, and back of the AHSM-HS are calculated for storage conditions. For the OS200FC TC, the average and the maximum dose rates on the side, top, and bottom are calculated.

Occupational doses during loading, transfer to the ISFSI, and maintenance and surveillance operations are provided in Chapter B.10. Radiation streaming concerns are also discussed in Chapter B.10. Site dose and occupational dose calculations are provided in Chapter B.10.

For accident conditions (e.g., cask drop, fire), the OS200FC TC neutron shield (water), including the steel skin (shown in Figure B.5.5-23), are assumed to be removed. The results of this analysis are addressed in Chapter B.11. Accident analyses involving the loaded AHSM-HS on the ISFSI pad are also discussed in Chapter B.11.

B.5.2 Source Specification

Design basis radioactive source terms are calculated with the TRITON\T-DEPL module of SCALE 6.0 [B5.17]. Radiological and thermal sources for qualification of the authorized contents are calculated with the SAS2H/ORIGEN-S modules of SCALE 4.4 [B5.1]. The fuel assembly at burnup and enrichment combinations shown in Table B.2.1-6 are employed in the fuel qualification calculations for the ranking of source terms (analyzed regions 1 and 2). Thermal sources calculated with SAS2H/ORIGEN-S are employed to develop the DHE.

B.5.2.1 Design Basis Assembly Description

A composite CE 16x16 assembly with the maximum initial heavy metal and cobalt content in each region is employed as the bounding fuel assembly design from a shielding standpoint. The neutron flux during reactor operations is peaked in the active fuel (in-core) region of the fuel assembly and drops off rapidly outside the active fuel region. Much of the fuel assembly hardware is outside of the active fuel region of the fuel assembly. To account for this reduction in neutron flux, the fuel assembly is divided into four exposure "regions." The four axial regions used in the source term calculation are: the bottom (nozzle) region, the active fuel region, the (gas) plenum region, and the top (nozzle) region. The bounding CE 16x16 fuel assembly materials and masses for each irradiation region are listed in Table B.5.5-9. The light elements that make up the fuel and materials for the various fuel assembly hardware are obtained from reference [B5.2] except for the cobalt content in stainless steel and Inconel for which higher values are employed for conservatism. The elemental compositions of the fuel assembly are listed in Table B.5.5-10 and Table B.5.5-11, respectively. The design basis source terms are generated using a heavy metal loading of 0.456 MTU per assembly. The fuel assembly and hardware masses are irradiated in the appropriate irradiation region in the SAS2H/ORIGEN-S and TRITON\T-DEPL models. To account for the reduction in neutron flux outside the active fuel regions, neutron flux (fluence) correction factors are applied to light element composition for each of these regions. The neutron flux correction factors are shown in Table B.5.5-12 [B5.3].

Bounding radiological sources for the authorized control components (CCs) are shown in Table B.5.5-19. The sources are calculated with a TRITON\T-DEPL model. Parameters employed in the model are provided in Table B.5.5-18 and a sketch is included in Figure B.5.5-11.

B.5.2.2 Source Ranking

The purpose of ranking is to determine BECT combinations that result in bounding gamma, neutron, and total dose rates.

B.5.2.2.1 Response Functions

Simplified shielding analysis models are created to generate a set of spatial and energy dependent dose rate equivalent values representing the shielding attenuation per source particle per energy group. Two MCNP5 models are developed: AHSM-HS quarter radial model including the roof vent and end-of-array side shield wall and 32PTH2 DSC in OS200FC TC quarter radial model. The AHSM-HS model allows an estimate of dose rates near the vent outlet on top of the storage module as well as on the side shield wall. There are two additional locations

near the AHSM-HS where the dose rates are substantially larger than at the other locations near the AHSM-HS: at the bottom air inlet vents in the front face of the module and air outlet vents on the AHSM-HS roof. The response function that simulates penetration and streaming of source particles to the vent opening on top of the AHSM-HS roof slab is used in the current analysis for ranking sources for the AHSM-HS. The OS200FC TC model allows an estimate of dose rates on the side of the transfer cask. Collectively, these locations are referred to as locations of interest. Source terms with the same source energy structure can then simply be multiplied by the response functions to get the dose rate at the locations of interest. It is also reasonable to expect that if some radiological source results in bounding dose rates at the location of interest, it would result in bounding dose rates at all other locations where dose rates are calculated.

However, shielding evaluations with full scale models may result in dose rates at the locations of interest that differ from those obtained herein using the response function since the ranking of the radiological sources (determination of the source that results in the highest dose rates) is the only concern in the current analysis. Therefore, the simplified shielding models of the OS200FC cask and the AHSM-HS storage module employed herein are acceptable for the purpose of determining the fuel assembly BECT parameters resulting in the bounding source.

Response function entries are determined for the important primary gamma energy range of 0.6 MeV to 3.0 MeV since this energy range contributed to more than 98% of the primary gamma dose rates for the zones depicted on Figure B.2.1-1. Neutron response functions are based on the Cm-244 Watt fission spectrum which account for the neutron radiation and the secondary gamma (n,γ) sources. The response functions for both the AHSM-HS and OS200FC TC are presented in Table B.5.5-13 and Table B.5.5-14, respectively.

B.5.2.2.2 Fuel Qualification Methodology

Fuel qualification is performed to determine acceptable combinations of burnup and enrichment for the spent fuel assemblies as shown in Table B.2.1-6. Radiation sources from each of these burnup and enrichment combinations are calculated using SAS2H/ORIGEN-S and are ranked in the order of their importance to dose rates. The cooling times employed for these evaluations are such that the resulting fuel assembly satisfies the decay heat limitations per Figure B.2.1-1, including a minimum cooling time of 5.0 years. Therefore, the calculated cooling times for the ranking of the radiological sources correspond to the minimum required cooling times for fuel assemblies in order to qualify for loading as a function of assembly enrichment and burnup. These sets of radiological sources are converted to sets of dose rates using the response functions. BECT combinations resulting in the largest dose rates are identified and employed in TRITON\T-DEPL depletion models to calculate design basis radiological source terms from four axial exposure regions of the design basis fuel assembly. The design basis radiological source terms calculated with TRITON\T-DEPL models are shown in Table B.5.5-21 through Table B.5.5-23.

The source terms are calculated using a constant cycle average specific power of 30 MW to maximize actinide production rate. One day of down time is conservatively assumed in the depletion models. The cobalt concentration used in the various hardware materials and the total for the entire fuel assembly are selected to maximize the gamma source terms. Boron concentration, moderator temperature, and density values are selected in the depletion model to

maximize buildup of isotopic activities such as Cm-244, resulting in a conservative calculation of neutron source terms.

The minimum required cooling times (and corresponding radiological sources utilized during the ranking) are determined as a function of assembly initial enrichment and burnup for each decay heat limit. Because the decay heat and radiological sources decrease with decreasing burnup for a given enrichment and cooling time, it is conservative to assume during the ranking that the required cooling time for a lower burnup assembly is the same as that for a higher burnup assembly with the same enrichment. Also, the decay heat and radiological sources generally increase slightly with decreasing enrichment for a given burnup and cooling time. Therefore, it is conservative to assume during the ranking that the required cooling time for a higher enrichment assembly is bounded by that for a lower enrichment assembly with the same burnup. The required cooling time for initial enrichments between two enrichment values is assumed to be bounded by that of the lower enrichment.

Dose rates below 14 GWd/MTU burnup and cooling times less than 5.0 years are essentially due to primary gamma radiation (PGR) only. A substantial portion (up to 30 %) of the PGR dose rate is due to the source in the 2.0 to 3.0 MeV energy range. The intensity of the PGR source in this energy range is mainly due to Rh-106 and Pr-144 isotopes with half-lives bounded by 1.015 years. Therefore, dose rates, as well as decay heat, from assemblies with burnup below 14 GWd/MTU are not very significant when a minimum cooling time of 5.0 years is employed for fuel qualification. As a result, decay heat and radiological sources from fuel with burnup below 14 GWd/MTU and an initial enrichment greater than 0.7 wt. % U-235 are bounded by the 14 GWd/MTU cases when ranking the fuel assemblies since 5.0 years is imposed as the minimum allowed cooling time.

Analyzed region 2 in Table B.2.1-6 was an extension of the DHE to encompass the burnup and enrichment combinations as shown. In analyzed region 1, each burnup and enrichment combination was analyzed using SAS2H/ORIGEN-S. For analyzed region 2, only some of the combinations were analyzed using SAS2H/ORIGEN-S. However, these combinations show excellent agreement with the DHE. As the DHE is a continuous function, the other combinations in analyzed region 2 not explicitly analyzed by SAS2H/ORIGEN-S are still encompassed by the DHE. As the enrichment decreases for constant burnup, the fraction of the dose rate due to neutrons increases. Imposing a 10 year minimum cooling time for spent fuel assemblies with a burnup and enrichment combination in analyzed region 2 ensure the design basis source is still bounding for all combinations in both analyzed regions 1 and 2. Additionally, the accident neutron source that was used for the 32PTH2 DSC in the AHSM-HS and OS200FC TC bounds all other neutron sources for authorized contents.

B.5.2.3 Decay Heat Equation

Decay heat sources at various cooling times are determined using SAS2H\ORIGEN-S. The sources are used in a regression analysis to determine parameters of the DHE. The DHE allows the calculation of decay heat for a single design basis assembly as a function of burnup, enrichment, and cooling time.

Decay heat values in watts per fuel assembly are very well represented with an equation of this form:

$$f(Bu,En,T) = P(Bu,En) \times (G \times \exp(-H \times T) + I \times \exp(-J \times T)),$$

where

$$P(Bu,En) = A + B \times Bu + C \times \ln(En) + D \times Bu\text{^}2 + E \times \ln(En)\text{^}2 + F \times Bu \times \ln(En),$$

and

$$A = -55.1,\ B = 55.4,\ C = 226,\ D = 0.691,\ E = 63.4$$

$$F = -19.7,\ G = 1.75,\ H = 0.483,\ I = 0.310,\ J = 0.022.$$

The variables in $f(Bu,En,T)$ correspond to assembly average burnup in GWd/MTU, assembly average enrichment in wt. % U-235, and cooling time in years. The following are the additional considerations when using the DHE.

- Fitting parameters of the DHE are determined using decay heat data at certain burnup and enrichment combinations. The DHE is only applicable to the burnup and enrichment combinations designated as analyzed regions 1 and 2 only in Chapter 2, Table B.2.1-6.

- Fitting parameters of the DHE are determined using decay heat data corresponding to cooling times in the range of 5 to 32 years. The decay heat values obtained beyond this range of cooling times are not fully validated. However, the DHE results in conservative decay heat values at cooling times greater than 32 years, and the extent of the conservatism increases with cooling times greater than 32 years.

- The DHE can under predict the decay heat values for cooling times between 5.0 to 6.0 years. However, the extent of the under prediction does not exceed 6%, and gradually decreases when the cooling time is 6.0 years. Therefore, a 6% margin should be added to the decay heat values predicted with the DHE.

- The DHE equation results in conservative decay heat values when cooling times are greater than 6.0 years. The extent of conservatism is within 3.0 % for cooling times between 6.0 to 28.0 years.

- The results predicted with the DHE are also applicable to fuel assemblies with control components (CCs).

B.5.2.4 Qualification of Fuel Assemblies with Reconstituted Fuel Rods

A reconstituted fuel assembly is defined as a fuel assembly where fuel rods are replaced with fuel or non-fuel (reconstituted) rods and could undergo further irradiation. It is assumed in the shielding analysis that the replacement rods have the same length and outer diameter as the fuel rods they replace. It is assumed when analyzing fuel assemblies with replacement rods undergoing further irradiation, the reconstitution occurred at the end of the first irradiation cycle.

Proprietary information withheld pursuant to 10 CFR 2.390

Proprietary information withheld pursuant to 10 CFR 2.390

Proprietary information withheld pursuant to 10 CFR 2.390

B.5.2.5 Qualification of Fuel Assemblies with Control Components

The 32PTH2 DSC is designed to accommodate up to 32 CE 16 x 16 class fuel assemblies with and without control components (CCs). Authorized CCs include Burnable Poison Rod Assemblies (BPRAs), Control Rod Assemblies (CRAs), Thimble Plug Assemblies (TPAs), Axial Power Shaping Rod Assemblies (APSRAs), Control Element Assemblies (CEAs), Vibration Suppression Inserts (VSIs), Orifice Rod Assemblies (ORAs), Neutron Source Assemblies (NSAs), and Neutron Sources. Nonfuel hardware that is positioned within the fuel assembly after the fuel assembly is discharged from the core (such as Guide Tubes or Instrument Tube Tie Rods) or Anchors, Guide Tube Inserts, BPRA Spacer Plates or other devices that are positioned and operated within the fuel assembly during reactor operation are also considered as CCs.

It is assumed that the CCs are not physically connected to any specific fuel assembly and can be removed from the assembly in which they were irradiated. It is expected that, for example, a 5 year cooled assembly can house a 15 year cooled CC. CEAs represent a limiting case from the radiation shielding standpoint for the CCs because they contain the maximum mass of cobalt compared to any other CC. Gamma source terms are determined for the major sections of the 5-finger CEAs in a CE 16x16 fuel assembly after 15 years of cooling. The resulting source terms are doubled to ensure that they are bounding when considering a minimum cooling time limit of 10 years for CCs. The effect on dose rates and heat load is discussed below.

PWRs typically operate in an All-Rods-Out mode, in which only the lead control rod bank is slightly inserted into the active fuel region. All other control rod banks are fully withdrawn from the active fuel region during normal operation. Therefore, it would be expected that only the tip of the nose cap section of the lead control rod bank would receive significant neutron irradiation. The analysis assumes that each CEA finger is fully inserted into the active fuel up to the top height of the B_4C pellet section. Therefore, the resulting gamma source terms are very conservative.

Design parameters of the bounding CEA are presented in Table B.5.5-18. The sections of the bounding CEA are shown schematically on a sketch in Figure B.5.5-11. The limiting gamma radiation source per finger is shown in Table B.5.5-19 for various sections of the 5-finger CEA.

The radiological source terms due to CCs affect the dose rate distributions near the OS200FC TC and the AHSM-HS. However, it is determined that the maximum value of the dose rates due to design basis radiological source terms without CCs remain bounding if the location of fuel assemblies containing CCs is limited to only the 12 fuel compartments designated as zone 2 per Figure B.2.1-1 to radial zone 2.

Proprietary information withheld pursuant to 10 CFR 2.390

B.5.2.6 Design Basis Source Term Determination

Response functions are used to determine the bounding BECT combination for the authorized contents. The design basis source terms are calculated by employing these bounding parameters for the shielding evaluation of the 32PTH2DSC in the OS200FC TC and the 32PTH2DSC in the AHSM-HS.

B.5.2.6.1 Gamma Source

Four TRITON/T-DEPL models are employed to determine gamma source terms for the four exposure regions of interest for each fuel assembly; the bottom, active fuel, plenum, and top regions. Each model includes the light element specification for the regions being evaluated and the source term output from ORIGEN-S provides the total gamma source for the active fuel region and only the light element source for the plenum, top, and bottom nozzle regions. To account for the reduction in neutron flux in the plenum and top and bottom regions the elemental compositions for these regions are multiplied by the appropriate flux factors given in Table B.5.5-12.

The TRITON\T-DEPL gamma source term is output in the CASK-81 energy group structure shown in Table B.5.5-20 [B5.7]. Gamma source terms for the active fuel region include contributions from actinides, fission products, and activation products. The bottom, plenum, and top nozzle regions include only the contribution from the activation products for each region. The design basis gamma source terms for the shielding evaluation of the 32PTH2 DSC in the AHSM-HS is shown in Table B.5.5-21. The design basis gamma source terms for the shielding

evaluation of the 32PTH2 DSC in the OS200FC TC are shown in Table B.5.5-22 and Table B.5.5-23.

Gamma source terms used in the MCNP5 shielding models are calculated by multiplying the assembly sources by the number of assemblies, in this case 32 assemblies for a fully loaded 32PTH2 DSC.

Almost 100% of the gamma spectrum from light elements is in the range of 0.70 MeV to 1.33 MeV, which corresponds exactly to two of the most prominent lines of Co-60. The principal fission product isotopes that contribute greater than 5% to the gamma source term in the energy range of 0.01 to 0.90 MeV are: Sr-90, Y-90, Rh-106, Cs-137, Pr-144, Eu-154, and Eu-155. Contributions from Y-90, Rh-106, Cs-137, Pr-144, and Eu-154 are dominant in the range of 0.90 to 1.50 MeV. Rh-106, Sm-147, and Ce-142 are the strongest emitters at energies greater than 2.0 MeV. The accuracy of gamma spectrum is dependent upon the energy. Gamma source terms computed for fission products tend to be more accurate than those for actinides because the calculation of their inventory has less uncertainty.

Immediately after discharge, the gamma emission at higher energies is dominated by actinides, particularly at energies greater than 4 MeV at all cooling times and energy greater than 3.5 MeV for cooling times after 10 years and is dominated by the contribution from Cm-244 [B5.1]. Thus the uncertainty for energies 3.0 MeV and greater is bounded with the precision with which the inventory of Cm-244 is calculated. Per SCALE 4.4 [B5.1], reported experimental Cm-244 densities are accurate within ± 20%. The gamma emission intensity from Cm, which is proportional to the quantity of Cm in the actinide inventory, is bounded by this value.

B.5.2.6.2 Neutron Source Term

One TRITON/T-DEPL model is required to determine the total design basis neutron source term for the active fuel region. At discharge, the neutron source is almost equally produced from Cm-242 and Cm-244. The other strong contributor is Cf-252, which is approximately 10% of the Cm intensity, but its share essentially vanishes after 6 years of cooling time because the half-life of Cf-252 is 2.65 years. The half-lives of Cm-242 and Cm-244 are 163 days and 18 years, respectively. Contributions from the next strongest emitters, Pu-238 and Pu-239, are lower by a factor of 1000 and 100 relative to Cm-244. Thus, the neutron spectrum for cooling times greater than or equal to 5 years is almost totally dominated by Cm-244 in both spontaneous fission and (α,n) components. The design basis neutron source terms for the shielding analysis of the 32PTH2 DSC in the AHSM-HS are shown in Table B.5.5-21. The design basis neutron source terms for the shielding analysis of the 32PTH2 DSC in the OS200FC TC are shown in Table B.5.5-22 and Table B.5.5-23.

The effect of subcritical neutron multiplication and source terms strength variation along the FA axis due to a variation of the axial burnup profile in the active fuel region are not accounted for when using SCALE depletion models. However, these effects are accounted for in the shielding analysis by applying correction factors when describing the source in MCNP5 input decks. Neutron source terms for use in the MCNP5 shielding models are calculated by multiplying the

fuel assembly source by the number of assemblies in the DSC fuel compartments. The magnitude of the neutron source is also increased to account for the axial distribution in the fuel, as discussed in Section B.5.4.2. The effect of the neutron subcritical multiplication and correction to the neutron source strength due to axial burnup profile variation is also accounted in the calculation of the response functions used for ranking the fuel assemblies

Total neutron source terms for use in the MCNP5 shielding models are calculated by multiplying the neutron source for each fuel assembly by the total number of assemblies, as well as $P_f/(1-k_{eff})$ to account for subcritical multiplication, where k_{eff} is assumed to be 0.4 for a dry DSC and 0.941 for a DSC filled with water (when the fuel is completely under water), and P_f is the neutron peaking factor discussed in section B.5.4.2. The assumed values of k_{eff} are conservative because they correspond to fresh, not depleted, fuel. The fixed source spectrum in MCNP5 is assumed to follow a Cm-244 spontaneous fission spectrum for all of the shielding calculations. It is based on the following relationship:

$$p(E) \sim \exp(-E/a)\sinh(bE)^{1/2},$$

with input parameters a=0.906 MeV and b=3.848 $(MeV)^{-1}$, as given in the MCNP5 manual [B5.8].

B.5.3 Model Specification

The neutron and gamma dose rates on the surface of the AHSM-HS and on the surface, 1, and 3 feet from the surface of the OS200FC TC are evaluated with the Monte Carlo transport code MCNP5 [B5.8]. In addition, the flux-to-dose-rate conversion factors specified by the ANSI/ANS 6.1.1-1977, shown in Table B.5.5-8, are used [B5.9].

B.5.3.1 Description of the Radial and Axial Shielding Configurations

Figure B.5.5-1 is a sketch of the AHSM-HS with a vertical cut-away through the center module and 32PTH2 DSC. Figure B.5.5-2 through Figure B.5.5-5 show various cuts through the AHSM-HS along the length of the 32PTH2 DSC. These figures illustrate the layout of the 32PTH2 DSC in the AHSM-HS and the major design features of the AHSH-HS, including the end and rear shield walls.

MCNP5 computer models are employed to determine the dose rates along the front wall surface, the rear shield wall surface, the vent openings, the roof surface, and on the surfaces of the side shield walls.

Figure B.5.5-6 through Figure B.5.5-10 shows the shielding configuration of the 32PTH2 DSC in the OS200FC TC.

B.5.3.2 Storage Configuration

The geometry and material design features of the AHSM-HS are modeled explicitly in MCNP5. In the MCNP5 coordinate system, the AHSM-HS/32PTH2 DSC length is in the z direction, the width is in the x direction, and the height is in the y direction. The MCNP5 model is a full 3-D representation of a single 32PTH2 DSC inside the AHSM-HS.

Proprietary information withheld pursuant to 10 CFR 2.390

Two MCNP5 models are developed for this calculation. The gamma model, containing a detailed segmentation of the thicker 32PTH2 DSC steel shield plugs and cover lids and AHSM-HS door, is utilized to calculate the gamma dose rates. The neutron model is utilized to calculate the neutron dose rates.

The AHSM-HS shielding performance was analyzed both with and without the dose reduction hardware in the inlet and outlet vents. The dose reduction hardware is discussed in Section B.5.4.8.

Various views of the MCNP5 model depicting the important AHSM-HS features, including the optional dose reduction hardware are shown in Figure B.5.5-12 through Figure B.5.5-19.

B.5.3.3 Loading and Transfer Configurations

The z-axis in the MCNP5 model coincides with the axis of the OS200FC TC and the 32PTH2 DSC. The dose rates at the surface, 1.5 feet and 3 feet from the surface of the 32PTH2 DSC/OS200FC TC are determined using MCNP5. Four different configurations associated with loading/unloading of the spent fuel are analyzed. These configurations are (1) transfer (normal) (2) decontamination, (3) welding, and (4) accident.

Definition of OS200FC TC and 32PTH2 DSC Configurations

Transfer (Normal) – The 32PTH2 DSC and annulus between the 32PTH2 DSC and OS200FC TC are assumed to be dry. The neutron shield is assumed to be full. The 32PTH2 DSC top shield plug, inner and outer top cover plates, and the OS200FC TC lid are installed. The MCNP5 model for this configuration is shown in Figure B.5.5-20.

Decontamination – The OS200FC TC is assumed to be full of water. The annulus between the 32PTH2 DSC and OS200FC TC is also filled with water. The neutron shield is assumed to be full. The top shield plug and the inner top cover plate are assumed to be installed and no temporary shielding is in place. The MCNP5 model for the decontamination configuration is shown in Figure B.5.5-21.

Welding – For welding operations the fuel is assumed to be completely dry. Temporary shielding of 3 inches of NS-3 or equivalent and 1 inch of steel or equivalent are assumed to cover the top shield plug and the inner cover plate which are installed. The 32PTH2 DSC/OS200FC TC annulus and the OS200FC TC neutron shield are assumed to be completely filled with water. The outer top cover plate is not installed in this configuration. The MCNP5 model for the welding configuration is shown in Figure B.5.5-22.

Accident – The condition of the OS200FC TC during an accident assumes the liquid neutron shield and steel skin are lost (neutron shield is torn off). This assumption maximizes a possible credible dose rate under an accident scenario. The fuel is analyzed as both intact and failed (fuel reconfiguration). For modeling the fuel as rubble, it is assumed that the entire fuel assembly mass is free to redistribute during the event, and therefore a single homogenized region containing all assembly materials is modeled. A uniform, combined spatial source distribution is used without axial peaking. The final reconfiguration volume is assumed to be compacted to 50% of the original fuel assembly volume. The MCNP5 model for the accident configuration is shown in Figure B.5.5-23 without reconfiguration and Figure B.5.5-24 with reconfiguration. Dose rate results for these four configurations are provided in Table B.5.5-4 through Table B.5.5-8.

B.5.3.4 Elemental Compositions and Densities of Shielding Materials

The fuel assembly layout within the 32PTH2 DSC is a Cartesian array inside the fuel compartments surrounded by sheets of poison material which are modeled as aluminum in the shielding calculations. The fuel assembly is homogenized within the assembly volume, assuming fresh fuel with no blankets, burnable absorbers, or fission product poisons. This assumption is conservative as it minimizes self-shielding in the source regions. The homogenized material compositions are shown in Table B.5.5-25 and Table B.5.5-26 for dry and wet fuel, respectively.

The wet fuel material compositions are used for the decontamination configuration. The material compositions of the remaining shielding materials are shown in Table B.5.5-27.

B.5.4 Shielding Evaluation

B.5.4.1 Computer Program

The Monte Carlo N-Particle (MCNP5) computer program [B5.8] determines the particle (neutron and/or photon) flux throughout three-dimensional geometric systems by using the Monte Carlo method. Particles can be generated by either particle interaction with the transport medium or extraneous sources incident upon the system. MCNP5 or MCNP is an industry standard code distributed by ORNL/RSICC.

MCNP5 was chosen for this application because of its ability to solve three-dimensional, deep penetration, radiation transport problems applicable to the NUHOMS® 32PTH2 system.

B.5.4.2 Spatial Distribution of Radiological Sources

The fixed source components are:

- a neutron source due to the active fuel regions of the 32 fuel assemblies,
- a gamma source due to the active fuel regions of the 32 fuel assemblies,
- a gamma source due to the plenum regions of the 32 fuel assemblies,
- a gamma source due to the top nozzle regions of the 32 fuel assemblies,
- a gamma source due to the bottom nozzle regions of the 32 fuel assemblies, and
- a gamma source due to control components, if loaded.

For the shielding calculations, the probability of a gamma radiation source particle being originated at any given axial location within the active region of the fuel assembly is proportional to the burnup of the fuel at this location. The axial intensity of the gamma radiation source (axial peaking factor) is assumed to be proportional to the burnup profile. The probability of a neutron radiation source particle at any given axial location within the active region of the fuel assembly is proportional to the fourth power (4.02) of burnup of the fuel in this location. A uniform distribution of radiological sources at the axial end regions of the fuel assemblies is employed. The axial burnup profile is obtained from reference [B5.16] and is shown in the third column of Table B.5.5-28.

The axial distributions (peaking factors) for both neutron and gamma sources in the active fuel region are shown in Table B.5.5-28 as a function of active fuel height. These distributions are used to describe radiological source terms strength along the Z axis of the active fuel region in MCNP5 models for bounding shielding evaluation and calculation of response functions employed during the ranking of assemblies. A distribution of the sources within the active fuel region in the X and Y direction is assumed to be uniform. The gamma and neutron peaking factors are also used to represent the number of particles in each axial segment of the fuel assembly active region. The number of particles in each axial segment is the total source strength × fractional segment width × normalized peaking factor. The fractional segment widths are also shown in Table B.5.5-28 as a percentage of the total active fuel length. The number of particles in each segment is an input to the MCNP5 shielding models. However, it is not necessary to

input the actual number of particles in each segment on the MCNP5 input card because MCNP5 will renormalize the distribution, although the relative number of particles between each segment must match the true particle distribution.

The computer codes utilized herein to calculate source terms intrinsically assume that the power is generated uniformly throughout the active fuel region of fuel assemblies. This discrepancy is corrected in the shielding models by using the peaking factors described. The total intensity of the neuron source calculated with the depletion models utilized herein need to be multiplied by the factor of 1.183 to account for normalization of the neutron source. Its physical meaning is the ratio of the true total strength of the neutron radiation source due to a fuel assembly with an axially non-uniform distribution to the strength from the assembly with a uniform distribution. Subcritical multiplication was accounted in the results by scaling depending on the 32PTH2 DSC configuration. For configurations where the 32PTH2 DSC is assumed to be dry, k_{eff}=0.40 was used. For the sole configuration where the 32PTH2 DSC is assumed to be completely filled with water, the decontamination configuration as discussed in Section B.5.3, k_{eff}=0.9410 was used. Together, the neutron and (n,γ) sources require a factor of 1.97 to account for both the peaking factor and subcritical multiplication in dry cases. The notes to Table B.5.5-21 through Table B.5.5-23 provide additional clarification.

B.5.4.3 Cross-Section Data

The cross-section data used in this analysis is the standard ENDF/B-VI continuous cross section data distributed with the MCNP5 code [B5.8]. Cross-sections are at a temperature of 300°K. Because continuous cross-section data are utilized, cross-section processing is not required.

B.5.4.4 Flux-to-Dose Rate Conversion

The flux distribution calculated by the MCNP5 code is converted to dose rates using the flux-to-dose rate conversion factors provided in ANSI/ANS-6.1.1-1977 [B5.9]. The gamma ray and neutron flux-to-dose rate conversion factors are shown in Table B.5.5-24.

B.5.4.5 Geometry of Shielding Model

Figure B.5.5-12 through Figure B.5.5-19 show the MCNP5 model for the 32PTH2 DSC in the AHSM-HS.

Figure B.5.5-20 through Figure B.5.5-24 show the MCNP5 models of the 32PTH2 DSC in the OS200FC TC for the various loading/transfer configurations.

B.5.4.6 Dose Rate Methodology Validation

The method employed to calculate the dose rate has been verified using measurements. A loaded NUHOMS®-24P in the HSM Model 80 loaded with B&W 15x15 Mark B fuel was compared against an MCNP model of the same. The MCNP model was developed to calculate dose rates at the locations where the dose rates were measured on the real system.

The results of this comparison are shown in Table B.5.5-29 as reproduced from Table B.5.5-26 of Chapter M.5 of the Standardized NUHOMS® System UFSAR [B5.6]. This validation was

previously employed to qualify the MCNP methodology for the Standardized NUHOMS® System.

The results show that MCNP conservatively predicts total dose rates compared to the measured data. Some conservatism in the methodology used to calculate the source terms still exists and likely contributed to the general overprediction of the calculated dose rates when compared to the measured dose rates.

In conclusion, this comparison provides a validation of the dose rate calculation methodology for the 32PTH2 DSC in the AHSM-HS and provides additional assurance that the dose rates calculated for the 32PTH2 DSC in the AHSM-HS are conservative.

B.5.4.7 Source Term Methodology Validation

Two different computer codes are in use for fuel qualification and the source term calculations. The first, SAS2H/ORIGEN-S, was employed in the ranking of the fuel assemblies and generating decay heat source utilized in the regression analysis to determine parameters of the DHE. It was selected for its computational efficiency and appropriate fidelity required to rank the assemblies based on their respective BECT combinations. TRITON\T-DEPL was employed to calculate the design basis source terms at the BECT combination resulting in the highest dose rate based on the response functions from ranking.

Evaluations of the existing data with SAS2H and the 44-group ENDF/B-V library used in the analysis are documented in References [B5.12] and [B5.13]. These comparisons all show generally good agreement between the calculations and measurements, and show no adverse trend as a function of burnup in the data that would suggest that the isotopic predictions, and therefore neutron and gamma source terms, would not be in good agreement. A similar conclusion is also reached by the results documented in the JAERI report [B5.14].

As documented in Reference [B5.15] and confirmed in the SAS2H analysis, the total neutron source with increasing burnup is dominated by spontaneous fission neutrons. Based on the results from the SAS2H analysis, the neutron source term is due almost entirely to the spontaneous fission of Cm-244 (greater than 85%). Further, a review of the measured Cm-244 content compared to the Cm-244 content predicted by SAS2H and the 44-group ENDF/B-V library documented in References [B5.12] and [B5.13] for burnups up to 46,460 MWd/MTU, it is concluded that the calculated values are within ±11 % of the measured values, with most of the predicted values within ±5% of measured. Further, there is no adverse trend as a function of burnup in the data that would indicate that the predicted Cm-244 content is significantly different at higher burnups.

Reference [B5.18], a newer compilation of data for high burnup fuel, has been generated for TRITON with the goal of extensive validation. Enrichments from 2.6 to 4.7 wt. % U-235 and burnups from 14 to 78 GWd/MTU were considered in the report. This study bridges the gap of previous references from 45 to 62 GWd/MTU, the current regulatory limit. The report concludes that the calculated isotopic results are generally found to be within the range of the experimental data for many important to shielding isotopes in the spent fuel. The report covers isotopes important to both radiological source and decay heat particularly at cooling times equal to or greater than 5 years.

According to calorimetric measurements of spent fuel assembly heat rates the code results in slightly under predicted values for BWR assemblies, and slightly over predicted values for PWR assemblies [B5.19]. At a confidence level associated with two standard deviations, the percentage differences lie in the range of 2.4-3.2 %. A review of uncertainties, differences between measured and calculated with SAS2H quantities of isotopes, decay heats and radiological sources is presented in Section S.2.3 of reference [B5.1]. Benchmarking by ORNL has investigated the decay heat source terms due to LEU fuel. It is observed that isotopes contributing to the neutron radiation source are also strong contributors to the decay heat sources. Two depletion models, TRITON and SAS2H, were utilized in the current analysis. It was observed that the TRITON models generally result in lower decay heat values when compared to the results from SAS2H.

The coupled approach using SAS2H/ORIGEN-S for ranking with TRITON\T-DEPL to develop the design basis source terms targets the correct BECT combination while providing an appropriately validated basis for the codes. Both the burnup and the enrichment ranges for authorized contents have been validated in publically available literature. The results of this report are reasonable when compared to the dose rates developed in the analysis and their relative strength compared to the exposure limits of 10 CFR Part 72.

Proprietary information withheld pursuant to 10 CFR 2.390

Proprietary information withheld pursuant to 10 CFR 2.390

B.5.5 Supplemental Information

B.5.5.1 References:

[B5.1] Oak Ridge National Laboratory, RSIC Computer Code Collection, "SCALE: A Modular Code System for Performing Standardized Computer Analysis for Licensing Evaluations for Workstations and Personal Computers," NUREG/CR-0200, Revision 6, ORNL/NUREG/CSD-2/V2/R6.

[B5.2] Ludwig, S.B., and J.P. Renier, "Standard- and Extended-Burnup PWR and BWR Reactor Models for the ORIGEN2 Computer Code," ORNL/TM-11018, Oak Ridge National Laboratory, December 1989.

[B5.3] Office of Civilian Radioactive Waste Management, "Characteristics of Potential Repository Wastes", DOE/RW-0184-R1, July 1992.

[B5.4] Not used.

[B5.5] Not used.

[B5.6] "Updated Final Safety Analysis Report for the Standardized NUHOMS® Horizontal Modular Storage System for Irradiated Nuclear Fuel," Revision 11, (US NRC Docket No. 72-1004) File Number NUH003.0103.

[B5.7] Oak Ridge National Laboratory, "CASK-81 22 Neutron, 18 Gamma-Ray, P3, Cross Sections for Shipping Cask Analysis", Report DLC-23.

[B5.8] "MCNP/MCNPX - Monte Carlo N-Particle Transport Code System Including MCNP5 1.40 and MCNPX 2.5.0 and Data Libraries," CCC-730, Oak Ridge National Laboratory, RSICC Computer Code Collection, January 2006.

[B5.9] American Nuclear Society, "American National Standard Neutron and Gamma-Ray Flux-to-Dose Rate Factors", ANSI/ANS-6.1.1-1977, La Grange Park, Illinois, March 1977.

[B5.10] Not used.

[B5.11] Not used.

[B5.12] M.D. DeHart and O.W. Hermann, "An Extension of the Validation of SCALE (SAS2H) Isotopic Predictions for PWR Spent Fuel," ORNL/TM-13317, September 1996.

[B5.13] O.W. Hermann, S.M. Bowman, M.C. Brady, C.V. Parks, "Validation of the SCALE System for PWR Spent Fuel Isotopic Composition Analyses," ORNL/TM-12667, March 1995.

[B5.14] Japan Atomic Energy Research Institute, "Technical Development on Burnup Credit for Spent LWR Fuels," JAERI-Tech 2000-071, September 21, 2000.

[B5.15] U.S. Nuclear Regulatory Commission, "Nuclide Importance to Criticality Safety, Decay Heating, and Source Terms Related to Transport and Interim Storage of High Burnup LWR Fuel," NUREG/CR-6700, Published January 2001, ORNL/TM-2000/284.

[B5.16] J.C. Wagner, M.D. DeHart, and C.V. Parks, "Recommendations for Addressing Axial Burnup in PWR Burnup Credit Analyses," NUREG/CR-6801, Oak Ridge National Laboratory.

[B5.17] SCALE 6: Modular Code System for Performing Standardized Computer Analyses for Licensing Evaluation for Workstations and Personal Computers., Oak Ridge National Laboratory, Radiation Shielding Information Center Code Package CCC-750, February 2009.

[B5.18] US Nuclear Regulatory Commission, "Uncertainties in Predicted Isotopic Compositions for High Burnup PWR Spent Nuclear Fuel," NUREG/CR-7012, Published January 2011, ORNL/TM-2010/41.

[B5.19] O.W. Herman, J.P. Renier, and C.V. Parks, "Technical Support for a Proposed Decay Heat Guide Using SAS2H/ORIGEN-S Data", NUREG-CR-5625, ORNL/CSD-130, Martin Marietta Energy Systems Inc., Oak Ridge Natl. Lab. (1994).

Table B.5.5-1
NUHOMS® 32PTH2 System Shielding Materials

Proprietary information withheld pursuant to 10 CFR 2.390

Table B.5.5-2
Summary of NUHOMS® 32PTH2 DSC in AHSM-HS, Bounding Maximum and Average Dose Rates

Dose Rate Location	Maximum Gamma (mrem/hr)	Gamma MCNP5 1σ Error	Maximum Neutron (mrem/hr)	Neutron MCNP5 1σ Error	Maximum Total[1] (mrem/hr)	Total MCNP5 1σ Error
AHSM-HS Roof (centerline)	5.70	0.026	3.04	0.031	8.74	0.020
AHSM-HS Roof Birdscreen	23.69	0.024	18.74	0.032	42.43	0.020
AHSM-HS End (Side) Shield Wall Surface	1.55	0.025	0.46	0.130	2.00	0.035
AHSM-HS Door Exterior Surface (within Door Perimeter)	3.61	0.046	1.74	0.037	5.35	0.033
AHSM-HS Front Birdscreen	207.63	0.12	75.53	0.49	247.75	0.10
Over Top Vent Shaft (Accident) [2]	1888.48	0.03	341.71	0.03	2230.19	0.03

Dose Rate Location	Gamma Average (mrem/hr)	Gamma MCNP5 1σ Error	Average Neutron (mrem/hr)	Neutron MCNP5 1σ Error	Average Total (mrem/hr)	Total MCNP5 1σ Error
Top of AHSM-HS Roof Slab	6.54	0.002	4.27	0.003	10.81	0.002
AHSM-HS End (Side) Shield Wall Surface	0.39	0.002	0.12	0.01	0.51	0.003
AHSM-HS Front	8.42	0.04	2.28	0.06	10.70	0.04
AHSM-HS 3' Thick Rear Shield Wall	0.09	0.01	0.02	0.02	0.11	0.01
Top of AHSM-HS Roof Slab (Accident) [2]	101.50	<0.01	25.17	0.01	126.67	<0.01

Notes:

(1) Gamma and Neutron dose rate peaks do not always occur at same location; therefore, the maximum of total dose rate is not always the sum of the gamma and neutron dose rate maximums.

(2) The dose rates are applied to the hypothetical accident condition. However, the values of the dose rates are determined when the top vent cover is in place. That means the exposure to radiation backscattering from top vent cover and vent liners included. This is extremely conservative because there is no backscattering from the top vent cover when the top vent cover is lost during the hypothetical accident. Therefore, the actual maximum and the average dose rates are lower by about the factor of two and six when the top vent cover is lost during the accident conditions, respectively.

Table B.5.5-3
Summary of NUHOMS® 32PTH2 DSC in AHSM-HS, Bounding Maximum and Average Dose Rates With Dose Rate Reduction Hardware

Proprietary information withheld pursuant to 10 CFR 2.390

Table B.5.5-4
Summary of NUHOMS® 32PTH2 DSC in OS200FC TC for Transfer Operations, Bounding Maximum and Average Dose Rates

Dose Rate Location	Distance	Maximum Neutron (mrem/hr)	Neutron MCNP5 1σ Error	Maximum Gamma (mrem/hr)	Gamma MCNP5 1σ Error	Maximum Total[(1)] (mrem/hr)	Total MCNP5 1σ Error
Side	Surface	2.93E+01	0.0021	1.98E+02	0.0028	2.02E+02	0.0025
	1.5 ft	1.81E+01	0.0019	1.15E+02	0.0023	1.29E+02	0.0023
	3 ft	1.27E+01	0.0018	7.98E+01	0.0025	9.25E+01	0.0022
Top	Surface	4.09E+00	0.0110	5.09E+02	0.0349	5.11E+02	0.0348
	1.5 ft	2.43E+00	0.0094	1.05E+02	0.0390	1.06E+02	0.0386
	3 ft	1.52E+00	0.0135	6.76E+01	0.0457	6.85E+01	0.0451
Bottom	Surface	2.10E+02	0.0094	5.95E+02	0.0125	8.05E+02	0.0095
	1.5 ft	5.23E+01	0.0114	2.56E+02	0.0142	3.08E+02	0.0120
	3 ft	2.10E+01	0.0154	1.32E+02	0.0173	1.53E+02	0.0150

Dose Rate Location	Distance	Average Neutron (mrem/hr)	Neutron MCNP5 1σ Error	Average Gamma (mrem/hr)	Gamma MCNP5 1σ Error	Average Total (mrem/hr)	Total MCNP5 1σ Error
Side	Surface	1.44E+01	0.0013	1.20E+02	0.0016	1.34E+02	0.0015
	1.5 ft	8.96E+00	0.0012	7.63E+01	0.0013	8.53E+01	0.0012
	3 ft	6.56E+00	0.0012	5.66E+01	0.0013	6.31E+01	0.0012
Top	Surface	2.06E+00	0.0100	5.59E+01	0.0174	5.79E+01	0.0168
	1.5 ft	1.18E+00	0.0075	3.65E+01	0.0231	3.76E+01	0.0224
	3 ft	8.37E-01	0.0068	2.92E+01	0.0259	3.01E+01	0.0252
Bottom	Surface	1.12E+01	0.0050	3.99E+01	0.0052	5.11E+01	0.0042
	1.5 ft	7.85E+00	0.0053	2.75E+01	0.0067	3.53E+01	0.0054
	3 ft	6.04E+00	0.0056	2.31E+01	0.0074	2.92E+01	0.0060

Note:

(1) Gamma and Neutron dose rate peaks do not always occur at same location; therefore, the maximum of total dose rate is not always the sum of the gamma plus neutron dose rate maximums.

Table B.5.5-5
Summary of NUHOMS® 32PTH2 DSC in OS200FC TC for Decontamination Operation, Bounding Maximum and Average Dose Rates

Dose Rate Location	Distance	Maximum Neutron (mrem/hr)	Neutron MCNP5 1σ Error	Maximum Gamma (mrem/hr)	Gamma MCNP5 1σ Error	Maximum Total[(1)] (mrem/hr)	Total MCNP5 1σ Error
Side	Surface	1.69E+03	0.0021	1.29E+03	0.0009	2.97E+03	0.0013
	1.5 ft	1.05E+03	0.0018	7.34E+02	0.0008	1.79E+03	0.0011
	3 ft	7.37E+02	0.0017	4.77E+02	0.0008	1.21E+03	0.0011
Top	Surface	4.05E+01	0.0105	3.71E+03	0.0102	3.71E+03	0.0102
	1.5 ft	2.42E+01	0.0126	2.61E+03	0.0104	2.62E+03	0.0104
	3 ft	1.58E+01	0.0151	1.78E+03	0.0129	1.78E+03	0.0129
Bottom	Surface	1.83E+03	0.0243	5.33E+02	0.0128	2.36E+03	0.0190
	1.5 ft	4.61E+02	0.0289	2.29E+02	0.0147	6.90E+02	0.0199
	3 ft	1.99E+02	0.0374	1.20E+02	0.0177	3.18E+02	0.0243

Dose Rate Location	Distance	Average Neutron (mrem/hr)	Neutron MCNP5 1σ Error	Average Gamma (mrem/hr)	Gamma MCNP5 1σ Error	Average Total (mrem/hr)	Total MCNP5 1σ Error
Side	Surface	7.41E+02	0.0012	6.05E+02	0.0009	1.35E+03	0.0008
	1.5 ft	4.72E+02	0.0012	3.53E+02	0.0005	8.25E+02	0.0007
	3 ft	3.52E+02	0.0012	2.53E+02	0.0005	6.05E+02	0.0007
Top	Surface	1.86E+01	0.0072	5.49E+02	0.0046	5.68E+02	0.0045
	1.5 ft	1.21E+01	0.0084	5.13E+02	0.0048	5.25E+02	0.0047
	3 ft	8.84E+00	0.0096	4.69E+02	0.0048	4.78E+02	0.0048
Bottom	Surface	1.56E+02	0.0087	8.70E+01	0.0024	2.43E+02	0.0057
	1.5 ft	9.77E+01	0.0099	4.95E+01	0.0035	1.47E+02	0.0067
	3 ft	7.08E+01	0.0109	3.40E+01	0.0045	1.05E+02	0.0075

Note:

(1) Gamma and Neutron dose rate peaks do not always occur at same location; therefore, the maximum of total dose rate is not always the sum of the gamma plus neutron dose rate maximums.

Table B.5.5-6
Summary of NUHOMS® 32PTH2 DSC in OS200FC TC for Welding Operation, Bounding Maximum and Average Dose Rates

Dose Rate Location	Distance	Maximum Neutron (mrem/hr)	Neutron MCNP5 1σ Error	Maximum Gamma (mrem/hr)	Gamma MCNP5 1σ Error	Maximum Total(1) (mrem/hr)	Total MCNP5 1σ Error
Side	Surface	2.07E+01	0.0028	2.82E+02	0.0679	2.83E+02	0.0677
	1.5 ft	1.29E+01	0.0025	9.16E+01	0.0026	9.54E+01	0.0027
	3 ft	9.01E+00	0.0026	6.02E+01	0.0028	6.92E+01	0.0025
Top	Surface	3.78E+00	0.0752	2.59E+03	0.0581	2.60E+03	0.0580
	1.5 ft	2.08E+00	0.0418	1.49E+03	0.0048	1.49E+03	0.0048
	3 ft	1.34E+00	0.0555	1.04E+03	0.0193	1.05E+03	0.0193
Bottom	Surface	2.11E+02	0.0092	5.97E+02	0.0124	8.08E+02	0.0094
	1.5 ft	5.12E+01	0.0116	2.53E+02	0.0142	3.04E+02	0.0120
	3 ft	2.06E+01	0.0174	1.32E+02	0.0171	1.53E+02	0.0150

Dose Rate Location	Distance	Average Neutron (mrem/hr)	Neutron MCNP5 1σ Error	Average Gamma (mrem/hr)	Gamma MCNP5 1σ Error	Average Total (mrem/hr)	Total MCNP5 1σ Error
Side	Surface	1.01E+01	0.0016	1.21E+02	0.0093	1.31E+02	0.0086
	1.5 ft	6.26E+00	0.0015	6.51E+01	0.0049	7.14E+01	0.0045
	3 ft	4.59E+00	0.0015	4.57E+01	0.0027	5.03E+01	0.0025
Top	Surface	1.31E+00	0.0121	3.95E+02	0.0117	3.97E+02	0.0116
	1.5 ft	9.25E-01	0.0125	3.60E+02	0.0118	3.61E+02	0.0118
	3 ft	7.07E-01	0.0133	3.29E+02	0.0122	3.30E+02	0.0122
Bottom	Surface	9.41E+00	0.0060	3.51E+01	0.0056	4.45E+01	0.0046
	1.5 ft	6.95E+00	0.0052	2.54E+01	0.0070	3.24E+01	0.0056
	3 ft	5.48E+00	0.0054	2.18E+01	0.0076	2.73E+01	0.0061

Note:

(1) Gamma and Neutron dose rate peaks do not always occur at same location; therefore, the maximum of total dose rate is not always the sum of the gamma plus neutron dose rate maximums.

Table B.5.5-7
Summary of NUHOMS® 32PTH2 DSC in OS200FC TC for Accident Conditions, Bounding Maximum and Average Dose Rates

Dose Rate Location	Distance	Maximum Neutron (mrem/hr)	Neutron MCNP5 1σ Error	Maximum Gamma (mrem/hr)	Gamma MCNP5 1σ Error	Maximum Total[(1)] (mrem/hr)	Total MCNP5 1σ Error
Side	Surface	2.88E+03	0.0012	4.00E+02	0.0050	3.15E+03	0.0012
	1.5 ft	1.79E+03	0.0011	2.33E+02	0.0045	1.98E+03	0.0012
	3 ft	1.21E+03	0.0010	1.47E+02	0.0044	1.35E+03	0.0011
Top	Surface	1.32E+02	0.0057	4.85E+02	0.0693	4.96E+02	0.0678
	1.5 ft	8.70E+01	0.0063	1.02E+02	0.0875	1.26E+02	0.0708
	3 ft	6.32E+01	0.0068	6.68E+01	0.0900	9.09E+01	0.0661
Bottom	Surface	5.44E+02	0.0148	6.07E+02	0.0242	1.15E+03	0.0145
	1.5 ft	1.99E+02	0.0047	2.53E+02	0.0283	4.12E+02	0.0182
	3 ft	1.32E+02	0.0050	1.42E+02	0.0337	2.29E+02	0.0218

Dose Rate Location	Distance	Average Neutron (mrem/hr)	Neutron MCNP5 1σ Error	Average Gamma (mrem/hr)	Gamma MCNP5 1σ Error	Average Total (mrem/hr)	Total MCNP5 1σ Error
Side	Surface	1.24E+03	0.0008	2.06E+02	0.0030	1.45E+03	0.0008
	1.5 ft	8.25E+02	0.0008	1.40E+02	0.0028	9.65E+02	0.0008
	3 ft	6.18E+02	0.0007	1.06E+02	0.0028	7.24E+02	0.0007
Top	Surface	7.31E+01	0.0034	7.72E+01	0.0249	1.50E+02	0.0129
	1.5 ft	5.03E+01	0.0033	4.56E-01	0.0092	5.07E+01	0.0033
	3 ft	3.96E+01	0.0033	3.02E+01	0.0494	6.98E+01	0.0215
Bottom	Surface	2.16E+02	0.0024	5.58E+01	0.0093	2.72E+02	0.0027
	1.5 ft	1.30E+02	0.0027	3.23E+01	0.0130	1.62E+02	0.0034
	3 ft	9.21E+01	0.0029	2.62E+01	0.0147	1.18E+02	0.0040

Note:

(1) Gamma and Neutron dose rate peaks do not always occur at same location; therefore, the maximum of total dose rate is not always the sum of the gamma plus neutron dose rate maximums.

Table B.5.5-8
Summary of NUHOMS® 32PTH2 DSC in OS200FC TC for Accident Conditions with Reconfiguration, Bounding Maximum and Average Dose Rates

Dose Rate Location	Distance	Maximum Neutron (mrem/hr)	Neutron MCNP5 1σ Error	Maximum Gamma (mrem/hr)	Gamma MCNP5 1σ Error	Maximum Total[1] (mrem/hr)	Total MCNP5 1σ Error
Side	Surface	2.36E+03	0.0024	3.19E+02	0.0058	2.67E+03	0.0022
	1.5 ft	1.50E+03	0.0021	2.10E+02	0.0054	1.70E+03	0.0020
	3 ft	1.03E+03	0.0020	1.48E+02	0.0051	1.18E+03	0.0019
Top	Surface	1.23E+02	0.0112	8.80E+01	0.1036	1.57E+02	0.0091
	1.5 ft	8.06E+01	0.0118	2.73E+01	0.0175	9.28E+01	0.0104
	3 ft	5.71E+01	0.0124	1.80E+01	0.0235	6.33E+01	0.0113
Bottom	Surface	1.02E+03	0.0198	6.02E+02	0.0234	1.62E+03	0.0152
	1.5 ft	3.04E+02	0.0195	2.45E+02	0.0275	5.49E+02	0.0163
	3 ft	1.61E+02	0.0085	1.20E+02	0.0356	2.72E+02	0.0196

Dose Rate Location	Distance	Average Neutron (mrem/hr)	Neutron MCNP5 1σ Error	Average Gamma (mrem/hr)	Gamma MCNP5 1σ Error	Average Total (mrem/hr)	Total MCNP5 1σ Error
Side	Surface	1.13E+03	0.0014	1.50E+02	0.0033	1.28E+03	0.0013
	1.5 ft	7.54E+02	0.0014	1.03E+02	0.0033	8.57E+02	0.0013
	3 ft	5.63E+02	0.0014	7.84E+01	0.0033	6.42E+02	0.0013
Top	Surface	7.09E+01	0.0065	2.73E+01	0.0189	9.81E+01	0.0070
	1.5 ft	4.71E+01	0.0061	6.75E-01	0.0133	4.78E+01	0.0060
	3 ft	3.67E+01	0.0059	8.44E+00	0.0429	4.52E+01	0.0093
Bottom	Surface	3.34E+02	0.0041	4.33E+01	0.0095	3.77E+02	0.0038
	1.5 ft	1.82E+02	0.0044	2.68E+01	0.0119	2.09E+02	0.0041
	3 ft	1.24E+02	0.0048	1.95E+01	0.0151	1.44E+02	0.0046

Note:

(1) Gamma and Neutron dose rate peaks do not always occur at same location; therefore, the maximum of total dose rate is not always the sum of the gamma plus neutron dose rate maximums.

Table B.5.5-9
Materials and Masses of Composite Design Basis Assembly

Proprietary information withheld pursuant to 10 CFR 2.390

Table B.5.5-10
Elemental Composition of Materials of Composite Design Basis Fuel Assembly

Element	Atomic Number	Material Composition, grams per kg of material			
		Zircaloy-4	Inconel X-750/ Inconel 625	Stainless Steel 302/304	Uranium Oxide Fuel
H	1	1.30E-02	-	-	-
Li	3	-	-	-	1.00E-03
B	5	3.30E-04	-	-	1.00E-03
C	6	1.20E-01	3.99E-01	8.00E-01	8.94E-02
N	7	8.00E-02	1.30E+00	1.30E+00	2.50E-02
O	8	9.50E-01	-	-	1.34E+02
F	9	-	-	-	1.07E-02
Na	11	-	-	-	1.50E-02
Mg	12	-	-	-	2.00E-03
Al	13	2.40E-02	7.98E+00	-	1.67E-02
Si	14	-	2.99E+00	1.00E+01	1.21E-02
P	15	-	-	4.50E-01	3.50E-02
S	16	3.50E-02	7.00E-02	3.00E-01	-
Cl	17	-	-	-	5.30E-03
Ca	20	-	-	-	2.00E-03
Ti	22	2.00E-02	2.49E+01	-	1.00E-03
V	23	2.00E-02	-	-	3.00E-03
Cr	24	1.25E+00	1.50E+02	1.90E+02	4.00E-03
Mn	25	2.00E-02	6.98E+00	2.00E+01	1.70E-03
Fe	26	2.25E+00	6.78E+01	6.88E+02	1.80E-02
Co	27	2.00E-02	1.00E+01	2.00E+00	1.00E-03
Ni	28	2.00E-02	7.22E+02	8.92E+01	2.40E-02
Cu	29	2.00E-02	4.99E-01	-	1.00E-03
Zn	30	-	-	-	4.03E-02
Zr	40	9.79E+02	-	-	-
Nb	41	-	8.98E+00	-	-
Mo	42	-	-	-	1.00E-02
Ag	47	-	-	-	1.00E-04
Cd	48	2.50E-04	-	-	2.50E-02
In	49	-	-	-	2.00E-03
Sn	50	1.60E+01	-	-	4.00E-03
Gd	64	-	-	-	2.50E-03
Hf	72	7.80E-02	-	-	-
W	74	2.00E-02	-	-	2.00E-03
Pb	82	-	-	-	1.00E-03
U	92	2.00E-04	-	-	881

Table B.5.5-11
Content of Light Elements of the Composite Design Basis Assembly

Element	Bottom Nozzle Region (Kg)	Active fuel Region (Kg)	Plenum Region (Kg)	Top Nozzle Region (Kg)	Total (Kg)
H	0	0.0017	0	0	0.0017
Li	0	0.0005	0	0	0.0005
B	0	0.0005	0	0	0.0005
C	0.0013	0.0564	0.0014	0.0011	0.0602
N	0.0020	0.0231	0.0021	0.0021	0.0293
O	0.0019	61.3643	0.0018	0.0000	61.3680
F	0	0.0049	0	0	0.0049
Na	0	0.0068	0	0	0.0068
Mg	0	0.0009	0	0	0.0009
Al	0.0019	0.0201	0	0.0041	0.0262
Si	0.0127	0.0090	0.0150	0.0127	0.0494
P	0.0005	0.0159	0.0007	0.0005	0.0177
S	0.0004	0.0045	0.0005	0.0004	0.0059
Cl	0	0.0024	0	0	0.0024
Ca	0	0.0009	0	0	0.0009
Ti	0.0059	0.0324	0	0.0129	0.0513
V	0	0.0039	0	0	0.0040
Cr	0.2653	0.3369	0.2868	0.2894	1.1783
Mn	0.0256	0.0115	0.0300	0.0259	0.0931
Fe	0.8449	0.3736	1.0348	0.8033	3.0565
Co	0.0048	0.0148	0.0030	0.0074	0.0300
Ni	0.2771	0.8648	0.1336	0.4728	1.7483
Cu	0.0002	0.0036	0	0.0003	0.0040
Zn	0	0.0184	0	0	0.0184
Zr	1.9452	124.1751	1.8564	0.0133	127.9900
Nb	0.0021	0.0106	0	0.0046	0.0174
Mo	0	0.0046	0	0	0.0046
Ag	0	0	0	0	0
Cd	0	0.0114	0	0	0.0114
In	0	0.0009	0	0	0.0009
Sn	0.0318	2.0310	0.0303	0.0002	2.0934
Gd	0	0.0011	0	0	0.0011
Hf	0.0002	0.0099	0.0001	0	0.0102
W	0	0.0035	0	0	0.0035
Pb	0	0.0005	0	0	0.0005

Table B.5.5-12
Flux Factors by Assembly Region

Region	Flux Factor
Bottom	0.20
Active Fuel (in-core)	1.00
Plenum	0.20
Top	0.10

Table B.5.5-13
AHSM-HS Response Functions

Response Functions for the AHSM-HS						
Maximum Energy (MeV)	**Zone 1**	**Relative Error[1]**	**Zone 2**	**Relative Error**	**Zone 3**	**Relative Error**
0.60	0.000E+00	-	3.96E-18	0.616	4.29E-16	0.067
0.80	0.000E+00	-	1.13E-17	0.314	3.42E-15	0.030
1.00	0.000E+00	-	7.20E-17	0.228	7.49E-15	0.021
1.33	1.095E-18	0.777	2.24E-16	0.110	1.70E-14	0.015
1.66	7.446E-19	0.722	8.14E-16	0.075	3.83E-14	0.011
2.00	2.428E-18	0.775	2.36E-15	0.050	7.29E-14	0.008
2.50	1.995E-17	0.286	5.83E-15	0.034	1.42E-13	0.006
3.00	5.070E-17	0.203	1.32E-14	0.021	2.69E-13	0.004
Neutron	2.452E-10	0.023	1.483E-9	0.034	4.559E-9	0.031

Note:

(1) High variance is acceptable because Zone 1 contributes negligibly to the external dose rates.

Table B.5.5-14
OS200FC TC Response Functions

Response functions for the OS200FC TC, dry						
Maximum Energy MeV)	Zone 1	Relative Error[1]	Zone 2	Relative Error	Zone 3	Relative Error
0.60	0.000E+00	-	0.000E+00	-	1.052E-17	0.937
0.80	0.000E+00	-	9.384E-18	0.810	7.001E-15	0.036
1.00	0.000E+00	-	1.204E-15	0.101	1.580E-13	0.009
1.33	7.217E-17	0.590	3.148E-14	0.029	2.130E-12	0.003
1.66	4.866E-16	0.222	2.628E-13	0.013	1.232E-11	0.002
2.00	4.243E-15	0.123	1.032E-12	0.008	3.635E-11	0.001
2.50	1.821E-14	0.075	3.025E-12	0.006	8.542E-11	0.001
3.00	5.582E-14	0.047	6.700E-12	0.004	1.603E-10	0.001
Neutron	1.436E-09	0.008	3.720E-09	0.010	1.235E-08	0.002

Note:

(1) High variance is acceptable because Zone 1 contributes negligibly to the external dose rates.

Table B.5.5-15
Additional Cooling Times (ΔT) in Years for Fuel Assemblies with 2% of Fuel Rods Reconstituted with Stainless Steel

Burn-up, GWD/ MTU	Cobalt Impurities (g/kg of Stainless Steel of the Replacement Rods)								Burn-up, GWD/ MTU	Cobalt Impurities (g/kg of Stainless Steel of the Replacement Rods)							
	0.3	0.5	0.8	1.0	1.25	1.5	1.75	2.0		0.3	0.5	0.8	1.0	1.25	1.5	1.75	2.0
14	0.0	0.0	0.0	0.0	0.0	0.0	0.0	0.0	**39**	0.0	0.5	1.4	1.9	2.6	3.1	3.7	4.2
15	0.0	0.0	0.0	0.0	0.0	0.0	0.0	0.0	**40**	0.0	0.5	1.4	1.9	2.6	3.1	3.7	4.2
16	0.0	0.0	0.0	0.0	0.0	0.0	0.0	0.0	**41**	0.0	0.5	1.4	1.9	2.6	3.1	3.7	4.2
17	0.0	0.0	0.0	0.0	0.0	0.0	0.0	0.0	**42**	0.0	0.5	1.3	1.9	2.5	3.1	3.6	4.1
18	0.0	0.0	0.0	0.0	0.0	0.0	0.0	0.0	**43**	0.0	0.3	1.2	1.7	2.3	2.9	3.4	3.9
19	0.0	0.0	0.0	0.0	0.0	0.0	0.0	0.0	**44**	0.0	0.2	1.1	1.6	2.3	2.8	3.4	3.9
20	0.0	0.0	0.0	0.0	0.0	0.0	0.0	0.0	**45**	0.0	0.1	1.0	1.5	2.2	2.7	3.3	3.8
21	0.0	0.0	0.0	0.0	0.0	0.0	0.0	0.3	**46**	0.0	0.0	0.9	1.4	2.0	2.6	3.1	3.6
22	0.0	0.0	0.0	0.0	0.0	0.0	0.3	0.8	**47**	0.0	0.0	0.7	1.3	1.9	2.5	3.0	3.5
23	0.0	0.0	0.0	0.0	0.0	0.2	0.7	1.2	**48**	0.0	0.0	0.6	1.2	1.8	2.4	2.9	3.4
24	0.0	0.0	0.0	0.0	0.0	0.6	1.1	1.6	**49**	0.0	0.0	0.5	1.0	1.6	2.2	2.7	3.2
25	0.0	0.0	0.0	0.0	0.4	1.0	1.5	2.0	**50**	0.0	0.0	0.3	0.9	1.5	2.0	2.6	3.1
26	0.0	0.0	0.0	0.2	0.8	1.4	2.0	2.5	**51**	0.0	0.0	0.2	0.7	1.3	1.9	2.4	2.9
27	0.0	0.0	0.0	0.6	1.2	1.8	2.3	2.8	**52**	0.0	0.0	0.0	0.5	1.1	1.7	2.2	2.7
28	0.0	0.0	0.4	1.0	1.6	2.2	2.7	3.2	**53**	0.0	0.0	0.0	0.3	1.0	1.5	2.1	2.6
29	0.0	0.0	0.8	1.3	2.0	2.5	3.1	3.6	**54**	0.0	0.0	0.0	0.1	0.8	1.3	1.9	2.4
30	0.0	0.3	1.2	1.7	2.4	2.9	3.5	4.0	**55**	0.0	0.0	0.0	0.0	0.5	1.1	1.6	2.1
31	0.0	0.7	1.5	2.1	2.7	3.3	3.8	4.3	**56**	0.0	0.0	0.0	0.0	0.3	0.9	1.4	1.9
32	0.1	0.7	1.6	2.1	2.7	3.3	3.9	4.3	**57**	0.0	0.0	0.0	0.0	0.2	0.7	1.3	1.8
33	0.2	0.9	1.8	2.3	2.9	3.5	4.0	4.5	**58**	0.0	0.0	0.0	0.0	0.0	0.5	1.0	1.5
34	0.2	0.9	1.8	2.3	2.9	3.5	4.0	4.5	**59**	0.0	0.0	0.0	0.0	0.0	0.3	0.8	1.3
35	0.3	0.9	1.8	2.3	2.9	3.5	4.0	4.5	**60**	0.0	0.0	0.0	0.0	0.0	0.0	0.6	1.1
36	0.3	0.9	1.8	2.3	3.0	3.5	4.1	4.5	**61**	0.0	0.0	0.0	0.0	0.0	0.0	0.4	0.8
37	0.0	0.5	1.4	1.9	2.6	3.1	3.7	4.2	**62**	0.0	0.0	0.0	0.0	0.0	0.0	0.2	0.7
38	0.0	0.6	1.5	2.0	2.6	3.2	3.8	4.3	**63**	0.0	0.0	0.0	0.0	0.0	0.0	0.0	0.5

Table B.5.5-16
Additional Cooling Times (ΔT) in Years for Fuel Assemblies with 3% of Fuel Rods Reconstituted with Stainless Steel

Burn-up, GWD/ MTU	Cobalt Impurities (g/kg of Stainless Steel of the Replacement Rods)								Burn-up, GWD/ MTU	Cobalt Impurities (g/kg of Stainless Steel of the Replacement Rods)							
	0.3	0.5	0.8	1.0	1.25	1.5	1.75	2.0		0.3	0.5	0.8	1.0	1.25	1.5	1.75	2.0
14	0.0	0.0	0.0	0.0	0.0	0.0	0.0	0.0	**39**	0.7	1.5	**2.6**	**3.2**	**3.9**	**4.6**	**5.2**	5.6
15	0.0	0.0	0.0	0.0	0.0	0.0	0.0	0.0	**40**	0.7	1.5	2.5	3.1	3.8	4.5	5.1	5.6
16	0.0	0.0	0.0	0.0	0.0	0.0	0.0	0.0	**41**	0.7	1.5	2.5	3.1	3.8	4.5	5.1	5.6
17	0.0	0.0	0.0	0.0	0.0	0.0	0.0	0.0	**42**	0.7	1.4	2.5	3.1	3.8	4.5	5.1	5.5
18	0.0	0.0	0.0	0.0	0.0	0.0	0.0	0.4	**43**	0.5	1.3	2.4	3.1	3.8	4.4	5.0	5.4
19	0.0	0.0	0.0	0.0	0.0	0.0	0.3	0.9	**44**	0.4	1.2	2.3	2.9	3.6	4.3	4.9	5.3
20	0.0	0.0	0.0	0.0	0.0	0.2	0.8	1.3	**45**	0.3	1.1	2.2	2.8	3.5	4.2	4.8	5.2
21	0.0	0.0	0.0	0.0	0.0	0.7	1.3	1.8	**46**	0.2	0.9	2.1	2.7	3.4	4.1	4.7	5.1
22	0.0	0.0	0.0	0.0	0.5	1.1	1.7	2.3	**47**	0.1	0.8	2.0	2.6	3.3	3.9	4.5	5.0
23	0.0	0.0	0.0	0.2	0.9	1.6	2.2	2.7	**48**	0.0	0.7	1.9	2.5	3.2	3.8	4.4	4.9
24	0.0	0.0	0.0	0.6	1.3	2.0	2.6	3.1	**49**	0.0	0.6	1.8	2.4	3.1	3.7	4.3	4.7
25	0.0	0.0	0.4	1.0	1.7	2.4	3.0	3.5	**50**	0.0	0.4	1.6	2.2	2.9	3.6	4.1	4.5
26	0.0	0.0	0.8	1.4	2.1	2.8	3.4	3.9	**51**	0.0	0.2	1.4	2.0	2.7	3.4	4.0	4.4
27	0.0	0.1	1.2	1.8	2.5	3.2	3.8	4.3	**52**	0.0	0.1	1.3	1.9	2.6	3.2	3.8	4.2
28	0.0	0.5	1.6	2.2	2.9	3.5	4.1	4.7	**53**	0.0	0.0	1.1	1.7	2.4	3.0	3.6	4.0
29	0.1	0.9	1.9	2.6	3.3	3.9	4.5	5.1	**54**	0.0	0.0	0.9	1.5	2.2	2.9	3.5	3.8
30	0.5	1.3	2.3	2.9	3.6	4.3	4.9	5.4	**55**	0.0	0.0	0.7	1.3	2.0	2.7	3.3	3.6
31	0.9	1.6	2.7	3.3	4.0	4.6	5.2	5.8	**56**	0.0	0.0	0.5	1.1	1.8	2.5	3.0	3.4
32	0.9	1.7	2.7	3.3	4.0	4.7	5.3	5.8	**57**	0.0	0.0	0.3	0.9	1.6	2.2	2.8	3.2
33	1.1	1.8	2.9	3.5	4.2	4.8	5.4	6.0	**58**	0.0	0.0	0.1	0.7	1.4	2.1	2.7	3.0
34	1.1	1.9	2.9	3.5	4.2	4.9	5.4	6.0	**59**	0.0	0.0	0.0	0.5	1.2	1.9	2.4	2.7
35	1.1	1.9	2.9	3.5	4.2	4.9	5.4	6.0	**60**	0.0	0.0	0.0	0.3	1.0	1.6	2.2	2.5
36	1.1	1.9	2.9	3.5	4.2	4.9	5.5	6.0	**61**	0.0	0.0	0.0	0.0	0.7	1.4	2.0	2.3
37	0.7	1.5	2.5	3.1	3.8	4.5	5.1	5.6	**62**	0.0	0.0	0.0	0.0	0.5	1.2	1.7	2.1
38	0.8	1.6	2.6	3.2	3.9	4.6	5.2	5.7	**63**	0.0	0.0	0.0	0.0	0.3	1.0	1.5	1.9

Table B.5.5-17
Additional Cooling Times (ΔT) in Years for Fuel Assemblies with 5% of Fuel Rods Reconstituted with Stainless Steel

Burn-up, GWD/ MTU	Cobalt Impurities (g/kg of Stainless Steel of the Replacement Rods)								Burn-up, GWD/ MTU	Cobalt Impurities (g/kg of Stainless Steel of the Replacement Rods)							
	0.3	0.5	0.8	1.0	1.25	1.5	1.75	2.0		0.3	0.5	0.8	1.0	1.25	1.5	1.75	2.0
14	0.0	0.0	0.0	0.0	0.0	0.0	0.0	0.4	**39**	1.8	2.8	4.2	4.9	5.8	6.6	7.3	7.9
15	0.0	0.0	0.0	0.0	0.0	0.0	0.3	1.0	**40**	1.8	2.8	4.2	4.9	5.8	6.6	7.3	7.9
16	0.0	0.0	0.0	0.0	0.0	0.2	0.9	1.6	**41**	1.8	2.8	4.2	4.9	5.8	6.6	7.3	7.9
17	0.0	0.0	0.0	0.0	0.0	0.8	1.5	2.1	**42**	1.7	2.8	4.1	4.8	5.7	6.5	7.2	7.8
18	0.0	0.0	0.0	0.0	0.5	1.3	2.0	2.7	**43**	1.6	2.6	3.9	4.7	5.6	6.3	7.0	7.7
19	0.0	0.0	0.0	0.2	1.1	1.8	2.5	3.2	**44**	1.5	2.5	3.8	4.6	5.5	6.2	6.9	7.6
20	0.0	0.0	0.0	0.6	1.5	2.3	3.0	3.6	**45**	1.4	2.4	3.8	4.5	5.4	6.1	6.8	7.5
21	0.0	0.0	0.3	1.1	2.0	2.8	3.5	4.1	**46**	1.2	2.3	3.6	4.4	5.2	6.0	6.7	7.3
22	0.0	0.0	0.8	1.6	2.4	3.2	3.9	4.6	**47**	1.1	2.2	3.5	4.3	5.1	5.9	6.6	7.2
23	0.0	0.0	1.2	2.0	2.9	3.7	4.4	5.0	**48**	1.0	2.1	3.4	4.2	5.0	5.8	6.5	7.1
24	0.0	0.3	1.6	2.4	3.3	4.1	4.8	5.4	**49**	0.9	1.9	3.2	4.0	4.8	5.6	6.3	7.0
25	0.0	0.7	2.1	2.8	3.7	4.5	5.2	5.8	**50**	0.7	1.7	3.0	3.8	4.7	5.4	6.1	6.8
26	0.1	1.1	2.5	3.2	4.1	4.9	5.6	6.2	**51**	0.5	1.6	2.9	3.7	4.5	5.3	6.0	6.6
27	0.5	1.5	2.8	3.6	4.5	5.3	6.0	6.6	**52**	0.4	1.4	2.7	3.5	4.3	5.1	5.8	6.5
28	0.8	1.9	3.2	4.0	4.9	5.7	6.4	7.0	**53**	0.2	1.2	2.6	3.3	4.2	5.0	5.7	6.3
29	1.2	2.3	3.6	4.4	5.2	6.0	6.7	7.4	**54**	0.0	1.0	2.4	3.1	4.0	4.7	5.4	6.1
30	1.6	2.6	4.0	4.7	5.6	6.4	7.1	7.7	**55**	0.0	0.8	2.1	2.9	3.8	4.5	5.2	5.9
31	1.9	3.0	4.3	5.1	5.9	6.7	7.4	8.1	**56**	0.0	0.6	1.9	2.7	3.5	4.3	5.0	5.6
32	2.0	3.0	4.4	5.1	6.0	6.8	7.5	8.1	**57**	0.0	0.4	1.8	2.5	3.4	4.1	4.8	5.5
33	2.2	3.2	4.5	5.3	6.1	6.9	7.6	8.3	**58**	0.0	0.2	1.5	2.3	3.1	3.9	4.6	5.3
34	2.2	3.2	4.5	5.3	6.2	6.9	7.6	8.3	**59**	0.0	0.0	1.3	2.0	2.9	3.7	4.4	5.0
35	2.2	3.2	4.5	5.3	6.2	6.9	7.6	8.3	**60**	0.0	0.0	1.1	1.8	2.7	3.4	4.1	4.8
36	2.2	3.2	4.5	5.3	6.2	6.9	7.6	8.3	**61**	0.0	0.0	0.8	1.6	2.4	3.2	3.9	4.5
37	1.8	2.8	4.2	4.9	5.8	6.6	7.3	7.9	**62**	0.0	0.0	0.6	1.4	2.2	3.0	3.7	4.3
38	1.9	2.9	4.3	5.0	5.9	6.7	7.4	8.0	**63**	0.0	0.0	0.4	1.2	2.0	2.8	3.5	4.1

Table B.5.5-18
Design Parameters for the 5-Finger CEA in a CE 16x16 Class Fuel Assembly

Proprietary information withheld pursuant to 10 CFR 2.390

Table B.5.5-19
Total Gamma Source Term (γ/s per Finger) Due to Sections of the 5-Finger CEA and Its Spectrum (10 Years Cooled)

Gamma Radiation Energy Range			Spectrum for Sections of the CEA				
E_{min}, MeV	to	E_{max}, MeV	First Nose Cap	Second Nose Cap	Third Nose Cap	Hollow Clad	B_4C Pellet Section
0.00e+00	to	5.00e-02	1.3302E-02	1.3292E-02	1.3283E-02	1.3213E-02	1.3356E-02
5.00e-02	to	1.00e-01	3.1848E-03	3.1847E-03	3.1847E-03	3.1847E-03	3.1845E-03
1.00e-01	to	2.00e-01	6.3356E-04	6.3351E-04	6.3355E-04	6.3348E-04	6.3352E-04
2.00e-01	to	3.00e-01	3.1496E-05	3.1493E-05	3.1492E-05	3.1477E-05	3.1497E-05
3.00e-01	to	4.00e-01	4.1253E-05	4.1252E-05	4.1254E-05	4.1255E-05	4.1250E-05
4.00e-01	to	6.00e-01	2.6068E-06	2.6068E-06	2.6070E-06	2.6073E-06	2.6066E-06
6.00e-01	to	8.00e-01	1.1161E-04	1.0685E-04	1.0224E-04	6.7427E-05	1.1540E-04
8.00e-01	to	1.00e+00	1.4099E-04	1.3640E-04	1.3195E-04	9.8350E-05	1.4465E-04
1.00e+00	to	1.33e+00	7.6618E-01	7.6620E-01	7.6620E-01	7.6631E-01	7.6613E-01
1.33e+00	to	1.66e+00	2.1636E-01	2.1636E-01	2.1639E-01	2.1641E-01	2.1635E-01
1.66e+00	to	2.00e+00	2.3467E-20	1.5969E-20	1.0124E-20	5.2640E-21	1.7532E-21
2.00e+00	to	2.50e+00	5.1770E-06	5.1771E-06	5.1774E-06	5.1780E-06	5.1768E-06
2.50e+00	to	3.00e+00	4.4234E-09	4.4234E-09	4.4236E-09	4.4243E-09	4.4230E-09
3.00e+00	to	4.00e+00	9.7594E-31	8.3024E-31	6.8397E-31	3.5397E-31	6.0375E-31
4.00e+00	to	5.00e+00	0.0	0.0	0.0	0.0	0.0
5.00e+00	to	6.50e+00	0.0	0.0	0.0	0.0	0.0
6.50e+00	to	8.00e+00	0.0	0.0	0.0	0.0	0.0
8.00e+00	to	1.00e+01	0.0	0.0	0.0	0.0	0.0
Total, normalized			1.0	1.0	1.0	1.0	1.0
Total Intensity, γ/s per Finger, per Section			2.5803E+13	2.7578E+13	1.0141E+14	1.9342E+13	8.1425E+11

Table B.5.5-20
CASK-81 Energy Group Structure

Neutron Group Number	E_{upper} (MeV)
1	14.9
2	12.2
3	10.0
4	8.18
5	6.36
6	4.96
7	4.06
8	3.01
9	2.46
10	2.35
11	1.83
12	1.11
13	0.550
14	0.111
15	3.35E-03
16	5.83E-04
17	1.01E-04
18	2.90E-05
19	1.07E-05
20	3.06E-06
21	1.12E-06
22[1]	4.14E-07

Gamma Group Number	E_{upper} (MeV)
23	10.0
24	8.0
25	6.5
26	5.0
27	4.0
28	3.0
29	2.5
30	2.0
31	1.66
32	1.33
33	1.0
34	0.8
35	0.6
36	0.4
37	0.3
38	0.2
39	0.1
40[2]	0.05

Notes:

1. Group 22 lower energy boundary is 1.00E-08 MeV
2. Group 40 lower energy boundary is 0.01 MeV

Table B.5.5-21
Bounding Radiological Source Term for Assemblies in Zone 1 through Zone 3 for 32PTH2 DSC in AHSM-HS, γ/(s·FA)

For Zone 1, Zone 2, and Zone 3 Positions[1]: Bounding Gamma and Neutron Source Terms 32PTH2 DSC in AHSM-HS: 31 GWD/MTU, 1.7 wt.%, 5.0 years cooling.						
E_{min}, MeV	to	E_{max}, MeV	Bottom Nozzle	Active fuel	Plenum	Top Nozzle
0.00e+00	to	5.00e-02	1.328E+12	1.726E+15	1.145E+12	1.547E+12
5.00e-02	to	1.00e-01	9.102E+10	3.599E+14	5.709E+10	1.394E+11
1.00e-01	to	2.00e-01	3.244E+10	3.036E+14	2.378E+10	3.373E+10
2.00e-01	to	3.00e-01	1.836E+09	8.555E+13	1.394E+09	1.675E+09
3.00e-01	to	4.00e-01	3.923E+09	6.202E+13	3.271E+09	2.206E+09
4.00e-01	to	6.00e-01	5.618E+10	6.439E+14	5.349E+10	4.943E+08
6.00e-01	to	8.00e-01	2.947E+10	1.822E+15	2.790E+10	6.170E+08
8.00e-01	to	1.00e+00	1.007E+11	2.523E+14	1.224E+11	9.672E+10
1.00e+00	to	1.33e+00	2.635E+13	1.506E+14	1.645E+13	4.065E+13
1.33e+00	to	1.66e+00	7.442E+12	4.413E+13	4.647E+12	1.148E+13
1.66e+00	to	2.00e+00	7.410E+02	1.562E+12	3.798E+02	1.184E+03
2.00e+00	to	2.50e+00	1.781E+08	3.086E+12	1.112E+08	2.747E+08
2.50e+00	to	3.00e+00	1.521E+05	1.179E+11	9.498E+04	2.347E+05
3.00e+00	to	4.00e+00	3.669E-05	1.093E+10	1.078E-11	8.030E-05
4.00e+00	to	5.00e+00	0	9.790E+06	0	0
5.00e+00	to	6.50e+00	0	3.929E+06	0	0
6.50e+00	to	8.00e+00	0	7.706E+05	0	0
8.00e+00	to	1.00e+01	0	1.637E+05	0	0
Total Gamma, γ/(s*FA)			3.544E+13	5.454E+15	2.253E+13	5.394E+13
Total Neutrons, n/(s*FA)			7.104E+08[2]			

Notes:

(1) The fuel zones are shown in Figure B.2.1-1 of Chapter B.2

(2) Neutron radiation source corresponds to the design basis fuel assembly at 57 GWD/MTU, 3.6 wt. % U-235 enrichment and a cooling time of 13.2 years. This is the neutron source resulting in the bounding neutron radiation dose rates from Zone 1 and 3. A neutron source strength of 8.05e+8 n/(s*FA) is employed in the shielding analysis.

Table B.5.5-22
Bounding Radiological Source Term for Assemblies in Zone 1 and Zone 3 for 32PTH2 DSC in OS200FC TC, γ/(s·FA)

For Zone 1 and Zone 3 Positions[1]: Bounding Gamma and Neutron Source Terms 32PTH2 DSC in OS200FC TC: 33 GWD/MTU, 1.7 wt.%, 5.2 years cooling						
E_{min}, MeV	to	E_{max}, MeV	Bottom Nozzle	Active fuel	Plenum	Top Nozzle
0.00e+00	to	5.00e-02	1.343E+12	1.703E+15	1.152E+12	1.576E+12
5.00e-02	to	1.00e-01	9.348E+10	3.513E+14	5.860E+10	1.431E+11
1.00e-01	to	2.00e-01	3.311E+10	2.938E+14	2.422E+10	3.464E+10
2.00e-01	to	3.00e-01	1.871E+09	8.304E+13	1.418E+09	1.720E+09
3.00e-01	to	4.00e-01	3.977E+09	5.955E+13	3.310E+09	2.265E+09
4.00e-01	to	6.00e-01	5.664E+10	6.521E+14	5.394E+10	5.011E+08
6.00e-01	to	8.00e-01	2.973E+10	1.908E+15	2.814E+10	6.448E+08
8.00e-01	to	1.00e+00	8.965E+10	2.615E+14	1.088E+11	8.623E+10
1.00e+00	to	1.33e+00	2.706E+13	1.553E+14	1.689E+13	4.175E+13
1.33e+00	to	1.66e+00	7.643E+12	4.512E+13	4.770E+12	1.179E+13
1.66e+00	to	2.00e+00	3.925E+02	1.446E+12	2.133E+02	5.837E+02
2.00e+00	to	2.50e+00	1.829E+08	2.711E+12	1.141E+08	2.821E+08
2.50e+00	to	3.00e+00	1.562E+05	1.095E+11	9.754E+04	2.410E+05
3.00e+00	to	4.00e+00	4.076E-05	1.017E+10	1.375E-11	8.924E-05
4.00e+00	to	5.00e+00	0	1.222E+07	0	0
5.00e+00	to	6.50e+00	0	4.907E+06	0	0
6.50e+00	to	8.00e+00	0	9.622E+05	0	0
8.00e+00	to	1.00e+01	0	2.043E+05	0	0
Total Gamma, γ/(s*FA)			3.635E+13	5.518E+15	2.309E+13	5.536E+13
[2]Total Neutrons, n/(s*FA)			3.504e+8			
[3]Total Neutrons for Accident Conditions, n/(s*FA)			7.104e+8			

Notes:

(1) The fuel zones are shown in Figure B.2.1-1 of Chapter B.2

(2) 4.17E+8 n/(s*FA) is employed in the shielding analysis

(3) Neutron radiation source corresponds to the design basis fuel assembly at 57 GWD/MTU, 3.6 wt. % U-235 enrichment and a cooling time of 13.2 years. This is the neutron source resulting in the bounding neutron radiation dose rates from Zone 1 and 3. A neutron source strength of 8.05e+8 n/(s*FA) is employed in the shielding analysis for accidents.

Table B.5.5-23
Bounding Radiological Source Term for Assemblies in the DSC Zone 2 for 32PTH2 DSC in OS200FC TC, γ/(s·FA)

Zone 2 Positions[1]: Bounding Gamma and Neutron Source Terms 32PTH2 DSC in OS200FC TC: 33 GWD/MTU, 1.7 wt.%, 5.0 years cooling.						
E_{min}, MeV	to	E_{max}, MeV	Bottom Nozzle	Active fuel	Plenum	Top Nozzle
0.00e+00	to	5.00e-02	1.400E+12	1.819E+15	1.206E+12	1.631E+12
5.00e-02	to	1.00e-01	9.599E+10	3.786E+14	6.019E+10	1.469E+11
1.00e-01	to	2.00e-01	3.427E+10	3.197E+14	2.513E+10	3.556E+10
2.00e-01	to	3.00e-01	1.941E+09	9.015E+13	1.474E+09	1.766E+09
3.00e-01	to	4.00e-01	4.151E+09	6.516E+13	3.463E+09	2.326E+09
4.00e-01	to	6.00e-01	5.960E+10	7.059E+14	5.677E+10	5.235E+08
6.00e-01	to	8.00e-01	3.126E+10	1.961E+15	2.960E+10	6.557E+08
8.00e-01	to	1.00e+00	1.052E+11	2.790E+14	1.279E+11	1.010E+11
1.00e+00	to	1.33e+00	2.778E+13	1.614E+14	1.734E+13	4.286E+13
1.33e+00	to	1.66e+00	7.848E+12	4.742E+13	4.897E+12	1.210E+13
1.66e+00	to	2.00e+00	7.519E+02	1.656E+12	3.881E+02	1.192E+03
2.00e+00	to	2.50e+00	1.877E+08	3.198E+12	1.172E+08	2.896E+08
2.50e+00	to	3.00e+00	1.604E+05	1.255E+11	1.001E+05	2.474E+05
3.00e+00	to	4.00e+00	4.093E-05	1.165E+10	1.381E-11	8.960E-05
4.00e+00	to	5.00e+00	0	1.232E+07	0	0
5.00e+00	to	6.50e+00	0	4.943E+06	0	0
6.50e+00	to	8.00e+00	0	9.699E+05	0	0
8.00e+00	to	1.00e+01	0	2.059E+05	0	0
Total Gamma, γ/(s*FA)			3.736E+13	5.832E+15	2.375E+13	5.686E+13
[2]Total Neutrons, n/(s*FA)			3.530e+8			
[3]Total Neutrons for Accident Conditions, n/(s*FA)			9.695e+8			

Notes:

(1) The fuel zones are shown in Figure B.2.1-1 of Chapter B.2

(2) 4.20E+8 n/(s*FA) is employed in the shielding analysis

(3) Neutron radiation source corresponds to the design basis fuel assembly at 63 GWD/MTU, 4.3 wt. % U-235 enrichment and a cooling time of 7.6 years. This is the neutron source resulting in the bounding neutron radiation dose rates from Zone 2. A neutron source strength of 1.11e+9 n/(s*FA) is employed in the shielding analysis for accidents.

Table B.5.5-24
ANSI/ANS-6.1.1-77 Flux to Dose Rate Conversion Factors

Gamma Energy, MeV	Gamma Flux-to-Dose-Rate Factor (mrem/hr)/(γ/cm^2-sec)	Neutron Energy, MeV	Neutron Flux-to-Dose-Rate Factor (mrem/hr)/(n/cm^2-sec)
0.01	3.96E-03	2.5E-08	3.67E-03
0.03	5.82E-04	1E-07	3.67E-03
0.05	2.90E-04	1.00E-06	4.46E-03
0.07	2.58E-04	1.00E-05	4.54E-03
0.10	2.83E-04	1.00E-04	4.18E-03
0.15	3.79E-04	0.001	3.76E-03
0.20	5.01E-04	0.01	3.56E-03
0.25	6.31E-04	0.10	2.17E-02
0.30	7.59E-04	0.50	9.26E-02
0.35	8.78E-04	1.00	1.32E-01
0.40	9.85E-04	2.50	1.25E-01
0.45	1.08E-03	5.00	1.56E-01
0.50	1.17E-03	7.00	1.47E-01
0.55	1.27E-03	10.00	1.47E-01
0.60	1.36E-03	14.00	2.08E-01
0.65	1.44E-03	20.00	2.27E-01
0.70	1.52E-03		
0.80	1.68E-03		
1.00	1.98E-03		
1.40	2.51E-03		
1.80	2.99E-03		
2.20	3.42E-03		
2.60	3.82E-03		
2.80	4.01E-03		
3.25	4.41E-03		
3.75	4.83E-03		
4.25	5.23E-03		
4.75	5.60E-03		
5.00	5.80E-03		
5.25	6.01E-03		
5.75	6.37E-03		
6.25	6.74E-03		
6.75	7.11E-03		
7.50	7.66E-03		
9.00	8.77E-03		
11.00	1.03E-02		
13.00	1.18E-02		
15.00	1.33E-02		

Table B.5.5-25
Homogenized Dry Fuel Assembly Region Compositions

	Mass Fraction, Dry			
Element	**Top**	**Plenum**	**Active Fuel**	**Bottom**
Hydrogen	1.07E-07	7.02E-06	2.561E-06	7.281E-06
Lithium			7.060E-07	
Boron-10	5.18E-10	3.39E-08	1.465E-07	3.512E-08
Boron-11	2.21E-09	1.44E-07	6.245E-07	1.497E-07
Carbon	6.68E-04	4.05E-04	8.749E-05	3.655E-04
Nitrogen	1.29E-03	5.97E-04	3.579E-05	5.728E-04
Oxygen	7.85E-06	1.63E-02	9.511E-02	1.618E-02
Fluorine			7.554E-06	
Sodium		1.78E-02	1.059E-05	1.759E-02
Magnesium			1.412E-06	
Aluminum	2.51E-03	1.30E-05	3.114E-05	5.442E-04
Silicon	7.71E-03	4.26E-03	1.403E-05	3.595E-03
Phosphorus	3.05E-04	1.92E-04	2.471E-05	1.528E-04
Sulfur	2.25E-04	1.47E-04	7.023E-06	1.262E-04
Chlorine			3.742E-06	
Calcium			1.412E-06	
Titanium	7.83E-03	1.08E-05	5.034E-05	1.670E-03
Vanadium	1.65E-07	1.08E-05	6.058E-06	1.120E-05
Chromium	1.76E-01	8.16E-02	5.233E-04	7.518E-02
Manganese	1.57E-02	8.53E-03	1.794E-05	7.269E-03
Iron	4.87E-01	2.94E-01	5.803E-04	2.393E-01
Cobalt	4.49E-03	8.64E-04	2.100E-05	1.357E-03
Nickel	2.86E-01	3.80E-02	1.337E-03	7.807E-02
Copper	1.57E-04	1.08E-05	5.560E-06	4.438E-05
Zinc			2.845E-05	
Zirconium	8.09E-03	5.29E-01	1.929E-01	5.484E-01
Niobium	2.82E-03		1.645E-05	5.971E-04
Molybdenum			7.060E-06	
Silver			7.060E-08	
Cadmium	2.07E-09	1.35E-07	1.770E-05	1.400E-07
Indium			1.412E-06	
Tin	1.32E-04	8.64E-03	3.155E-03	8.961E-03
Gadolinium			1.765E-06	
Hafnium	6.45E-07	4.21E-05	1.537E-05	4.369E-05
Tungsten	1.65E-07	1.08E-05	5.352E-06	1.120E-05
Lead			7.060E-07	
Bismuth			2.824E-07	
Uranium-235	1.18E-11	7.68E-10	3.601E-02	7.964E-10
Uranium-238	1.64E-09	1.07E-07	6.700E-01	1.112E-07
Density (g/cm^3)	1.27	1.80	3.82	3.35

Table B.5.5-26
Homogenized Flooded Fuel Assembly Region Compositions

	Mass Fraction, Wet			
Element	**Top**	**Plenum**	**Active Fuel**	**Bottom**
Hydrogen	4.337E-02	6.345E-02	4.569E-03	1.215E-02
Lithium			6.772E-07	
Boron-10	3.173E-10	1.466E-08	2.326E-06	1.536E-08
Boron-11	1.353E-09	6.250E-08	9.916E-06	6.549E-08
Carbon	4.089E-04	1.755E-04	8.392E-05	3.258E-04
Nitrogen	7.891E-04	2.583E-04	3.433E-05	5.106E-04
Oxygen	3.442E-01	5.106E-01	1.275E-01	1.108E-01
Fluorine			7.246E-06	
Sodium		7.697E-03	1.016E-05	1.568E-02
Magnesium			1.354E-06	
Aluminum	1.535E-03	5.612E-06	2.987E-05	4.851E-04
Silicon	4.719E-03	1.843E-03	1.345E-05	3.205E-03
Phosphorus	1.865E-04	8.295E-05	2.370E-05	1.362E-04
Sulfur	1.380E-04	6.348E-05	6.737E-06	1.125E-04
Chlorine			3.589E-06	
Calcium			1.354E-06	
Titanium	4.797E-03	4.677E-06	4.829E-05	1.489E-03
Vanadium	1.012E-07	4.677E-06	5.811E-06	9.986E-06
Chromium	1.075E-01	3.532E-02	5.019E-04	6.702E-02
Manganese	9.631E-03	3.691E-03	1.720E-05	6.480E-03
Iron	2.979E-01	1.272E-01	5.566E-04	2.133E-01
Cobalt	2.752E-03	3.739E-04	2.014E-05	1.209E-03
Nickel	1.751E-01	1.645E-02	1.282E-03	6.960E-02
Copper	9.607E-05	4.677E-06	5.333E-06	3.957E-05
Zinc			2.729E-05	
Zirconium	4.955E-03	2.289E-01	1.850E-01	4.889E-01
Niobium	1.727E-03		1.578E-05	5.323E-04
Molybdenum			6.772E-06	
Silver			6.772E-08	
Cadmium	1.265E-09	5.846E-08	1.698E-05	1.248E-07
Indium			1.354E-06	
Tin	8.097E-05	3.741E-03	3.026E-03	7.988E-03
Gadolinium			1.693E-06	
Hafnium	3.947E-07	1.824E-05	1.474E-05	3.894E-05
Tungsten	1.012E-07	4.677E-06	5.134E-06	9.986E-06
Lead			6.772E-07	
Bismuth			2.709E-07	
Uranium-235	7.197E-12	3.325E-10	3.454E-02	7.100E-10
Uranium-238	1.005E-09	4.643E-08	6.426E-01	9.915E-08
Density (g/cm^3)	2.08	2.36	3.98	3.75

Table B.5.5-27
Elemental Compositions of Shielding Materials

Element	ASME SA-36	ASME SA-240 Type 304	ASME SA-240 Type 316	ASME SB-209 Type 6061	ASTM B29 Chemical-Copper Lead	Fill Gas	Water	Air	Concrete	NS-3[1]
H	-	-	-	-	-	-	11.2	3.13E-7	0.00567	4.85
He	-	-	-	-	-	100	-	7.24E-7	-	-
C	0.26	0.08	0.08	-	-	-	-	1.31E-4	-	9.35
N	-	0.1	0.1	-	-	-	-	7.55E-1	-	-
O	-	-	-	-	-	-	88.8	2.32E-1	0.50019	57.05
Ne	-	-	-	-	-	-	-	1.27E-5	-	-
Na	-	-	-	-	-	-	-	-	0.01702	-
Mg	-	-	-	0.1	-	-	-	-	-	-
Al	-	-	-	97.738	-	-	-	-	0.04578	17.89
Si	0.4	0.75	0.75	0.6	-	-	-	-	0.31710	3.36
P	0.04	0.45	0.45	-	-	-	-	-	-	-
S	0.05	0.3	0.3	-	-	-	-	-	-	-
Ar	-	-	-	-	-	-	-	1.29E-2	-	-
K	-	-	-	-	-	-	-	-	0.01917	-
Ca	-	-	-	-	-	-	-	-	0.08286	5.61
Ti	-	-	-	0.15	-	-	-	-	-	-
Cr	-	18.5	17	0.038	-	-	-	-	-	-
Mn	-	2	2	0.15	-	-	-	-	-	-
Fe	99.25	68.57	64.82	0.7	0.0015	-	-	-	0.01221	0.56
Ni	-	9.25	12	-	0.0015	-	-	-	-	-
Cu	-	-	-	0.275	0.06	-	-	-	-	-
Zn	-	-	-	0.25	0.001	-	-	-	-	-
As	-	-	-	-	0.00033	-	-	-	-	-
Kr								3.30E-6	-	-
Mo	-	-	2.5	-	-	-	-	-	-	-
Ag	-	-	-	-	0.015	-	-	-	-	-
Sn	-	-	-	-	0.00033	-	-	-	-	-
Sb	-	-	-	-	0.00033	-	-	-	-	-
Xe	-	-	-	-	-	-	-	3.94E-7	-	-
Pb	-	-	-	-	99.9	-	-	-	-	-
Bi	-	-	-	-	0.02	-	-	-	-	-
Density (g/cm^3)	7.82	7.92	8.03	2.7	11.17	.18E-3	0.958	0.001225	2.3	1.729

Table B.5.5-28
Axial Distribution of Radiological Sources in Shielding Models

In core Zone	In core Zone (% of height)	Gamma	Neutron[1]
1	2.78	0.573	0.107
2	8.33	0.917	0.706
3	13.89	1.066	1.293
4	19.44	1.106	1.499
5	25	1.114	1.543
6	30.56	1.111	1.527
7	36.11	1.106	1.499
8	41.69	1.101	1.472
9	47.22	1.097	1.451
10	52.78	1.093	1.430
11	58.33	1.089	1.409
12	63.89	1.086	1.393
13	69.44	1.081	1.368
14	75	1.073	1.327
15	80.56	1.051	1.221
16	86.11	0.993	0.972
17	91.67	0.832	0.477
18	97.22	0.512	0.068
Average Peaking Factor		1.0	1.183

Note:

1) Peaking factors for the axial distribution of neutron source are obtained by taking the peaking factors for the gamma radiation source to the power of 4.02.

Table B.5.5-29
Comparison of Calculated vs. Measured Dose Rates for Code Validation

Description	Maximum Measured Dose Rate, mrem/hr		Maximum Calculated with MCNP		Ratio, Calculated/ Measured
			mrem/hr	MCNP 1σ error, %	
In front of HSM Front Bird Screen	Neutron	0.6	1.43	2.4	2.4
	Gamma	30	281.98	6.8	9.4
	Total	30.6	283.42	6.8	9.3
Above HSM Roof Bird Screen	Neutron	3	2.53	1.6	0.8
	Gamma	130	661.46	2.0	5.1
	Total	133	663.99	2.0	5.0
On HSM Door	Neutron	3	7.36	1.1	2.5
	Gamma	7	13.17	2.1	1.9
	Total	10	20.53	1.4	2.1

Proprietary information withheld pursuant to 10 CFR 2.390

Figure B.5.5-1
NUHOMS® 32PTH2 System in AHSM-HS Shielding Configuration – Side View at Centerline of DSC

Proprietary information withheld pursuant to 10 CFR 2.390

Figure B.5.5-2
NUHOMS® 32PTH2 System in AHSM-HS Shielding Configuration – Head-on View at z = 300 cm (Roof Vent Caps not Shown)

Proprietary information withheld pursuant to 10 CFR 2.390

Figure B.5.5-3
NUHOMS® 32PTH2 System in AHSM-HS Shielding Configuration – Head-on View at z = 300 cm (Roof Vents Shown)

Proprietary information withheld pursuant to 10 CFR 2.390

Figure B.5.5-4
NUHOMS® 32PTH2 System in AHSM-HS Shielding Configuration – Head-on View at z = 560 cm (DSC Top)

Proprietary information withheld pursuant to 10 CFR 2.390

Figure B.5.5-5
NUHOMS® 32PTH2 System in AHSM-HS Shielding Configuration – Head-on View at z = 120 cm (DSC Bottom)

Proprietary information withheld pursuant to 10 CFR 2.390

Figure B.5.5-6
NUHOMS® 32PTH2 System in OS200FC TC Side Shielding Configuration – Normal Configuration

Proprietary information withheld pursuant to 10 CFR 2.390

Figure B.5.5-7
NUHOMS® 32PTH2 System in OS200FC TC Top Shielding Configuration

Proprietary information withheld pursuant to 10 CFR 2.390

Figure B.5.5-8
NUHOMS® 32PTH2 System in OS200FC TC Bottom Shielding Configuration

Proprietary information withheld pursuant to 10 CFR 2.390

Figure B.5.5-9
NUHOMS® 32PTH2 System in OS200FC TC Shielding Configuration for Accident with Reconfiguration

Proprietary information withheld pursuant to 10 CFR 2.390

Figure B.5.5-10
NUHOMS® 32PTH2 System in OS200FC TC Shielding Configuration for Accident with Reconfiguration Cross-Section

Proprietary information withheld pursuant to 10 CFR 2.390

Figure B.5.5-11
Axial Sections of 5-Finger CEA (Sketch not to Scale)

Proprietary information withheld pursuant to 10 CFR 2.390

Figure B.5.5-12
32PTH2 DSC within AHSM-HS MCNP5 Model, x-z View, Cut-through at y = 5 cm

Proprietary information withheld pursuant to 10 CFR 2.390

Figure B.5.5-13
32PTH2 DSC within AHSM-HS MCNP5 Model, x-y View, Cut-through at z = 280 cm

Proprietary information withheld pursuant to 10 CFR 2.390

Figure B.5.5-14
32PTH2 DSC within AHSM-HS MCNP5 Model, x-y View, Cut-through at z = 200 cm

Proprietary information withheld pursuant to 10 CFR 2.390

Figure B.5.5-15
32PTH2 DSC within AHSM-HS MCNP5 Model, y-z View, Cut-through at x = -90 cm

Proprietary information withheld pursuant to 10 CFR 2.390

Figure B.5.5-16
32PTH2 DSC within AHSM-HS MCNP5 Model, x-y View, Cut-through at z = 280 cm

Proprietary information withheld pursuant to 10 CFR 2.390

Figure B.5.5-17
32PTH2 DSC within AHSM-HS MCNP5 Model, z-y View, Cut-through at x = -109 cm

Proprietary information withheld pursuant to 10 CFR 2.390

Figure B.5.5-18
32PTH2 DSC within AHSM-HS MCNP5 Model, x-y View, Cut-through at z = 7 cm

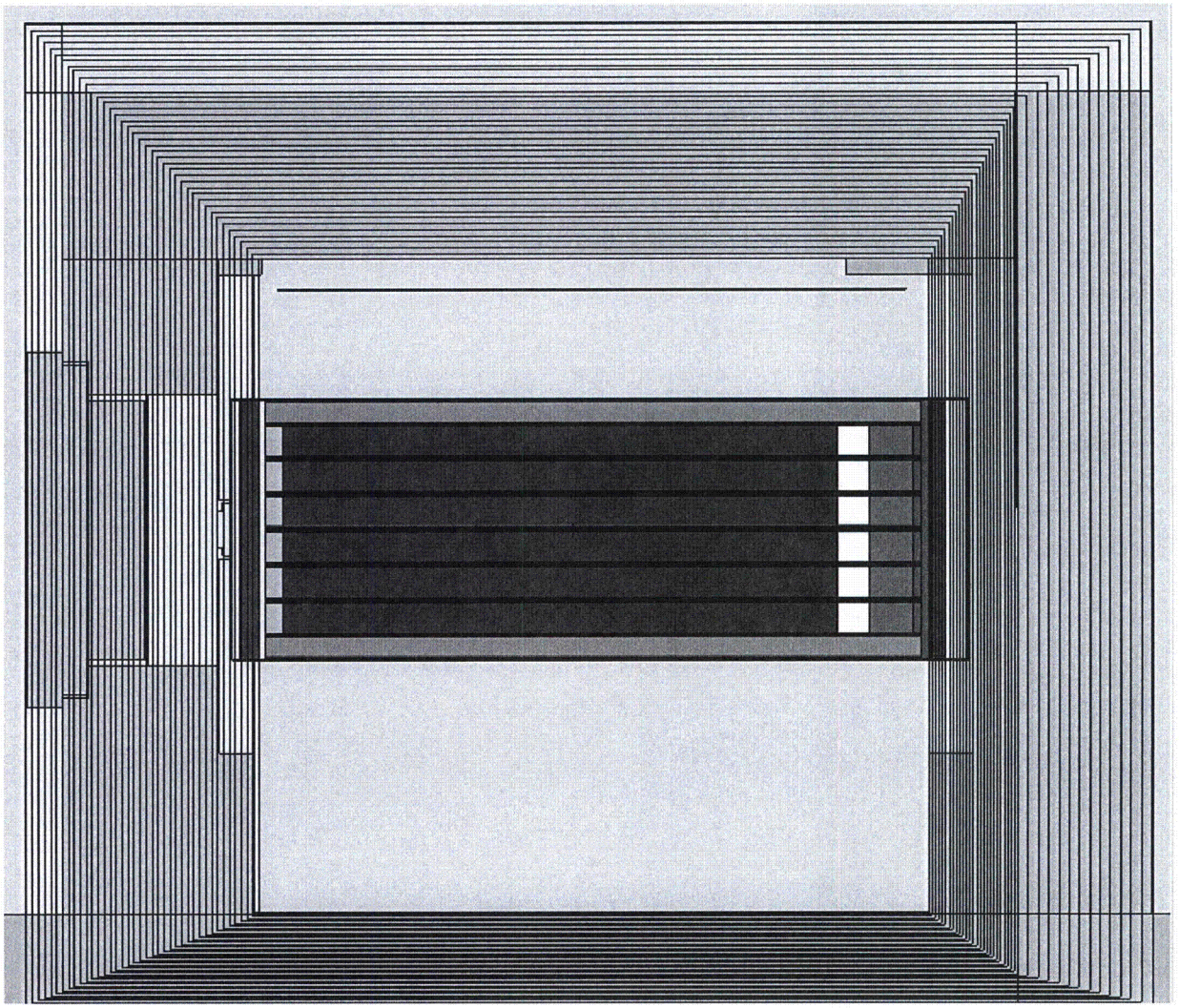

Figure B.5.5-19
32PTH2 DSC within AHSM-HS MCNP5 Model, z-y View, Cut-through at x = 2 cm

Proprietary information withheld pursuant to 10 CFR 2.390

Figure B.5.5-20
32PTH2 DSC in OS200FC TC MCNP5 Model, Transfer (Normal) Configuration

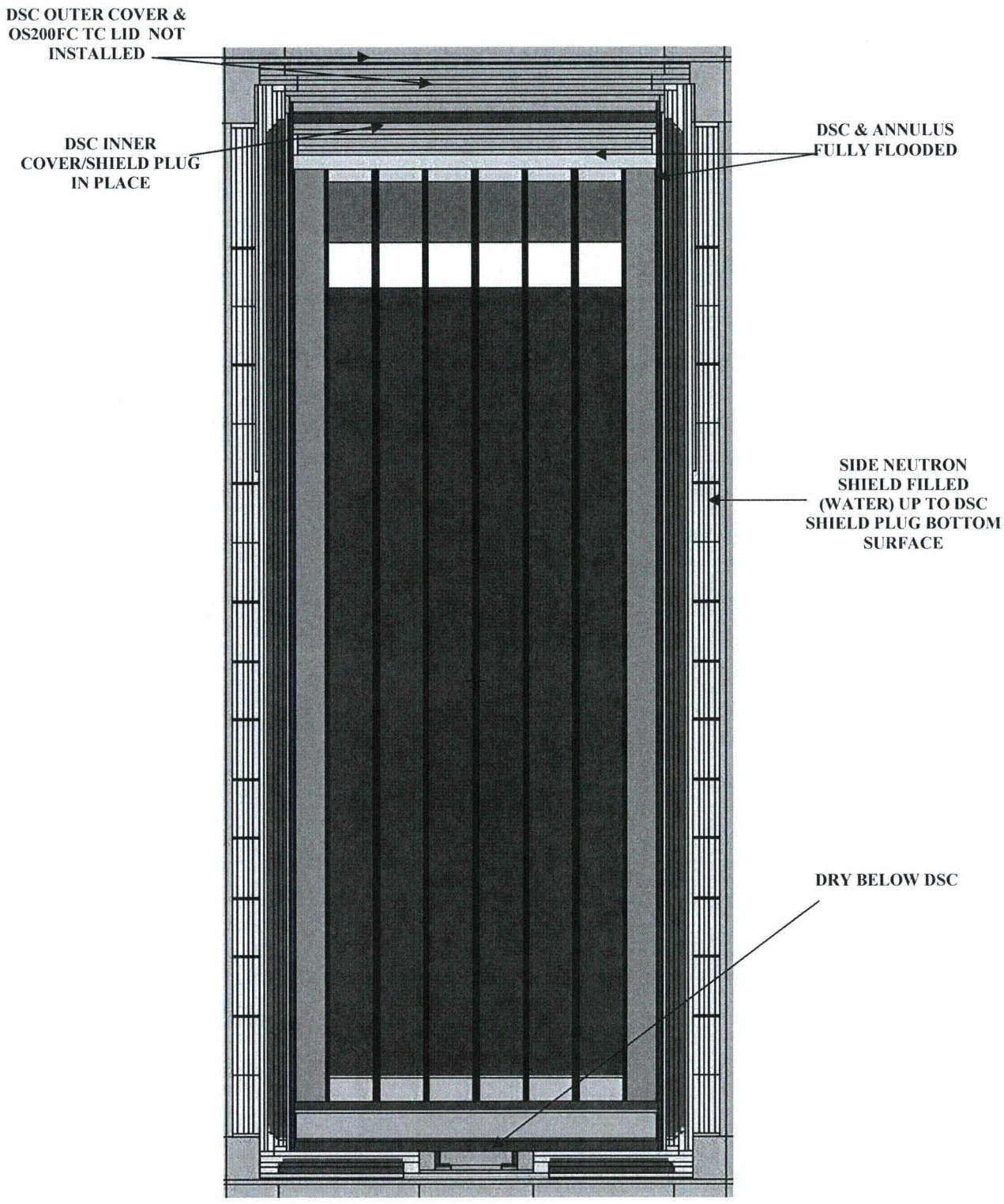

Figure B.5.5-21
32PTH2 DSC in OS200FC TC MCNP5 Model, Decontamination Configuration

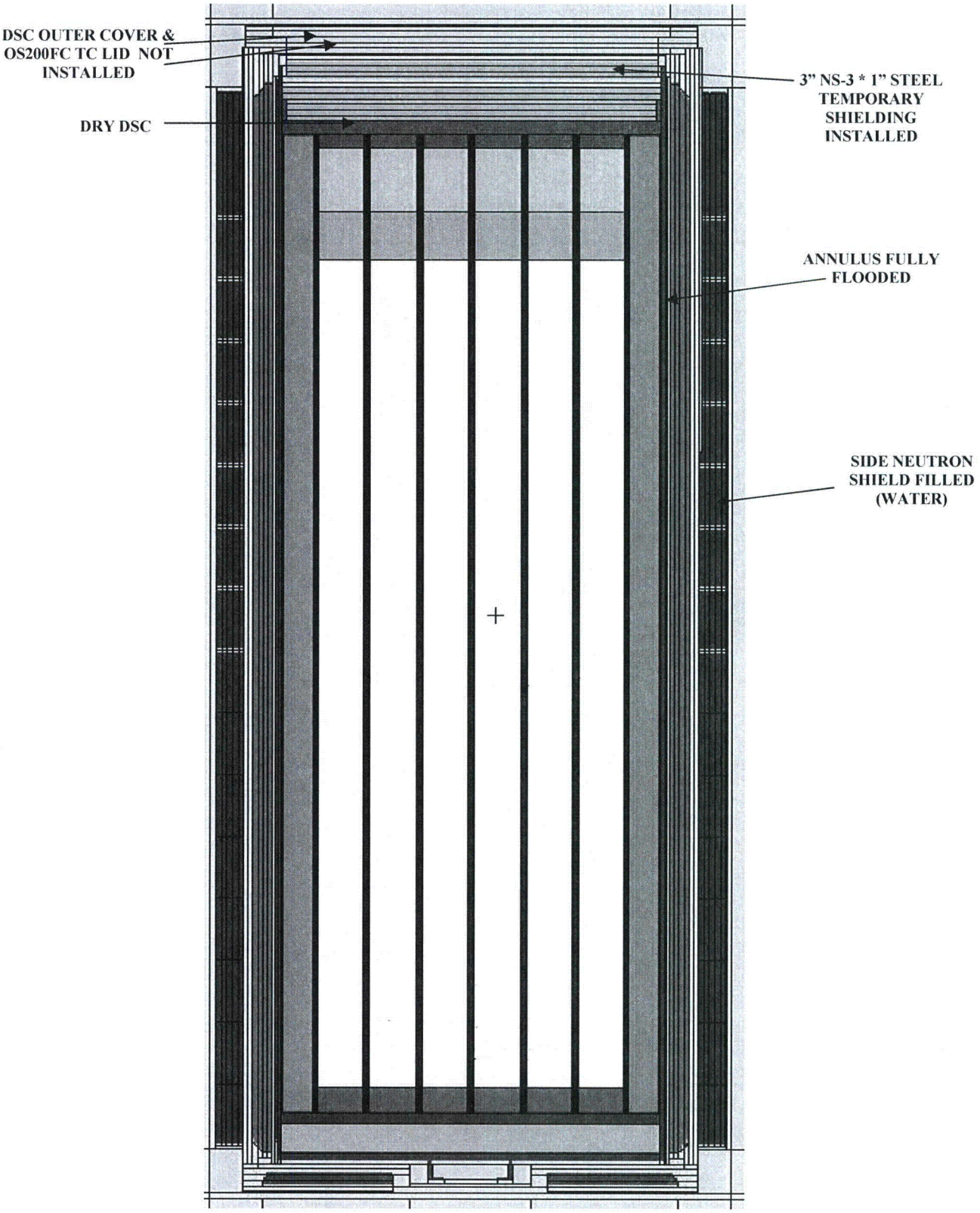

Figure B.5.5-22
32PTH2 DSC in OS200FC TC MCNP5 Model, Welding Configuration

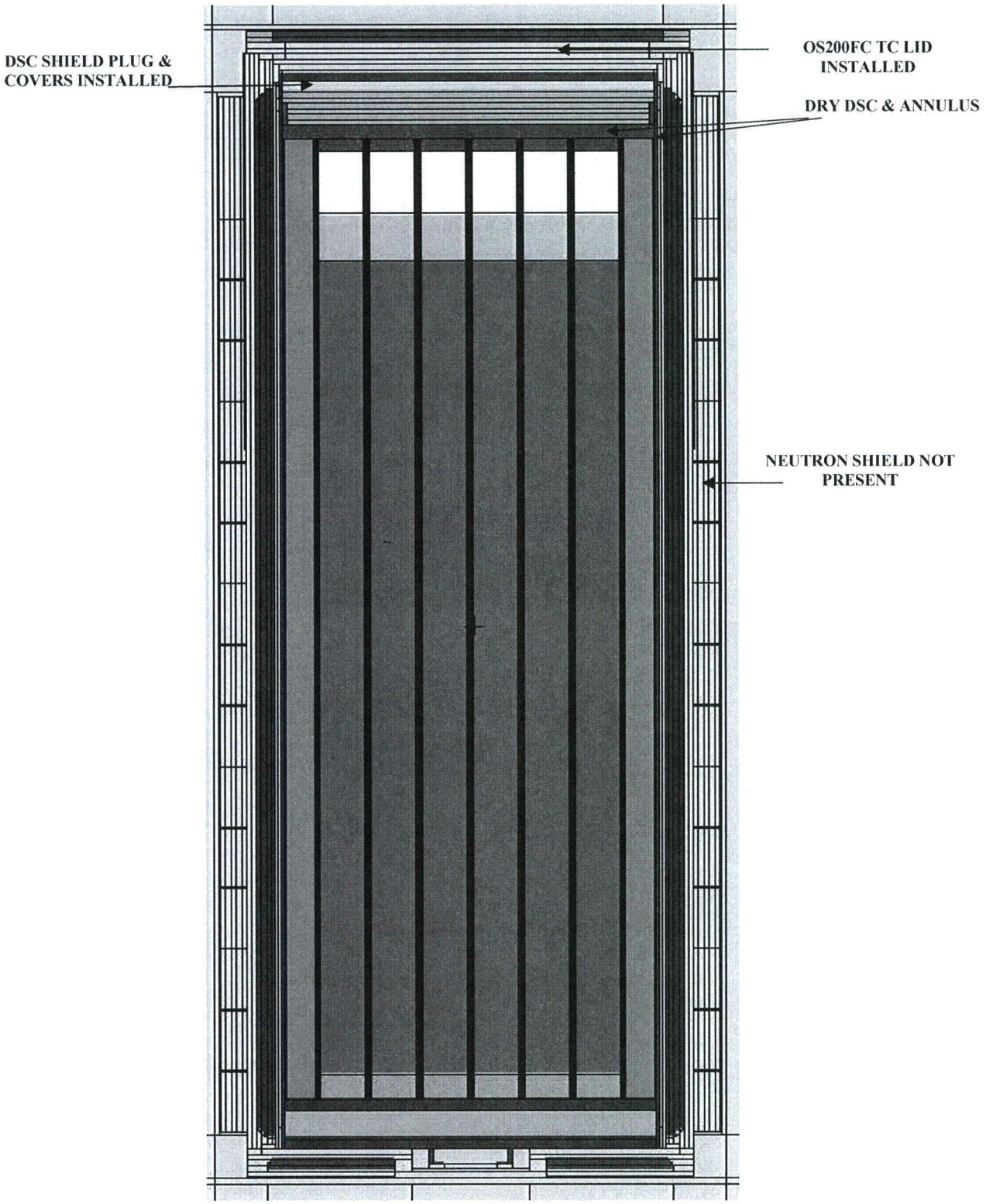

Figure B.5.5-23
32PTH2 DSC in OS200FC TC MCNP5 Model, Accident Configuration without Reconfiguration

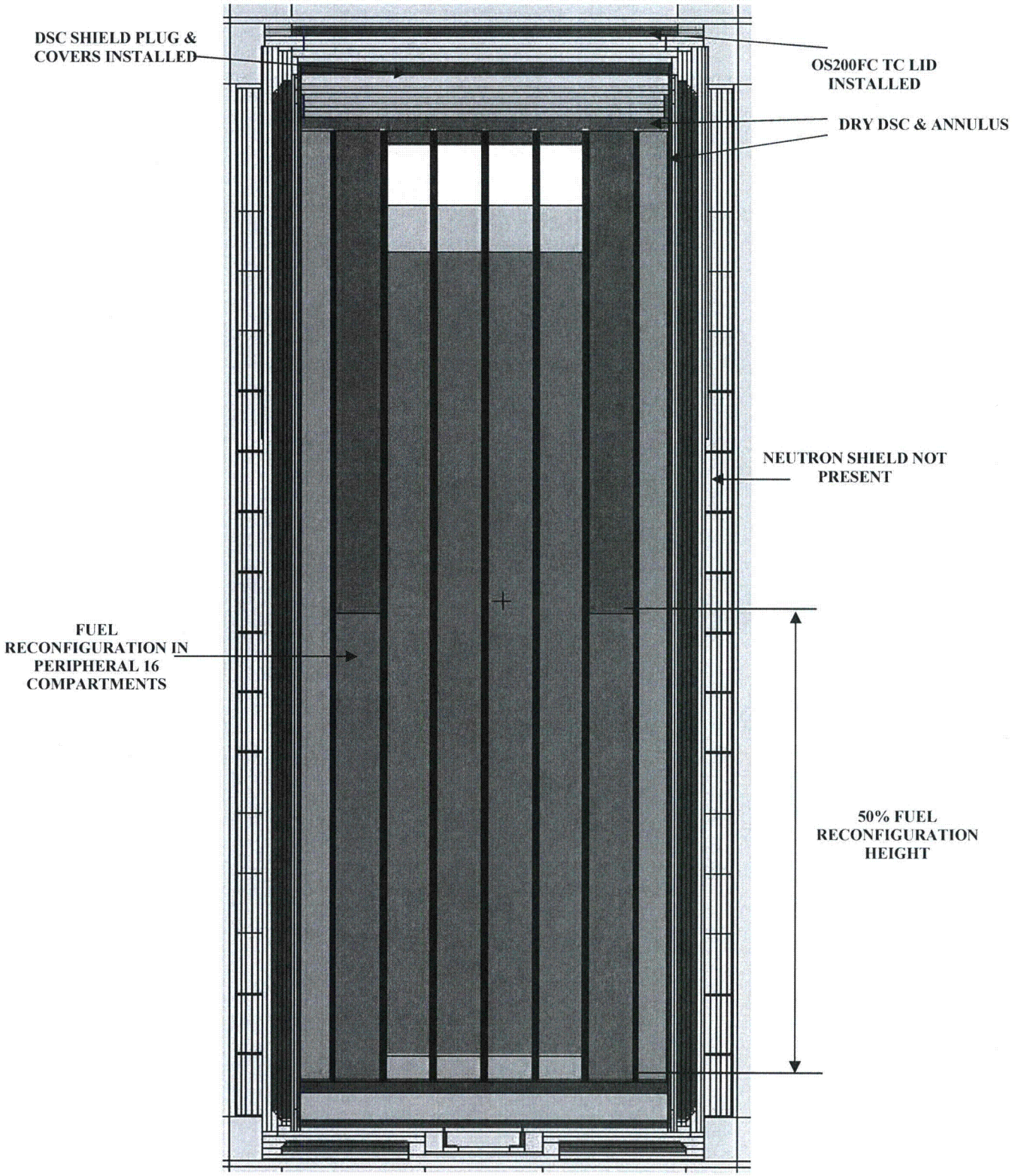

Figure B.5.5-24
32PTH2 DSC in OS200FC TC MCNP5 Model, Accident Configuration with Reconfiguration

B.6 CRITICALITY EVALUATION

The design criteria for the NUHOMS® 32PTH2 Dry Shielded Canister (DSC) requires that the fuel loaded in the 32PTH2 DSC remain subcritical under normal and accident conditions as defined in 10 CFR Part 72. The criticality analysis presented herein is identical to the analysis prepared for 32PTH1 DSC and described in Appendix U.6 of the UFSAR for the Standardized NUHOMS® System [B6.5].

The 32PTH2 DSC system's criticality safety is ensured by fixed neutron absorbers in the basket, soluble boron in the pool and favorable basket assembly geometry. Burnup credit is not taken in this criticality evaluation. The 32PTH2 DSC basket uses an aluminum/B_4C metal matrix composite as its fixed neutron poison material. This material is suitable for long-term use in the radiation and thermal environments of the 32PTH2 DSC. Justification for the use of 90% B-10 credit for the poison materials is provided in Chapter B.9 which also addresses the issues identified in the NUREG-1536 [B6.4].

Each 32PTH2 DSC basket is provided with aluminum transition rails. In addition, depending on the boron content in the basket poison plates, three basket types designated as type B, type C, and type D are employed. The only difference between the basket types is the fixed poison loading. Table B.6.6-1 lists the minimum B-10 poison loading required for the poison materials and the corresponding poison content modeled in the analysis for each basket type.

In addition to utilizing three (3) different fixed poison loadings, a minimum soluble boron concentration of 2600 ppm in the spent fuel pool is credited in the analysis.

B.6.1 Discussion and Results

Figure B.6.6-1 shows the cross section of the 32PTH2 DSC. The 32PTH2 DSC stainless steel basket consists of an "egg-crate" plate design for aluminum and neutron absorber plates. The fuel assemblies are housed in 32 stainless steel fuel compartment tubes. The basket assembly structure, including the fuel compartment tubes, is held together with stainless steel insert plates and the poison and aluminum plates that form the "egg-crate" structure. The basket compartment structure is connected to perimeter transition rail assemblies, made of aluminum. The fuel compartment tube structure is connected to perimeter transition rail assemblies as shown on the drawings in Chapter B.1, Section B.1.5.2. The poison/aluminum plates are located between the fuel compartment tubes, as shown in Figure B.6.6-1.

The criticality analysis presented herein is performed for a 32PTH2 DSC in the NUHOMS® OS200FC Transfer Cask (TC) during all loading (includes unloading) and transfer operations. This analysis also bounds all conditions of storage in the AHSM-HS. The OS200FC TC consists of an inner stainless steel shell, lead gamma shield, a stainless steel structural shell and a hydrogenous neutron shield. This analysis is applicable to any licensed cask of similar construction including those with liquid or solid hydrogenous neutron shields. The 32PTH2 DSC/OS200FC TC configuration is shown to be subcritical under normal, off-normal and accident conditions of loading, transfer and storage.

The design characteristics of the CE 16x16 class fuel assembly are summarized in Table B.6.6-4. The fuel rod and control component dimensions are presented in Table B.6.6-5. The intact fuel criticality analysis includes the most reactive fuel assembly position and the most reactive configuration for the basket. Criticality calculations are performed to determine the maximum allowed initial enrichment as a function of basket type which is listed in Table B.6.6-2. The damaged fuel criticality analysis determines the most reactive damaged fuel assembly configuration. Damaged assembly criticality calculations are performed to determine the maximum allowed initial enrichment as a function of basket type. These results are shown in Table B.6.6-3. The calculations determine k_{eff} with the CSAS5 control module of SCALE6 [B6.1] for each initial enrichment, including all uncertainties to assure criticality safety under all credible conditions.

Control components (CCs) are also authorized for storage in the 32PTH2 DSCs. The authorized CCs are burnable poison rod assemblies (BPRAs), control rod assemblies (CRAs), thimble plug assemblies (TPAs), axial power shaping rod assemblies (APSRAs), control element assemblies (CEAs), vibration suppressor inserts (VSIs), orifice rod assemblies (ORAs), neutron source assemblies (NSAs), and neutron sources. Non-fuel hardware that is positioned within the fuel assembly after the fuel assembly is discharged from the core (such as Guide Tubes or Instrument Tube Tie Rods) or Anchors, Guide Tube Inserts, BPRA Spacer Plates, or other devices that are positioned and operated within the fuel assembly during reactor operation are also considered as CCs.

The results of the evaluation demonstrate that the maximum calculated k_{eff}, including statistical uncertainty, are less than the upper subcritical limit (USL) determined from a statistical analysis of benchmark criticality experiments. The statistical analysis procedure includes a confidence band with an administrative safety margin of 0.05.

B.6.2 Package Fuel Loading

The 32PTH2 DSC is capable of transferring and storing a maximum of 32 intact CE 16x16 class PWR fuel assemblies. In addition, a maximum of 16 damaged and 16 remaining intact, (for a total of 32) PWR fuel assemblies can also be stored within the 32PTH2 DSC. The reactivity of a 32PTH2 DSC loaded with less than 32 PWR fuel assemblies is lower than that calculated for a fully loaded 32PTH2 DSC since the more absorbing borated water replaces the fuel in the empty locations. This is demonstrated in the analysis. Reconstituted fuel assemblies, where the fuel pins are replaced by lower enriched fuel pins or non-fuel pins that displace the same amount of borated water in the active fuel region, are considered intact fuel assemblies in the criticality evaluation. Both intact and damaged fuel assemblies are evaluated with CCs, and discrete burnable absorbers (DBAs).

The CE 16x16 class fuel parameters and CC dimensions that are employed in the analysis are presented in Table B.6.6-5. Reload fuel from other manufacturers with the same parameters are also considered as authorized contents.

For the CE 16x16 class fuel assembly, CCs are also included as authorized contents. The only change to the package fuel loading in order to evaluate the addition of these CCs, is replacing the borated water in the water holes with $^{11}B_4C$. Since these CCs displace borated moderator in the assembly guide and/or instrument tubes, an evaluation is performed to determine the potential impact of the storage of CCs that extend into the active fuel region on the system reactivity. For CCs such as CRAs and BPRAs no credit is taken for the cladding and absorbers; rather the CCs are modeled as $^{11}B_4C$ in the entire tube of the respective design. Thus, the highly borated moderator in the tube is modeled as $^{11}B_4C$. The inclusion of more B-11 and carbon enhances neutron scattering, causing the neutron population in the fuel assembly to be slightly increased, which increases reactivity. Therefore, these calculations bound any CC design that is compatible with a CE 16x16 class fuel assembly. The CCs that do not extend into the active fuel region of the assembly do not have any effect on the reactivity of the system as evaluated because only the active fuel region is modeled in this evaluation with periodic boundary conditions making the model infinite in the axial direction. The fuel assembly dimensions reported in Table B.6.6-5 remain unchanged for the CC cases. The models that include CCs only differ in that the region inside the guide tubes and instrument tube are modeled as $^{11}B_4C$ instead of moderator. Additionally, the presence of non-multiplying sources like the NSAs has no impact on criticality calculations.

Since the criticality analysis models simulate only the active fuel height; any CC that is inserted into the fuel assembly such that it does not extend into the active fuel region, is considered authorized for storage without adjustment to the initial enrichment as required for control components that extend into the active fuel region. For example, TPAs or ORAs are permitted for storage within a fuel assembly without adjusting the minimum soluble boron content in the spent fuel pool or DSC cavity (2600 ppm) or maximum initial enrichment given in Table B.6.6-2 and Table B.6.6-3, since TPAs or ORAs do not extend into the active fuel region.

B.6.3 Model Specification

The following subsections describe the physical models and materials of the 32PTH2 DSC as loaded and transferred in the NUHOMS® OS200FC TC (or other TCs of similar design) used for input to the CSAS5 module of SCALE6 [B6.1] to perform the criticality evaluation. The reactivity of the 32PTH2 DSC under storage conditions is bounded by the OS200FC TC analysis with zero internal moderator density case. The OS200FC TC analysis with zero internal moderator density case bounds the storage conditions in the AHSM-HS because (1) the canister internals are always dry (purged and backfilled with He) while in the AHSM-HS, and (2) the OS200FC TC contains materials such as steel and lead which provide close reflection of fast neutrons back into the fuel basket while the AHSM-HS materials (concrete) are much further from the sides of the 32PTH2 DSC and thereby tend to reflect thermalized neutrons back to the canister which are absorbed in the canister materials reducing the system reactivity. The criticality analysis methodology for the intact and damaged fuel assemblies in the 32PTH2 DSC are according to the requirements in reference [B6.4].

B.6.3.1 Description of Calculation Model

The OS200FC TC and 32PTH2 DSC are explicitly modeled using the appropriate geometry options in KENO V.a of the CSAS5 control module in SCALE6. Several models are developed to evaluate the fabrication tolerances of the canister, fuel OD, fuel clad outer diameter, fuel assembly locations, initial enrichments, fixed poison loading, soluble boron concentration and storage of CCs (BPRAs, CRAs, TPAs, APSRAs, VSIs, ORAs, NSAs, etc.) with the fuel.

The criticality evaluation is performed using an "egg-crate" section length of 13.48 inches in the basket. The actual "egg-crate" length is 15.0 inches in the active fuel region of the assembly. This represents a more reactive design than the actual basket because of the shorter "egg-crate" section length. Utilizing a shorter section length in the model ensures that the model is conservative since the amount of poison per unit length is minimized. The key basket dimensions utilized in the calculation are shown in Table B.6.6-6.

The fixed poison modeled in the calculation is based on a poison plate thickness of 0.075 inches. The important parameter is the minimum B-10 areal density; therefore the modeled thickness of the poison plate does not affect the results of the calculation.

The basic KENO model, as discussed above, is a 13.48-inch axial section and full-radial cross section of the 32PTH2 DSC and OS200FC TC with periodic boundary conditions at the axial boundaries (top and bottom) and reflective boundary conditions at the radial boundaries (sides). This axial section essentially models one building block of the egg crate basket structure. Periodic boundary conditions ensure that the resulting KENO model is essentially infinite in the axial direction. The model does not explicitly include the water neutron shield; however the infinite array of casks without the neutron shield does contain non-borated water between the casks and in the 32PTH2 DSC - OS200FC TC gap. For the purpose of storage, the 32PTH2 DSC/OS200FC TC configuration is not expected to encounter any regions containing fresh water once the fuel assemblies are loaded. Therefore, this hypothetical configuration that models an infinite array of casks in close reflection is conservative.

The fuel assemblies within the basket are modeled as arrays of fuel pins and guide/instrument tubes. Spacer grids are not modeled since their effect on reactivity is insignificant. The fuel compartments surround each fuel assembly that are in-turn bounded by the basket plates consisting of 0.370" aluminum/poison plates. These plates are arranged to represent an egg-crate structure with the 0.295"- aluminum and 0.075"-poison plates. The thermal expansion and egg-crate slot gaps are not modeled (conservative) assuming plate continuity, thus replacing the more absorbing borated water (internal moderator) with aluminum. Additionally, the drawings in Chapter B.1, Section B.1.5.2 show that the thickness of the basket support plates determine spacing between two compartments. This thickness of 0.375" is greater than the 0.370" specification of the poison-aluminum plate that would exist between the compartments, below the support plates. As a result, this creates space for borated water during loading. This space is conservatively removed in this KENO model by increasing the aluminum thickness of the poison-aluminum plate to increase the overall thickness to 0.375". KENO model plots in 2D for the various views of the basket compartment are shown in Figure B.6.6-2 through Figure B.6.6-7.

The 32PTH2 DSC basket poison plates are located at all the faces where six fuel assemblies are lined up. Thus, all the interior 16 fuel assemblies are surrounded by poison plates on all four faces and the outer 16 fuel assemblies do not have poison plates on the radially outward-looking face. The fuel assembly and poison plate positions (and the aluminum plate positions) in the KENO model of the basket are shown in Figure B.6.6-8. Even though the poison and aluminum plates are modeled as discrete plates around the fuel compartment, they are all continuous, running from one end of the basket to the other, across the 32PTH2 DSC.

The basket assembly structure is connected to the 32PTH2 DSC shell by perimeter transition rail assemblies. The transition rail material is aluminum. The rails provide a structural function as well as provide a heat conduction path from the basket to the 32PTH2 DSC shell. The rails are modeled as aluminum between the outside of the "egg-crate" structure of the basket and the inner diameter (ID) of the 32PTH2 DSC shell.

A list of all the geometry units used in the basic KENO model is shown in Table B.6.6-7. Figure B.6.6-9 shows the various radial "cylinders" utilized in the KENO model surrounding the fuel assemblies. Basically, this shows the 32PTH2 DSC and OS200FC TC as modeled.

The first model developed uses nominal dimensions for the fuel compartments, fuel compartment thickness, and poison plate thickness. The fuel assemblies are centered in the fuel compartment. This basic KENO model is used to determine the most reactive assembly-to-assembly pitch, and to determine the most reactive 32PTH2 DSC geometry configuration accounting for manufacturing tolerances. The calculational model employs the most reactive configuration identified above and is used to determine the maximum allowable initial enrichment as a function of basket type (fixed poison loading) for a minimum soluble boron concentration of 2600 ppm in the spent fuel pool or DSC cavity. The KENO plot of this model for the CE 16x16 assembly class is shown in Figure B.6.6-10.

The design basis intact assembly KENO model is utilized as the starting KENO model for the damaged assembly calculations. This model is modified to evaluate the various damaged fuel

configurations such as single shear, double shear, optimum pitch, axial fuel shifting beyond the poison plates and missing rods. These models are then utilized to determine the most reactive damaged fuel configuration. The calculational KENO model for damaged fuel criticality analysis employs this most reactive damaged configuration.

The CE 16x16 class fuel assemblies have five guide tubes. Each guide tube occupies the space of four fuel rods in the assembly. The damaged fuel models are initially evaluated without guide tubes for simplicity. Once the most reactive damaged fuel configuration is determined, the guide tubes are included in a sensitivity evaluation to determine the most reactive modeling of guide tubes. Three models are evaluated herein for this purpose: (1) Five large cylindrical guide tubes in the five guide tube locations, (2) Square guide tubes (with equivalent surface area) placed in the five guide tube locations, and (3) Four smaller cylindrical guide tubes (with equivalent surface area) in place of one large cylindrical guide tube. The three guide tube models considered are illustrated in Figure B.6.6-17. The calculational damaged fuel KENO model also includes the most reactive guide tube modeling and is used to determine the maximum allowable initial enrichment as a function of basket type for a minimum soluble boron concentration of 2600 ppm in the spent fuel pool or DSC cavity. Representative illustrations of the damaged assembly KENO models for the various damaged assembly configurations are included in Figure B.6.6-13 through Figure B.6.6-16.

B.6.3.2 Package Regional Densities

The Oak Ridge National Laboratory (ORNL) SCALE 6 code package [B6.1] contains a standard material data library for common elements, compounds, and mixtures. All the material specifications employed in the criticality analysis are obtained from this data library.

Table B.6.6-8 provides a complete list of all the relevant materials used for the criticality evaluation.

B.6.4 Criticality Calculations

This section describes the analysis methodology utilized for the criticality analysis. The analyses are performed with the CSAS5 module of the SCALE6 system. A series of calculations are performed to determine the most reactive configuration for the system with 32 CE 16x16 class fuel assemblies loaded without CCs at 2600 ppm minimum soluble boron concentration in the spent fuel pool or DSC cavity. The most reactive credible configuration was determined to be an infinite array of flooded systems, each containing 32 fuel assemblies, with minimum fuel compartment tube ID, nominal fuel compartment tube thickness, poison thickness of 0.075 inches, minimum assembly-to-assembly pitch, maximum pellet OD, minimum fuel clad thickness, and maximum clad OD.

A series of calculations is also performed to determine the relative reactivity of the various damaged fuel configurations. The most reactive damaged fuel configuration occurs in the double shear scenario, at maximum sheared row displacement, with the five large cylindrical guide tubes. All damaged assembly calculations model 32 damaged assemblies in the 32PTH2 DSC for simplicity. The most reactive credible configuration that is modeled is an infinite array of flooded systems, each containing 32 damaged fuel assemblies, with minimum fuel compartment tube ID, nominal fuel compartment tube thickness, poison thickness of 0.075 inches, minimum assembly-to-assembly pitch, maximum pellet OD, minimum fuel clad thickness, and maximum clad OD.
Finally, using the most reactive credible configurations, each determined for intact and damaged assemblies, the maximum initial enrichment (with and without CCs) is calculated as a function of basket poison material (Type B-D) for a minimum soluble boron concentration of 2600 ppm in the spent fuel pool or DSC cavity.

B.6.4.1 Calculation Method

B.6.4.1.1 Computer Codes

The CSAS5 control module of SCALE6 [B6.1] is used to calculate the effective multiplication factor (k_{eff}) of the fuel in the OS200FC TC (bounds fuel in AHSM-HS). The CSAS5 control module allows simplified data input to the functional modules BONAMI, NITAWL, and KENO V.a. These modules process the required cross sections and calculate the k_{eff} of the system. BONAMI-S performs resonance self-shielding calculations for nuclides that have Bondarenko data associated with their cross sections. NITAWL applies a Nordheim resonance self-shielding correction to nuclides having resonance parameters. Finally, KENO V.a calculates the k_{eff} of a three-dimensional system. A sufficiently large number of neutron histories are run so that the standard deviation is below 0.0010 for all calculations.

B.6.4.1.2 Physical and Nuclear Data

The physical and nuclear data required for the criticality analysis include the fuel assembly geometry data and cross-section data. Table B.6.6-5 provides the pertinent geometry data for criticality analysis for the CE 16x16 class fuel assembly and CCs evaluated in the 32PTH2 DSC.

The criticality analysis used the 44-group cross-section library built into the SCALE system. ORNL used ENDF/B-V data to develop this broad-group library specifically for criticality analysis of a wide variety of thermal systems.

B.6.4.1.3 Bases and Assumptions

The analytical results reported in Chapter B.3, Section B.3.6 demonstrate that the OS200FC TC containment boundary and canister basket structure do not experience any significant distortion under normal, off-normal or accident conditions although, the outer 16 basket assembly compartments experience a relative deflection of -0.096" in the y-direction. The fuel assembly drop analyses documented in Section B.3.5 also demonstrate that the fuel rods do not experience any deformation significant enough to cause a change in the fuel geometry. Therefore, for normal, and off-normal or accident conditions, the OS200FC TC geometry is identical except for the neutron shield and neutron shield jacket (outer skin). As discussed above, the neutron shield and neutron shield jacket (outer skin) are conservatively removed and the interstitial space modeled as water.

The 32PTH2 DSC and OS200FC TC is modeled in KENO V.a using the available geometry input. This option allows a model to be constructed that uses regular geometric shapes to define the material boundaries. The following conservative assumptions are also incorporated into the criticality calculations for intact fuel:

1. No integral burnable absorbers, such as gadolinia, erbia or any other absorbers are included.

2. CCs that extend into the active fuel region, such as BPRAs, CRAs, APSRAs, CEAs, and NSAs are conservatively assumed to exhibit the neutronic properties of $^{11}B_4C$. There is negligible absorption from any of these hardware and are collectively referred to as CCs.

3. Water in the 32PTH2 DSC cavity contains a minimum of 2600 PPM soluble boron at optimum density. The soluble boron is mixed with the moderator. By varying the moderator density from 50% to 100% of full density, the density of water at which the reactivity is maximized is determined.

4. Fresh fuel is assumed. No credit taken for fissile depletion due to burnup or fission product poisoning.

5. For intact fuel, the maximum planar average initial fuel enrichment is modeled as uniform everywhere throughout the assembly. Natural uranium blankets and axial or radial enrichment zones are modeled as enriched uranium at the maximum planar average initial enrichment.

6. All fuel rods are filled with full density fresh water in the pellet/cladding gap.

7. Only a 13.48-inch section of the basket (actual is 15.0-inches) with fuel assemblies is explicitly modeled with periodic axial boundary conditions, therefore the model is

effectively infinitely long and the actual poison height for each section is conservatively modeled to be approximately 1.52 inches shorter.

8. The neutron shield and stainless steel neutron shield jacket (outer skin) of the OS200FC TC are conservatively removed and the infinite array of OS200FC TCs are pushed close together with the moderator (fresh water) in the interstitial spaces.

9. The MMC poison plates are modeled with a B-10 content that is 90% of the minimum specified B-10 content.

10. The fuel rods are modeled assuming a stack density of 97.5% theoretical density with no allowance for dishing or chamfer. This assumption conservatively increases the total fuel content in the model.

11. Temperature at 20 °C (293 K).

12. All stainless steel is modeled as SS304. The small differences in the composition of the various stainless steels have no effect on results of the calculation.

13. All zirconium based materials in the fuel are modeled as Zircaloy-4. The small differences in the composition of the various clad / guide tube materials have no effect on the results of the calculation.

14. The thermal expansion and egg-crate gaps are conservatively replaced with the basket material wherever present. This results in replacing the soluble boron moderator in the gap regions with aluminum; thereby decreasing the neutron absorption around the fuel.

15. The transition rails between the basket and the canister shell are modeled as aluminum with no credit for borated water in the gaps between components.

16. The cask containment boundary and canister basket structure do not experience any significant distortion under accident conditions based on the results from Chapter B.3. The -0.096" deflection of the outer 16 basket assembly compartments does not affect the reactivity of the system, under accident conditions. This is justified in Section B.6.4.2.2.

In addition, the damaged fuel criticality calculations also employ the following conservative assumptions:

17. The gross damage resulting from a cask-drop accident is assumed to be either a single-ended or double-ended rod shear with flooding in borated water (during fuel loading and unloading operations). A maximum of 4 inches of fuel may be uncovered by the poison plates due to shifting of the sheared rods.

18. The cases with bare fuel (no clad) and rubble are not modeled since replacing the clad with borated water results in an increase in absorption. Hence, damaged fuel cases are modeled with the presence of the clad around the fuel pellet.

19. The bent or bowed fuel rod cases after the drop accidents assume that the fuel is intact but that the rod pitch is allowed to vary from its nominal fuel rod pitch.

20. The single-ended fuel rod shear cases assume that fuel rods that form one assembly face shear in one place and are displaced to new locations. The fuel pellets are assumed to remain in the fuel rods.

21. The double-ended fuel rod shear cases assume that fuel rods that form one assembly face, shear in two places and the sheared fuel rod pieces are separated from the parent fuel rods.

B.6.4.1.4 Determination of k_{eff}

The Monte Carlo calculations performed with CSAS5 (KENO V.a) use a flat neutron starting distribution. The total number of histories traced for each calculation is approximately 800,000. This number of histories is sufficient to achieve source convergence and produce standard deviations of less than 0.0010 in Δk_{eff}. The maximum k_{eff} for the calculation is determined with the following formula:

$$k_{eff} = k_{KENO} + 2\sigma_{KENO}$$

B.6.4.2 Fuel Loading Optimization

B.6.4.2.1 Determination of the Most Reactive Intact Fuel Configuration

The fuel-loading configuration of the 32PTH2 DSC/OS200FC TC affects the reactivity of the package. Several series of analyses determined the most reactive configuration for the 32PTH2 DSC/OS200FC TC.

1. Fuel assembly position (Assembly pitch)

The first set of analyses evaluates the effect of fuel assembly position within the fuel compartments. The evaluated positions are: 1) Fuel assemblies centered within their compartments, 2) Fuel assemblies positioned radially outward relative to the center of the basket, and 3) Fuel assemblies positioned radially inward relative to the center of the basket. The basket dimensions are modeled using nominal values. The results of the evaluation are provided in Table B.6.6-9. The results demonstrate that the most reactive position is with the fuel assemblies positioned radially inward relative to the center of the basket.

Proprietary information withheld pursuant to 10 CFR 2.390

Proprietary information withheld pursuant to 10 CFR 2.390

Proprietary information withheld pursuant to 10 CFR 2.390

In Table B.6.6-6, the 32PTH2 DSC wall thickness modeled is shown to be greater than the maximum thickness. The analysis in Table B.6.6-18 shows that modeling the wall thickness as reported results in a higher k_{eff} for the system. The two thickness values evaluated are 0.50" and 0.61". The thickness of 0.50" represents a value below the design minimum including the corrosion allowance while the value 0.61" is the design minimum with the corrosion allowance. For a thickness of 0.50" three sensitivity evaluations are performed as described: 1) The DSC ID

Proprietary information withheld pursuant to 10 CFR 2.390

8. *Reconstituted Fuel Rod Study*

The analysis performed in this section uses the most reactive configuration from the previous evaluations. This evaluation is performed to determine the effect of using fuel assemblies reconstituted with stainless steel rods. For analysis purposes, up to 16 reconstituted fuel rods are evaluated herein since the results indicate that a higher number of rods will further reduce the reactivity. The rods have a diameter equal to the clad OD of the fuel rod and span the length of the active fuel region. An illustration of a fuel assembly with reconstituted fuel rods is shown in Figure B.6.6-11. All fuel assemblies contain an equal number of stainless steel rods. The locations of the rods are selected systematically since not all possible configurations can be practically evaluated, and it is expected that a different placement for the same amount of reconstituted fuel rods produces reactivity differences that are statistically insignificant. The results in Table B.6.6-19 show that as the number of reconstituted fuel rods increases per fuel assembly, the reactivity decreases. These results also indicate that the reactivity reduction is expected to continue with more than 16 rods and from a criticality standpoint there is no restriction on the number of reconstituted rods per assembly as long as each rod displaces the same amount of moderator in the active fuel region as that of a fuel rod.

9. *Empty Fuel Compartment Location Study*

The analysis performed in this section uses the most reactive configuration from previous evaluations. The evaluation determines the effect of short loading the 32PTH2 DSC. For analysis purposes, up to six empty compartment locations are modeled within the DSC. An illustration of a KENO model with up to six empty compartments empty is shown in Figure B.6.6-12. The results in Table B.6.6-20 show that as the number of empty fuel compartment locations increases, the reactivity decreases. From a criticality standpoint, there is no restriction on the number of empty compartments in the 32PTH2 DSC.

10. *Discrete Burnable Absorber Study*

The analysis performed in this section uses the most reactive configuration from the previous evaluations. This evaluation determines the effect of the presence of Discrete Burnable Absorbers (DBAs) on the system reactivity. For analysis purposes, up to 16 DBAs are evaluated. The rods have a diameter equal to the clad OD of the fuel rods and span the axial fuel length. The DBAs are conservatively modeled as $^{11}B_4C$ with no credit taken for the presence of any residual B-10. The DBA locations employed are the same as those employed for the reconstituted fuel rod study as shown in Figure B.6.6-11. All fuel assemblies in the DSC are modeled with the same number of DBAs for this purpose of the evaluation. The results in Table B.6.6-21 show that as the number of DBAs increases per fuel assembly, the reactivity decreases. From a criticality standpoint, there is no restriction on the number of DBAs per assembly.

B.6.4.2.2 Determination of the Maximum Initial Enrichment for Intact Fuel

The analysis performed in this section is performed using the most reactive configuration determined in section B.6.4.2.1, above. This configuration is employed to determine the maximum allowable initial enrichment as a function of basket type (poison plate loading) for a minimum soluble boron concentration of 2600 ppm in the spent fuel pool or DSC cavity. Only the fixed poison loading is changed for each model. The 32PTH2 DSC/OS200FC TC model for this evaluation differs from the actual design in the following ways:

- The B-10 content of the poison plates is at the minimum required for reactivity control for each basket type per Table B.6.6-1.
- The neutron shield and the neutron shield jacket (outer skin) of the cask are conservatively replaced with water between the array of casks.
- The worst case geometry and material configurations, as determined in Section B.6.4.2.1 above, are modeled.

Proprietary information withheld pursuant to 10 CFR 2.390

- The maximum allowable initial enrichment as a function of fixed poison loading is shown in Table B.6.6-2 for intact fuel.

Three (3) different fixed poison plate loadings (basket types B, C and D) are employed in the criticality calculations. The minimum soluble boron concentration is 2600 ppm in the spent fuel pool or DSC cavity. The maximum allowable initial enrichment is 5.10 wt. % U-235. Respectively the results for the intact CE 16x16 class fuel assembly calculations as a function of moderator density, with and without CCs are listed in Table B.6.6-22 and Table B.6.6-23.

B.6.4.2.3 Determination of the Most Reactive Damaged Fuel Configurations

There are several mechanisms by which a fuel rod may be breached. These mechanisms may occur while the fuel is loaded in the reactor core, in the spent fuel pool, during transport, while in temporary dry storage, and while in permanent dry storage. In addition, the type and extent of fuel rod breach can be broken down into several categories. For this calculation, the method by which the fuel rod is breached is not as important as the extent of the resultant damage. The methodology used for the damaged fuel criticality evaluations in the 32PTH2 DSC is according to the requirements in reference [B6.4]. The gross damage resulting from a cask-drop accident is assumed to be a single-ended rod shear, double-ended rod shear, or fuel rod reconfiguration during a re-flood of the 32PTH DSC. The bent or bowed fuel rod cases assume that the fuel is intact but not in its nominal fuel rod pitch. It is possible that the fuel rods may be crushed inwards or bowed outwards to a certain degree. Therefore, this is evaluated by varying the fuel rod pitch from a minimum pitch, based on clad OD, to a maximum, based on the fuel compartment size. All pitch variations assume a uniform rod pitch throughout the entire fuel matrix.

The single-ended fuel rod shear cases assume that a fuel rod shears in one place and is displaced to a new location. The fuel pellets are assumed to remain in the fuel rod. This case is evaluated by displacing one row of rods from the base fuel assembly matrix at small increments towards the side of the fuel compartment. The base fuel assembly matrix is at nominal pitch and positioned in the "inward" position within the 32PTH2 DSC to maximize the separation distance between the fuel array and the sheared row of fuel rods. A smaller rod pitch for the base fuel assembly matrix was not chosen because it is shown from the pitch cases that decreasing the rod pitch decreases reactivity. Increasing the base fuel assembly rod pitch will increase reactivity. However, since the resulting model is similar to and is bounded by the rod pitch variation cases presented below, it is not duplicated here.

The double-ended fuel rod shear cases assume that the fuel rod shears in two places and the intact fuel rod piece is separated from the parent fuel rod. Three resulting conditions are exhibited by the occurrence of a double-ended rod shear. These include: the fuel rod piece remains in place, it is displaced in the same plane, or it is displaced to a different plane. The "remain in place" situation results in no deviation from the base fuel assembly matrix, and is therefore considered trivial and is not evaluated separately. The fuel rod piece displaced in the same plane is equivalent to the single-ended rod shear case discussed above and is not re-evaluated in these cases. The fuel rod piece displaced in a different plane results in two possibilities: an added rod or a removed rod. As in the single-ended shear cases, the base fuel assembly matrix will be positioned in the "inward" position of the 32PTH2 DSC to allow room

for a row of displaced fuel rods. In the first model, one full length rod is added to the base assembly that results in a 16x17 array, with two rows detached. In the second model, the base assembly is reduced by one row and two rows of rods that are half the length of the base assembly rods are added. The nominal rod pitch is used for the base fuel matrix just as in the single-ended shear rod cases. The analysis for the double-ended shear configuration is carried out with the minimum fuel compartment size.

The first step is to determine the most reactive damaged fuel assembly geometry. This was completed using a fixed poison loading of 18 mg B-10/cm^2, a soluble boron concentration 2600 ppm in the spent fuel pool or DSC cavity and an assembly enrichment of 5.10 wt. % U-235. All 32 assembly locations were modeled with damaged fuel assemblies. In addition, all the damaged fuel sensitivity calculations are carried out with internal moderator replacing the guide tubes. This was done for simplicity and is not expected to impact the results of this evaluation. The design basis damaged assembly calculations, however, employ the guide tubes in their respective KENO models. The intent of these calculations is to determine the most reactive damaged assembly configurations, not to meet the USL. The various analyses are described below:

1. *Rod Pitch Study*

   The first set of damaged fuel analyses is a study of the effect of the fuel rod pitch on system reactivity. KENO models with rod pitches ranging from a minimum corresponding to the clad OD to a maximum limited by the fuel compartment internal width are developed. An additional variation in this evaluation was performed by using the maximum compartment internal width to determine the most reactive configuration. A KENO model plot at maximum pitch is shown in Figure B.6.6-13. The results of the rod pitch study are shown in Table B.6.6-24. These results indicate that the optimum pitch occurs at near maximum pitch. These results also indicate that the increase in reactivity due to an increase in the fuel rod pitch is offset (within statistical uncertainty of the method) by a reduction in the reactivity due to the increased assembly-to-assembly pitch when the compartment width is increased. The most reactive case is indicated in bold text in Table B.6.6-24. This study also demonstrates that the results of the parametric study in Section B.6.4.2.1 for fuel compartment ID are also applicable to the damaged assembly evaluations.

2. *Single-Ended Rod Shear Study*

   The next set of analyses performed is for the single ended rod shear. This study evaluates the reactivity effect of the fuel assembly when the peripheral row of rods is separated from the rest of the assembly. The displacement of the sheared row of rods varies radially from fuel assembly up to a maximum that is governed by the fuel assembly width and the fuel compartment width.

   The KENO model plot shown in Figure B.6.6-14, displays the orientation of the displaced rods relative to the base assembly. The amount of fuel remains the same, i.e., no new fuel is added to the system. Nominal rod pitch is used for the 16 by 15 array. In the cask drop accident scenarios, it is more likely that the fuel assembly will be crushed as a result of the drop and therefore cause local decreases in the rod pitch of the

assembly. However, the rod pitch studies outlined above show that a decrease in the fuel rod pitch results in a decrease in system reactivity. Therefore, the single-ended rod shear study evaluations, the rod pitch is modeled at nominal value.

The shear distance between adjacent rods is measured from the outer surface of the rods. The shear distance that produces the nominal pitch, is compared with the nominal pitch case employed in the rod pitch study without guide tubes to benchmark the model to be used for the single shear analysis. This distance of $D = 0.310$ *cm* results in a k_{eff} difference that is statistically insignificant when compared to the nominal pitch configuration employed in the rod pitch study. An example plot of a single-ended shear configuration is shown in Figure B.6.6-15. The results of this evaluation are shown in Table B.6.6-25. The results for most reactive case are shown as bold text. The results indicate that there exists an optimum shear row separation distance where the reactivity is highest.

3. *Double-Ended Rod Shear Study*

The double-ended rod shear evaluations model a row (16 by 1 arrays) of dislocated rods severed at different sections axially and then displaced to other sections of the 32PTH2 DSC in order to define a bounding condition for fuel rod location following a double-ended rod shear. Two different models were considered for this study. In the first case, 10 sections of the 13.48" egg crate model are stacked together where half of the sections contain a 16x15 array and the extra 16x2 array of rods free to displace, while the other half contains a 16x15 array. In the second case, the model contains the same 10 sections and all sections contain the 16x15 array and the 16x2 sheared array of rods. In order to ensure that the model with the 10 stacks of the 13.48" sections is bounding or similar in reactivity, it is compared to the single 13.48" design basis model. The new model is then modified to include the description of the sheared rods. The shear distance between adjacent rods is measured from the outer surface of the rods. As demonstrated in Table B.6.6-26 the shear distance that results in an effective nominal pitch ($D = 0.310$ *cm*) as compared with the most reactive intact model at nominal pitch and it is concluded that it results in a reactivity that is statistically insignificant. This comparison is performed by modeling one of the row of the sheared rods with water. An example plot of a double ended shear configuration is shown in Figure B.6.6-16. The results of this evaluation are shown in Table B.6.6-26. The results for most reactive case are shown as bold text. The modeling of 10-egg-crate sections with periodic axial boundary conditions produces a k_{eff} difference that is statistically insignificant when compared to the single egg crate section with periodic axial boundary conditions. Using the 10-egg-crate modeling technique, two kinds of models were created for the purpose of the double-ended rod shear study. In the first model, the sheared rods have the same length as the rest of the rods in the intact assembly. In the second model, the sheared rods have half the length of the rest of the rods in the intact assembly. The bounding case, as indicated in the table, is the full length sheared rods at maximum separation from the base assembly.

4. *Shifting of Fuel Beyond Poison*

This study analyzes the effect of shifting of loose rods beyond the height of the poison plates. The model assumes that a four-inch axial section of the entire fuel assembly shifts beyond the poison plates. The height of the axial shift, four inches, is more than the maximum difference between the basket height and the canister cavity height (about 3.5 inches). These models conservatively bound all the cases associated with the shifting of fuel rods beyond poison. This evaluation is performed using nominal pitch employing a variation of the 10-egg-crate section model described in the previous evaluation. For this study, an additional four inches of shifted fuel is included in the model. The results of these evaluations are shown in Table B.6.6-28. The result for the most reactive case is shown as bold text. These results show that the double shear analysis bounds the shifting of individual sheared fuel rods or a full assembly, beyond the poison plate.

5. *Most Reactive Guide Tube Model*

As described in Section B.6.3.1, modeling of the CE 16x16 class fuel assembly in KENO, for damaged fuel was modified in order to simplify the definition of the damaged fuel assemblies. The most reactive damaged fuel model determined previously is evaluated herein with the three variations of guide tube models to determine the effect on reactivity

The damaged fuel model sensitivity evaluation is performed with the following three different guide tube representations:

- The design basis intact fuel model is modified to the most reactive damaged fuel model obtained with five large cylinder guide tubes.
- Four cylindrical guide tubes are modeled in the lattice locations occupied by a single guide tube. The dimensions of the equivalent guide tubes are derived such that the surface area occupied by the large guide tubes is conserved.
- Five square guide tubes replace the large cylindrical guide tubes. The dimensions of the square guide tubes are derived such that the surface area occupied by the large cylinder is conserved.

An illustration of the four cylinder guide tube modeling and the square guide tube modeling are presented in Figure B.6.6-18 and Figure B.6.6-19, respectively.

The results of the damaged fuel models indicate that the double shear study results in a higher k_{eff}. However, to determine the most reactive guide tube model, the maximum case for the rod pitch and the double shear separation distances of 0.692 cm and 0.923 cm are considered.

The results presented in Table B.6.6-27, show that the most reactive case results from modeling the five large cylindrical guide tubes in the model with the maximum double

shear separation of 0.923 cm. This model is illustrated in Figure B.6.6-20 and Figure B.6.6-21.

6. *Missing Rods Evaluation*

Due to the presence of soluble boron in the moderator, the reactivity effect of missing fuel rods is negative since the fissile fuel rods are replaced with soluble boron and will result in a reduction in k_{eff}. This is demonstrated in this sensitivity study where the most reactive rod pitch case is re-evaluated with up to 16 missing rods. The locations of the missing rods are selected systematically since not all possible configurations can be practically evaluated. It is expected that a different placement for the same number of missing rods would produce reactivity differences that are statistically insignificant. The results in Table B.6.6-29 show that there is a reduction in system reactivity when fuel rods are removed from the assemblies. This implies that there is no limit to the number of missing rods for each damaged assembly.

B.6.4.2.4 Determination of the Maximum Initial Enrichment for Damaged Fuel

The maximum initial enrichment for damaged fuel assemblies is determined for each basket, with and without CCs. The most reactive damaged fuel model is based on the double shear model with maximum separation distance between the sheared row of rods and the base assembly with five large cylindrical guide tubes and is employed to determine the maximum initial enrichment for each basket type, with and without CCs, for a minimum soluble boron concentration of 2600 ppm in the spent fuel pool. Table B.6.6-3 shows these results for damaged fuel assemblies with and without CCs.

The 32PTH2 DSC/OS200FC TC model for this evaluation differs from the design in the following ways:

- The B-10 content of the poison plates is the minimum required for reactivity control for each basket type per Table B.6.6-1.
- Damaged assemblies are loaded in all 32 fuel compartments.
- The neutron shield and the neutron shield jacket (outer skin) of the cask are conservatively replaced with water between the array of casks.
- The worst case geometry and material configurations, from Section B.6.4.2.1 and Section B.6.4.2.3 above are modeled.

Proprietary information withheld pursuant to 10 CFR 2.390

Three (3) different fixed poison loadings (basket types B, C, and D) are employed in the criticality calculations. A minimum soluble boron concentration of 2600 ppm in the spent fuel

pool or DSC cavity is employed in these calculations. The results for cases without CCs are presented in Table B.6.6-30 and the results for cases with CCs are presented in Table B.6.6-31.

B.6.4.3 Criticality Results

Table B.6.6-32 lists the bounding results for intact fuel for all conditions of storage. The highest calculated k_{eff}, including 2σ uncertainty, is the case with an initial enrichment of 4.95 wt. % U-235, 2600 ppm boron with CCs in a Type C Basket. The maximum allowed initial enrichment values (with and without CCs) as a function of fixed poison loading and a soluble boron concentration of 2600 ppm are shown in Table B.6.6-2 for intact fuel.

Table B.6.6-33 lists the bounding results for damaged fuel assemblies for all conditions of storage. The highest calculated k_{eff}, including 2σ uncertainty, is the case with an initial enrichment of 5.10 wt. % U-235, 2600 ppm boron without CCs, in a Type D Basket. The maximum allowed initial enrichment values (with and without CCs) as a function of fixed poison loading and a soluble boron concentration of 2600 ppm are shown in Table B.6.6-3.

These criticality calculations were performed with CSAS5 of SCALE6. For each case, the result includes (1) the KENO-calculated k_{KENO}, (2) the one sigma uncertainty σ_{KENO}, and (3) the final k_{eff}, which is equal to $k_{KENO} + 2\sigma_{KENO}$.

The criterion for subcriticality is that:

$$k_{KENO} + 2\sigma_{KENO} \leq USL,$$

Where USL is the upper subcritical limit established by an analysis of benchmark criticality experiments.

From Section B.6.5 the minimum USL over the parameter range is 0.9410. From Table B.6.6-33 for the most reactive case,

$$k_{KENO} + 2\sigma_{KENO} = 0.9378 + 2\ (0.0007) = 0.9392 \leq 0.9410.$$

B.6.5 Criticality Benchmark Experiments

The criticality safety analysis of the 32PTH2 DSC System uses the CSAS5 module of the SCALE6 system [B6.1] and is described briefly in section B.6.4.1.1.

The analysis presented herein uses the fresh fuel assumption for criticality analysis. The analysis employs the 44-group ENDF/B-V cross-section library because it has a small bias, as determined by 118 benchmark calculations. The Upper Subcritical Limit (USL-1) was determined using the results of these 118 benchmark calculations.

The benchmark problems used to perform this verification are representative of benchmark arrays of commercial light water reactor (LWR) fuels with the following characteristics:

(1) Water moderation.

(2) Boron neutron absorbers.

(3) Unirradiated light water reactor type fuel (no fission products or "burnup credit") near room temperature (vs. reactor operating temperature).

(4) Close reflection.

(5) Uranium oxide.

The 118 uranium oxide experiments were chosen to model a wide range of parameters that include uranium enrichment, fuel pin pitch, assembly separation, soluble boron concentration and control elements in order to test the ability of the code to accurately calculate k_{eff}. These experiments are discussed in detail in Reference [B6.2].

B.6.5.1 Benchmark Experiments and Applicability

A summary of all of the pertinent parameters for each experiment is included in Table B.6.6-34 along with the results of each run. The best correlation is observed for fuel assembly separation distance with a correlation of 0.69. All other parameters show much lower correlation ratios indicating no real correlation. All parameters were evaluated for trends and to determine the most conservative USL.

The USL is calculated in accordance to NUREG/CR-6361 [B6.2]. USL Method 1 (USL-1) applies a statistical calculation of the bias and its uncertainty plus an administrative margin (0.05) to the linear fit of results of the experimental benchmark data. The basis for the administrative margin is from reference [B6.3]. Results from the USL evaluation are presented in Table B.6.6-35.

The criticality evaluation used the same cross section set, fuel materials, and similar material/geometry options that were used in the 118 benchmark calculations shown in Table B.6.6-34. The modeling techniques and the applicable parameters listed in Table B.6.6-36 for the

actual criticality evaluations fall within the range of those addressed by the benchmarks in Table B.6.6-34.

B.6.5.2 Results of Benchmark Calculations

The results from the comparisons of physical parameters of each of the fuel assembly types (bounding for both intact and damaged assembly configurations) to the applicable USL values are presented in Table B.6.6-36. The USL value is determined to be 0.9410.

B.6.6 Appendix

B.6.6.1 References

[B6.1] SCALE 6: Modular Code System for Performing Standardized Computer Analyses for Licensing Evaluation for Workstations and Personal Computers, Oak Ridge National Laboratory, Radiation Shielding Information Center Code Package CCC-750, February 2009.

[B6.2] U.S. Nuclear Regulatory Commission, "Criticality Benchmark Guide for Light-Water-Reactor fuel in Transportation and Storage Packages," NUREG/CR-6361, Published March 1997, ORNL/TM-13211.

[B6.3] U.S. Nuclear Regulatory Commission, "Recommendations for Preparing the Criticality Safety Evaluation of Transportation Packages," NUREG/CR-5661, Published April 1997, ORNL/TM-11936.

[B6.4] U.S. Nuclear Regulatory Commission, "Standard Review Plan for Dry Cask Storage Systems," NUREG-1536, Revision 1, Published July 2010.

[B6.5] Transnuclear, Inc., Updated Final Safety Analysis Report for the Standardized NUHOM® Horizontal Modular Storage System for Irradiated Nuclear Fuel, Revision 11, USNRC Docket No. 72-1004.

Table B.6.6-1
Minimum B-10 Content in the Neutron Poison Plates

Basket Assembly Type	Minimum B-10 Content MMC (mg/cm^2)	B-10 Content Used in Criticality Evaluation (mg/cm^2)
B	15.0	13.5
C	20.0	18.0
D	32.0	28.8

Table B.6.6-2
Maximum Planar Average Initial Enrichment for Each Configuration (Intact Fuel)

Fuel Assembly Class[1]	Maximum Planar Average Initial Enrichment (wt. % U-235) as a Function of Basket Assembly Type (Fixed Poison Plate Loading) and Minimum Soluble Boron Concentration of 2600 ppm.			
		Basket Type		
		B	C	D
CE 16x16 Class Fuel Assembly	With CC	4.75	4.95	5.10
	Without CC	4.80	5.05	5.10

Notes:

(1) Reload fuel from other manufacturers with parameters shown in Table B.6.6-4 is also acceptable.

Table B.6.6-3
Maximum Planar Average Initial Enrichment for Each Configuration (Damaged Fuel)

Fuel Assembly Class[1]	Maximum Planar Average Initial Enrichment (wt. % U-235) as a Function of Basket Assembly Type (Fixed Poison Plate Loading) and Minimum Soluble Boron Concentration of 2600 ppm.			
		B	C	D
CE 16x16 Class Fuel Assembly	With CC	4.45	4.60	4.90
	Without CC	4.50	4.70	5.10

Notes:

(1) Reload fuel from other manufacturers with parameters shown in Table B.6.6-4 is also acceptable.

Table B.6.6-4
CE 16x16 Class Fuel Assembly Design Characteristics

Proprietary information withheld pursuant to 10 CFR 2.390

Table B.6.6-5
CE 16x16 Fuel Rod and Control Component Dimensions

Proprietary information withheld pursuant to 10 CFR 2.390

Table B.6.6-6
NUHOMS® 32PTH2 Basket Assembly Dimensions

Proprietary information withheld pursuant to 10 CFR 2.390

Table B.6.6-7
Description of the Basic KENO Model Units

(Part 1 of 2)

Geometry Units	Description
1	Fuel Pin Cell
2	Guide Tube
3	Instrument Tube
21 - 23	Basket Cells with Poison along the West Face of F/A
31 - 33	Basket Cells without Poison along North Face of F/A
41 - 43	Basket Cells without Poison along the East Face of F/A
51 - 53	Basket Cells with Poison along the South Face of F/A
25,35,45,55	Arrays that define the West, North, East and South Faces of the Basket Cell without fuel
61 - 63	Basket Cells without Poison along the West Face of F/A
71 - 73	Basket Cells without Poison along North Face of F/A
81 - 83	Basket Cells without Poison along the East Face of F/A
91 - 93	Basket Cells without Poison along the South Face of F/A
65,75,85,95	Arrays that define the West, North, East and South Faces of the Basket Cell without fuel and poison
201	Basket Cell with Fuel Assembly Positions 201, 202, 205, 206 representing the South West Interior Positions
204	Basket Cell with Fuel Assembly Positions 203, 204, 207, 208, 235, 236 representing the South East Positions
211	Basket Cell with Fuel Assembly Positions 211, 212, 215, 216, 231, 232 representing the North West Positions
214	Basket Cell with Fuel Assembly Positions 213, 214, 217, 218, 233, 234, 237, 238 representing the North East Positions
202	Basket Cell with Fuel Assembly Positions 225, 226 representing West Facing Corner (South West) Positions
203	Basket Cell with Fuel Assembly Positions 221, 222 representing South Facing Corner (South West) Positions
205	Basket Cell with Fuel Assembly Positions 223, 224 representing the South Facing Corner (South East) Positions
212	Basket Cell with Fuel Assembly Positions 227, 228 representing West Facing Corner (North West) Positions
241 - 245	Array of Basket Cells defining the outer 16 locations
245	Array of Basket Cells defining the inner 16 locations
10	Global Unit

Table B.6.6-7
Description of the Basic KENO Model Units
(Part 2 of 2)

Geometry Units	Description
101-108	Additional Fuel Pin Cell – Rod Pitch Study
111-118	Additional Fuel Pin Cell – Rod Pitch and Single Shear Study
122,124,126,128	Additional Fuel Pin Cell –Single and Double Shear Study
11	Uncovered Fuel Pin Cell – 4" fuel shift study
20	Uncovered Empty Guide Tube – 4" fuel shift study
3	Empty fuel cell – missing rods study
2, 7, 8, 9	Square Guide Tube Definition
401	Basket Cell with Fuel Assembly Positions 401, 402, 405, 406 representing the South West Interior Positions
404	Basket Cell with Fuel Assembly Positions 403, 404, 407, 408, 435, 436 representing the South East Positions
411	Basket Cell with Fuel Assembly Positions 411, 412, 415, 416, 431, 432 representing the North West Positions
414	Basket Cell with Fuel Assembly Positions 427, 428 representing the North East Positions
402	Basket Cell with Fuel Assembly Positions 435, 436 representing West Facing Corner (South West) Positions
403	Basket Cell with Fuel Assembly Positions 421, 422 representing South Facing Corner (South West) Positions
405	Basket Cell with Fuel Assembly Positions 423, 424 representing the South Facing Corner (South East) Positions
412	Basket Cell with Fuel Assembly Positions 437, 438
415	Basket Cell with Fuel Assembly Positions 413, 414, 417, 418, 433, 434 representing West Facing Corner (North West) Positions
416	Basket Cell With Fuel Assembly Positions 403, 404, 407, 408
441 - 445	Array of Basket Cells defining the outer 16 locations
445	Array of Basket Cells defining the inner 16 locations

Table B.6.6-8
Material Property Data

(Part 1 of 2)

Material	ID	Density g/cm^3	Element	Weight %	Atom Density (atoms/b-cm)
UO_2 (Enrichment - 5.1 wt. %)	1	10.686	U-235	4.4955	1.23081E-03
			U-238	83.6511	2.26135E-02
			O	11.8534	4.76886E-02
Zircaloy-4	2	6.560	Zr	98.23	4.2541E-02
			Sn	1.45	4.8254E-04
			Fe	0.21	1.4856E-04
			Cr	0.10	7.5978E-05
			Hf	0.01	2.2133E-06
Water (Pellet Clad Gap)	3	0.998	H	11.1	6.6769E-02
			O	88.9	3.3385E-02
Stainless Steel (SS304)	4	7.940	C	0.080	3.1877E-04
			Si	1.000	1.7025E-03
			P	0.045	6.9468E-05
			Cr	19.000	1.7473E-02
			Mn	2.000	1.7407E-03
			Fe	68.375	5.8545E-02
			Ni	9.500	7.7402E-03
Borated Water (2600 ppm Boron)	5	1.000	H	11.162	6.67515E-02
			O	88.578	3.33757E-02
			B10	0.048	2.88211E-05
			B11	0.212	1.16009E-04
$^{11}B_4C$ in CC	7	2.520	B11	78.57	1.08305E-01
			C	21.43	2.70763E-02
Aluminum	8	2.702	Al	100.0	6.0307E-02
Water	10	0.998	H	11.1	6.6769E-02
			O	88.9	3.3385E-02
Lead	11	11.344	Pb	100.0	3.2969E-02

Table B.6.6-8
Material Property Data

(Part 2 of 2)

Material	ID	Density g/cm3	Compound	Wt %	Element	Atom Density (atoms/b-cm)
MMC Poison Plate for Type B Basket (13.5 mg B-10/cm^2)	9	2.693	B_4C	18.240	B10	4.26140E-03
					B11	1.71527E-02
			Al	81.760	C	5.35352E-03
					Al	4.91425E-02
MMC Poison Plate for Type C Basket (18.0 mg B-10/cm^2)	9	2.693	B_4C	24.319	B10	5.68163E-03
					B11	2.28693E-02
			Al	75.681	C	7.13773E-03
					Al	4.54887E-02
MMC Poison Plate for Type D Basket (28.8 mg B-10/cm^2)	9	2.693	B_4C	38.911	B10	9.09075E-03
					B11	3.65914E-02
			Al	61.089	C	1.14205E-02
					Al	3.67180E-02

Table B.6.6-9
Evaluation of Assembly Position within Fuel Compartment

Model Description	k_{KENO}	1σ	k_{eff}
Fuel Assembly Position Within The Fuel Compartment – Outward			
Internal Moderator Density = 50 %	0.8905	0.0008	0.8921
Internal Moderator Density = 60 %	0.9038	0.0007	0.9052
Internal Moderator Density = 70 %	0.9062	0.0007	0.9076
Internal Moderator Density = 80 %	0.9058	0.0007	0.9072
Internal Moderator Density = 90 %	0.9001	0.0007	0.9015
Internal Moderator Density = 100 %	0.8919	0.0008	0.8935
Fuel Assembly Position Within The Fuel Compartment – Centered			
Internal Moderator Density = 50 %	0.9051	0.0007	0.9065
Internal Moderator Density = 60 %	0.9208	0.0007	0.9222
Internal Moderator Density = 70 %	0.9253	0.0007	0.9267
Internal Moderator Density = 80 %	0.9265	0.0007	0.9279
Internal Moderator Density = 90 %	0.9218	0.0008	0.9234
Internal Moderator Density = 100 %	0.9151	0.0008	0.9167
Fuel Assembly Position Within The Fuel Compartment – Inward			
Internal Moderator Density = 50 %	0.9073	0.0006	0.9085
Internal Moderator Density = 60 %	0.9224	0.0007	0.9238
Internal Moderator Density = 70 %	0.9289	0.0007	0.9303
Internal Moderator Density = 80 %	**0.9306**	**0.0007**	**0.9320**
Internal Moderator Density = 90 %	0.9242	0.0008	0.9258
Internal Moderator Density = 100 %	0.9175	0.0008	0.9191

Table B.6.6-10
Fuel Compartment Tube Internal Dimension Evaluation Results

Model Description	k_{KENO}	1σ	k_{eff}
Proprietary information withheld pursuant to 10 CFR 2.390			
Internal Moderator Density = 50 %	0.9048	0.0007	0.9062
Internal Moderator Density = 60 %	0.9184	0.0007	0.9198
Internal Moderator Density = 70 %	0.9257	0.0007	0.9271
Internal Moderator Density = 80 %	0.9239	0.0008	0.9255
Internal Moderator Density = 90 %	0.9204	0.0007	0.9218
Internal Moderator Density = 100 %	0.9141	0.0007	0.9155
Proprietary information withheld pursuant to 10 CFR 2.390			
Internal Moderator Density = 50 %	0.9073	0.0006	0.9085
Internal Moderator Density = 60 %	0.9224	0.0007	0.9238
Internal Moderator Density = 70 %	0.9289	0.0007	0.9303
Internal Moderator Density = 80 %	0.9306	0.0007	0.9320
Internal Moderator Density = 90 %	0.9242	0.0008	0.9258
Internal Moderator Density = 100 %	0.9175	0.0008	0.9191
Proprietary information withheld pursuant to 10 CFR 2.390			
Internal Moderator Density = 50 %	0.9089	0.0006	0.9101
Internal Moderator Density = 60 %	0.9261	0.0006	0.9273
Internal Moderator Density = 70 %	0.9324	0.0007	0.9338
Internal Moderator Density = 80 %	**0.9328**	**0.0007**	**0.9342**
Internal Moderator Density = 90 %	0.9281	0.0007	0.9295
Internal Moderator Density = 100 %	0.9226	0.0007	0.9240

Table B.6.6-11
Fuel Compartment Tube Wall Thickness Evaluation Results

Model Description	k_{KENO}	1σ	k_{eff}
Proprietary information withheld pursuant to 10 CFR 2.390			
Internal Moderator Density = 50 %	0.9092	0.0007	0.9106
Internal Moderator Density = 60 %	0.9236	0.0007	0.9250
Internal Moderator Density = 70 %	0.9313	0.0008	0.9329
Internal Moderator Density = 80 %	0.9326	0.0007	0.9340
Internal Moderator Density = 90 %	0.9282	0.0007	0.9296
Internal Moderator Density = 100 %	0.9213	0.0007	0.9227
Proprietary information withheld pursuant to 10 CFR 2.390			
Internal Moderator Density = 50 %	0.9089	0.0006	0.9101
Internal Moderator Density = 60 %	0.9261	0.0006	0.9273
Internal Moderator Density = 70 %	0.9324	0.0007	0.9338
Internal Moderator Density = 80 %	**0.9328**	**0.0007**	**0.9342**
Internal Moderator Density = 90 %	0.9281	0.0007	0.9295
Internal Moderator Density = 100 %	0.9226	0.0007	0.9240
Proprietary information withheld pursuant to 10 CFR 2.390			
Internal Moderator Density = 50 %	0.9093	0.0007	0.9107
Internal Moderator Density = 60 %	0.9247	0.0006	0.9259
Internal Moderator Density = 70 %	0.9311	0.0007	0.9325
Internal Moderator Density = 80 %	0.9307	0.0009	0.9325
Internal Moderator Density = 90 %	0.9295	0.0007	0.9309
Internal Moderator Density = 100 %	0.9219	0.0007	0.9233

Table B.6.6-12
Poison Plate Thickness Evaluation Results

Model Description	k_{KENO}	1σ	k_{eff}
Proprietary information withheld pursuant to 10 CFR 2.390			
Internal Moderator Density = 50 %	0.9089	0.0008	0.9105
Internal Moderator Density = 60 %	0.9255	0.0008	0.9271
Internal Moderator Density = 70 %	0.9312	0.0007	0.9326
Internal Moderator Density = 80 %	0.9317	0.0008	0.9333
Internal Moderator Density = 90 %	0.9285	0.0007	0.9299
Internal Moderator Density = 100 %	0.9212	0.0006	0.9224
Proprietary information withheld pursuant to 10 CFR 2.390			
Internal Moderator Density = 50 %	0.9089	0.0006	0.9101
Internal Moderator Density = 60 %	0.9261	0.0006	0.9273
Internal Moderator Density = 70 %	0.9324	0.0007	0.9338
Internal Moderator Density = 80 %	**0.9328**	**0.0007**	**0.9342**
Internal Moderator Density = 90 %	0.9281	0.0007	0.9295
Internal Moderator Density = 100 %	0.9226	0.0007	0.9240
Proprietary information withheld pursuant to 10 CFR 2.390			
Internal Moderator Density = 50 %	0.9104	0.0007	0.9118
Internal Moderator Density = 60 %	0.9243	0.0007	0.9257
Internal Moderator Density = 70 %	0.9311	0.0007	0.9325
Internal Moderator Density = 80 %	0.9327	0.0007	0.9341
Internal Moderator Density = 90 %	0.9295	0.0008	0.9311
Internal Moderator Density = 100 %	0.9206	0.0007	0.9220

Table B.6.6-13
Fuel Pellet OD Evaluation Results

Model Description	k_{KENO}	1σ	k_{eff}
Proprietary information withheld pursuant to 10 CFR 2.390			
Internal Moderator Density = 50 %	0.9101	0.0007	0.9115
Internal Moderator Density = 60 %	0.9241	0.0007	0.9255
Internal Moderator Density = 70 %	0.9315	0.0007	0.9329
Internal Moderator Density = 80 %	**0.9341**	**0.0009**	**0.9359**
Internal Moderator Density = 90 %	0.9298	0.0007	0.9312
Internal Moderator Density = 100 %	0.9225	0.0006	0.9237
Proprietary information withheld pursuant to 10 CFR 2.390			
Internal Moderator Density = 50 %	0.9089	0.0006	0.9101
Internal Moderator Density = 60 %	0.9261	0.0006	0.9273
Internal Moderator Density = 70 %	0.9324	0.0007	0.9338
Internal Moderator Density = 80 %	0.9328	0.0007	0.9342
Internal Moderator Density = 90 %	0.9281	0.0007	0.9295
Internal Moderator Density = 100 %	0.9226	0.0007	0.9240
Proprietary information withheld pursuant to 10 CFR 2.390			
Internal Moderator Density = 50 %	0.9087	0.0008	0.9103
Internal Moderator Density = 60 %	0.9240	0.0007	0.9254
Internal Moderator Density = 70 %	0.9323	0.0007	0.9337
Internal Moderator Density = 80 %	0.9333	0.0007	0.9347
Internal Moderator Density = 90 %	0.9274	0.0007	0.9288
Internal Moderator Density = 100 %	0.9210	0.0008	0.9226

Table B.6.6-14
Fuel Clad Thickness Evaluation Results

Model Description	k_{KENO}	1σ	k_{eff}
Proprietary information withheld pursuant to 10 CFR 2.390			
Internal Moderator Density = 50 %	0.9054	0.0007	0.9068
Internal Moderator Density = 60 %	0.9213	0.0007	0.9227
Internal Moderator Density = 70 %	0.9282	0.0007	0.9296
Internal Moderator Density = 80 %	0.9305	0.0008	0.9321
Internal Moderator Density = 90 %	0.9258	0.0008	0.9274
Internal Moderator Density = 100 %	0.9211	0.0007	0.9225
Proprietary information withheld pursuant to 10 CFR 2.390			
Internal Moderator Density = 50 %	0.9101	0.0007	0.9115
Internal Moderator Density = 60 %	0.9241	0.0007	0.9255
Internal Moderator Density = 70 %	0.9315	0.0007	0.9329
Internal Moderator Density = 80 %	0.9341	0.0009	0.9359
Internal Moderator Density = 90 %	0.9298	0.0007	0.9312
Internal Moderator Density = 100 %	0.9225	0.0006	0.9237
Proprietary information withheld pursuant to 10 CFR 2.390			
Internal Moderator Density = 50 %	0.9151	0.0008	0.9167
Internal Moderator Density = 60 %	0.9306	0.0008	0.9322
Internal Moderator Density = 70 %	0.9357	0.0008	0.9373
Internal Moderator Density = 80 %	**0.9370**	**0.0007**	**0.9384**
Internal Moderator Density = 90 %	0.9318	0.0007	0.9332
Internal Moderator Density = 100 %	0.9240	0.0008	0.9256

Table B.6.6-15
Fuel Clad OD Evaluation Results

Model Description	k_{KENO}	1σ	k_{eff}
Proprietary information withheld pursuant to 10 CFR 2.390			
Internal Moderator Density = 50 %	0.9146	0.0007	0.9160
Internal Moderator Density = 60 %	0.9306	0.0008	0.9322
Internal Moderator Density = 70 %	**0.9375**	**0.0007**	**0.9389**
Internal Moderator Density = 80 %	0.9369	0.0007	0.9383
Internal Moderator Density = 90 %	0.9316	0.0007	0.9330
Internal Moderator Density = 100 %	0.9252	0.0007	0.9266
Proprietary information withheld pursuant to 10 CFR 2.390			
Internal Moderator Density = 50 %	0.9151	0.0008	0.9167
Internal Moderator Density = 60 %	0.9306	0.0008	0.9322
Internal Moderator Density = 70 %	0.9357	0.0008	0.9373
Internal Moderator Density = 80 %	0.9370	0.0007	0.9384
Internal Moderator Density = 90 %	0.9318	0.0007	0.9332
Internal Moderator Density = 100 %	0.9240	0.0008	0.9256
Proprietary information withheld pursuant to 10 CFR 2.390			
Internal Moderator Density = 50 %	0.9136	0.0008	0.9152
Internal Moderator Density = 60 %	0.9277	0.0007	0.9291
Internal Moderator Density = 70 %	0.9333	0.0008	0.9349
Internal Moderator Density = 80 %	0.9363	0.0007	0.9377
Internal Moderator Density = 90 %	0.9302	0.0007	0.9316
Internal Moderator Density = 100 %	0.9226	0.0007	0.9240
Proprietary information withheld pursuant to 10 CFR 2.390			
Internal Moderator Density = 50 %	0.9176	0.0007	0.9190
Internal Moderator Density = 60 %	0.9305	0.0007	0.9319
Internal Moderator Density = 70 %	0.9371	0.0008	0.9387
Internal Moderator Density = 80 %	0.9375	0.0008	0.9391
Internal Moderator Density = 90 %	0.9331	0.0007	0.9345
Internal Moderator Density = 100 %	0.9275	0.0008	0.9291

Table B.6.6-16
Effect of Replacing Vertical Gap with Borated Water

Model Description	k_{KENO}	1σ	k_{eff}
Most Reactive without Gap	**0.9375**	**0.0007**	**0.9389**
Internal Moderator Density = 50 %	0.9135	0.0007	0.9149
Internal Moderator Density = 60 %	0.9279	0.0008	0.9295
Internal Moderator Density = 70 %	0.9325	0.0007	0.9339
Internal Moderator Density = 80 %	0.9354	0.0007	0.9368
Internal Moderator Density = 90 %	0.9312	0.0006	0.9324
Internal Moderator Density = 100 %	0.9251	0.0007	0.9265

Table B.6.6-17
AREVA Fuel Evaluation

Model Description	k_{KENO}	1σ	k_{eff}
Most Reactive Model	**0.9375**	**0.0007**	**0.9389**
Internal Moderator Density = 50 %	0.9069	0.0007	0.9083
Internal Moderator Density = 60 %	0.9240	0.0007	0.9254
Internal Moderator Density = 70 %	0.9320	0.0007	0.9334
Internal Moderator Density = 80 %	0.9338	0.0008	0.9354
Internal Moderator Density = 90 %	0.9324	0.0008	0.9340
Internal Moderator Density = 100 %	0.9263	0.0007	0.9277

Table B.6.6-18
DSC Shell Thickness Variation

Model Description	k_{KENO}	1σ	k_{eff}
Most Reactive Model	**0.9375**	**0.0007**	**0.9389**
Most Reactive Case with DSC Shell Thickness of 0.50", Fresh Water Between Rail and DSC Gap			
Internal Moderator Density = 50 %	0.9153	0.0008	0.9168
Internal Moderator Density = 60 %	0.9295	0.0007	0.9308
Internal Moderator Density = 70 %	0.9362	0.0007	0.9375
Internal Moderator Density = 80 %	0.9368	0.0008	0.9383
Internal Moderator Density = 90 %	0.9330	0.0007	0.9344
Internal Moderator Density = 100 %	0.9244	0.0006	0.9257
Most Reactive Case with DSC Shell Thickness of 0.61", Fresh Water Between Rail and DSC Gap			
Internal Moderator Density = 50 %	0.9148	0.0007	0.9163
Internal Moderator Density = 60 %	0.9304	0.0007	0.9318
Internal Moderator Density = 70 %	0.9356	0.0008	0.9372
Internal Moderator Density = 80 %	0.9365	0.0007	0.9379
Internal Moderator Density = 90 %	0.9327	0.0007	0.9341
Internal Moderator Density = 100 %	0.9260	0.0007	0.9274
Most Reactive Case with DSC Shell Thickness of 0.50", Borated Water Between Rail and DSC Gap			
Internal Moderator Density = 50 %	0.9155	0.0007	0.9168
Internal Moderator Density = 60 %	0.9301	0.0006	0.9313
Internal Moderator Density = 70 %	0.9362	0.0008	0.9377
Internal Moderator Density = 80 %	0.9357	0.0007	0.9371
Internal Moderator Density = 90 %	0.9326	0.0007	0.9341
Internal Moderator Density = 100 %	0.9245	0.0007	0.9259
Most Reactive Case with DSC Shell Thickness of 0.61", Borated Water Between Rail and DSC Gap			
Internal Moderator Density = 50 %	0.9174	0.0007	0.9188
Internal Moderator Density = 60 %	0.9312	0.0008	0.9327
Internal Moderator Density = 70 %	0.9372	0.0007	0.9387
Internal Moderator Density = 80 %	0.9364	0.0009	0.9382
Internal Moderator Density = 90 %	0.9319	0.0007	0.9333
Internal Moderator Density = 100 %	0.9276	0.0008	0.9292
Most Reactive Case with DSC Shell Thickness of 0.50", No DSC Gap, DSC OD - 69.5"			
Internal Moderator Density = 50 %	0.9159	0.0007	0.9173
Internal Moderator Density = 60 %	0.9287	0.0010	0.9307
Internal Moderator Density = 70 %	0.9366	0.0007	0.9379
Internal Moderator Density = 80 %	0.9359	0.0007	0.9374
Internal Moderator Density = 90 %	0.9326	0.0007	0.9340
Internal Moderator Density = 100 %	0.9251	0.0007	0.9265

Table B.6.6-19
Reconstituted Fuel Rod Study for Most Reactive System

Model Description	k_{KENO}	1σ	k_{eff}
0 Reconstituted rods	**0.9375**	**0.0007**	**0.9389**
2 Reconstituted rods	0.9329	0.0007	0.9343
4 Reconstituted rods	0.9272	0.0007	0.9286
6 Reconstituted rods	0.9234	0.0007	0.9248
8 Reconstituted rods	0.9191	0.0007	0.9205
10 Reconstituted rods	0.9132	0.0007	0.9146
12 Reconstituted rods	0.9086	0.0008	0.9102
14 Reconstituted rods	0.9066	0.0006	0.9078
16 Reconstituted rods	0.9010	0.0007	0.9024

Table B.6.6-20
Empty Fuel Compartment Locations Study

Model Description	k_{KENO}	1σ	k_{eff}
0 Empty locations	**0.9375**	**0.0007**	**0.9389**
2 Empty locations	0.8932	0.0008	0.8948
4 Empty locations	0.8792	0.0007	0.8806
6 Empty locations	0.8615	0.0007	0.8629

Table B.6.6-21
Discrete Burnable Absorber Study

Model Description	k_{KENO}	1σ	k_{eff}
0 DBAs	**0.9375**	**0.0007**	**0.9389**
2 DBAs	0.9358	0.0007	0.9372
4 DBAs	0.9344	0.0007	0.9358
6 DBAs	0.9333	0.0007	0.9347
8 DBAs	0.9328	0.0007	0.9342
10 DBAs	0.9311	0.0008	0.9327
12 DBAs	0.9291	0.0008	0.9307
14 DBAs	0.9266	0.0007	0.9280
16 DBAs	0.9270	0.0008	0.9286

Table B.6.6-22
CE 16x16 Class Assembly without CCs Final Results (Intact Fuel)

Model Description	k_{KENO}	1σ	k_{eff}
Enrichment = 4.80 wt. % U-235, Soluble Boron = 2600 ppm, Type B Basket			
Internal Moderator Density = 50 %	0.9155	0.0008	0.9171
Internal Moderator Density = 60 %	0.9284	0.0008	0.9300
Internal Moderator Density = 70 %	**0.9326**	**0.0007**	**0.9340**
Internal Moderator Density = 80 %	0.9305	0.0007	0.9319
Internal Moderator Density = 90 %	0.9247	0.0007	0.9261
Internal Moderator Density = 100 %	0.9172	0.0007	0.9186
Enrichment = 5.05 wt. % U-235, Soluble Boron = 2600 ppm, Type C Basket			
Internal Moderator Density = 50 %	0.9144	0.0007	0.9158
Internal Moderator Density = 60 %	0.9287	0.0008	0.9303
Internal Moderator Density = 70 %	0.9333	0.0007	0.9347
Internal Moderator Density = 80 %	**0.9343**	**0.0007**	**0.9357**
Internal Moderator Density = 90 %	0.9294	0.0007	0.9308
Internal Moderator Density = 100 %	0.9236	0.0007	0.9250
Enrichment = 5.10 wt. % U-235, Soluble Boron = 2600 ppm, Type D Basket			
Internal Moderator Density = 50 %	0.8910	0.0007	0.8924
Internal Moderator Density = 60 %	0.9064	0.0008	0.9080
Internal Moderator Density = 70 %	0.9163	0.0007	0.9177
Internal Moderator Density = 80 %	0.9168	0.0007	0.9182
Internal Moderator Density = 90 %	**0.9172**	**0.0008**	**0.9188**
Internal Moderator Density = 100 %	0.9119	0.0006	0.9131

Table B.6.6-23
CE 16x16 Class Assembly with CCs Final Results (Intact Fuel)

Model Description	k_{KENO}	1σ	k_{eff}
Enrichment = 4.75 wt. % U-235, Soluble Boron = 2600 ppm, Type B Basket			
Internal Moderator Density = 50 %	0.9064	0.0007	0.9078
Internal Moderator Density = 60 %	0.9240	0.0007	0.9254
Internal Moderator Density = 70 %	0.9319	0.0008	0.9335
Internal Moderator Density = 80 %	**0.9351**	**0.0007**	**0.9365**
Internal Moderator Density = 90 %	0.9348	0.0008	0.9364
Internal Moderator Density = 100 %	0.9295	0.0007	0.9309
Enrichment = 4.95 wt. % U-235, Soluble Boron = 2600 ppm, Type C Basket			
Internal Moderator Density = 50 %	0.9009	0.0007	0.9023
Internal Moderator Density = 60 %	0.9190	0.0007	0.9204
Internal Moderator Density = 70 %	0.9299	0.0007	0.9313
Internal Moderator Density = 80 %	0.9341	0.0008	0.9357
Internal Moderator Density = 90 %	**0.9359**	**0.0007**	**0.9373**
Internal Moderator Density = 100 %	0.9340	0.0008	0.9356
Enrichment = 5.10 wt. % U-235, Soluble Boron = 2600 ppm, Type D Basket			
Internal Moderator Density = 50 %	0.8822	0.0007	0.8836
Internal Moderator Density = 60 %	0.9017	0.0008	0.9033
Internal Moderator Density = 70 %	0.9146	0.0007	0.9160
Internal Moderator Density = 80 %	0.9246	0.0008	0.9262
Internal Moderator Density = 90 %	**0.9281**	**0.0007**	**0.9295**
Internal Moderator Density = 100 %	0.9266	0.0007	0.9280

Table B.6.6-24
Rod Pitch Study Results

Model Description	k_{KENO}	1σ	k_{eff}
CE 16x16 Class Fuel Assembly			
Pitch=0.384", IMD=100%	0.7117	0.0009	0.7135
Pitch=0.400", IMD=100%	0.7548	0.0009	0.7566
Pitch=0.417", IMD=100%	0.7924	0.0010	0.7944
Pitch=0.433", IMD=100%	0.8241	0.0009	0.8259
Pitch=0.450", IMD=100%	0.8524	0.0007	0.8538
Pitch=0.466", IMD=100%	0.8752	0.0008	0.8768
Pitch=0.482", IMD=100%	0.8959	0.0007	0.8973
Pitch=0.499", IMD=100%	0.9131	0.0007	0.9145
Pitch=0.506", IMD=100%	0.9192	0.0008	0.9208
Pitch=0.515", IMD=050%	0.9265	0.0007	0.9279
Pitch=0.515", IMD=060%	0.9376	0.0007	0.9390
Pitch=0.515", IMD=070%	0.9427	0.0007	0.9441
Pitch=0.515", IMD=080%	0.9396	0.0007	0.9410
Pitch=0.515", IMD=090%	0.9350	0.0007	0.9364
Pitch=0.515", IMD=100%	0.9251	0.0007	0.9265
Pitch=0.531", IMD=050%	0.9368	0.0007	0.9382
Pitch=0.531", IMD=060%	0.9486	0.0007	0.9500
Pitch=0.531", IMD=070%	0.9514	0.0007	0.9528
Pitch=0.531", IMD=080%	0.9479	0.0007	0.9493
Pitch=0.531", IMD=090%	0.9399	0.0009	0.9417
Pitch=0.531", IMD=100%	0.9295	0.0006	0.9307
Pitch=0.548", IMD=050%	0.9416	0.0007	0.9430
Pitch=0.548", IMD=060%	0.9516	0.0007	0.9530
Pitch=0.548", IMD=070%	**0.9517**	**0.0007**	**0.9531**
Pitch=0.548", IMD=080%	0.9456	0.0007	0.9470
Pitch=0.548", IMD=090%	0.9362	0.0008	0.9378
Pitch=0.548", IMD=100%	0.9218	0.0007	0.9232
Maximum Compartment Width and Increased Pitch			
Pitch=0.554", IMD=050%	0.9419	0.0007	0.9433
Pitch=0.554", IMD=060%	0.9512	0.0007	0.9526
Pitch=0.554", IMD=070%	0.9485	0.0008	0.9501
Pitch=0.554", IMD=080%	0.9416	0.0007	0.9430
Pitch=0.554", IMD=090%	0.9316	0.0007	0.9330
Pitch=0.554", IMD=100%	0.9161	0.0007	0.9175

Table B.6.6-25
Single Ended Rod Shear Study Results

Model Description	k_{KENO}	1σ	k_{eff}
CE 16x16 Class Fuel Assembly			
Nominal Pitch, IMD=70% (1)	0.9358	0.0007	0.9372
D=0.000 cm, IMD=70%	0.9309	0.0007	0.9323
D=0.238 cm, IMD=70%	0.9340	0.0007	0.9354
D=0.310 cm, IMD=70% (2)	0.9353	0.0007	0.9367
D=0.475 cm, IMD=70%	0.9368	0.0007	0.9382
D=0.713 cm, IMD=70%	0.9383	0.0008	0.9399
D=1.188 cm, IMD=70%	**0.9406**	**0.0007**	**0.9420**
D=1.425 cm, IMD=70%	0.9403	0.0007	0.9417
D=1.663 cm, IMD=70%	0.9387	0.0008	0.9403
D=1.900 cm, IMD=70%	0.9366	0.0007	0.9380

Notes:

(1) This model is the same as that evaluated in Table B.6.6-24, at the nominal pitch with 100% internal moderator density.

(2) This case is the model benchmarked with the configuration described in note (1).

Table B.6.6-26
Double Ended Rod Shear Study Results – Model 1

(Part 1 of 2)

Model Description	k_{KENO}	1σ	k_{eff}
Comparison of Single 13.48" Section with 10 – 13.48" Section Models, IMD = 070%			
10 – 13.48" Section	0.9374	0.0007	0.9388
1 – 13.48" Section	0.9375	0.0007	0.9389
D = 0.310 cm	0.9374	0.0007	0.9388
Full Length Sheared Rods			
D = 0.000 cm			
IMD=050%	0.9291	0.0008	0.9307
IMD=060%	0.9459	0.0007	0.9473
IMD=070%	0.9509	0.0008	0.9525
IMD=080%	0.9504	0.0008	0.9520
IMD=090%	0.9461	0.0007	0.9475
IMD=100%	0.9376	0.0007	0.9390
D = 0.231 cm			
IMD=050%	0.9321	0.0006	0.9333
IMD=060%	0.9474	0.0007	0.9488
IMD=070%	0.9521	0.0007	0.9535
IMD=080%	0.9525	0.0007	0.9539
IMD=090%	0.9487	0.0007	0.9501
IMD=100%	0.9421	0.0006	0.9433
D = 0.462 cm			
IMD=050%	0.9342	0.0007	0.9356
IMD=060%	0.9496	0.0007	0.9510
IMD=070%	0.9540	0.0008	0.9556
IMD=080%	0.9548	0.0007	0.9562
IMD=090%	0.9510	0.0006	0.9522
IMD=100%	0.9422	0.0007	0.9436
D = 0.692 cm			
IMD=050%	0.9357	0.0007	0.9371
IMD=060%	0.9515	0.0007	0.9529
IMD=070%	0.9567	0.0007	0.9581
IMD=080%	**0.9569**	**0.0008**	**0.9585**
IMD=090%	0.9519	0.0008	0.9535
IMD=100%	0.9430	0.0007	0.9444
D = 0.923 cm			
IMD=050%	0.9382	0.0007	0.9396
IMD=060%	0.9523	0.0008	0.9539
IMD=070%	0.9553	0.0007	0.9567
IMD=080%	**0.9569**	**0.0008**	**0.9585**
IMD=090%	0.9502	0.0007	0.9516
IMD=100%	0.9414	0.0007	0.9428

Table B.6.6-26
Double Ended Rod Shear Study Results – Model 2

(Part 2 of 2)

Model Description	k_{KENO}	1σ	k_{eff}
Double Shear - Model 2 Half Length Sheared Rods			
D = 0.000 cm, IMD=100%	0.9315	0.0007	0.9329
D = 0.231 cm, IMD=100%	0.9347	0.0007	0.9361
D = 0.468 cm, IMD=100%	0.9345	0.0007	0.9359
D = 0.692cm, IMD=100%	0.9365	0.0008	0.9381
D = 0.923 cm, IMD=100%	0.9331	0.0008	0.9347
Model 2 - D = 0.692 cm			
IMD=050%	0.9240	0.0006	0.9252
IMD=060%	0.9409	0.0007	0.9423
IMD=070%	**0.9480**	**0.0008**	**0.9496**
IMD=080%	0.9475	0.0007	0.9489
IMD=090%	0.9428	0.0007	0.9442
Model 2 - D = 0.923 cm			
IMD=050%	0.9265	0.0007	0.9279
IMD=060%	0.9409	0.0007	0.9423
IMD=070%	0.9477	0.0008	0.9493
IMD=080%	0.9466	0.0008	0.9482
IMD=090%	0.9428	0.0008	0.9444

Table B.6.6-27
Most Reactive Guide Tube Model

(Part 1 of 2)

Model Description	k_{KENO}	1σ	k_{eff}
Double Shear 0.692 cm- Large Cylinder Guide Tubes – 7x7			
IMD=050%	0.9350	0.0008	0.9366
IMD=060%	0.9506	0.0007	0.9520
IMD=070%	0.9568	0.0007	0.9582
IMD=080%	0.9574	0.0009	0.9592
IMD=090%	0.9531	0.0008	0.9547
IMD=100%	0.9478	0.0007	0.9492
Double Shear 0.923 cm- Large Cylinder Guide Tubes – 7x7			
IMD=050%	0.9351	0.0007	0.9365
IMD=060%	0.9491	0.0007	0.9505
IMD=070%	0.9570	0.0007	0.9584
IMD=080%	**0.9583**	**0.0007**	**0.9597**
IMD=090%	0.9531	0.0007	0.9545
IMD=100%	0.9467	0.0007	0.9481
Double Shear -0.692 cm– 4 Cylinder Guide Tubes – 16x16			
IMD=050%	0.9344	0.0007	0.9358
IMD=060%	0.9510	0.0007	0.9524
IMD=070%	0.9571	0.0007	0.9585
IMD=080%	0.9574	0.0006	0.9586
IMD=090%	0.9554	0.0007	0.9568
IMD=100%	0.9483	0.0007	0.9497
Double Shear -0.923 cm– 4 Cylinder Guide Tubes – 16x16			
IMD=050%	0.9352	0.0007	0.9366
IMD=060%	0.9514	0.0007	0.9528
IMD=070%	0.9557	0.0007	0.9571
IMD=080%	0.9566	0.0007	0.9580
IMD=090%	0.9527	0.0007	0.9541
IMD=100%	0.9452	0.0007	0.9466

Table B.6.6-27
Most Reactive Guide Tube Model

(Part 2 of 2)

Double Shear -0.692 cm – Square Guide Tubes – 16x16			
IMD=050%	0.9337	0.0007	0.9351
IMD=060%	0.9493	0.0006	0.9505
IMD=070%	0.9573	0.0008	0.9589
IMD=080%	0.9570	0.0007	0.9584
IMD=090%	0.9529	0.0006	0.9541
IMD=100%	0.9468	0.0008	0.9484
Double Shear -0.923 cm – Square Guide Tubes – 16x16			
IMD=050%	0.9348	0.0007	0.9362
IMD=060%	0.9504	0.0007	0.9518
IMD=070%	0.9567	0.0006	0.9579
IMD=080%	0.9562	0.0008	0.9578
IMD=090%	0.9519	0.0006	0.9531
IMD=100%	0.9442	0.0006	0.9454
Most Reactive Rod Pitch – Square Guide Tubes			
IMD=050%	0.9400	0.0008	0.9416
IMD=060%	0.9521	0.0007	0.9535
IMD=070%	0.9536	0.0007	0.9550
IMD=080%	0.9487	0.0007	0.9501
IMD=090%	0.9401	0.0007	0.9415
IMD=100%	0.9276	0.0006	0.9288
Most Reactive Rod Pitch – 4 Cylinder Guide Tubes			
IMD=050%	0.9414	0.0007	0.9428
IMD=060%	0.9528	0.0007	0.9542
IMD=070%	0.9542	0.0006	0.9554
IMD=080%	0.9496	0.0007	0.9510
IMD=090%	0.9402	0.0006	0.9414
IMD=100%	0.9281	0.0006	0.9293

Table B.6.6-28
4" Fuel Shift Study

Model Description	k_{KENO}	1σ	k_{eff}
IMD=050%	0.9224	0.0008	0.9240
IMD=060%	0.9379	0.0007	0.9393
IMD=070%	**0.9412**	**0.0007**	**0.9426**
IMD=080%	0.9407	0.0008	0.9423
IMD=090%	0.9357	0.0007	0.9371
IMD=100%	0.9260	0.0007	0.9274

Table B.6.6-29
Missing Rods Study

Model Description	k_{KENO}	1σ	k_{eff}
Missing 0	**0.9542**	**0.0006**	**0.9554**
Missing 1	0.9517	0.0006	0.9529
Missing 2	0.9504	0.0007	0.9518
Missing 4	0.9489	0.0006	0.9501
Missing 6	0.9461	0.0007	0.9475
Missing 8	0.9422	0.0007	0.9436
Missing 10	0.9406	0.0007	0.9420
Missing 12	0.9382	0.0007	0.9396
Missing 14	0.9342	0.0007	0.9356
Missing 16	0.9335	0.0006	0.9347

Table B.6.6-30
CE 16x16 Class Assembly without CCs Final Results (Damaged Fuel)

Model Description	k_{KENO}	1σ	k_{eff}
Enrichment = 4.50 wt. % U-235, Soluble Boron = 2600 ppm, Type B Basket			
Internal Moderator Density = 50 %	0.9157	0.0007	0.9171
Internal Moderator Density = 60 %	0.9301	0.0006	0.9313
Internal Moderator Density = 70 %	0.9323	0.0006	0.9335
Internal Moderator Density = 80 %	**0.9325**	**0.0007**	**0.9339**
Internal Moderator Density = 90 %	0.9252	0.0006	0.9264
Internal Moderator Density = 100 %	0.9160	0.0008	0.9176
Enrichment = 4.70 wt. % U-235, Soluble Boron = 2600 ppm, Type C Basket			
Internal Moderator Density = 50 %	0.9131	0.0007	0.9145
Internal Moderator Density = 60 %	0.9280	0.0008	0.9296
Internal Moderator Density = 70 %	**0.9338**	**0.0006**	**0.9350**
Internal Moderator Density = 80 %	0.9315	0.0007	0.9329
Internal Moderator Density = 90 %	0.9285	0.0007	0.9299
Internal Moderator Density = 100 %	0.9222	0.0007	0.9236
Enrichment = 5.10 wt. % U-235, Soluble Boron = 2600 ppm, Type D Basket			
Internal Moderator Density = 50 %	0.9080	0.0008	0.9096
Internal Moderator Density = 60 %	0.9284	0.0007	0.9298
Internal Moderator Density = 70 %	0.9365	0.0007	0.9379
Internal Moderator Density = 80 %	**0.9378**	**0.0007**	**0.9392**
Internal Moderator Density = 90 %	0.9364	0.0006	0.9376
Internal Moderator Density = 100 %	0.9297	0.0007	0.9311

Table B.6.6-31
CE 16x16 Class Assembly with CCs Final Results (Damaged Fuel)

Model Description	k_{KENO}	1σ	k_{eff}
Enrichment = 4.45 wt. % U-235, Soluble Boron = 2600 ppm, Type B Basket			
Internal Moderator Density = 50 %	0.9080	0.0006	0.9092
Internal Moderator Density = 60 %	0.9242	0.0007	0.9256
Internal Moderator Density = 70 %	0.9340	0.0007	0.9354
Internal Moderator Density = 80 %	**0.9375**	**0.0008**	**0.9391**
Internal Moderator Density = 90 %	0.9359	0.0008	0.9375
Internal Moderator Density = 100 %	0.9301	0.0007	0.9315
Enrichment = 4.60 wt. % U-235, Soluble Boron = 2600 ppm, Type C Basket			
Internal Moderator Density = 50 %	0.9012	0.0007	0.9026
Internal Moderator Density = 60 %	0.9203	0.0007	0.9217
Internal Moderator Density = 70 %	0.9313	0.0007	0.9327
Internal Moderator Density = 80 %	0.9348	0.0008	0.9364
Internal Moderator Density = 90 %	**0.9355**	**0.0009**	**0.9373**
Internal Moderator Density = 100 %	0.9320	0.0007	0.9334
Enrichment = 4.90 wt. % U-235, Soluble Boron = 2600 ppm, Type D Basket			
Internal Moderator Density = 50 %	0.8909	0.0007	0.8923
Internal Moderator Density = 60 %	0.9125	0.0006	0.9137
Internal Moderator Density = 70 %	0.9253	0.0007	0.9267
Internal Moderator Density = 80 %	0.9339	0.0007	0.9353
Internal Moderator Density = 90 %	**0.9366**	**0.0007**	**0.9380**
Internal Moderator Density = 100 %	0.9345	0.0007	0.9359

Table B.6.6-32
Summary of Criticality Results for Intact Fuel Assemblies

Model Description	k_{KENO}	1σ	k_{eff}
Regulatory Requirements			
Dry Storage (Bounded by infinite array of undamaged storage canisters)	0.5454	0.0004	0.5462
Accident Loading Conditions (Optimum Moderator Density)	**0.9359**	**0.0007**	**0.9373**
Normal Loading and Unloading Conditions (Maximum Moderator Density)	0.9340	0.0008	0.9356

Table B.6.6-33
Summary of Criticality Results for Damaged Fuel Assemblies

Model Description	k_{KENO}	1σ	k_{eff}
Regulatory Requirements			
Dry Storage (Bounded by infinite array of damaged storage canisters)	0.5356	0.0004	0.5364
Accident Loading Conditions (Optimum Moderator Density)	**0.9378**	**0.0007**	**0.9392**
Normal Loading and Unloading Conditions (Maximum Moderator Density)	0.9345	0.0007	0.9359

Table B.6.6-34
Benchmark Experiments

(Part 1 of 3)

Experiment ID	U-235 Enrichment in wt%	Fuel Rod Pitch (cm)	H_2O/UO_2 Volume Ratio	Boron Loading (PPM)	Separation Distance (cm)	AEG	k_{eff}	σ
b1645so1	2.46	1.41	1.015	1068	1.78	32.79	0.9958	0.0009
b1645so2	2.46	1.41	1.015	1156	1.78	32.74	0.9999	0.0009
bw1231b1	4.02	1.511	1.139	1152	-	31.13	0.9953	0.0008
bw1231b2	4.02	1.511	1.139	3389	-	29.89	0.9961	0.0007
bw1273m	2.46	1.511	1.376	1675	-	32.22	0.9952	0.0007
bw1484a1	2.46	1.636	1.841	15	1.64	34.53	0.9975	0.0008
bw1484a2	2.46	1.636	1.841	72	4.92	35.15	0.9922	0.0008
bw1484b1	2.46	1.636	1.841	1037	-	33.93	0.9982	0.0008
bw1484b2	2.46	1.636	1.841	769	1.64	34.57	0.9964	0.0008
bw1484b3	2.46	1.636	1.841	143	4.92	35.23	0.9970	0.0007
bw1484c1	2.46	1.636	1.841	-	1.64	34.62	0.9924	0.0009
bw1484c2	2.46	1.636	1.841	-	1.64	35.22	0.9951	0.0009
bw1484s1	2.46	1.636	1.841	432	1.64	34.50	0.9987	0.0007
bw1484s2	2.46	1.636	1.841	514	1.64	34.54	0.9991	0.0008
bw1484sl	2.46	1.636	1.841	-	6.54	35.39	0.9954	0.0009
bw1645s1	2.46	1.209	0.383	746	1.78	30.10	0.9981	0.0008
bw1645s2	2.46	1.209	0.383	886	1.78	29.98	1.0018	0.0007
bw1810a	2.46	1.636	1.841	1239	-	33.94	0.9990	0.0006
bw1810b	2.46	1.636	1.841	1170	-	33.95	0.9991	0.0006
bw1810cr	2.46	1.636	1.841	1499	-	33.13	0.9970	0.0010
bw1810d	2.46	1.636	1.841	1654	0.18973	33.08	0.9963	0.0008
bw1810e	2.46	1.636	1.841	1579	-	33.14	0.9982	0.0008
bw1810f	2.46	1.636	1.841	1337	-	33.95	1.0034	0.0008
bw1810gr	2.46	1.636	1.841	1776	-	32.92	0.9991	0.0016
bw1810h	2.46	1.636	1.841	1899	-	32.93	0.9993	0.0008
bw1810i	2.46	1.636	1.841	1250	-	33.94	1.0017	0.0007
bw1810j	2.46	1.636	1.532	1635	-	33.12	0.9991	0.0008
epru65b	2.35	1.562	1.196	463	-	33.38	0.9986	0.0010
epru65	2.35	1.562	1.196	-	-	33.92	0.9966	0.0010
epru75b	2.35	1.905	2.408	568	-	35.29	0.9992	0.0010
epru75	2.35	1.905	2.408	-	-	35.86	0.9966	0.0008
epru87b	2.35	2.21	3.687	286	-	36.31	0.9999	0.0007
epru87	2.35	2.21	3.687	-	-	36.61	0.9983	0.0008
nse71sq	4.74	1.26	1.823	-	-	33.74	1.0007	0.0018
nse71w1	4.74	1.26	1.823	-	-	33.98	0.9941	0.0017
nse71w2	4.74	1.26	1.823	-	-	34.38	0.9992	0.0020
p2438ba	2.35	2.032	2.918	-	5.05	36.20	0.9972	0.0009
p2438slg	2.35	2.032	2.918	-	8.39	36.26	0.9960	0.0008

Table B.6.6-34
Benchmark Experiments

(Part 2 of 3)

Experiment ID	U-235 Enrichment in wt%	Fuel Rod Pitch (cm)	H_2O/UO_2 Volume Ratio	Boron Loading (PPM)	Separation Distance (cm)	AEG	k_{eff}	σ
p2438ss	2.35	2.032	2.918	-	6.88	36.24	0.9969	0.0008
p2438zr	2.35	2.032	2.918	-	8.79	36.26	0.9958	0.0007
p2615ba	4.31	2.54	3.883	-	6.72	35.70	0.9973	0.0010
p2615ss	4.31	2.54	3.883	-	8.58	35.73	0.9991	0.0009
p2615zr	4.31	2.54	3.883	-	10.92	35.74	0.9984	0.0015
p2827l1	2.35	2.032	2.918	-	13.72	36.21	1.0014	0.0007
p2827l2	2.35	2.032	2.918	-	11.25	36.27	0.9991	0.0008
p2827l3	4.31	2.54	3.883	-	20.78	35.66	1.0100	0.0009
p2827l4	4.31	2.54	3.883	-	19.04	35.70	1.0075	0.0008
p2827slg	2.35	2.032	2.918	-	8.31	36.28	0.9957	0.0010
p3314ba	4.31	1.892	1.6	-	4.8	33.17	1.0007	0.0009
p3314bc	4.31	1.892	1.6	-	3.53	33.21	1.0004	0.0010
p3314bf1	4.31	1.892	1.6	-	3.6	33.23	1.0027	0.0009
p3314bf2	4.31	1.892	1.6	-	4.94	33.21	1.0024	0.0010
p3314bs1	2.35	1.684	1.6	-	3.86	34.83	0.9952	0.0009
p3314bs2	2.35	1.684	1.6	-	3.46	34.81	0.9936	0.0008
p3314bs3	4.31	1.892	1.6	-	7.23	33.41	0.9979	0.0011
p3314bs4	4.31	1.892	1.6	-	6.63	33.38	0.9996	0.0009
p3314slg	4.31	1.892	1.6	-	10.86	33.99	0.9974	0.0009
p3314ss1	4.31	1.892	1.6	-	3.38	33.95	0.9988	0.0009
p3314ss2	4.31	1.892	1.6	-	11.55	33.75	1.0018	0.0009
p3314ss3	4.31	1.892	1.6	-	4.47	33.88	0.9985	0.0010
p3314ss4	4.31	1.892	1.6	-	8.36	33.75	0.9969	0.0009
p3314ss5	2.35	1.684	1.6	-	7.8	34.93	0.9957	0.0011
p3314ss6	4.31	1.892	1.6	-	10.52	33.52	1.0009	0.0009
p3314w1	4.31	1.892	1.6	-	-	34.37	1.0010	0.0009
p3314w2	2.35	1.684	1.6	-	-	35.20	0.9974	0.0008
p3314zr	4.31	1.892	1.6	-	2.83	33.95	1.0003	0.0018
p3602bb	4.31	1.892	1.6	-	8.3	33.29	1.0030	0.0009
p3602bs1	2.35	1.684	1.6	-	4.8	34.75	1.0003	0.0008
p3602bs2	4.31	1.892	1.6	-	9.83	33.32	1.0035	0.0011
p3602n11	2.35	1.684	1.6	-	8.98	34.73	1.0029	0.0010
p3602n12	2.35	1.684	1.6	-	9.58	34.81	1.0039	0.0009
p3602n13	2.35	1.684	1.6	-	9.66	34.92	1.0006	0.0009
p3602n14	2.35	1.684	1.6	-	8.54	35.01	0.9987	0.0009
p3602n21	2.35	2.032	2.918	-	10.36	36.25	0.9997	0.0009
p3602n22	2.35	1.892	2.918	-	11.2	36.18	1.0016	0.0009
p3602n31	4.31	1.892	1.6	-	14.87	33.19	1.0083	0.0010
p3602n32	4.31	1.892	1.6	-	15.74	33.29	1.0069	0.0009
p3602n33	4.31	1.892	1.6	-	15.87	33.39	1.0064	0.0010
p3602n34	4.31	1.892	1.6	-	15.84	33.45	1.0045	0.0010

Table B.6.6-34
Benchmark Experiments

(Part 3 of 3)

Experiment ID	U-235 Enrichment in wt%	Fuel Rod Pitch (cm)	H_2O/UO_2 Volume Ratio	Boron Loading (PPM)	Separation Distance (cm)	AEG	k_{eff}	σ
	4.31	1.892	1.6	-	15.45	33.50	1.0049	0.0009
p3602n36	4.31	2.54	1.6	-	13.82	33.57	1.0021	0.0009
p3602n41	4.31	2.54	3.883	-	12.89	35.49	1.0126	0.0009
p3602n42	4.31	2.54	3.883	-	14.12	35.65	1.0098	0.0008
p3602n43	4.31	1.684	3.883	-	12.44	35.73	1.0038	0.0008
p3602ss1	2.35	1.684	1.6	-	8.28	34.85	1.0028	0.0013
p3602ss2	4.31	1.684	1.6	-	13.75	33.39	1.0039	0.0010
p3926l1	2.35	1.684	1.6	-	10.06	34.83	1.0003	0.0008
p3926l2	2.35	1.684	1.6	-	10.11	34.92	1.0000	0.0007
p3926l3	2.35	1.684	1.6	-	8.5	35.04	0.9977	0.0008
p3926l4	4.31	1.892	1.6	-	17.74	33.31	1.0069	0.0009
p3926l5	4.31	1.892	1.6	-	18.18	33.39	1.0058	0.0009
p3926l6	4.31	1.892	1.6	-	17.43	33.49	1.0024	0.0009
p3926sl1	2.35	1.684	1.6	-	6.59	35.05	0.9945	0.0008
p3926sl2	4.31	1.892	1.6	-	12.97	33.56	1.0000	0.0009
p4267b1	4.31	1.89	1.59	2150	-	31.78	0.9969	0.0008
p4267b2	4.31	1.89	1.59	2550	-	31.52	1.0022	0.0010
p4267b3	4.31	1.715	1.09	1030	-	30.99	1.0042	0.0009
p4267b4	4.31	1.715	1.09	1820	-	30.50	0.9987	0.0009
p4267b5	4.31	1.715	1.09	2550	-	30.09	1.0005	0.0008
p4267sl1	4.31	1.89	1.59	-	-	33.45	1.0010	0.0010
p4267sl2	4.31	1.715	1.09	-	-	31.94	0.9989	0.0009
p62ft231	4.31	1.891	1.6	-	5.67	32.89	1.0026	0.0009
p71f14f3	4.31	1.891	1.6	-	5.19	32.79	1.0002	0.0009
p71f14v3	4.31	1.891	1.6	-	5.19	32.86	0.9988	0.0009
p71f14v5	4.31	1.891	1.6	-	5.19	32.84	0.9989	0.0009
p71f214r	4.31	1.891	1.6	-	5.19	32.87	0.9975	0.0009
pat80l1	4.74	1.6	3.807	-	2	35.00	1.0015	0.0019
pat80l2	4.74	1.6	3.807	-	2	35.08	0.9968	0.0018
pat80ss1	4.74	1.6	3.807	-	2	34.99	1.0000	0.0016
pat80ss2	4.74	1.6	3.807	-	2	35.06	0.9961	0.0019
w3269a	5.7	1.422	1.93	-	-	33.13	0.9966	0.0017
w3269c	3.7	1.105	1.432	-	-	33.75	0.9964	0.0016
w3269sl1	3.7	1.105	1.432	-	-	33.35	0.9953	0.0016
w3269sl2	5.7	1.422	1.932	-	-	33.08	1.0038	0.0009
w3269w1	2.72	1.524	1.494	-	-	33.48	0.9951	0.0018
w3269w2	5.7	1.422	1.932	-	-	33.17	1.0010	0.0010
w3385sl1	5.74	1.422	1.933	-	-	33.23	0.9965	0.0010
w3385sl2	5.74	2.011	5.067	-	-	35.89	1.0019	0.0009
Correlation	**0.37**	**0.42**	**0.17**	**0.12**	**0.69**	**-0.04**		

Table B.6.6-35
USL Functions

Parameter	Applicable Range	USL Function	
Boron Loading (PPM)	[15, 3389]	0.9430+ 3.7407E-07*X	
Separation Distance (cm)	[0.18973, 20.78]	0.9402 + 5.5740E-04*X	X < 7.6786
		0.9445	X >= 7.6786
AEG	[29.91, 36.61]	0.9464 - 9.6498E-05*X	X > 30.882
		0.9434	X <= 30.882
U-235 Enrichment (wt. %)	[2.3500, 5.7400]	0.9391 + 1.2693E-03*X	X < 3.7304
		0.9439	X >= 3.7304
H_2O/UO_2 Volume Ratio	[0.3830, 5.0670]	0.9416 + 7.3841E-04*X	X < 2.4039
		0.9433	X >= 2.4039
Pitch (cm)	[1.1050 , 2.5400]	0.9343 + 5.2322E-03*X	X < 1.8386
		0.9440	X >= 1.8386

Table B.6.6-36
USL Evaluations

	Intact Fuel		Damaged Fuel	
Parameter	**Value From Limiting Analysis**	**Bounding USL**	**Value From Limiting Analysis**	**Bounding USL**
Boron Loading (PPM)	2600	0.9440	2600	0.9440
AEG	31.7	0.9433	31.60	0.9434
Separation Distance (cm)	2.217	0.9414	1.902	0.9413
U-235 Enrichment (wt. %)	4.75	0.9439	4.45	0.9440
H_2O/UO_2 Volume Ratio	1.731	0.9429	1.731	0.9429
Pitch (cm)	**1.2852**	**0.9410**	**1.2852**	**0.9410**

Proprietary information withheld pursuant to 10 CFR 2.390

Figure B.6.6-1
NUHOMS® 32PTH2 DSC Cross Section

Proprietary information withheld pursuant to 10 CFR 2.390

Figure B.6.6-2
Basket Views and Dimensions

Proprietary information withheld pursuant to 10 CFR 2.390

Figure B.6.6-3
Basket Model Compartment Wall (View G)
(Not to Scale)

Periodic Boundary at the Top of Model

Proprietary information withheld pursuant to 10 CFR 2.390

Figure B.6.6-4
Basket Model Compartment Wall (View F)

(Not to Scale)

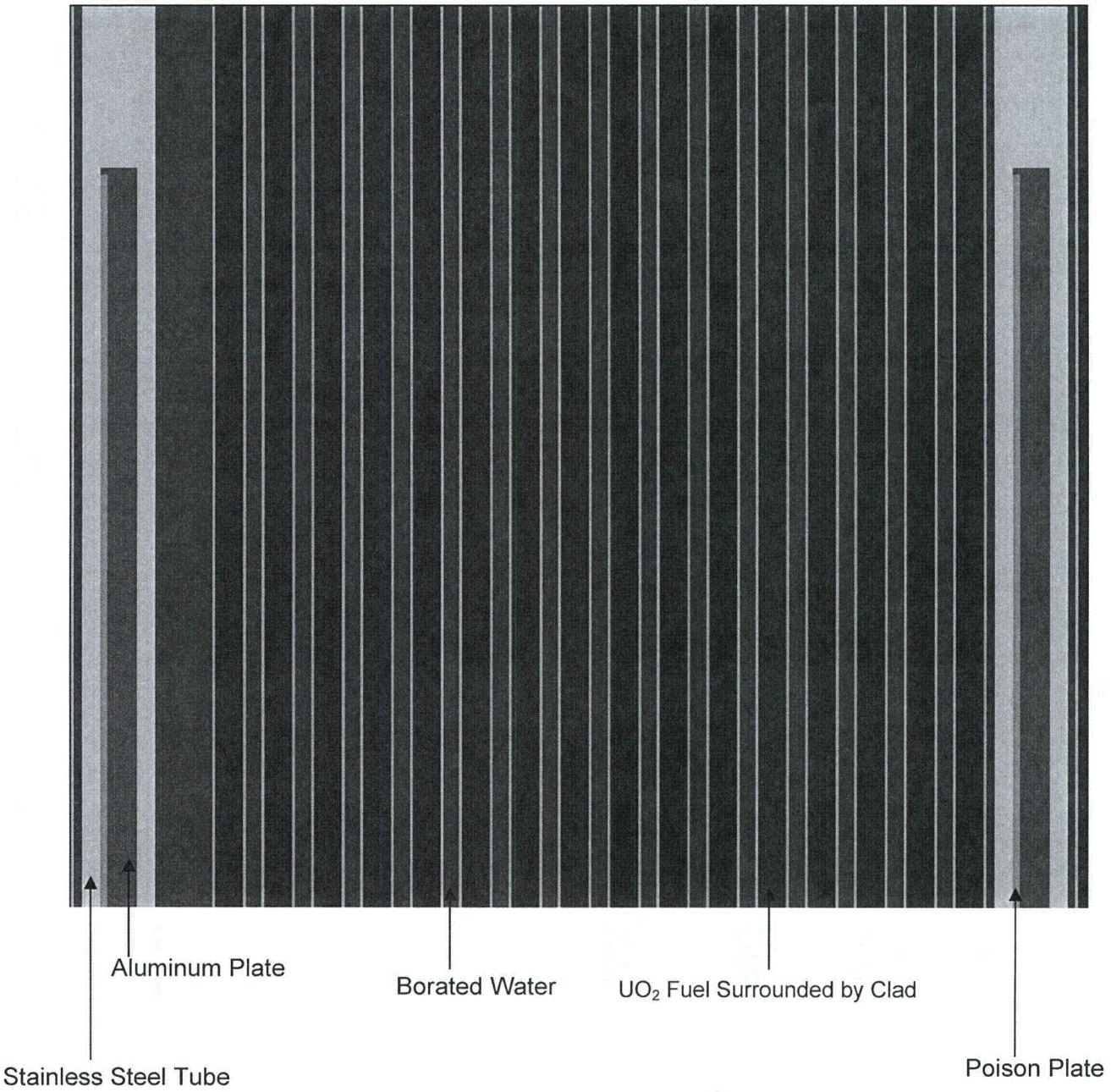

Figure B.6.6-5
Basket Model Compartment Wall with Fuel Assembly (View G)
(Not to Scale)

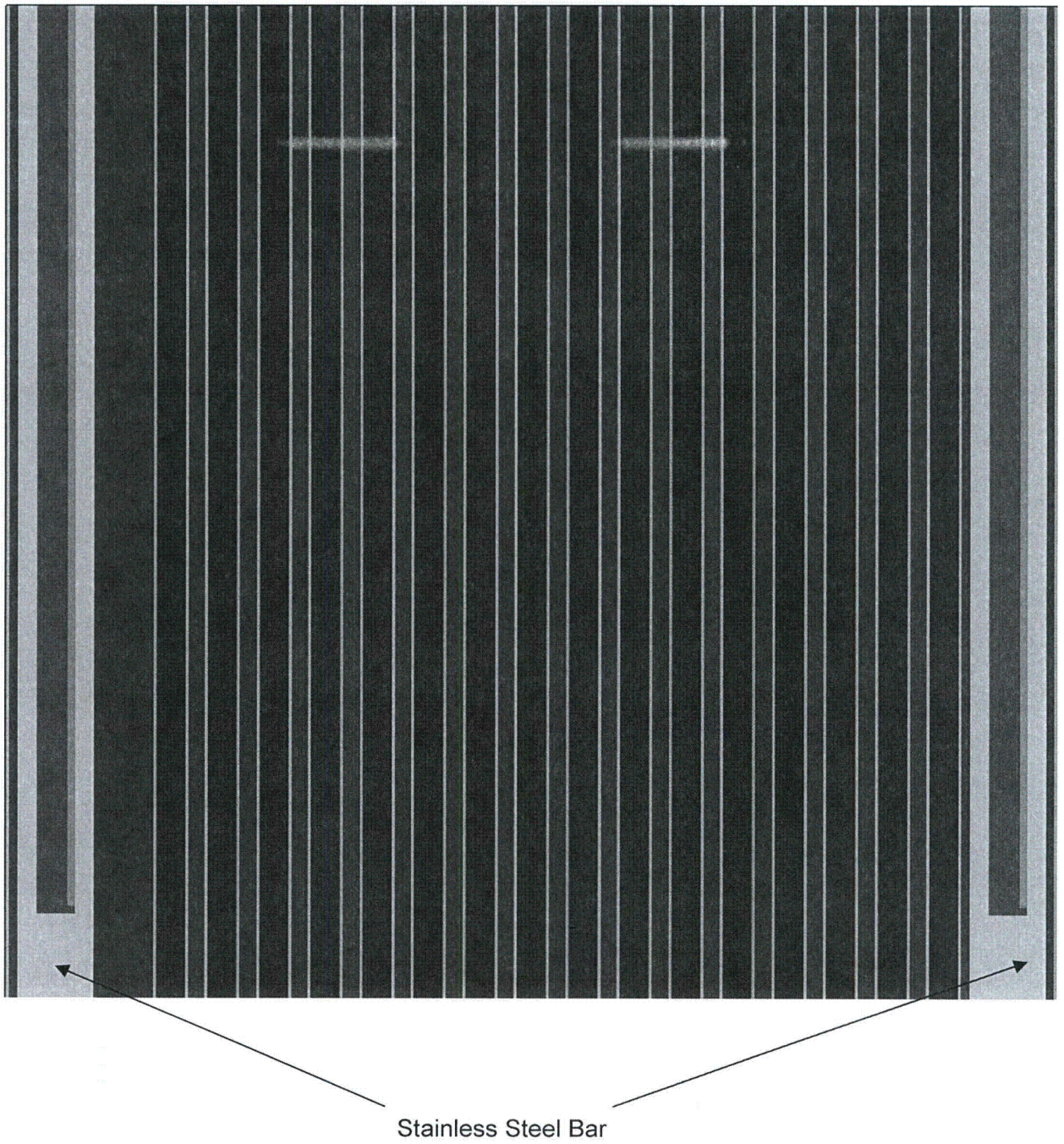

Figure B.6.6-6
Basket Model Compartment Wall with Fuel Assembly (View F)
(Not to Scale)

Proprietary information withheld pursuant to 10 CFR 2.390

Figure B.6.6-7
Basket Compartment with CE 16x16 Fuel Assembly

(Not to Scale)

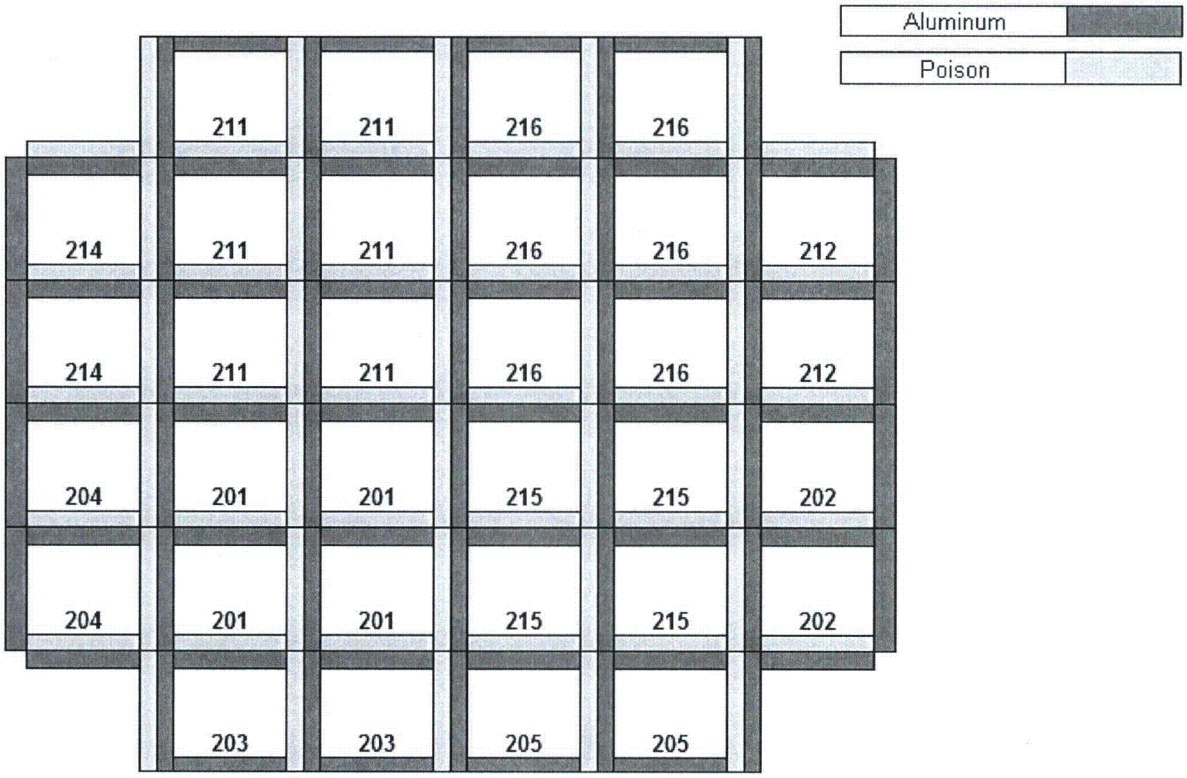

Figure B.6.6-8
Fuel Position and Poison Plate Location in the 32PTH2 DSC Design
(Not to Scale)

Proprietary information withheld pursuant to 10 CFR 2.390

Figure B.6.6-9
Canister and Transfer Cask Description in the KENO Model
(Not to Scale)

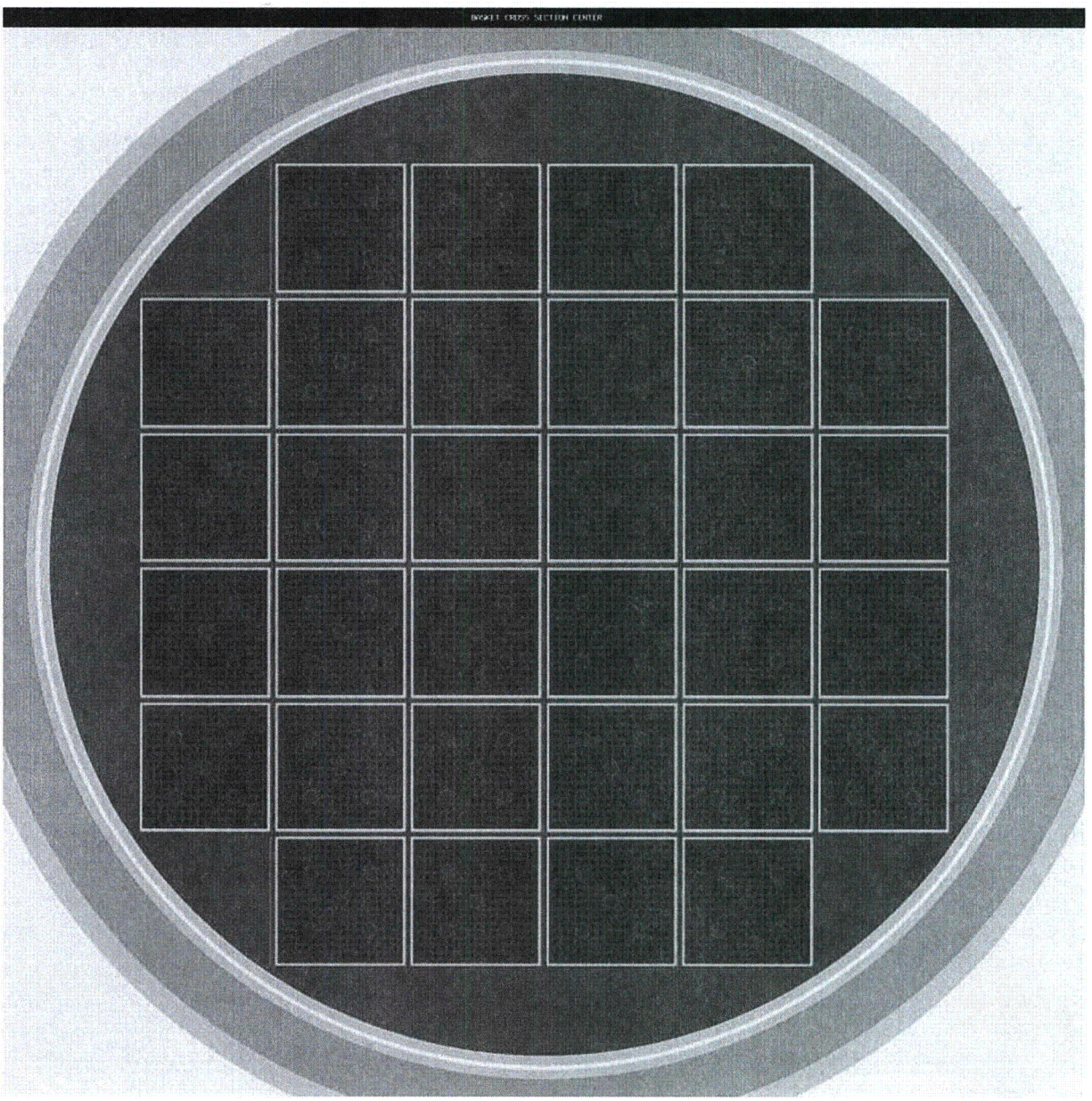

Figure B.6.6-10
CE 16x16 Class Assembly KENO Model

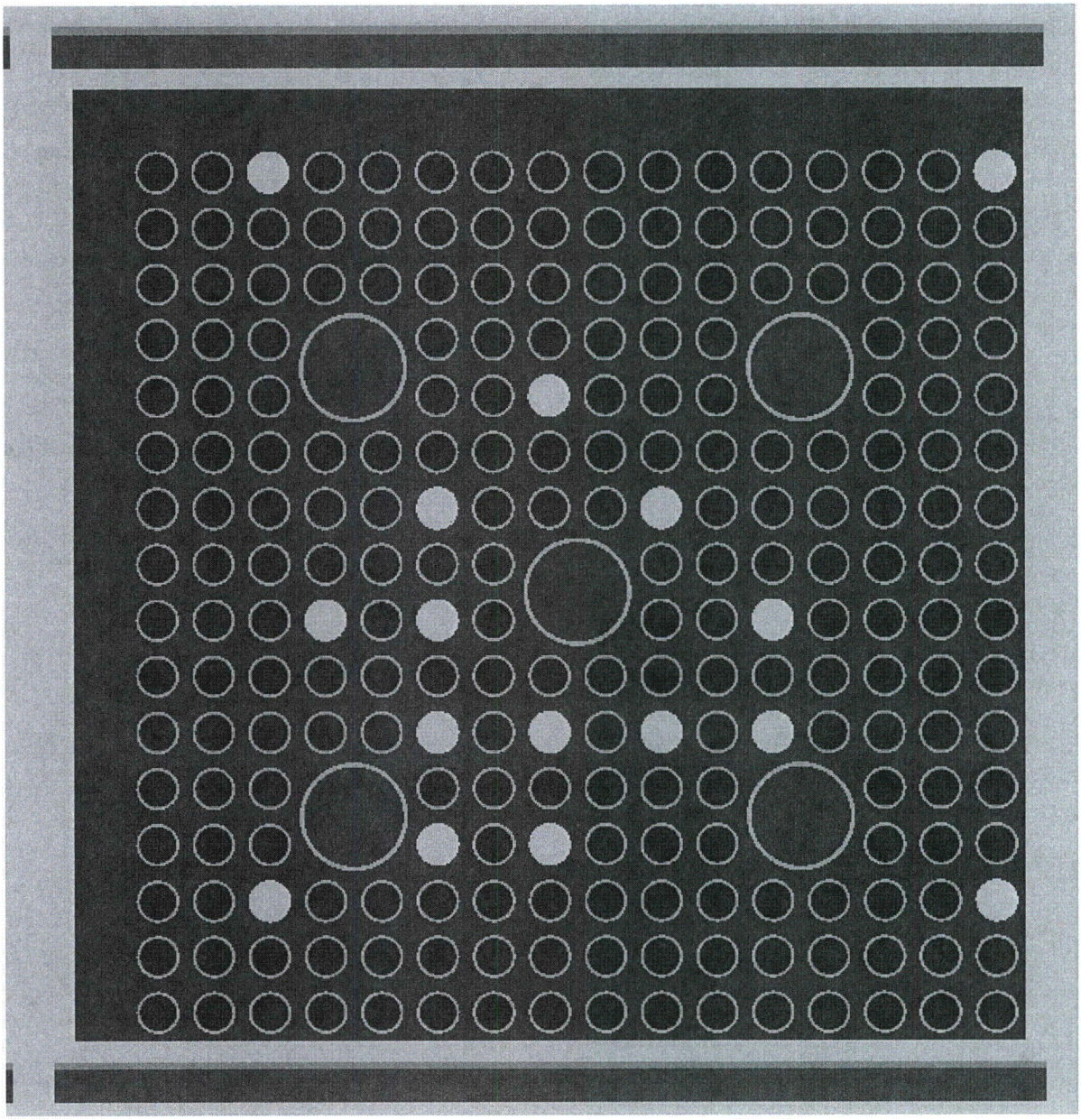

Figure B.6.6-11
Example of Reconstituted Fuel Rod Locations, 16 shown

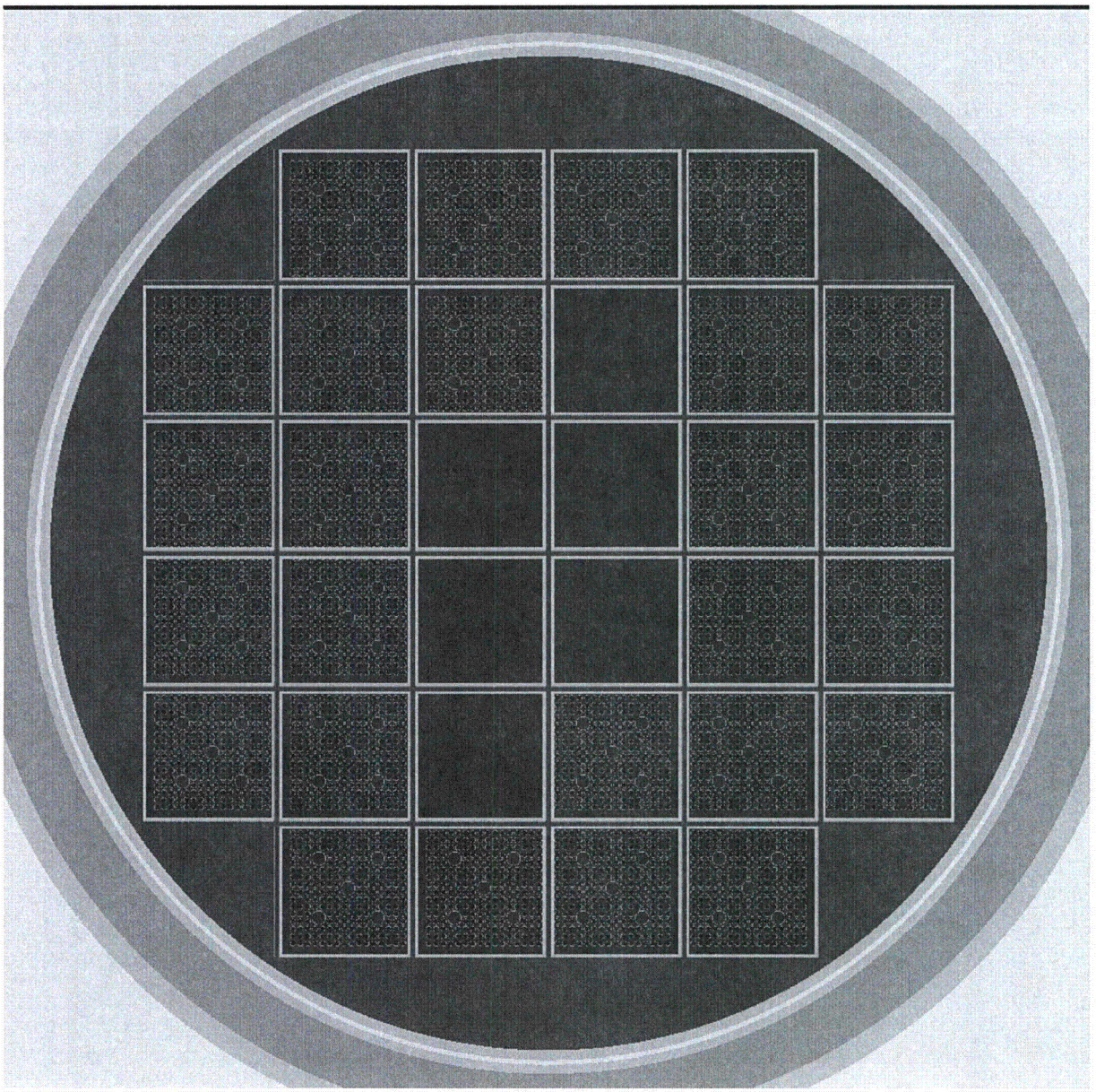

Figure B.6.6-12
Example of Empty Fuel Compartment Location, 6 shown

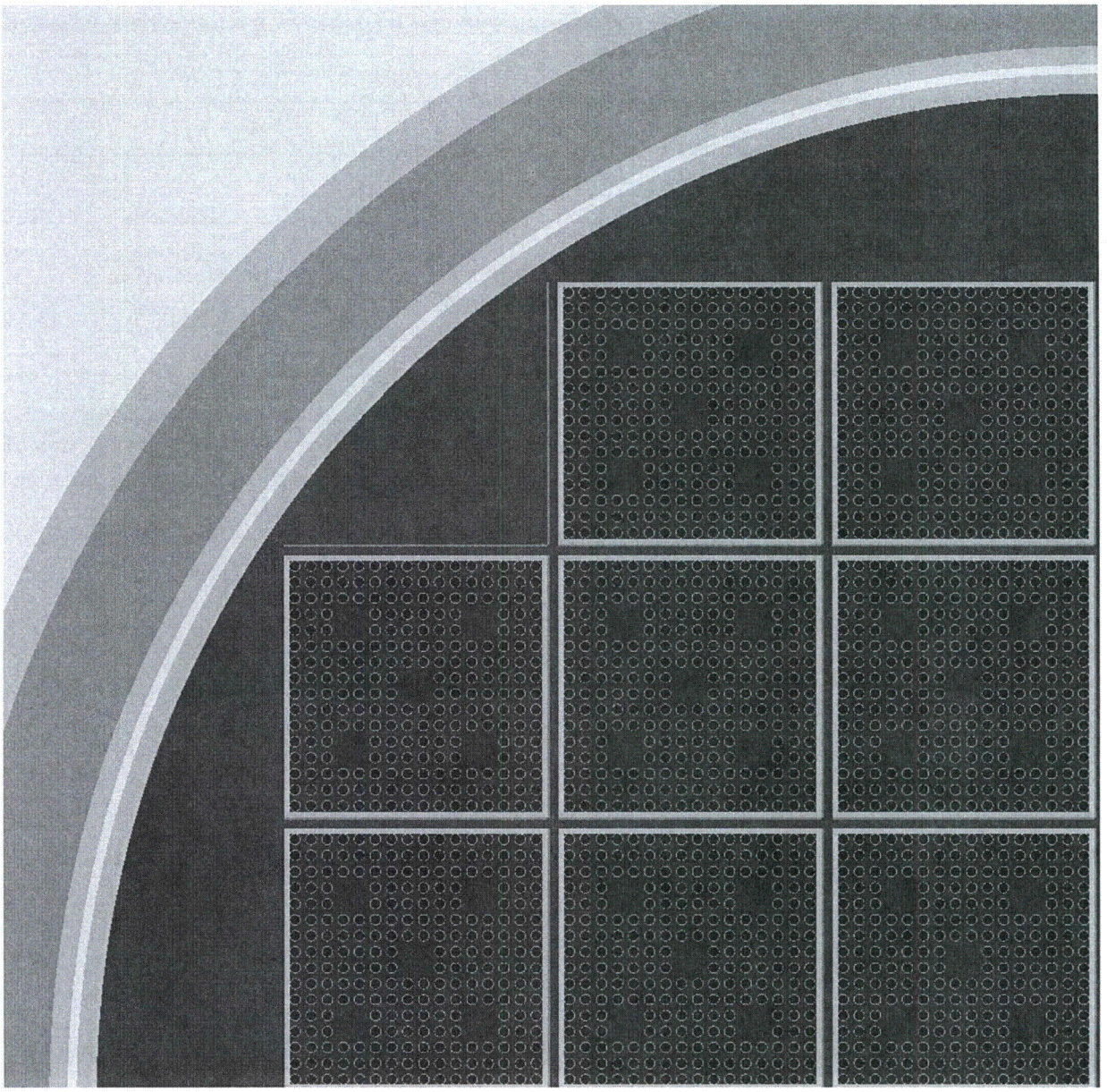

Figure B.6.6-13
Optimum Pitch KENO Model without CCs

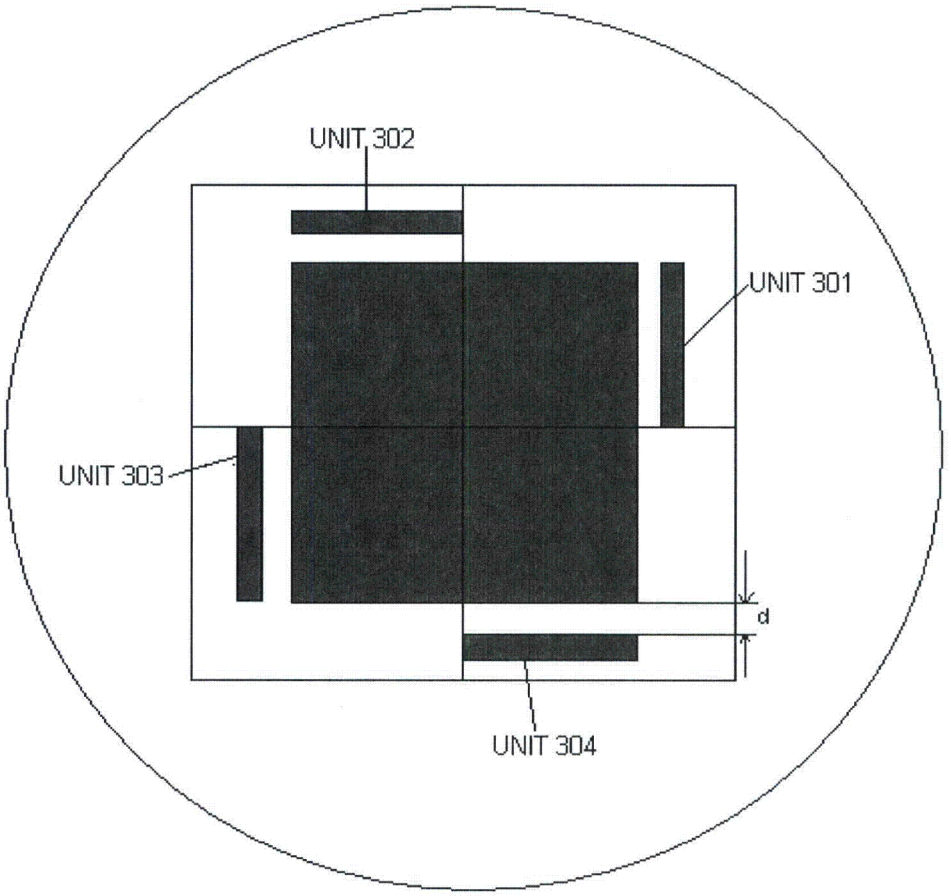

Notes:

(1) The separation distance "d" applies to all the UNITS.

(2) The figure is not to scale.

Figure B.6.6-14
Illustration of Displacement of Single and Double Sheared Rods

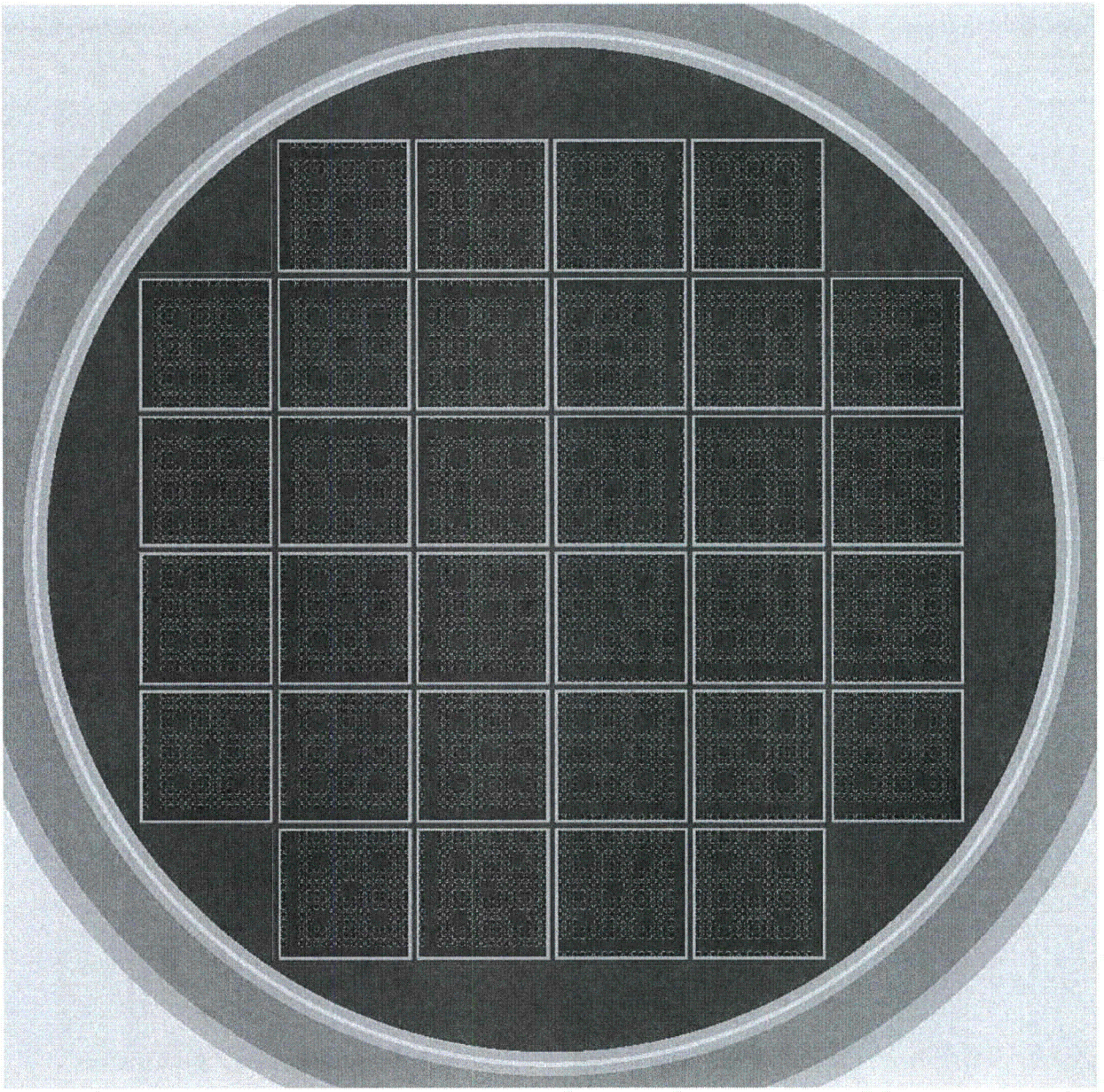

Figure B.6.6-15
Single Shear KENO Model – Maximum Displacement

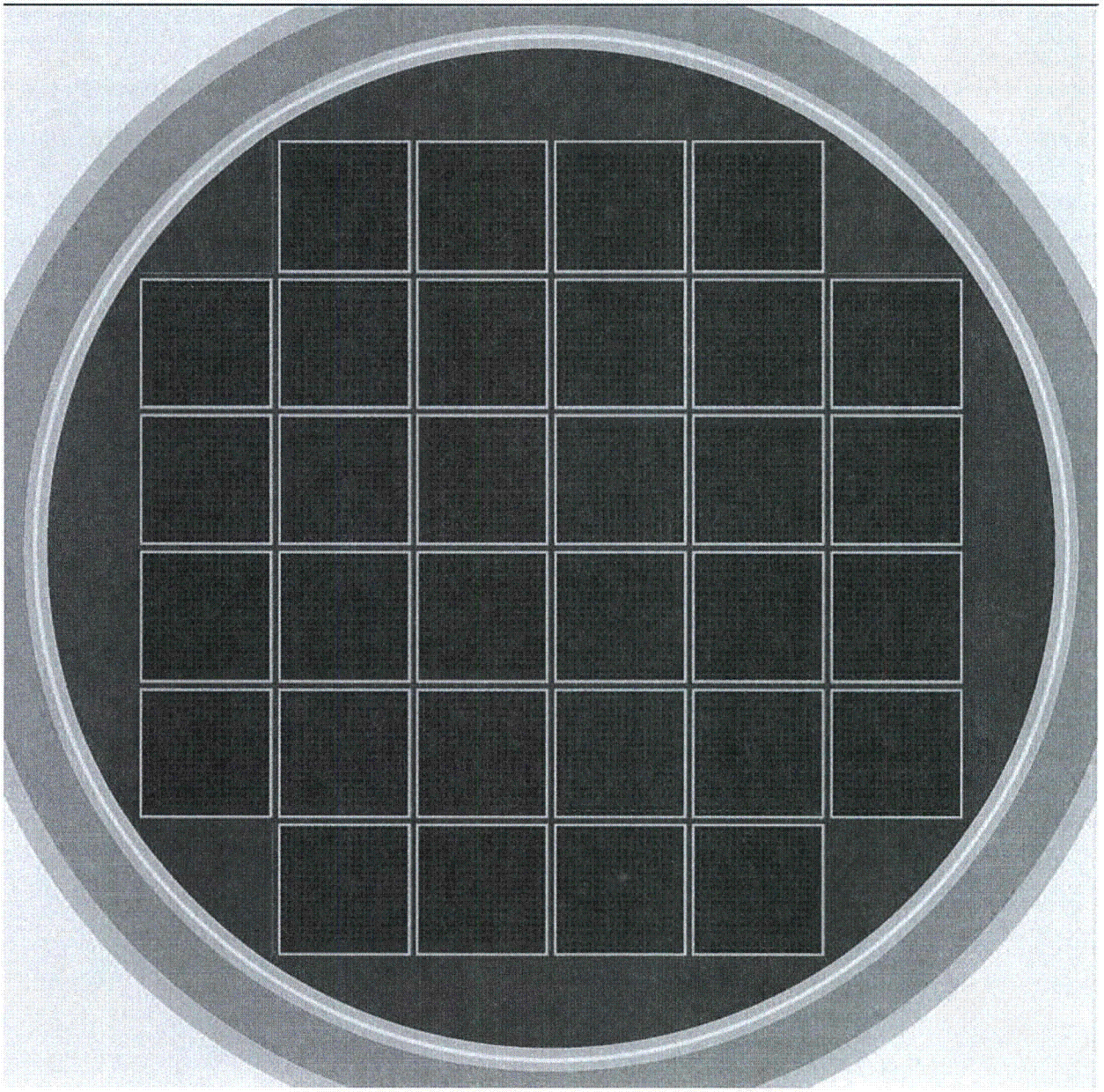

Figure B.6.6-16
Double Shear KENO Model – Maximum Displacement

Proprietary information withheld pursuant to 10 CFR 2.390

Figure B.6.6-17
Guide Tube KENO Modeling

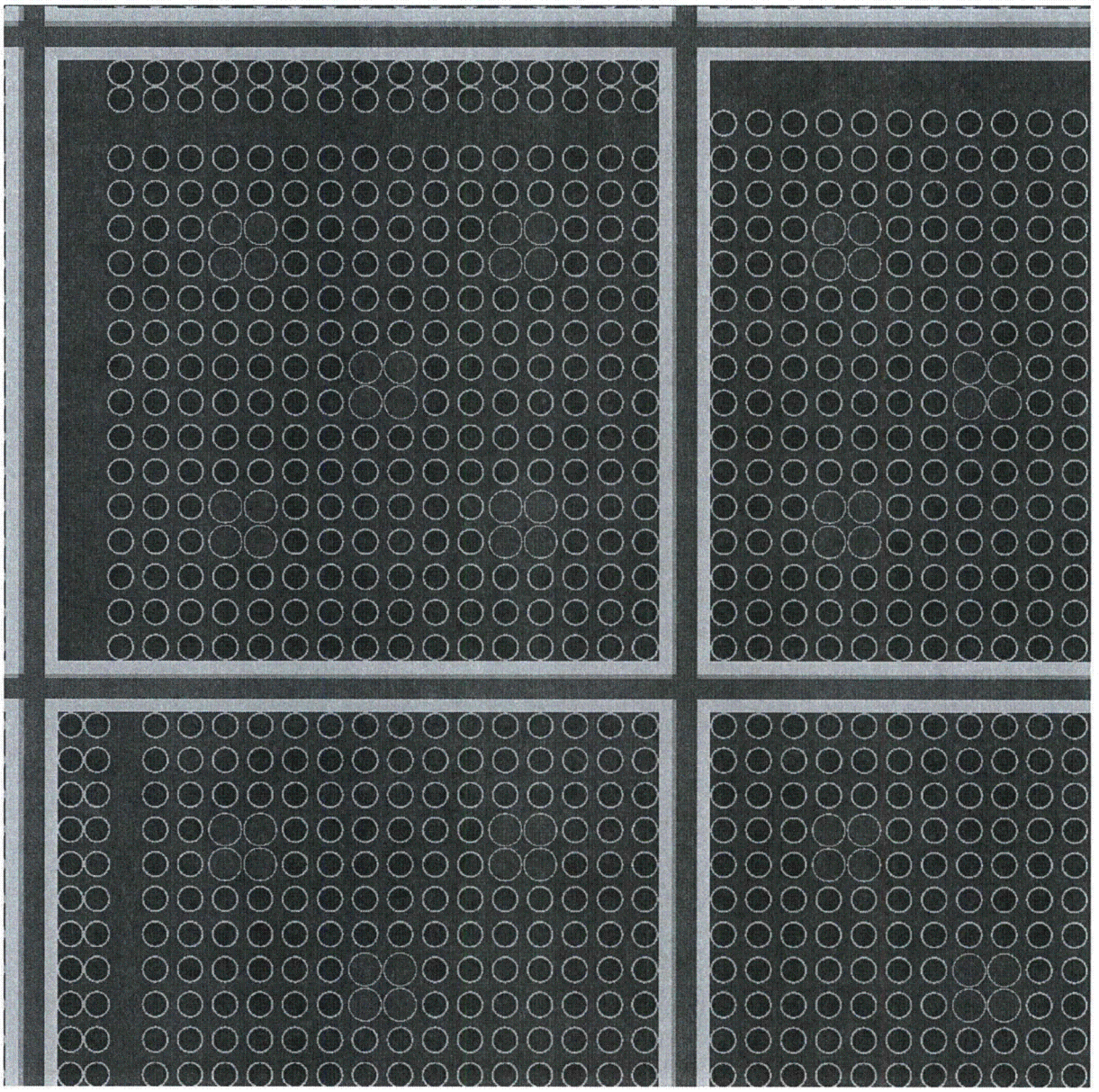

Figure B.6.6-18
Four Cylinder Guide Tube - KENO Model

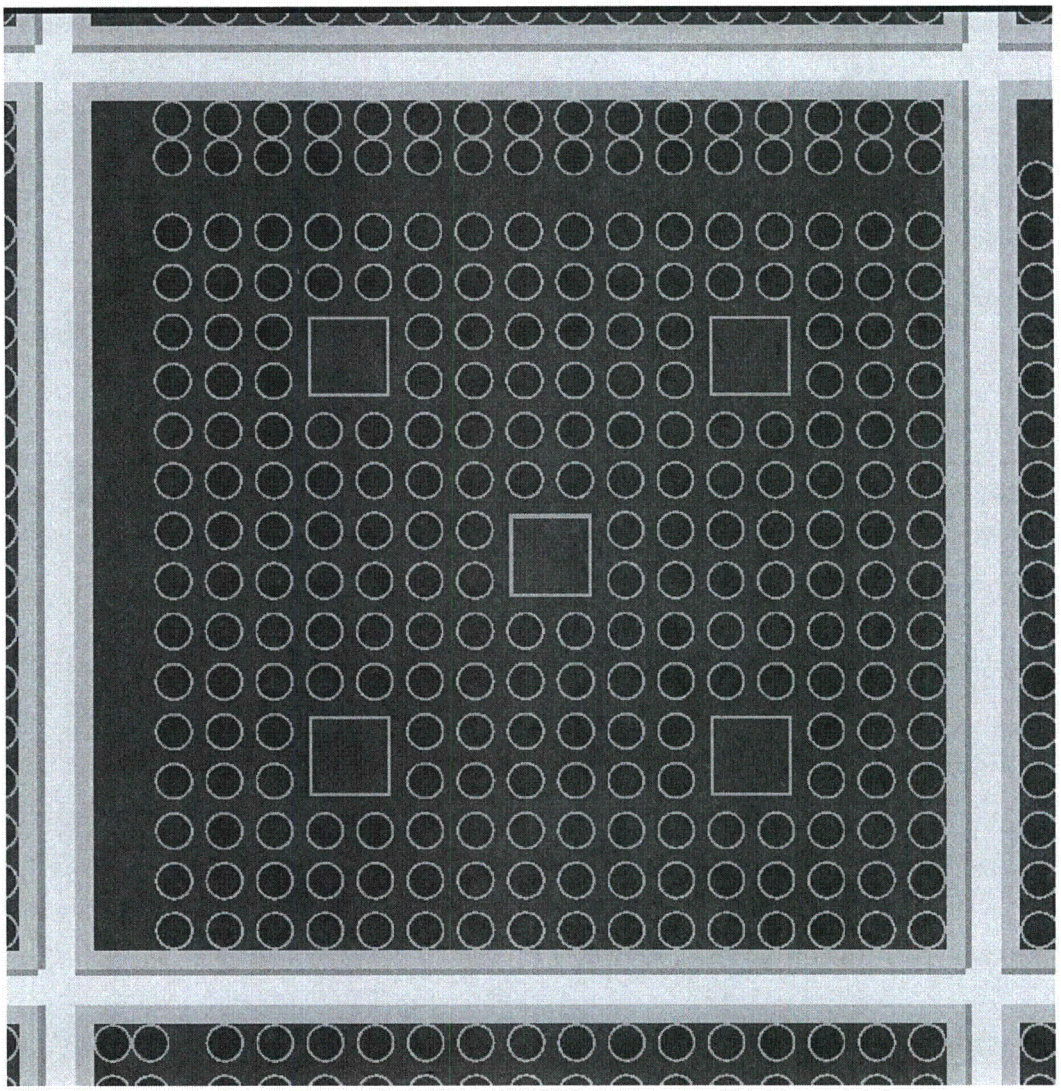

Figure B.6.6-19
Square Guide Tube – KENO Model

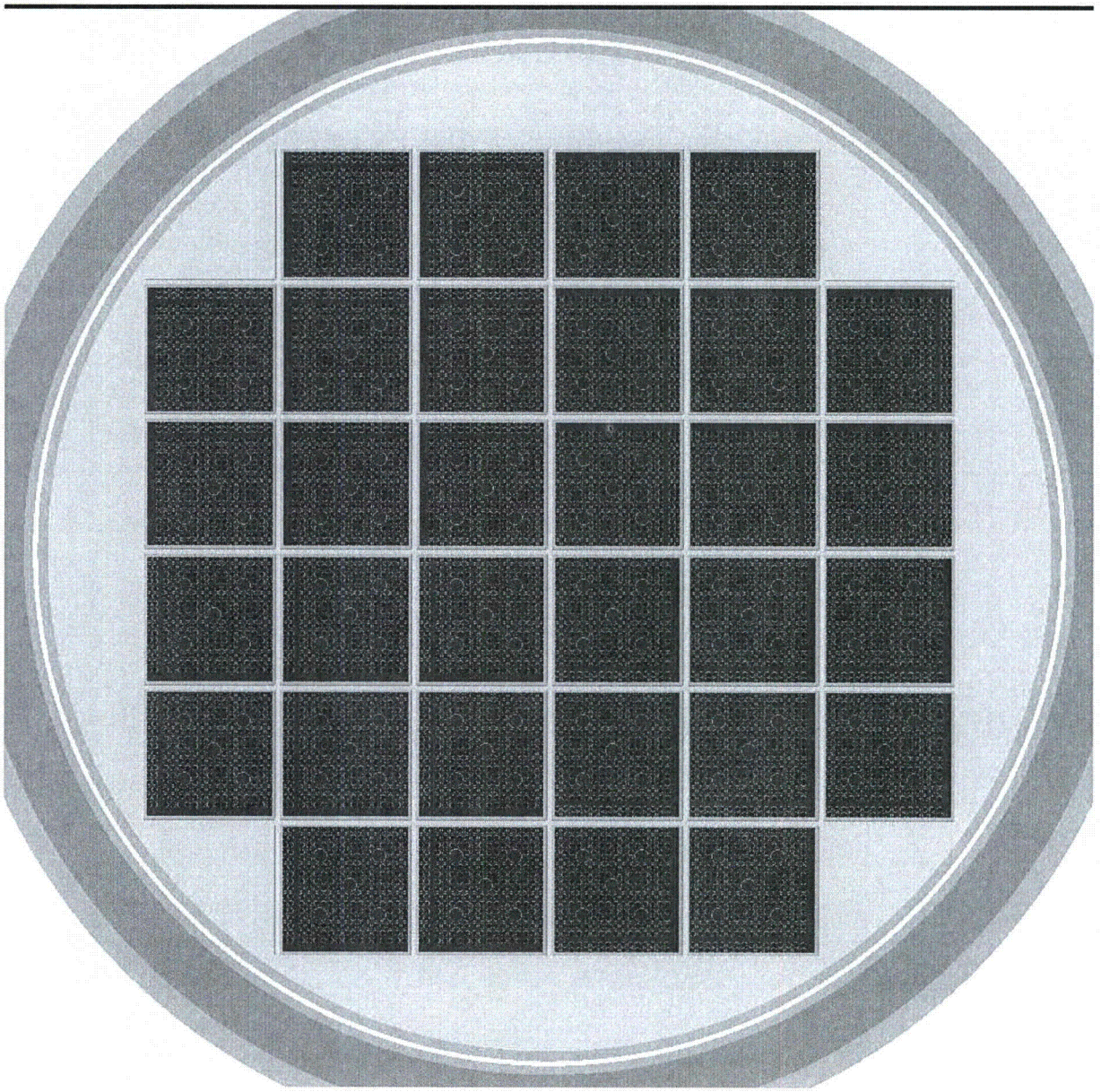

Figure B.6.6-20
Design Basis Damaged Fuel KENO Model

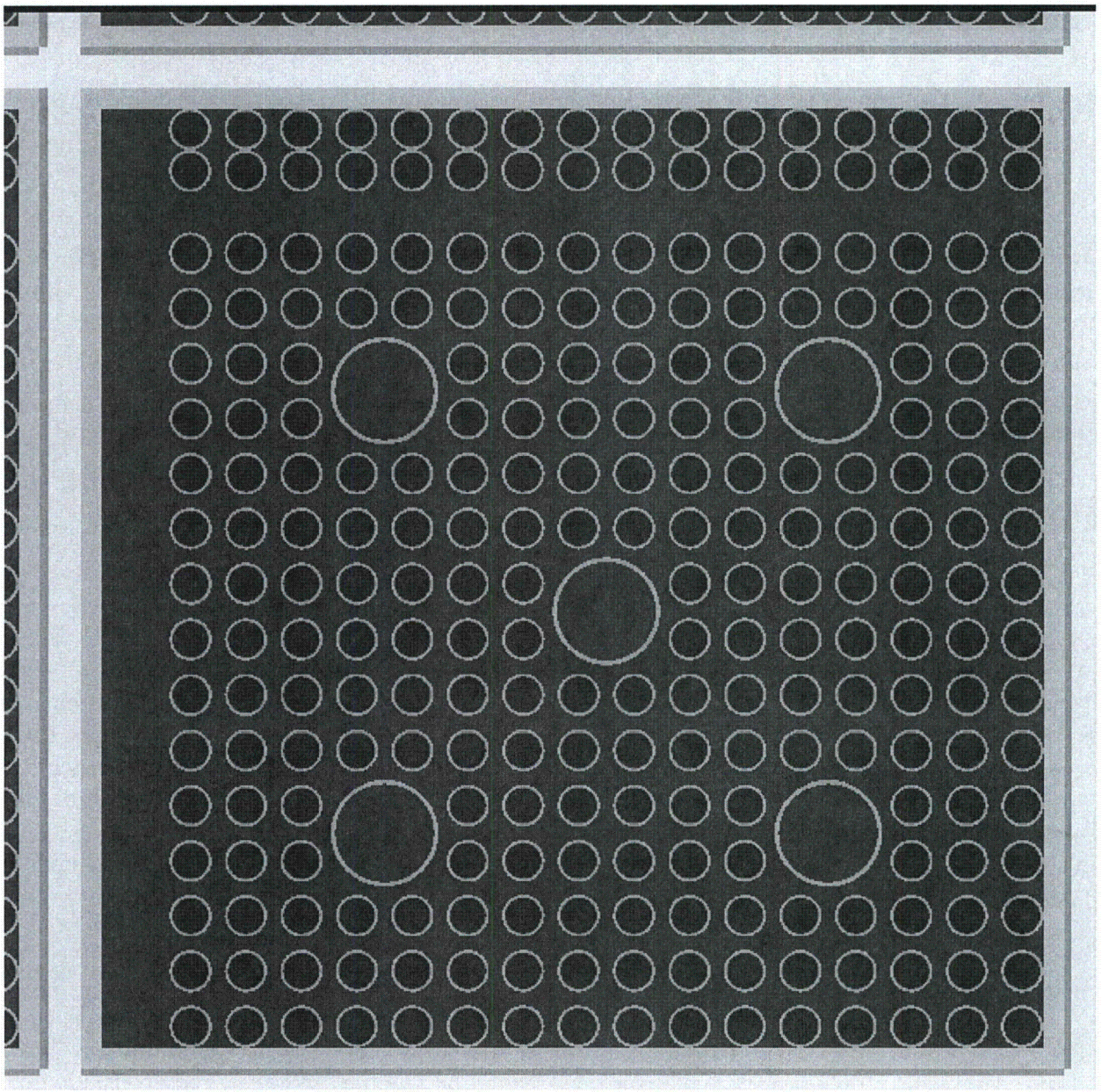

Figure B.6.6-21
Design Basis Damaged Fuel KENO Model – Fuel Compartment View

B.10 RADIATION PROTECTION

B.10.1 Ensuring that Occupational Radiation Exposures Are as Low as Reasonably Achievable (ALARA)

To ensure that occupational radiation exposures are ALARA for the NUHOMS® 32PTH2 system, two primary factors were considered: (1) minimizing occupational exposure during 32PTH2 DSC loading and transfer, and (2) minimizing storage dose rates when the 32PTH2 DSC is stored in the AHSM-HS at the ISFSI. Occupational exposure is minimized by shielding design of the 32PTH2 DSC and the OS200FC TC as well as procedures associated with loading and transfer. Storage dose rates are minimized by thick concrete shielding present in the AHSM-HS roof, use of self-shielding by placing AHSM-HSs directly adjacent to one another, and by facing the lowest dose rate side of the AHSM-HS arrays toward the limiting boundary of the facility, where possible.

B.10.1.1 Policy Considerations

The 32PTH2 DSC, OS200FC TC, and AHSM-HS design incorporates various methods of shielding and design features to minimize occupational radiation exposures. The licensee's existing radiation safety and ALARA policies for the plant should be applied to the ISFSI. The ALARA program should follow the general guidelines of Regulatory Guides 1.8 [B10.4], 8.8 [B10.1], 8.10 [B10.3] and 10 CFR Part 20 [B10.6]. ISFSI personnel should be trained in the proper operation of the NUHOMS® 32PTH2 system and updated on ALARA practices and dose reduction techniques. This training includes operations, inspections, repair, and maintenance. Proper training of personnel helps to minimize exposure to radiation such that the total individual and collective exposure to personnel in all phases of operation and maintenance are kept ALARA. Implementation of ISFSI systems and equipment procedures should be reviewed by the licensee to ensure exposures are ALARA during all phases of operations, maintenance and surveillance.

B.10.1.2 Design Considerations

The NUHOMS® 32PTH2 system takes into account radiation protection considerations, which ensure that occupational radiation exposures are ALARA. The fuel will be stored dry inside the sealed, heavily shielded 32PTH2 DSC and AHSM-HS. Shield plugs at the ends of the 32PTH2 DSC provide shielding for welding operations and during onsite 32PTH2 DSC transfer. OS200FC TC lead shielding and neutron shielding provide required shielding during transfer activities. The AHSM-HS walls, roof and shield walls provide shielding during storage. The 32PTH2 DSC will not be opened nor fuel removed while at the ISFSI, unless the ISFSI is specifically licensed for these purposes. Storage of the fuel in the dry, leak-tight 32PTH2 DSC eliminates the possibility of leakage of contaminated liquids, particulate materials, or radioactive gases. The exterior of the OS200FC TC is decontaminated prior to transfer to the ISFSI, thereby minimizing exposure of personnel to surface contamination. The 32PTH2 DSC outside surface is also contamination free (clean surface) due to the use of inflatable seals in the annulus between the OS200FC TC and 32PTH2 DSC during loading operations. The NUHOMS® 32PTH2 system contains no active components which require periodic maintenance or surveillance thereby

minimizing potential personnel dose due to maintenance activities. This method of spent fuel storage minimizes radiation exposure and eliminates the potential for personnel contamination. The NUHOMS® design configuration has been demonstrated to provide appropriate design features for reduction of doses and for facilitating decontamination in similar systems. Regulatory Position 2 of Regulatory Guide 8.8 [B10.1] is incorporated into the design considerations, as described below:

- Regulatory Position 2a on access control is met by use of a fence with a locked gate that surrounds the ISFSI and prevents unauthorized access.

- Regulatory Position 2b on radiation shielding is met by the heavy shielding attributes of the NUHOMS® 32PTH2 system which minimizes personnel exposures.

- Regulatory Position 2c on process instrumentation and controls is met by designing the instrumentation for a long service life and locating readouts in a low dose rate location. The use of thermocouples for temperature measurements located in embedded thermowells provides reliable, easily maintainable instrumentation for this monitoring function.

- Regulatory Position 2d on control of airborne contaminants may be applicable for vacuum drying operations of 32PTH2 DSCs containing damaged fuel. Monitoring of the vacuum drying system discharge and diversion to the gaseous radwaste system or other appropriate filtration systems will be implemented. No significant surface contamination is expected because the exterior of the OS200FC TC is decontaminated prior to transfer to the ISFSI and the exterior of the 32PTH2 DSC is also contamination free.

- Regulatory Position 2e on crud control is not applicable to the ISFSI because there are no systems at the ISFSI that could transport crud. The leak-tight 32PTH2 DSC design ensures that spent fuel crud will not be released or transferred from the 32PTH2 DSC.

- Regulatory Position 2f on decontamination is met because the OS200FC TC is decontaminated prior to transfer to the ISFSI. The OS200FC TC accessible surfaces are designed to facilitate decontamination.

- Regulatory Position 2g on radiation monitoring does not apply since no leakage of radioactive material is possible. There is no need for airborne radioactivity monitoring because the 32PTH2 DSCs are sealed and leak-tight. Airborne radioactivity due to damaged fuel is discussed under Regulatory Position 2d above. Area radiation monitors are not required because the ISFSI will not be occupied on a regular basis.

- Regulatory Position 2h on resin and sludge treatment systems is not applicable to the ISFSI because there are no radioactive systems containing resins or sludge associated with the ISFSI.

- Regulatory Position 2i concerning other miscellaneous ALARA items is not applicable because these items refer to radioactive systems not present at the ISFSI.

B.10.1.3 Operational Considerations

The operational requirements are incorporated into the radiation protection design features described in Section B.10.2 since the NUHOMS® 32PTH2 system is heavily shielded to minimize occupational exposure.

The 32PTH2 DSCs contain no radioactive liquids and, for intact fuel assemblies, are not expected to contain any radioactive gases. Additionally, the 32PTH2 DSC is designed to be leak-tight.

The NUHOMS® 32PTH2 system is designed to be essentially maintenance free. It is a passive system without any moving parts.

The only anticipated maintenance procedures are the visual inspection of the bird screens on the AHSM-HS ventilation inlet and outlet openings, and periodic maintenance of the thermocouples. Maintenance operations on the OS200FC TC, transfer equipment and other auxiliary equipment are performed in a low dose environment during periods when fuel movement is not occurring. Maintenance activities that could involve significant radiation exposure of personnel should be carefully planned.

The ISFSI contains no systems that process liquids or gases or contain, collect, store, or transport radioactive liquids or solids other than payloads identified in Chapter B.2. Therefore, the ISFSI meets ALARA requirements since there are no systems to be maintained or repaired other than those systems previously discussed.

B.10.2 Radiation Protection Design Features

B.10.2.1 NUHOMS® 32PTH2 System Design Features

The NUHOMS® 32PTH2 system has design features which ensure a high degree of integrity for the confinement of radioactive materials and reduction of direct radiation exposures to ALARA. These features are described below.

- The 32PTH2 DSCs are loaded, sealed, and leak-tested prior to transfer to the ISFSI.
- The fuel will not be unloaded nor will the 32PTH2 DSCs be opened at the ISFSI unless the ISFSI is specifically licensed for these purposes.
- The fuel is stored in a dry inert environment inside the 32PTH2 DSCs so that no radioactive liquid is available for leakage.
- The 32PTH2 DSCs are sealed and tested leak-tight with a helium atmosphere to prevent oxidation of the fuel. The leak-tight design features are described in Chapter B.7.
- The 32PTH2 DSCs are heavily shielded on both ends to reduce external dose rates. The shielding design features are discussed in Chapter B.5.
- No radioactive material will be discharged during storage since the 32PTH2 DSC is designed, fabricated and tested to be leak-tight.

Geometric attenuation, enhanced by air and ground dispersion, provides additional shielding for distant locations at restricted area and site boundaries. However, the contribution of the skyshine dose rate must be considered for distant locations. The total dose rate estimation, including skyshine, is provided in this chapter.

Proprietary information withheld pursuant to 10 CFR 2.390

B.10.2.2 Assumptions

Dose rates calculated in the immediate vicinity of the AHSM-HS loaded with a NUHOMS® 32PTH2 DSC are presented in Chapter B.5, which provides a detailed description of source term configuration, shielding analysis models, and expected dose rates. Dose rates for longer distances (off-site dose rates) are presented in this section for the design basis fuel load.

The Monte-Carlo computer code MCNP5, version 1.4 (MCNP), reference [B10.2], is used to calculate the dose rates at the required locations around the AHSM-HS arrays.

The assumptions used to generate the geometry of the AHSM-HS and shield walls for the MCNP runs are summarized below.

- Two different configurations are analyzed: a 2x10 back-to-back array of AHSM-HSs and two 1x10 front-to-front arrays of AHSM-HSs. Figure B.10.2-1 and Figure B.10.2-2 provide a sketch of the general configurations, respectively.

- The AHSM-HS arrays are modeled as a box enveloping the AHSM-HSs and 3 foot shield walls on the back (for the two 1x10 arrays only) and two sides. Source particles are then started on the surfaces of the box.

- The ISFSI pad is modeled as a concrete pad, approximately 108 feet by 84 feet by 3 feet thick. The remaining volume below ground level is modeled as soil. The dimensions of the pad model have a negligible effect on dose rates, so it is acceptable to use a generic pad size that is representative of a typical ISFSI.

- For the 2x10 array, the AHSM-HS interiors are filled with air. Most particles that enter the AHSM-HS will therefore pass through unhindered.

- For the two 1x10 arrays, the AHSM-HS "source array" interiors are filled with air. The "shield array" is modeled as concrete. This requires that the dose rates be processed, as described in Section B.10.2.4.

- The "universe" is a sphere surrounding the AHSM-HS. The radius of this sphere is more than 10 mean free paths (gamma) greater than that of the outermost detector.

The assumptions used to generate the AHSM-HS surface sources for the MCNP runs are summarized below.

- The AHSM-HS surface sources are generated using the AHSM-HS surface dose rates calculated in Chapter B.5.

- Each AHSM-HS is assumed to be filled with a NUHOMS® 32PTH2 DSC containing 32 design basis fuel assemblies (see Chapter B.5).

The assumptions used for the MCNP computer runs are summarized below.

- The ANSI/ANS-6.1.1-1977 flux-to-dose-rate factors from reference [B10.8] are used in the MCNP calculations. They can also be found in Chapter B.5.

- Source particles are generated on the AHSM-HS surface with initial directions following a cosine distribution. Radiation fluxes outside thick shields such as the AHSM-HS walls and roof tend to have forward peaked angular distributions that are reasonably approximated by a cosine function. Vents through shielding regions such as the AHSM-HS vents tend to collimate particles such that a semi-isotropic assumption is not appropriate. However, the use of a hard spectrum to specify the AHSM-HS surface flux is sufficiently conservative.

- Point detectors are used to calculate all of the dose rates on all sides of the AHSM-HS arrays. All detectors have been placed three feet above ground level.

B.10.2.3 Source Specification

Source information required by MCNP includes gamma and neutron spectra for the AHSM-HS array surfaces, total gamma and neutron activities for each AHSM-HS array face and total gamma and neutron activities for the entire ISFSI. Chapter B.5 provides the AHSM-HS surface dose rates and energy-dependent fluxes for each surface of the AHSM-HS. The spectra and dose rate data are presented in Table B.10.2-1 for gammas and Table B.10.2-2 for neutrons. The flux spectrum is input as the MCNP ERG source variable.

The activity of each surface is determined by multiplying the sum of the group fluxes by the area of the surface and by a conversion factor (0.5) to convert the surface flux to a current. This is required in order to represent the MCNP surface source as a current. The conversion factor is introduced because the current is mathematically half of the flux. This calculation is performed for the roof, sides, back and front of the AHSM-HS. The sum of the surface activities is then input as the tally multiplier for each of the MCNP tallies to scale the results by the total number of particles in the problem.

B.10.2.3.1 2x10 Back-to-Back Array

A box that envelops the AHSM-HS array and shield walls, as modeled in MCNP, approximates the 2x10 back-to-back array of AHSM-HSs. The dimensions of the box also include the width of the AHSM-HS end shield walls. As discussed above, the total activity of each face of the box is calculated by multiplying the current (half of the flux) by the area of the face. The activity calculation results are presented in Table B.10.2-3.

B.10.2.3.2 Two 1x10 Front-to-Front Arrays

Two boxes that envelop the AHSM-HS arrays and shield walls, as modeled in MCNP, approximate the two 1x10 front-to-front arrays of AHSM-HSs. The dimensions of each box also include the width of the AHSM-HS side and back shield walls. As discussed above, the total activity of each face of the box is calculated by multiplying the current (half of the flux) by the area of the face. The activity calculation results are presented in Table B.10.2-4.

B.10.2.4 Dose Rate Calculations

Point detectors are placed at the following distance as measured from each face of the "box": 6.095 m (20 ft), 10 m, 20 m, 30 m, 40 m, 50 m, 60 m, 70 m, 80 m, 90 m, 100 m, 200 m, 300 m, 400 m, 500 m, and 600 m. Each point detector is placed 91 cm (~3 feet) above the ground.

For the 2x10 back-to-back array of AHSM-HSs, the dose rates are calculated from the midpoints of the front and side of the array.

For the two 1x10 front-to-front arrays of AHSM-HSs, the dose rates are calculated from the midpoints of the back of the "source array" and "shield array" and halfway between the two arrays on the side. Due to the problem symmetry, the total dose rate at the back of the array

would be the sum of the dose rate results for the back of the "source" and "shield" arrays. The source strength is doubled in the FM card for the side tally since the model contains only one source array.

B.10.2.5 ISFSI Dose Rates

The dose rates at various distances from the front and side of the 2x10 back-to-back array of AHSM-HSs are presented in Table B.10.2-5 and Table B.10.2-6, respectively. The dose rates at various distances from the back and side of the two 1x10 front-to-front arrays of AHSM-HSs are presented in Table B.10.2-7 and Table B.10.2-8, respectively.

The annual dose limit from 10 CFR 72.104, reference [B10.5], is 25 mrem to any individual beyond the controlled area. Assuming 100% occupancy, the total annual exposure can be calculated by multiplying the dose rate by 8760 hours. Table B.10.2-9 and Figure B.10.2-3 present the annual exposure at various distances from the front and side of the 2x10 array. Table B.10.2-10 and Figure B.10.2-4 present the annual exposure at various distances from the back and side of the two 1x10 arrays. Based on these values, distances of at least 300 m from the front of the 2x10 array and 200 m from the sides of both arrays and the back of the two 1x10 arrays (when loaded with design basis fuel) are required to meet the annual dose rate limit for both configurations.

The dose rates from a typical ISFSI are evaluated by the licensee in a 10 CFR Part 72.212 evaluation to address the site-specific ISFSI layout and its time phased installation.

Dose rates at the site boundary will depend on specific ISFSI parameters such as storage array configuration, number of stored 32PTH2 DSCs, characteristics of stored fuel, fuel loading patterns, site geography, etc. Berms, walls, removable shields, or preferential loading of "cooler" fuel in the outer cells of the 32PTH2 DSC may be used to keep the site boundary dose rate within the 10 CFR 72.104 limits. Shields attached to the AHSM-HS must be evaluated for their potential impact on all normal, off-normal and accident scenarios to ensure that they do not introduce an unreviewed safety question as part of the site analysis performed as required by 10 CFR 72.104 and 10 CFR 72.212 [B10.5].

Table B.10.2-1
AHSM-HS Gamma Spectrum

AHSM-HS Surface Segment →	Front	Top	Rear	Side
Energy Group Upper Limit (MeV)	Flux [γ/(s·cm^2)]			
0.05	285.9	36.98	0.52	2.36
0.1	7647.78	1114.41	12.33	55.97
0.2	7721.22	1269.04	14.51	71.72
0.3	2542.01	402.26	5.59	28.38
0.4	1002.74	209.56	3.16	16.49
0.6	184.67	215.46	4.42	23.2
0.8	45.19	102.57	2.4	13.82
1	20.65	66	1.74	10.15
1.33	21.7	69.16	2.03	12.03
1.66	16.76	42.49	1.45	8.04
2	15.13	30.97	1.23	5.9
2.5	24.12	41.15	1.57	7.33
3	11.59	19.45	1.13	4.19
4	27.6	38.56	2.08	7.71
5	22.88	32.16	1.79	6.58
6.5	20.49	30.4	1.77	6.18
8	12.54	25.38	1.16	3.92
10	1.65	6.24	0.25	0.64
15	0.08	0.11	0.008	0.03
Total Flux [γ/(s• cm^2)]	19624.7	3752.35	59.138	284.64
Dose Rate [mrem/hr]	8.42	3.10	0.09	0.39

Table B.10.2-2
AHSM-HS Neutron Spectrum

AHSM-HS Surface Segment →	Front	Top	Rear	Side
Energy Group Upper Limit (MeV)	Flux [n/(s•cm^2)]			
4.14E-07	2.93E+02	1.87E+02	2.83E+00	1.49E+01
1.12E-06	1.03E+01	1.08E+01	6.97E-02	3.33E-01
3.06E-06	9.33E+00	1.04E+01	6.89E-02	3.24E-01
1.01E-05	1.06E+01	1.18E+01	8.03E-02	3.71E-01
2.90E-05	9.22E+00	9.78E+00	6.62E-02	3.14E-01
1.01E-04	1.00E+01	1.07E+01	7.40E-02	3.49E-01
5.83E-04	1.30E+01	1.30E+01	8.75E-02	4.45E-01
3.35E-03	1.16E+01	1.07E+01	7.22E-02	3.78E-01
1.11E-01	2.02E+01	1.45E+01	9.97E-02	5.52E-01
5.50E-01	6.87E+00	4.66E+00	3.15E-02	2.08E-01
1.11	2.54E+00	1.29E+00	1.27E-02	9.00E-02
1.83	5.51E-01	7.64E-01	9.03E-03	8.10E-02
2.35	2.84E-01	5.12E-01	8.22E-03	8.50E-02
2.46	1.90E-02	1.26E-01	1.93E-03	1.80E-02
3.01	8.40E-02	1.39E-01	1.29E-03	1.60E-02
4.06	3.50E-02	7.50E-02	7.27E-04	8.00E-03
4.96	4.00E-03	4.90E-02	5.50E-04	6.00E-03
6.36	5.00E-03	4.00E-02	3.64E-04	7.00E-03
8.18	2.00E-03	1.80E-02	7.72E-05	2.00E-03
10	1.46E-05	4.00E-03	1.85E-05	2.56E-04
12.2	0.00E+00	7.45E-04	1.77E-06	5.72E-05
14.9	0.00E+00	0.00E+00	1.65E-06	3.31E-06
Total Flux [n/(s• cm^2)]	3.97E+02	2.86E+02	3.51E+00	1.85E+01
Dose Rate [mrem/hr]	2.28	1.73	0.02	0.12

Table B.10.2-3
2x10 AHSM-HS Array Surface Activity Calculation

Proprietary information withheld pursuant to 10 CFR 2.390

Table B.10.2-4
1x10 AHSM-HS Array Surface Activity Calculation

Proprietary information withheld pursuant to 10 CFR 2.390

Table B.10.2-5
2x10 Array of AHSM-HSs Front Dose Rates

Distance (m)	Gamma Dose Rate (mrem/hr)	Uncertainty	Neutron Dose Rate (mrem/hr)	Uncertainty	Total Dose Rate (mrem/hr)	Uncertainty
6.1	2.39E+00	4.00E-04	1.02E+00	2.40E-03	3.41E+00	7.71E-04
10	1.44E+00	5.00E-04	6.29E-01	3.00E-03	2.07E+00	9.77E-04
20	5.34E-01	7.00E-04	2.55E-01	4.60E-03	7.89E-01	1.56E-03
30	2.61E-01	1.10E-03	1.32E-01	6.50E-03	3.93E-01	2.31E-03
40	1.48E-01	1.20E-03	7.94E-02	8.70E-03	2.28E-01	3.13E-03
50	9.37E-02	1.80E-03	5.06E-02	1.06E-02	1.44E-01	3.90E-03
60	6.35E-02	2.10E-03	3.45E-02	1.26E-02	9.80E-02	4.64E-03
70	4.51E-02	2.70E-03	2.42E-02	1.88E-02	6.93E-02	6.80E-03
80	3.30E-02	2.60E-03	1.71E-02	1.52E-02	5.01E-02	5.47E-03
90	2.49E-02	3.10E-03	1.29E-02	2.44E-02	3.78E-02	8.57E-03
100	1.93E-02	3.50E-03	9.85E-03	2.01E-02	2.92E-02	7.17E-03
200	2.68E-03	9.80E-03	1.04E-03	2.59E-02	3.72E-03	1.01E-02
300	5.75E-04	9.40E-03	2.60E-04	5.81E-02	8.34E-04	1.92E-02
400	1.67E-04	1.30E-02	8.07E-05	6.55E-02	2.48E-04	2.31E-02
500	5.69E-05	1.51E-02	2.89E-05	1.09E-01	8.58E-05	3.82E-02
600	2.31E-05	1.22E-02	1.18E-05	1.14E-01	3.49E-05	3.95E-02

Table B.10.2-6
2x10 Array of AHSM-HSs Side Dose Rates

Distance (m)	Gamma Dose Rate (mrem/hr)	Uncertainty	Neutron Dose Rate (mrem/hr)	Uncertainty	Total Dose Rate (mrem/hr)	Uncertainty
6.1	1.78E-01	1.30E-03	2.04E-01	6.30E-03	3.82E-01	3.41E-03
10	1.18E-01	1.50E-03	1.50E-01	6.30E-03	2.68E-01	3.59E-03
20	6.07E-02	2.20E-03	8.38E-02	8.40E-03	1.44E-01	4.96E-03
30	3.92E-02	2.80E-03	5.41E-02	1.11E-02	9.32E-02	6.54E-03
40	2.77E-02	3.80E-03	3.57E-02	1.24E-02	6.34E-02	7.18E-03
50	2.04E-02	3.10E-03	2.54E-02	1.42E-02	4.58E-02	7.99E-03
60	1.57E-02	4.40E-03	1.81E-02	1.65E-02	3.39E-02	9.07E-03
70	1.24E-02	4.70E-03	1.39E-02	2.15E-02	2.62E-02	1.16E-02
80	9.87E-03	5.70E-03	9.98E-03	1.93E-02	1.98E-02	1.01E-02
90	7.91E-03	4.90E-03	7.43E-03	2.32E-02	1.53E-02	1.15E-02
100	6.49E-03	8.00E-03	6.02E-03	2.66E-02	1.25E-02	1.35E-02
200	1.15E-03	1.52E-02	8.10E-04	4.70E-02	1.97E-03	2.13E-02
300	2.78E-04	4.58E-02	1.91E-04	5.75E-02	4.69E-04	3.59E-02
400	7.51E-05	2.87E-02	6.28E-05	7.39E-02	1.38E-04	3.71E-02
500	2.37E-05	1.97E-02	1.84E-05	4.03E-02	4.21E-05	2.08E-02
600	9.62E-06	3.39E-02	9.53E-06	2.06E-01	1.91E-05	1.04E-01

Table B.10.2-7
Two 1x10 Arrays of AHSM-HSs Back Dose Rates

Distance (m)	Gamma Dose Rate (mrem/hr)	Uncertainty	Neutron Dose Rate (mrem/hr)	Uncertainty	Total Dose Rate (mrem/hr)	Uncertainty
6.1	1.08E-01	1.70E-03	1.75E-01	1.38E-03	2.83E-01	1.07E-03
10	8.60E-02	1.95E-03	1.43E-01	1.57E-03	2.29E-01	1.22E-03
20	5.41E-02	2.38E-03	8.97E-02	2.30E-03	1.44E-01	1.69E-03
30	3.75E-02	3.41E-03	5.85E-02	2.48E-03	9.60E-02	2.02E-03
40	2.74E-02	3.81E-03	3.98E-02	3.13E-03	6.72E-02	2.42E-03
50	2.07E-02	3.53E-03	2.81E-02	3.21E-03	4.88E-02	2.38E-03
60	1.61E-02	3.92E-03	2.01E-02	4.04E-03	3.62E-02	2.84E-03
70	1.27E-02	3.99E-03	1.49E-02	4.38E-03	2.76E-02	2.99E-03
80	1.02E-02	4.96E-03	1.15E-02	5.37E-03	2.17E-02	3.68E-03
90	8.28E-03	7.84E-03	8.53E-03	5.93E-03	1.68E-02	4.90E-03
100	6.82E-03	8.76E-03	6.56E-03	5.56E-03	1.34E-02	5.23E-03
200	1.23E-03	1.10E-02	8.64E-04	1.24E-02	2.09E-03	8.24E-03
300	2.97E-04	1.99E-02	2.09E-04	1.84E-02	5.07E-04	1.39E-02
400	8.28E-05	2.09E-02	6.79E-05	1.58E-02	1.51E-04	1.35E-02
500	2.83E-05	2.57E-02	2.35E-05	2.91E-02	5.18E-05	1.93E-02
600	1.06E-05	1.80E-02	1.02E-05	3.07E-02	2.08E-05	1.77E-02

Table B.10.2-8
Two 1x10 Arrays of AHSM-HSs Side Dose Rates

Distance (m)	Gamma Dose Rate (mrem/hr)	Uncertainty	Neutron Dose Rate (mrem/hr)	Uncertainty	Total Dose Rate (mrem/hr)	Uncertainty
6.1	8.23E-01	9.00E-04	4.33E-01	2.90E-03	1.26E+00	1.16E-03
10	4.24E-01	1.30E-03	2.59E-01	5.20E-03	6.84E-01	2.13E-03
20	1.36E-01	2.20E-03	1.11E-01	5.80E-03	2.47E-01	2.88E-03
30	6.68E-02	3.30E-03	6.37E-02	7.40E-03	1.30E-01	3.99E-03
40	4.05E-02	5.50E-03	4.02E-02	7.70E-03	8.07E-02	4.72E-03
50	2.68E-02	3.90E-03	2.81E-02	1.15E-02	5.49E-02	6.18E-03
60	1.94E-02	5.00E-03	2.00E-02	1.25E-02	3.94E-02	6.81E-03
70	1.44E-02	5.00E-03	1.47E-02	1.52E-02	2.91E-02	8.07E-03
80	1.11E-02	5.30E-03	1.11E-02	2.04E-02	2.22E-02	1.06E-02
90	8.77E-03	1.07E-02	8.23E-03	1.73E-02	1.70E-02	1.00E-02
100	6.92E-03	6.50E-03	6.47E-03	2.43E-02	1.34E-02	1.22E-02
200	1.16E-03	1.64E-02	8.21E-04	3.57E-02	1.98E-03	1.76E-02
300	2.62E-04	1.69E-02	1.90E-04	3.66E-02	4.52E-04	1.82E-02
400	8.31E-05	6.83E-02	5.92E-05	6.90E-02	1.42E-04	4.91E-02
500	2.62E-05	4.28E-02	2.11E-05	5.69E-02	4.72E-05	3.47E-02
600	1.16E-05	7.08E-02	8.55E-06	6.62E-02	2.02E-05	4.95E-02

Table B.10.2-9
Annual Exposure for 2x10 Array of AHSM-HSs

Distance (m)	Front		Side	
	Dose Rate (mrem/hr)	Exposure (mrem)	Dose Rate (mrem/hr)	Exposure (mrem)
6.1	3.41E+00	29914	3.82E-01	3344
10	2.07E+00	18126	2.68E-01	2351
20	7.89E-01	6909	1.44E-01	1266
30	3.93E-01	3441	9.32E-02	817
40	2.28E-01	1994	6.34E-02	555
50	1.44E-01	1264	4.58E-02	402
60	9.80E-02	858	3.39E-02	297
70	6.93E-02	607	2.62E-02	230
80	5.01E-02	439	1.98E-02	174
90	3.78E-02	331	1.53E-02	134
100	2.92E-02	256	1.25E-02	110
200	3.72E-03	33	1.97E-03	17
300	8.34E-04	7.3	4.69E-04	4.1
400	2.48E-04	2.2	1.38E-04	1.21
500	8.58E-05	0.75	4.21E-05	0.37
600	3.49E-05	0.31	1.91E-05	0.17

Table B.10.2-10
Annual Exposure for Two 1x10 Arrays of AHSM-HSs

Distance (m)	Back		Side	
	Dose Rate (mrem/hr)	Exposure (mrem)	Dose Rate (mrem/hr)	Exposure (mrem)
6.1	2.83E-01	2482	1.26E+00	11008
10	2.29E-01	2004	6.84E-01	5989
20	1.44E-01	1259	2.47E-01	2166
30	9.60E-02	841	1.30E-01	1143
40	6.72E-02	589	8.07E-02	707
50	4.88E-02	427	5.49E-02	481
60	3.62E-02	317	3.94E-02	346
70	2.76E-02	241	2.91E-02	255
80	2.17E-02	190	2.22E-02	194
90	1.68E-02	147	1.70E-02	149
100	1.34E-02	117	1.34E-02	117
200	2.09E-03	18	1.98E-03	17
300	5.07E-04	4.4	4.52E-04	4.0
400	1.51E-04	1.32	1.42E-04	1.25
500	5.18E-05	0.45	4.72E-05	0.41
600	2.08E-05	0.18	2.02E-05	0.18

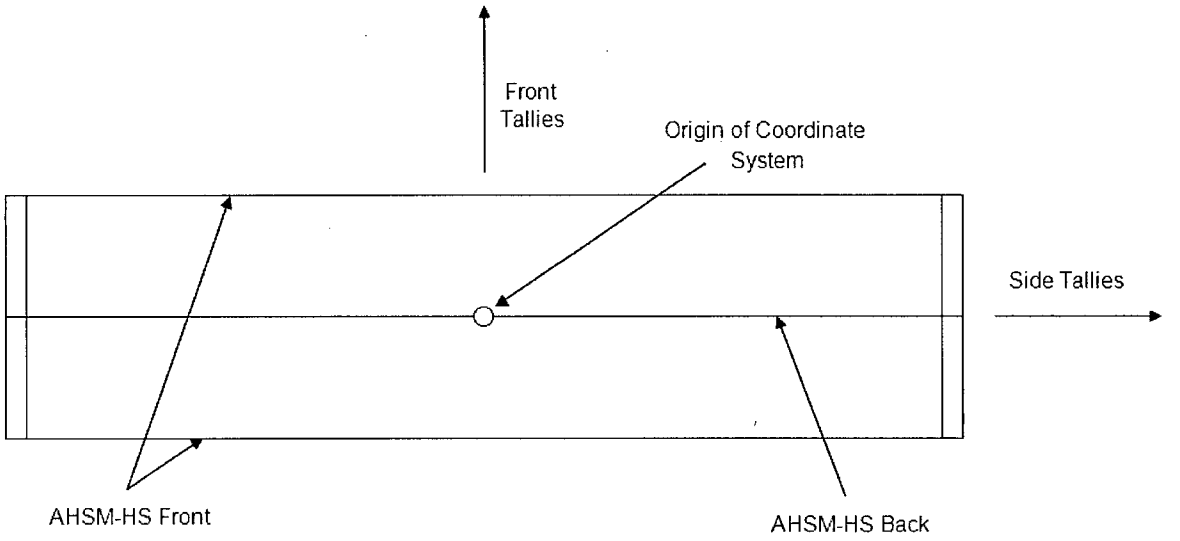

Figure B.10.2-1
2x10 Back-to-Back AHSM-HS Array Layout (sketch not to scale)

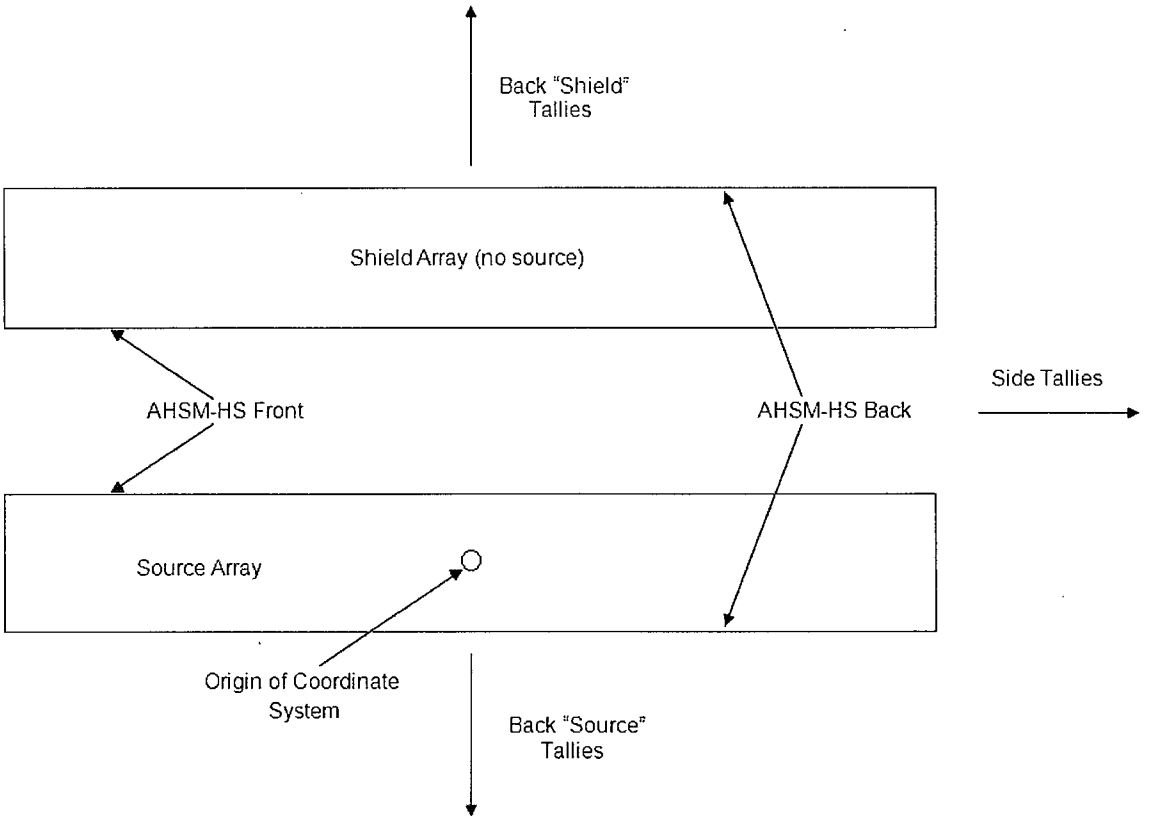

Figure B.10.2-2
Two 1x10 Front-to-Front AHSM-HS Arrays Layout (sketch not to scale)

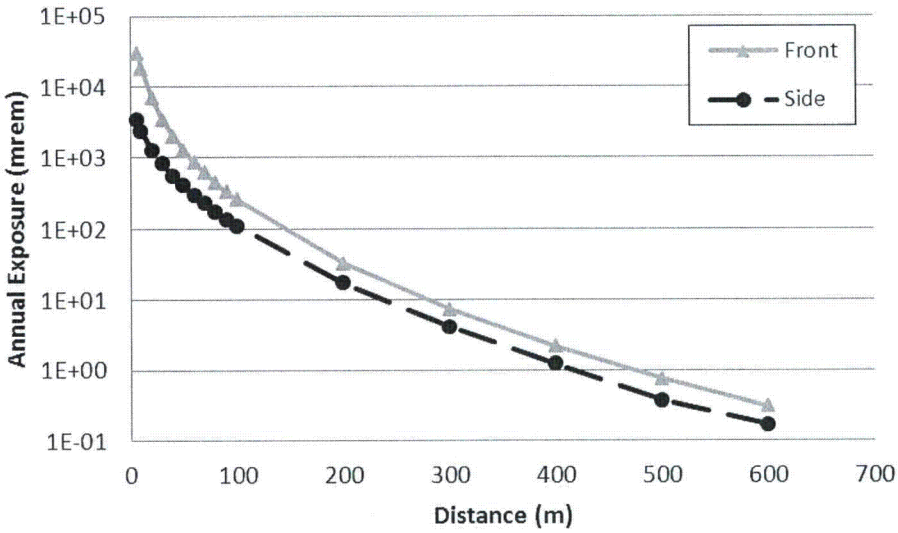

Figure B.10.2-3
Annual Exposure for 2x10 Array of AHSM-HSs

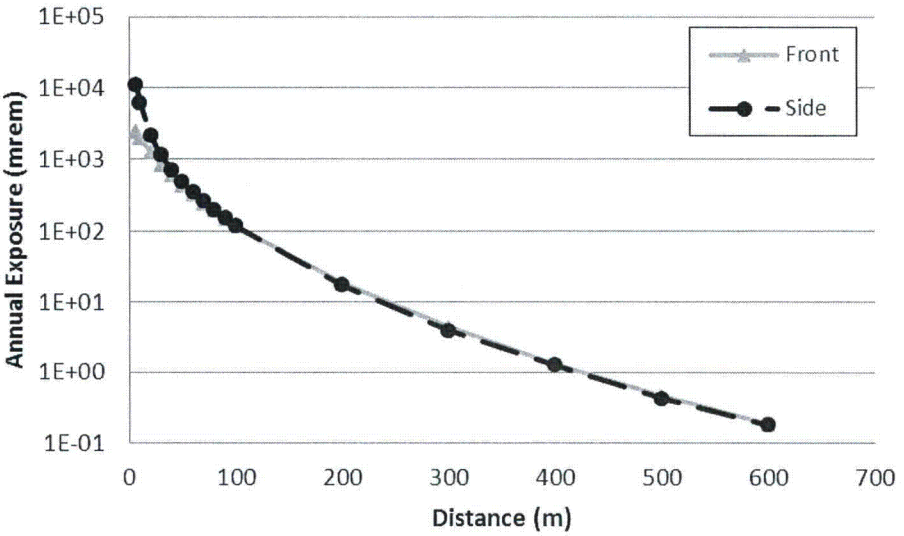

Figure B.10.2-4
Annual Exposure for Two 1x10 Arrays of AHSM-HSs

B.10.3 Estimated Onsite and Offsite Dose Assessment

This section provides estimates of occupational and off-site doses for typical ISFSI configurations.

Assumed annual occupancy times, including the anticipated maximum total hours per year for any individual and total person-hours per year for all personnel for each radiation area during normal operation and anticipated operational occurrences, will be evaluated by the licensee in a 10 CFR 72.212 [B10.5] evaluation to address the site specific ISFSI layout, inspection, and maintenance requirements. In addition, the estimated annual collective person rem doses associated with loading operations will be addressed by the licensee in a 10 CFR 72.212 evaluation.

B.10.3.1 Occupational Exposures

B.10.3.1.1 32PTH2 DSC Loading, Transfer and Storage Operations

Table B.10.3-1 shows the estimated occupational exposures to ISFSI personnel during loading, transfer, and storage of the 32PTH2 DSC (time and manpower may vary depending on individual ISFSI practices). The assumed task times and number of personnel required, and total resultant doses are listed in this table. Temporary shielding can be used by the licensee to maintain doses ALARA.

Licensees may elect to use different equipment and/or different procedures than assumed in the evaluation. Unique steps are sometimes necessary at the individual site to load the canister, complete closure operations, and place the canister in the AHSM-HS. Specifically, the licensee may choose to modify the sequence of operations in order to achieve reduced dose rates for a larger number of steps, with the end result of reduced total exposure. The only requirement is that the licensee practice ALARA with respect to the total exposure received for a loading campaign. These estimated durations, person-loading and dose rates are not limits.

The average distance for a given operation takes into account that the operator may be in contact with the OS200FC TC, but this duration will be limited. For draining activities, vacuum drying, and leak testing, the attachment of fittings will take place closer to the OS200FC TC than the operation of the pump and vacuum drying system. For decontamination activities, although operators could be near the OS200FC TC for some activities, other parts of the operation could be performed from farther away. For this reason, 1 foot to 3 feet is an appropriate average distance for these operations.

The operator's hands may be in a high dose rate location momentarily, for example when connecting couplings or vacuum fittings at the vent and siphon ports. This does not translate into a whole-body dose, and therefore, these localized streaming effects are not considered here.

For operations near the top end of the 32PTH2 DSC, most of the work will take place around the perimeter (top edge of 32PTH2 DSC/OS200FC TC) and a smaller portion will take place directly over the shield plug.

The areas of highest operational dose (potential streaming paths) are the front of a loaded AHSM-HS at the air inlet vent, at the OS200FC TC side surface with a dry 32PTH2 DSC (outer top cover plate welding, transfer operations) and at the 32PTH2 DSC/OS200FC TC annulus. Operating procedures and personnel training minimize personnel exposure in these areas. The guidance of Regulatory Guide 8.34 [B10.7] is to be employed in defining the on-site occupational dose and monitoring requirements.

Based on historical Transnuclear experience loading NUHOMS® DSCs into various horizontal storage modules, the total exposures for one loading campaign are generously overestimated. For the purpose of the analysis, activities listed in Table B.10.3-1 are assumed if the operator or worker is continuously present in the field. In reality, ALARA is fully in force and the operator or worker would minimize the time spent in the field or temporary shielding would be added to reduce total campaign exposures. For NUHOMS® DSCs containing 32 PWR spent fuel assemblies and heat loads up to 33 kW per DSC, total operational exposure to load a single DSC is generally under 400 person-mrem.

B.10.3.1.2 32PTH2 DSC Retrieval Operations

Occupational exposures to ISFSI personnel during 32PTH2 DSC retrieval are similar to those exposures calculated for 32PTH2 DSC insertion. Dose rates for retrieval operations will be lower than those for insertion operations due to radioactive decay of the spent fuel inside the AHSM-HS. Therefore, the dose rates for 32PTH2 DSC retrieval are bounded by the dose rates calculated for insertion.

B.10.3.1.3 32PTH2 DSC Fuel Unloading Operations

The process of unloading the 32PTH2 DSC is similar to that used for loading the 32PTH2 DSC. The same ALARA procedures utilized for loading should also be applied to unloading. Occupational exposures to plant personnel are bounded by those exposures calculated for 32PTH2 DSC loading.

B.10.3.1.4 Maintenance Operations

The dose rate for surveillance activities is obtained from Table B.10.2-5 and Table B.10.2-6 for the 2x10 back-to-back array of AHSM-HSs and Table B.10.2-7 and Table B.10.2-8 for the two 1x10 front-to-front arrays of AHSM-HSs. The 20 foot (6.1 m) dose rate is a conservative estimate for surveillance activities. The AHSM-HS surface dose rates provided in Chapter B.5 and listed in Table B.10.2-1 and Table B.10.2-2 are a conservative estimate for thermocouple maintenance activities including calibration and repair. The surface dose rates calculated in Chapter B.5 also provide a conservative estimate of a dose rate at 3 feet from the AHSM-HS which may be encountered during operations associated with removal of debris from AHSM-HS vents.

The ISFSI licensee will evaluate the additional dose to station personnel from ISFSI operations, based on the particular storage configuration and site personnel requirements.

B.10.3.1.5 Doses During ISFSI Array Expansion

ISFSI expansion should be planned to eliminate the need for entry into an AHSM-HS adjacent to a loaded AHSM-HS. The reduction in shielding between the side of an array with an installed shield wall Proprietary information withheld pursuant to 10 CFR 2.390 versus shielding between the inside of an empty AHSM-HS and an adjacent loaded AHSM-HS Proprietary information withheld pursuant to 10 CFR 2.390 is very significant. Pre-planning to limit entry into a AHSM-HS when it is not separated from a loaded AHSM-HS by at least one empty AHSM-HS Proprietary information withheld pursuant to 10 CFR 2.390 is recommended. Similarly, during array expansion, when the shield wall is removed, personnel access to the area should be controlled. For a AHSM-HS separated from a loaded AHSM-HS by an empty AHSM-HS, the resulting dose will be less than that specified for the side dose rate of an array with an installed shield wall so long as the vents in the empty AHSM-HS are outfitted with appropriate dose reduction hardware.

B.10.3.2 Public Exposure

The only off-site dose to the public from the ISFSI is from direct and skyshine radiation at or beyond the controlled area of the ISFSI (as defined by 10 CFR 72.106). Table B.10.2-5 and Table B.10.2-6 show the radiation dose rates in the vicinity of a 2x10 back-to-back array of AHSM-HSs. Table B.10.2-7 and Table B.10.2-8 show the radiation dose rates in the vicinity of two 1x10 front-to-front arrays of AHSM-HSs. The collective off-site dose is a function of the number and arrangement of the AHSM-HSs on the ISFSI, the proximity of the ISFSI to the site boundary, and other plant considerations to be addressed by the licensee in accordance with 10 CFR 72.212.

Each cask user or general licensee must perform a site-specific analysis as required by 10 CFR 72.212(b) to demonstrate compliance with 10 CFR 72.104(a) for normal operations and anticipated occurrences. The general licensee may consider site-specific conditions, such as actual distances to the nearest real person, topography, array configurations, characteristics of stored fuel, and use of engineered features, such as berms, walls, or additional shield blocks, in their analysis of public doses. The site-specific analysis must also include the doses received from other fuel cycle activities (e.g., reactor operations) in the region.

Table B.10.3-1
Exposure Estimation for a Single 32PTH2 DSC Loading
(for information only)
(Part 1 of 2)

Location	Task Description	No. of Workers	Duration (hr)	Area Dose Rate (mrem/hr)	Total Exposure (person-mrem)
Auxiliary Building and Fuel Pool	Place the 32PTH2 DSC into the OS200FC TC	2	2	2	8
	Fill the OS200FC TC/32PTH2 DSC Annulus with Clean Water and Install the Inflatable Seal	3	1	2	6
	Fill the 32PTH2 DSC Cavity with Water (borated for PWRs)	1	6	2	12
	Place the OS200FC TC Containing the 32PTH2 DSC in the Fuel Pool	5	0.5	2	5
	Verify and Load the Candidate Fuel Assemblies into the 32PTH2 DSC	3	5	2	30
	Place the Top Shield Plug on the 32PTH2 DSC	2	1	2	4
	Remove the OS200FC TC/32PTH2 DSC from the Fuel Pool and Place them in the Decon Area	5	0.5	2	5
		1	0.033	107	3.6
		1	0.667	79	52
OS200FC TC Decontamination Area	Decontaminate the Outer Surface of the OS200FC TC	1	1.75	79	138
		1	1	2	2
	Decontaminate the Top Region of the OS200FC TC and 32PTH2 DSC	1	0.5	2	1
		1	0.5	104	52
		1	0.5	123	61
	Drain Water from the 32PTH2 DSC Cavity	1	0.083	107	8.9
	Remove OS200FC TC/32PTH2 DSC Annulus Seal and Set-Up Welding Machine	1	0.167	1322	220
		1	0.75	92	69
		1	0.5	59	30
	Weld the Inner Top Cover Plate to the 32PTH2 DSC Shell and Perform NDE (PT)	6	2	2	24
		1	0.33	502	167
	Drain 32PTH2 DSC Cavity	1	0.25	92	23
		1	0.017	502	8.4
		1	0.5	2	1
	Vacuum Dry and Backfill the 32PTH2 DSC with Helium	1	0.5	59	30
		2	30	2	120
	Helium Leak Test the Shield Plug Weld	2	1	2	4
	Seal Weld the Prefabricated Plugs to the Vent and Siphon Port and Perform NDE (PT)	1	0.5	92	46
	Fit-Up the 32PTH2 DSC Top Cover Plate	1	0.25	502	126
		1	0.5	92	46
	Weld the Outer Top Cover Plate to 32PTH2 DSC Shell, Perform NDE (PT), and Drain the OS200FC TC/32PTH2 DSC Annulus	1	1	59	59
		1	0.167	502	84
		2	14	2	56
		1	0.333	502	167
	Install The OS200FC TC Lid	2	0.667	82	110

Table B.10.3-1
Exposure Estimation for a Single 32PTH2 DSC Loading
(for information only)
(Part 2 of 2)

Location	Task Description	No. of Workers	Duration (hr)	Area Dose Rate (mrem/hr)	Total Exposure (person-mrem)
Reactor/Fuel Building Bay	Ready the OS200FC TC Support Skid and Transfer Trailer for the Service	2	2	2	8
	Place the OS200FC TC onto the Skid and Trailer	2	0.25	79	39
	Secure the OS200FC TC to the Skid	1	0.25	79	20
ISFSI Site	Ready The OS200FC TC Support Skid and Transfer Trailer for the Service	2	2	negligible	0
	Transfer the OS200FC TC to ISFSI	6	1	negligible	0
	Position the OS200FC TC in Close Proximity with the AHSM-HS	3	1	negligible	0
	Remove the OS200FC TC Lid	2	0.67	63	84
	Align and Dock the OS200FC TC with the AHSM-HS	2	0.25	97	49
	Position and Align Ram with OS200FC TC	2	0.5	58	58
	Remove Ram Access Cover Plate	1	0.083	158	13
	Transfer the 32PTH2 DSC from the OS200FC TC to the AHSM-HS	3	0.5	negligible	0
	Lift the Ram Back onto the Trailer and Un-Dock the OS200FC TC from the	2	0.083	31	5
	Install AHSM-HS Access Door	2	0.5	15	15
Totals		N/A	87	N/A	2070

B.10.4 Supplemental Information

B.10.4.1 References

[B10.1] U.S. Nuclear Regulatory Commission, Regulatory Guide 8.8, Information Relevant to Ensuring That Occupational Exposures at Nuclear Power Stations will be As Low As Is Reasonably Achievable, Revision 3, June 1978.

[B10.2] "MCNP/MCNPX - Monte Carlo N-Particle Transport Code System Including MCNP5 1.40 and MCNPX 2.5.0 and Data Libraries," CCC-730, Oak Ridge National Laboratory, RSICC Computer Code Collection, January 2006.

[B10.3] U.S. Nuclear Regulatory Commission, Regulatory Guide 8.10, Operating Philosophy for Maintaining Occupational Radiation Exposures as low as is reasonably Achievable , Revision 1-R, May 1977.

[B10.4] U.S. Nuclear Regulatory Commission, Regulatory Guide 1.8, Qualification and Training of Personnel for Nuclear Power Plants, Revision 2, April 1987.

[B10.5] Title 10 Code of Federal Regulations Part 72, Licensing Requirements for the Independent Storage of Spent Nuclear Fuel and High-Level Radioactive Waste.

[B10.6] Title 10 Code of Federal Regulations Part 20, Standards for Protection Against Radiation.

[B10.7] U.S. Nuclear Regulatory Commission, Regulatory Guide 8.34, Monitoring Criteria and Methods to Calculate Occupational Radiation Doses, July 1992.

[B10.8] American Nuclear Society, "American National Standard Neutron and Gamma Flux-to-Dose Rate Factors". ANSI/ANS-6.1.1-1977, American Nuclear Society, La Grange Park, Illinois, March 1977.

B.11 ACCIDENT ANALYSES

Sections of this Chapter have been identified as "No change" due to the addition of the NUHOMS® 32PTH2 system to the Advanced NUHOMS® System. For these sections, the description or analysis presented in the corresponding sections of the UFSAR for the Advanced NUHOMS® System with a 24PT1-DSC or 24PT4-DSC loaded in the AHSM is also applicable to the system with a 32PTH2 DSC loaded in the AHSM-HS.

This Chapter describes the postulated off-normal and accident events that might occur during storage of the 32PTH2 DSC in an AHSM-HS at an ISFSI. In addition, this Chapter also addresses the potential causes of these events, their detection and consequences, and the corrective course of action to be taken by ISFSI personnel. Accident analyses demonstrate that the functional integrity of the system is maintained by:

- Maintaining sub-criticality within margins defined in Chapter B.6
- Maintaining confinement boundary integrity
- Ensuring fuel retrievability and
- Maintaining doses within 10 CFR 72.106 limits (< 5 rem).

The Accident Dose Calculations sections report the expected doses resulting from the postulated event in terms of whole body doses only. The leaktight canister design and the maintenance of confinement boundary integrity under all credible off-normal and accident scenarios ensures no radiation leakage from the 32PTH2 DSC, thereby limiting dose consequences to direct and scattered radiation doses without any associated inhalation or ingestion doses.

B.11.1 Off-Normal Operations

Off-normal operations are design events of the second type (Design Event II) as defined in ANSI/ANS 57.9 [B11.1]. Design Event II conditions consist of that set of events that, although not occurring regularly, can be expected to occur with moderate frequency, or on the order of once during a calendar year of ISFSI operation.

For the Advanced NUHOMS® System, off-normal events could occur during fuel loading, trailer towing, 32PTH2 DSC transfer and other operations. The two off-normal events, which bound the range of off-normal conditions, are:

1. A "jammed" 32PTH2 DSC during loading or unloading of the AHSM-HS

2. The extreme ambient temperatures of -40°F (winter) and +117°F (summer)

These two events envelop the range of expected off-normal structural loads and temperatures acting on the Advanced NUHOMS® System.

B.11.1.1 Off-Normal Transfer Loads

No change to the Off-Normal Transfer Loads section as described in Chapter 11, Section 11.1.1.

B.11.1.1.1 Postulated Cause of the Event

No change to the Postulated Cause of the Event section as described in Chapter 11, Section 11.1.1.1.

B.11.1.1.2 Detection of the Event

If the 32PTH2 DSC were to jam or bind during transfer, the hydraulic pressure in the ram would increase. The maximum ram push/pull forces are limited by design features to a maximum load of 110/80 kips. Override controls are available to the operator to increase the ram force up to its maximum 110/80 kips design load, or to interrupt the transfer operation at any time.

During the transfer operation, the force exerted on the 32PTH2 DSC by the hydraulic ram is that required to first overcome the static frictional resisting force between the OS200FC TC rails and the 32PTH2 DSC. Once the 32PTH2 DSC begins to slide, the resisting force is a function of the sliding friction coefficient between the 32PTH2 DSC and the OS200FC TC rails and/or between the 32PTH2 DSC and the AHSM-HS support rails. If motion is prevented, the hydraulic pressure increases, thereby increasing the force on the 32PTH2 DSC until the hydraulic ram system pressure limit is reached. This limit is controlled so that adequate force is available to overcome variations in surface finish, etc., but is sufficiently low to ensure that component damage does not occur.

The maximum ram design force is sufficient to overcome any potentially higher resistance loads due to sticking of the 32PTH2 DSC in either the OS200FC TC or the AHSM-HS. The 110 kips

design basis for the hydraulic ram system corresponds to the maximum force that can be developed with a coefficient of friction equal to 1.0.

B.11.1.1.3 Analysis of Effects and Consequences

The 32PTH2 DSC and the AHSM-HS are designed and analyzed for off-normal transfer loads of 110 kips (maximum force that the ram is able to develop), during insertion (loading) and 80 kips during retrieval (unloading) operations. These analyses are discussed in Chapter B.3.

For either loading or unloading of the 32PTH2 DSC under off-normal conditions, the stresses on the shell assembly components are demonstrated to be within the ASME Service Level B allowable stress limits. Therefore, permanent deformation of the 32PTH2 DSC shell components does not occur. In addition, the loads are applied to the outer bottom cover plate, which is not part of the confinement boundary. The internal basket assembly components are unaffected by these loads based on clearances provided between the basket components and the 32PTH2 DSC internal envelope.

There is no breach of the confinement boundary and, therefore, no potential for release of radioactive material exists.

B.11.1.1.4 Corrective Actions

The required corrective action is to reverse the direction of the force being applied to the 32PTH2 DSC by the ram, and return the 32PTH2 DSC to its previous position. Since no permanent deformation of the 32PTH2 DSC occurs, the sliding transfer of the 32PTH2 DSC to its previous position is unimpeded. The transfer cask alignment is then rechecked, and the transfer cask repositioned as necessary before attempts at transfer are renewed.

B.11.1.2 Extreme Ambient Temperatures

No change to the Extreme Ambient Temperatures section as described in Chapter 11, Section 11.1.2.

B.11.1.2.1 Postulated Cause of the Event

No change to the Postulated Cause of the Event section as described in Chapter 11, Section 11.1.2.1.

B.11.1.2.2 Detection of Event

No change to the Detection of Event section as described in Chapter 11, Section 11.1.2.2.

B.11.1.2.3 Analysis of Effects and Consequences

Thermal analyses of the NUHOMS® 32PTH2 system with the 32PTH2 DSC and CE 16x16 Class fuel for extreme ambient conditions are presented in Chapter B.4. The effects of extreme ambient temperatures on the NUHOMS® 32PTH2 system are discussed in Chapter B.3.

B.11.1.2.4 Corrective Actions

As shown in the analyses described in Chapters B.3 and B.4, the extreme ambient temperatures analyzed do not adversely impact operation of the NUHOMS® 32PTH2 system.

B.11.1.3 Radiological Impact from Off-Normal Operations

No change to the Radiological Impact from Off-Normal Operations section as described in Chapter 11, Section 11.1.3.

B.11.2 Postulated Accidents

The discussion in Section 11.2 for the 24PT1-DSC applies to the 32PTH2 DSC. References to Chapter 3 sections and tables apply to the corresponding section/tables presented/referenced in Chapter B.3, as appropriate.

The accidents postulated for the 32PTH2 system are shown in Table B.11.2-1.

B.11.2.1 Earthquake

B.11.2.1.1 Cause of Accident

No change to the Cause of Accident section as described in Chapter 11, Section 11.2.1.1.

B.11.2.1.2 Accident Analysis

Both linear and non-linear analyses are performed to determine the seismic response of the NUHOMS® 32PTH2 system. Non-linear (contact) elastic and linear elastic analyses are used in the structural evaluation of the 32PTH2 DSC shell assembly and AHSM-HS, respectively, to determine stresses and/or forces and moments within these components. Non-linear analyses are used for the seismic stability analyses to determine the maximum sliding and rocking response of the AHSM-HS array.

The stress analyses results due to seismic loads for the 32PTH2 DSC and the AHSM-HS are summarized in Section B.3.6. The non-linear seismic stability analyses are discussed in Section B.11.2.1.2.1.

Proprietary information withheld pursuant to 10 CFR 2.390

Proprietary information withheld pursuant to 10 CFR 2.390

Proprietary information withheld pursuant to 10 CFR 2.390

Maximum (enveloping of all analyses) sliding displacements are on the order of 52 inches (4.3 ft) in the X-direction and 66 inches (5.5 ft) in the Y-direction. These maximum sliding displacements are well within the clear distance of 8 ft. to the edge of the basemat available for sliding of the array assembly in each horizontal direction. Maximum tipping/uplift is less than 1.0 inch for the worst-case analysis.

The LS-DYNA analyses demonstrate that the response of the AHSM-HS assembly is dominated by sliding of the AHSM-HSs and that the rocking response is negligibly small.

Proprietary information withheld pursuant to 10 CFR 2.390

B.11.2.1.2.3 Modal Frequencies of AHSM-HS Loaded with 32PTH2 DSC

The natural frequencies of the loaded AHSM-HS are determined by performing a frequency analysis using the ANSYS [B11.6] finite element analytical model shown in Figure B.3.6-12. First mode global frequencies of the loaded AHSM-HS in each orthogonal direction are on the order of 21 Hz in the global X (transverse) direction, and in the rigid range of the input design spectrum (above 33 Hz) in the global Z (longitudinal) and Y (vertical) directions.

Proprietary information withheld pursuant to 10 CFR 2.390

B.11.2.1.2.5 32PTH2 DSC Seismic Stress Analysis

The seismic analysis of the 32PTH2 DSC inside the AHSM-HS is discussed in Section B.3.6.1.

B.11.2.1.2.6 AHSM-HS Seismic Analysis

The seismic analysis of the AHSM-HS is discussed in Section B.3.6.2. For the stress evaluations, an equivalent static analysis of the AHSM-HS is performed using the ANSYS model described in Section B.3.6.2.3.1 for 1.5g longitudinal, 1.6g transverse and 1.0g vertical accelerations

applied uniformly to the AHSM-HS. The seismic evaluation of the connections between AHSM-HS roof unit and the base and the connections between AHSM-HSs are conservatively performed using seismic accelerations of 2.25g in the longitudinal and the transverse directions, and 1.0g in the vertical direction.

The responses for each orthogonal direction are combined using the SRSS method.

As described in Section B.3.6.2, the seismic analysis results are incorporated in the loading combinations C4C (Table B3.6-25) and C5S (Table B3.6-26) for the concrete and the support structure components, respectively.

B.11.2.1.2.7 OS200FC Transfer Cask (TC) Seismic Analysis

The OS200FC TC, when mounted on the transfer trailer during a 1.5g earthquake, is subjected to stresses which are bounded by the 80 inch OS200FC TC drop analysis. The stress analysis of the OS200/OS200FC TC is documented in Appendix U of the Standardized NUHOMS® UFSAR [B11.7].

B.11.2.1.3 Accident Dose Calculations

No change to the Accident Dose Calculations section as described in Chapter 11, Section 11.2.1.3.

B.11.2.1.4 Corrective Actions

No change to the Corrective Actions section as described in Chapter 11, Section 11.2.1.4.

B.11.2.2 Tornado Wind Pressure and Tornado Missiles

B.11.2.2.1 Cause of Accident

No change to the Cause of Accident section as described in Chapter 11, Section 11.2.2.1.

B.11.2.2.2 Accident Analysis

The applicable design parameters for the design basis tornado (DBT) for the NUHOMS® 32PTH2 system are not changed from those presented in Section 2.2.1.

Tornado pressure drop effects on the 32PTH2 DSC are enveloped by internal design basis pressure analyses.

The determination of the tornado wind pressures and tornado missile loads acting on the AHSM-HS are not changed from those detailed for the AHSM in Section 3.6.2.2.

Stability analyses are performed to determine the response of the AHSM-HS to tornado wind pressure loads. The stability analyses are performed using closed-form calculation methods to

determine sliding and overturning response of the AHSM-HS array. A single AHSM-HS with both the end and the rear shield walls is conservatively selected for the analyses.

Stresses due to tornado wind pressures are bounded by those due to seismic accelerations, as described in Section B.3.6.2.

In addition, the AHSM-HS is evaluated for tornado missiles. The adequacy of the AHSM-HS to resist tornado missile loads is addressed using empirical formulae given in [B11.14].

B.11.2.2.2.1 Effect of Design Basis Tornado (DBT) Wind Pressure Loads on AHSM-HS

As described in Section B.3.6.2.2, the AHSM-HS is qualified for maximum velocity pressure of 344 lb/ft^2 determined from the tornado wind velocity parameters given in [B.11.8]. DBT generated design wind loads are determined using the provisions of Chapter 6 of [B11.13] and are summarized in Table B.3.6-24. As shown in Table B.3.6-24, the bounding values calculated from [B.11.13] and those used in Section 11.2.2.2.1 are used in the evaluations.

A single stand-alone AHSM-HS is protected by shield walls on either side and at the rear. For an AHSM-HS array, the critical AHSM-HS is on the windward end of the array. This AHSM-HS has an end shield wall to protect the AHSM-HS from tornado missile impacts. The shield wall is subjected to the 397 lb/ft^2 windward pressure load. The leeward side of the same end AHSM-HS in the array has no appreciable suction load due to the proximity of the adjacent AHSM-HS. The 208 lb/ft^2 suction load is applicable to the end shield wall on the opposite end module in the array. A suction of 442 lb/ft^2 is also applied to the roof unit of each AHSM-HS in the array.

A stability analysis is performed to evaluate the effects of overturning and sliding due to the postulated DBT. A single, freestanding AHSM-HS with two end shield walls and rear shield wall is used for this analysis.

The pressure drop has no effect on the AHSM-HS, since the AHSM-HS is an open structure, due to the presence of the inlet and outlet vents.

The stress analysis of the DBT wind pressures are bounded by those due to seismic accelerations, as described in Section B.3.6.2.

B.11.2.2.2.1.1 AHSM-HS Overturning Analysis

For the DBT wind overturning analysis, the overturning moment and the resulting stabilizing moments are calculated.

The stabilizing moment (M_{st}) for the windward module plus end shield walls is (using minimum component weights):

$$M_{st} = W(d + d_s) + W_s\left(d_s/2 + 2d + d_s\right) + W_s\left(d_s/2\right)$$

Where: W = 427 kips, weight of AHSM-HS + 32PTH2 DSC

W_s = 176 kips, weight of end module shield wall

d = 58.0", horizontal distance between center of gravity of AHSM-HS to the outer edge of the module.

d_s = 36" , thickness of the shield wall

Therefore: M_{st} = 73,226 kip-in.

and the overturning moment (M_{to}) for the windward module plus shield wall due to DBT wind pressure is:

$M_{to} = [(W_1 + W_2) A_w h/2 + W_3 A_r(d + d_s)]12$

Where: W_1 = 0.397 kip/ft.^{2}, wind load, windward wall

W_2 = 0.208 kip/ft^2, wind load, leeward wall

h = 18.5 ft, wall height

W_3 = 0.442 kip/ft.^{2}, wind uplift on roof

A_r = 323.9 ft.^{2}, roof unit area (including shield walls)

A_w = 382.4 ft.^{2}, wall area

d_s = 3 ft. thickness of the end shield wall

d = 7.84 ft., half of the transverse dimension of the roof

Therefore: M_{to} = 44,303 kip-in.

Because the overturning moment is smaller than the stabilizing moment, the freestanding AHSM-HS will not overturn. The resulting factor of safety against overturning effects for the DBT wind loads is 1.65.

B.11.2.2.2.1.2 AHSM –HS Sliding Analysis

To evaluate the potential for sliding of a single, free-standing AHSM-HS, the sliding force generated by the postulated DBT wind pressure is compared to the sliding resistance provided by friction between the base of the AHSM-HS and the ISFSI basemat.

The force (F_{sl}) required to slide the end module in an array is:

$F_{sl} = [W+2W_s - W_3A_r]\mu$

Where: μ= 0.6, coefficient of friction [B11.9]

W, W_s, W_3 and A_r are defined above.

Substituting gives:

$$F_{sl} = 382.0 \text{ kips}$$

The sliding force (F_{hw}) generated by DBT wind pressure for a single AHSM-HS is:

$$F_{hw} = (W_1 + W_2) A_w$$

Where: W_1, W_2 and A_w are as defined above.

Substituting gives:

$$F_{hw} = 231.0 \text{ kips}$$

Because the horizontal force generated by the postulated DBT is smaller than the force required to slide the end module in an AHSM-HS array, the AHSM-HS will not slide. The factor of safety against sliding of the AHSM-HS due to DBT wind loads is 1.65.

B.11.2.2.2.2 AHSM-HS Missile Impact Analysis

B.11.2.2.2.2.1 Local Damage Evaluation

Local missile impact effects consist of (a) missile penetration into the target, (b) missile perforation through the target and (c) spalling and scabbing of the target. This also includes punching shear in the region of the target. The missiles characterization is based on [B11.8]. The AHSM-HS outlet vent caps are not designed to resist direct impact from tornado missiles. In a worst case scenario debris may cause blocking of the outlet vents. This blocked vent accident scenario is addressed in Section B.11.2.7.

As per the ACI Code [B11.9] if the concrete thickness is at least 20% greater than that required to prevent perforation, the punching shear requirement of the code need not be checked. Several empirical formulas are available which are used to predict local damage effects.

The following enveloping missiles are considered for local damage of the AHSM-HS:

- Utility pole
- Armor piercing artillery shell
- Steel pipe

Large deformable missiles such as automobiles do not penetrate the structure. Therefore, the local effects from an automobile are evaluated using punching shear criteria of the ACI Code [B11.9].

The following empirical formulas are used to determine the local damage effects:

Reinforced Concrete Target

(a) Modified NDRC formulas for penetration depth [B11.14]:

$$x = [4KNWd(v_o/1000d)^{1.8}]^{0.5} \qquad \text{for } x/d \leq 2.0$$

$$x = \{[KNW(v_o/1000d)^{1.8}] + d\} \qquad \text{for } x/d > 2.0$$

where, x = Missile penetration depth, inches

K = concrete penetrability factor = $180/\sqrt{fc'}$

N = projectile shape factor

= 0.72 flat nosed

= 0.84 blunt nosed

= 1.0 bullet nosed (spherical end)

= 1.14 very sharp nose

W= weight of missile, lbs

v_o = striking velocity of missile, fps

d = effective projectile diameter, inches.

for a solid cylinder, d = diameter of projectile and

for a non-solid cylinder, $d = (4A_c/\pi)^{1/2}$

A_c= projectile impact area, in^2

(b) Modified NDRC formula for perforation thickness [B11.14]:

$$(e/d) = 3.19(x/d) - 0.718(x/d)^2 \qquad \text{for } x/d \leq 1.35$$

$$(e/d) = 1.32 + 1.24\,(x/d) \qquad \text{for } 1.35 \leq x/d \leq 13.5$$

where e= perforation thickness, in.

In order to provide an adequate margin of safety the design thickness $t_d = 1.2\ e$ [B11.9].

(c) Modified NDRC formula for scabbing thickness [B11.14]:

$$(s/d) = 7.91(x/d) - 5.06(x/d)^2 \qquad \text{for } x/d \leq 0.65$$

$$(s/d) = 2.12 + 1.36\,(x/d) \qquad \text{for } 0.65 \leq x/d \leq 11.75$$

Where: s = scabbing thickness, in.

In order to provide an adequate margin of safety the design thickness $t_d = 1.2$ s [B11.9].

The concrete targets of the AHSM-HS which may be subjected to local damage due to missile impact are:

- 44" thick roof
- 42" thick (minimum) front wall
- 36" thick end shield wall with 14" thick side wall
- 36" thick rear shield wall with 12" thick rear wall
- 32" thick concrete shielding door with ¾" steel plate on inside surface

To provide array expansion flexibility, two empty AHSM-HSs (with total walls thickness of 14"x4=56") may be installed in lieu of a 36" end shield wall.

B.11.2.2.2.2.1.1 Local Missile Impact Effects of Utility Pole Missile

The wood missiles (utility pole missile) do not have sufficient strength to penetrate a concrete target and the scabbing thickness required for wood missiles is substantially less than that required for a steel missile with the same mass and velocity. Practical wooden pole missiles are not capable of causing local damage to walls 12 inches thick, or greater for the missile velocities considered. Because none of the concrete targets are less than 12 inch thick, the postulated wood missiles will not cause local damage to the AHSM-HS concrete structure.

B.11.2.2.2.2.1.2 Local Missile Impact Effects of Armor Piercing Artillery Shell

Concrete Wall Evaluation:

d = diameter of missile = 8"

W = 276 lbs

V_o = 185 fps

f_c' = 5000 psi

K = $180/\sqrt{5000} = 2.55$

N = 0.84 blunt nosed

Penetration thickness $x = \sqrt{[4*2.55*0.84*276*8(185/(1000*8))^{1.8}]} = 4.6$" for $x/d = 0.58 \leq 2$

Perforation thickness $e = 8*[3.19(0.58) - 0.718(0.58)^2] = 12.9$" for $x/d = 0.58 < 1.35$

Required Perforation thickness = 1.2*12.9" = 15.5"

Scabbing thickness, $s = 8*[7.91(0.58) - 5.06(0.58)^2] = 23.1$" for $x/d = 0.58 < 0.65$

Required scabbing thickness = 1.2*23.1 = 27.7"

AHSM-HS Door Evaluation:

Required perforation thickness of concrete is 15.5" which is less than 32". Therefore, the missile will not perforate the concrete in the AHSM-HS door. The missile will not cause scabbing of the concrete since the door thickness is greater than that required to avoid scabbing. A ¾" steel plate added to the rear surface of the door provides further protection against scabbing of the concrete.

B.11.2.2.2.2.1.3 Local Missile Impact Effects of 12 Inch Diameter Steel Pipe Missile

Concrete Wall Evaluation:

Diameter of missile = 12.75" (Outer diameter of 12" dia Sch 40 pipe)

Contact surface area = A_c = 15.7 in^2 (cross section metal area of 12" dia Sch 40 pipe)

Effective diameter = $d = (4*15.7/\pi)^{1/2} = 4.47$ inches

W = 1500 lbs

v_o = 205 fps

f_c' = 5000 psi

K = $180/\sqrt{5000} = 2.55$

N = 0.72 flat nosed

Penetration thickness x = 15.2 in for $x/d > 2$

Perforation thickness e = 24.75 inches

Required perforation thickness 1.2*24.75 = 29.7 inches

Scabbing thickness = s = 30.15 inches

Required scabbing thickness = 1.2*30.15 = 36.2 inches

The thickness of the roof (44" thick), front wall (42" thick) and the end shield walls (36" thick +14" thick wall = 50") are sufficient to prevent perforation and scabbing of the concrete.

AHSM-HS Door Evaluation:

The required perforation thickness is 29.7". The thickness of concrete in the door is 32". Therefore, the missile will not perforate the concrete in the door. A ¾" steel plate added to the rear surface of the door provides further protection against scabbing of the concrete.

B.11.2.2.2.2.2 Massive Missile Impact Analysis

The AHSM-HS stability and potential damage due to impact of the postulated DBT massive missile consisting of a 4000 lb. automobile, 20 sq. ft. frontal area traveling at 195 ft/sec., is evaluated. The massive missile is assumed to impact the shield wall of an end AHSM-HS in an array. Using the principles of conservation of momentum with a coefficient of restitution of zero, the analysis presented below demonstrates that the end AHSM-HS remains stable and the missile energy is dissipated by sliding or slight tipping of the AHSM-HS.

Using conservation of momentum, the missile impact force equals the change in linear (sliding) or angular (overturning) momentum of the AHSM-HS. The AHSM-HS velocities immediately after impact are:

Sliding: $V = (m*vi) / (M+m)$ (Eq. 11.2-1)

Overturning: $\omega_a = (m*d_m*v_i)/(m*d_m^2 + I_A)$ (Eq. 11.2-2)

Where,

V = initial linear velocity of module after impact

v_i = 195 ft/sec = initial velocity of missile (conservative)

ω_A = initial rotational velocity about bottom right corner of the module and end shield walls (Figure B.11.2-12)

d_m = Vertical distance of the CG of the missile from A (Figure B.11.2-12) = 198 inches

m = 4000/386.4 = 10.35 lb-sec^2/in = mass of the missile

M = (427+2*176)*1000/386.4 = 2,016 lb-sec^2 /in = Mass of loaded AHSM-HS + End Shield walls

d = 115.6 in (Elevation of the CG of the loaded AHSM-HS

I_A = Mass moment of inertia of loaded AHSM-HS about point A (Figure B.11.2-12)

$I_A = 4.647 \times 10^7$ lb-sec^2-in

Sliding:

From Eq. 11.2-1 above: V = 11.95 in/sec = 1.0 ft/sec

For an impact at the bottom of the AHSM-HS wall, the kinetic energy imparted to the AHSM-HS is absorbed by sliding friction between the concrete of the AHSM-HS and the basemat. Coefficient of friction is 0.6 [B11.9].

Assuming that the missile impact load results in sliding of the AHSM-HS and equating the kinetic energy generated by the moving AHSM-HS to the work done by sliding friction force gives:

$$\mu * g * (M+m) * \Delta = (M+m)*V^2/2$$

$$\Delta = 0.31"$$

Therefore, a massive missile impact on a single AHSM-HS will slide the complete AHSM-HS approximately 0.31 inches sideways. This sliding distance would be significantly reduced due to the presence of more than one AHSM-HS side by side. Considering a three array module:

$$M = [3*(427) + 2*176]*1000/386.4$$

$$= 4226.2 \text{ lb-sec}^2/\text{in}$$

$$V = 5.72 \text{ in/sec} = 0.48 \text{ ft/sec}$$

$$\Delta = 0.071"$$

Therefore, the sliding displacement of the AHSM-HSs due to a massive missile impact is insignificant and will not cause any structural damage.

Overturning:

When the massive missile impacts at the top of the AHSM-HS, the missile energy is absorbed by plastic deformation of the missile and in rotation of the AHSM-HS. Therefore, equating the loss of kinetic energy to increase in the potential energy:

$$I_A \omega_A^2 /2 = M *g*d [\cos(\beta+\alpha-90)-\cos\beta] \quad \text{(Figure B.11.2-12)}$$

From Eq. 11.2-2 above: $\omega_A = 0.1023$ rad/sec

$$\beta = \tan^{-1} \{(58+36)/ 115.6)= 39.1°$$

$$M = 2016 \text{ lb-sec}^2/\text{in}$$

$$\cos(39.1+\alpha-90) - \cos (39.116) = 0.0027$$

$$\cos(39.1+\alpha- 90) = 0.0027 +0.7759 = 0.7786$$

$$90-\alpha = 39.1-38.87 = 0.23 °$$

Therefore, a loaded AHSM-HS rotates a maximum of 0.23° from vertical. The loaded AHSM-HS is stable against overturning as tip-over does not occur until the CG rotates past the edge point (point A Figure B.11.2-12) to an angle of more than 39.1° [= $\tan^{-1}$(94/115.6)].

Displacement at top of AHSM-HS =222*tan(0.23) =0.89". The maximum uplift at one edge = 188*tan(0.23) = 0.76". However, this tipping displacement is prevented by the seismic ties and keys, which connect the AHSM-HS to the adjacent AHSM-HS.

B.11.2.2.3 Accident Dose Calculations

The increase in the dose rates at the localized impact location following the missile impact accident is expected to be bounded by the dose rates at the AHSM-HS vents, calculated to be 2230 mrem/hour based on the maximum dose rate below the roof vent caps and 250 mrem/hour based on the maximum front inlet vent surface dose rate as calculated in Appendix B.5, Table B.5-2. This is consistent with the structural analysis results which are performed without the presence of the roof vent caps and demonstrate that there is no full penetration.

Proprietary information withheld pursuant to 10 CFR 2.390

This corresponds to a 21 fold increase in the back surface dose rate. For the two 1x10 arrays of AHSH-HSs, approximately 60% of the dose rate at distances greater than 50 m is attributable to the back surface. Therefore, it is reasonable to expect the dose rates at distances great than 50 m to increase by no more than a factor 13. Note that this is an extremely conservative estimate since it assumes that every AHSM-HS in the array receives a missile impact to the back surface. Appendix B.10, Table B.10-7 indicates that the back dose rate for the two 1x10 AHSM-HS arrays is 1.34E-2 mrem/hr at 100 m and 5.18E-5 mrem/hr at 500 m. Under the accident conditions described herein, these dose rates would increase to 1.74E-1 mrem/hr and 6.73E-4 mrem/hr at 100 m and 500 m, respectively. For an exposure duration of 8 hours, this corresponds to a received exposure of less than 1.5 mrem at 100 m and less than 0.007 mrem at 500 m.

Proprietary information withheld pursuant to 10 CFR 2.390

This corresponds to a 24 fold increase in the roof surface dose rate. Since the dose rates from the front of the 2x10 AHSM-HS array have the largest contribution from the roof (5.98E-3 mrem/hr of 2.92E-2 mrem/hr at 100 m and 2.91E-5 mrem/hr of 8.58E-5 at 500 m) and the largest dose rates over a given distance, the front of the 2x10 AHSM-HS array is considered for this analysis. Assuming the contribution to the dose rate increases by a factor of 24, the dose rates from Appendix B.10, Table B.10-5 would increase to 1.67E-1 mrem/hr and 7.55E-4 mrem/hr at 100 m and 500 m, respectively. For an exposure duration of 8 hours, this corresponds to a received exposure of less than 1.5 mrem at 100 m and less than 0.007 mrem at 500 m.

Therefore, the dose consequences for a duration of 8 hours are that the total exposures are calculated to be less than 3 mrem at 100 m and less than 0.015 mrem at 500 m. Note that these calculations conservatively assume that all the 20 modules are subjected to missile impact and that all the roof vent caps are removed.

Recovery from this event can be performed in a planned and deliberate manner to replace the shield wall(s) and roof vent cap(s), if required. This requires temporary shielding during removal and replacement of the wall(s), or, if needed, removal of the AHSM-HS from service. At no time is there a danger of a release of radioactive materials to the general public.

B.11.2.2.4 Corrective Actions

Evaluation of AHSM-HS damage as a result of a tornado-generated missile is to be performed to assess the need for temporary shielding and AHSM-HS repairs to return the AHSM-HSs to pre-tornado design conditions.

B.11.2.3 Flood

B.11.2.3.1 Cause of Accident

No change to the Cause of Accident section as described in Chapter 11, Section 11.2.3.1.

B.11.2.3.2 Accident Analysis

No change to the Cause of Accident section as described in Chapter 11, Section 11.2.2.2.

B.11.2.3.2.1 AHSM-HS Flooding Analysis

Because the AHSM-HS is open to the atmosphere, static differential pressure due to flooding is not a design load.

The maximum drag force, F, acting on the AHSM-HS due to a 15 fps flood water velocity is calculated as follows [B11.11]:

$$F = (v^2/2g)C_dA\rho_w$$

Where:

- v = 15 fps, flood water velocity
- C_D = 2.0, drag coefficient for flat plate
- A = 18.5 ft., AHSM-HS area per foot length
- ρ_w = 62.4 lb/ft^3, flood water density
- F = Drag force (lb.)
- g = 32.2 ft/s^2 = Acceleration due to gravity

The resulting flood induced pressure load of 8.07 kips/ft. is applied normally to the end module shield wall of a stand-alone AHSM-HS.

B.11.2.3.2.1.1 AHSM-HS Overturning Analysis

The factor of safety against overturning of a single AHSM-HS with shield walls, for the postulated flooding conditions, is calculated by summing moments about the bottom outside corner of a single, free-standing AHSM-HS. A net weight of 266.1 kips for a loaded AHSM-HS plus 102.8 kips for the upstream end shield wall, including buoyancy effects, is used to calculate the stabilizing moment resisting the overturning moment applied to the AHSM-HS by the flood water drag force. The stabilizing moment is:

$$M_{st} = 266.1x52 + 102.8x(110+18)$$

$$= 26{,}996 \text{ kip-in.}$$

The maximum drag force due to the postulated water current velocity of 15 fps is calculated in Section B.11.2.3.2.1 as 8.07 kips/ft. acting over the entire height and width of an end shield wall of a single free-standing AHSM-HS. Therefore, the overturning moment due to the postulated flood current is:

$$M_{ot} = 8.07 \text{ kips/ft.} \times 20.67 \text{ ft.} \times (18.5x12/2)$$

$$= 18{,}516 \text{ kip-in.}$$

The factor of safety (F.S.) against overturning for a single, freestanding AHSM-HS due to the postulated design basis flood water velocity is given by:

$$\text{F.S.} = 26{,}996 / 18{,}516 = 1.46$$

B.11.2.3.2.1.2 AHSM-HS Sliding Analysis

The factor of safety against sliding of a freestanding single AHSM-HS due to the maximum postulated flood water velocity of 15 fps is calculated using methods similar to those described above. The effective weight of the AHSM-HS including the 32PTH2 DSC and end shield wall acting vertically downward, less the effects of buoyancy acting vertically upward is 368.9 kips. The friction force resisting sliding of the AHSM-HS is equal to the product of the net weight of the AHSM-HS and 32PTH2 DSC and the coefficient of friction for concrete placed against another concrete surface such as that between the AHSM-HS and basemat, which is 0.6 [B11.9]. Therefore, the force resisting sliding of the AHSM-HS is 0.6 x 368.9 or 221.34 kips. The drag force acting on a single AHSM-HS is 8.07 kips/ft x20.67 ft = 166.8 kips total acting on the side wall of a single AHSM-HS, due to a flood velocity of 15 fps. The resulting factor of safety against sliding of a single free standing AHSM-HS due to the design basis flood water velocity is 1.33.

B.11.2.3.2.2 32PTH2 DSC Flood Analyses

The 32PTH2 DSC is evaluated for the design basis 50-foot hydrostatic head of water producing external pressure of 21.7 psi on the 32PTH2 DSC shell and outer cover plates. A pressure of 22 psi is used for the structural evaluations.

The stress analyses for the 32PTH2 DSC due to flooding pressure are addressed in Section B.3.6.1.

B.11.2.3.2.3 Thermal Evaluation of Flood Accident

The NUHOMS® 32PTH2 system was evaluated for the impact of a worst case flood accident which completely covers the AHSM-HS. The thermal consequences of such an accident are beneficial. The 32PTH2 DSC shell temperatures are shown in Tables B.4.6-16 and B.4.6-17 for the design basis decay heats. The maximum temperature of the 32PTH2 DSC is higher than the saturation temperature of water. Under these conditions, the water which contacts the 32PTH2 DSC surface would eventually boil, providing an extremely effective heat removal mechanism for the 32PTH2 DSC. Therefore, the thermal effects of the flood accident are bounded by the other thermal accidents which are considered in this section.

B.11.2.3.3 Accident Dose Calculations

The radiation dose due to flooding of the AHSM-HS is negligible. The radioactive material inside the 32PTH2 DSC will remain confined in the 32PTH2 DSC and, therefore, will not contaminate the encroaching flood water. The minimal amount of contamination that may be on the outside surface of the 32PTH2 DSC is not sufficient to be a radiological hazard if it were to be washed off the 32PTH2 DSC outer surface.

B.11.2.3.4 Corrective Action

If flooding should occur, any silt deposits can be removed using a pump suction hose, or fire hose inserted through the inlet vent, to suck the silt out, or produce a high velocity water flow to flush the silt through the AHSM inlet vent. The corrosion inhibiting design features of the 32PTH2 DSC are addressed in Chapter B.3, Section B.3.4.

B.11.2.4 Fire/Explosion

The discussion in Section 11.2.4 for the 24PT1-DSC is applicable to the 32PTH2 DSC, with the exception that a specific evaluation of the hypothetical fire event has been performed for the 32PTH2 DSC and the results are presented in Chapter B.4, Section B.4.5.4.

B.11.2.5 Accidental Drop of the 32PTH2 DSC Inside the Transfer Cask

B.11.2.5.1 Cause of Accident

This section addresses the structural integrity of the 32PTH2 DSC shell and internal basket assemblies when subjected to postulated cask drop accident conditions. Drops are postulated for

the 32PTH2 DSC when positioned inside the OS200FC TC and cannot occur once the 32PTH2 DSC is transferred into the AHSM-HS.

B.11.2.5.1.1 Cask Handling and Transfer Operation

No change to the Cask Handling and Transfer Operation section as described in Chapter 11, Section 11.2.5.1.1.

B.11.2.5.1.2 32PTH2 DSC Drop Accident Scenarios

Transfer of the loaded 32PTH2 DSC from the Spent Fuel Pool Building to the ISFSI basemat is carried out utilizing the OS200FC TC which is horizontally mounted and secured to the transfer trailer skid. At the ISFSI basemat, the transfer skid is backed up against the AHSM-HS front wall and restrained to it by the skid restraints. Once the OS200FC TC is docked and aligned to the AHSM-HS opening, a hydraulic ram is used to push the 32PTH2 DSC out of the OS200FC TC and into the AHSM-HS. The AHSM-HS door is then installed, thus, completing the transfer operations.

At no time during the transfer loading (or unloading) operations is there a need for any lifts of the OS200FC TC with the loaded 32PTH2 DSC. Therefore, the vertical end drops for the Advanced NUHOMS® System are non-mechanistic, not credible events, and consequently no end drops are postulated. Sliding of the 32PTH2 DSC out of the OS200FC TC or tilting of the OS200FC TC in such a way as to result in a corner drop are also non-mechanistic, highly unlikely events. Nevertheless, for conservatism, a corner drop is postulated and evaluated for the Advanced NUHOMS® System.

Based on the configuration of the OS200FC TC mounted on the trailer skid during transfer operations, the bounding drop distance from the bottom of the OS200FC TC is approximately 68". However, for conservatism, a drop height of 80" is used for the side and corner drop evaluations.

In spite of the highly incredible nature of any scenario that could lead to a drop accident for the OS200FC TC, the following drop scenarios are conservatively selected for design of the 32PTH2 DSC:

1. A 75g horizontal side drop applied in an equivalent static analysis or an initial velocity associated with an 80" drop height is applied if a dynamic analysis is performed

2. A 25g oblique corner drop at an angle of 30° to the horizontal, onto the corner of the OS200FC TC in an equivalent static analysis or an initial velocity associated with an 80" drop height is applied if a dynamic analysis is performed.

As discussed above, a vertical end drop is not credible because the 32PTH2 DSC is not handled in the vertical orientation once it is loaded onto the transfer trailer. However, for purposes of bounding the 25g corner drop, and as part of 10 CFR Part 50 and 10 CFR Part 71 evaluations, the 32PTH2 DSC is also analyzed for a 75g end drop.

B.11.2.5.1.3 Transfer Cask Drop Surface Conditions

No change to the Transfer Cask Drop Surface Conditions section as described in Chapter 11, Section 11.2.5.1.3.

B.11.2.5.2 Accident Analysis

The stress analyses of the 32PTH2 DSC resulting from the postulated drop scenarios are summarized in Chapter B.3, Section B.3.6.1.

B.11.2.5.3 Accident Dose Calculations

The postulated accident condition for the OS200 FC TC assumes that after a drop event, the water in the neutron shield is lost. The loss of neutron shield is modeled as described in Chapter B.5, Section B.5.3 by conservatively considering the loss of water and the steel skin. Also, damaged fuel is modeled as fuel rubble that falls to the bottom of the fuel compartment of the basket. The dose rates due to the fuel rubble model are bounded by the results from assuming intact fuel in damaged fuel locations at far distances. The accident condition dose rates from Chapter B.5, Section B.5.1 are summarized in Table B.11.2-3 for the 32PTH2 DSC loaded with design basis fuel. The radioactive source terms for the accident analysis models result in neutron dose rates that are maximized and are bounding.

Table B.11.2-3 shows the accident condition dose rates at 1, 100 and 500 meters from the side of the OS200FC TC. The average dose rate at the transfer cask surface with the loss of the neutron shield is 1450 mrem/hr (206 mrem/hr gamma and 1240 mrem/hr neutron). The only potential off-site dose consequences would be additional direct and air scattered radiation if the accident were to occur sufficiently close to the site boundary. It is assumed that eight hours would be required to either recover the neutron shield or to add temporary shielding while arranging recovery operations. As a result, it is estimated that on-site workers at an average distance of 1 meter would receive an additional dose of 1.6 rem (200 mrem/hr for 8 hours). The dose received by a person located 100 meters away from the NUHOMS® 32PTH2 system installation for an assumed duration of 8 hours would be less than 2.5 mrem with the OS200FC TC. The dose to an off-site person located 500 meters away for the assumed 8 hour duration would be less than 0.02 mrem with the OS200FC TC. These exposures are well within the limits of 10 CFR Part 72.106 for an accident condition.

Water bags or other neutron absorbing material could be wrapped around the transfer cask to reduce the surface dose rate to an acceptable level for recovery operations, thus minimizing exposure of personnel in the vicinity. The actual local and off-site dose rates, recovery time and operations needed to retrieve the OS200FC TC, and the required actions to be performed following the event, depend upon the severity of the event, site characteristics, and the resultant OS200FC TC and trailer/skid damage.

B.11.2.5.4 Corrective Actions

No change to the Corrective Actions section as described in Chapter 11, Section 11.2.5.4.

B.11.2.6 Lightning

No change to the Lightning section as described in Chapter 11, Section 11.2.6. AHSM-HS lightning protection equipment, if required by plant criteria, is considered a miscellaneous attachment and is allowed by the AHSM-HS design.

B.11.2.7 Blockage of Air Inlet and Outlet Openings

No change to the Blockage of Air Inlet and Outlet Openings section as described in Chapter 11, Section 11.2.7. Analyses results for the 32PTH2 DSC are presented in Chapter B.3 and B.4. References to bounding Chapter 11 analyses correspond to the pertinent Chapter B.11 section.

B.11.2.8 Accidental Pressurization of the 32PTH2 DSC

No change to the Accidental Pressurization of the 24PT1-DSC section as described in Chapter 11, Section 11.2.8. Analysis results for the 32PTH2 DSC are presented in Chapter B.4.

B.11.2.9 Burial

No change to the Burial section as described in Chapter 11, Section 11.2.9.

References to bounding Chapter 11 analysis correspond to the pertinent Chapter B.11 section.

Table B.11.2-1 Postulated Accident Loading Identification

Accident Load Type	Section Reference	NUHOMS® 32PTH2 System Component Potentially Affected			
		32PTH2 DSC Shell Assembly	32PTH2 DSC Internal Basket	32PTH2 DSC Support Structure	AHSM-HS
Earthquake	B.11.2.1	X	X	X	X
Extreme Wind and Tornado Missiles	B.11.2.2				X
Flood	B.11.2.3	X			X
Fire/Explosion	B.11.2.4	X	X		X
Accident Cask Drop	B.11.2.5	X	X		
Lightning	B.11.2.6				X
Blockage of Air Inlet and Outlet Openings	B.11.2.7	X	X	X	X
Accidental Pressurization of the 32PTH2-DSC	B.11.2.8	X			
AHSM-HS Burial	B.11.2.9	X			X

Table B.11.2-2 Summary of AHSM-HS Sliding/Uplift Displacements

Proprietary information withheld pursuant to 10 CFR 2.390

Table B.11.2-3 Summary of 32PTH2 DSC, OS200FC TC Accident Dose Rates

Dose Rate Location	Maximum Gamma (mrem/hr)	Gamma MCNP 1σ Error	Maximum Neutron (mrem/hr)	Neutron MCNP 1σ Error	Maximum Total[1] (mrem/hr)	Total MCNP 1σ Error
Cask 1 m (Radial) Accident Condition	5.24E+01	0.0006	1.34E+02	0.0052	1.87E+02[2]	0.0038
Cask 100 m (Radial) Accident Condition	1.72E-01	0.0005	1.19E-01	0.0029	2.91E-01	0.0012
Cask 500 m (Radial) Accident Condition	1.25E-03	0.0010	7.67E-04	0.0032	2.02E-03	0.0014

Note:

(1) Gamma and neutron dose rate peaks do not always occur at same location; therefore, the total dose rate is not always the sum of the gamma plus neutron dose rate.

(2) The total dose rate using the rubble model is 191 mrem/hour.

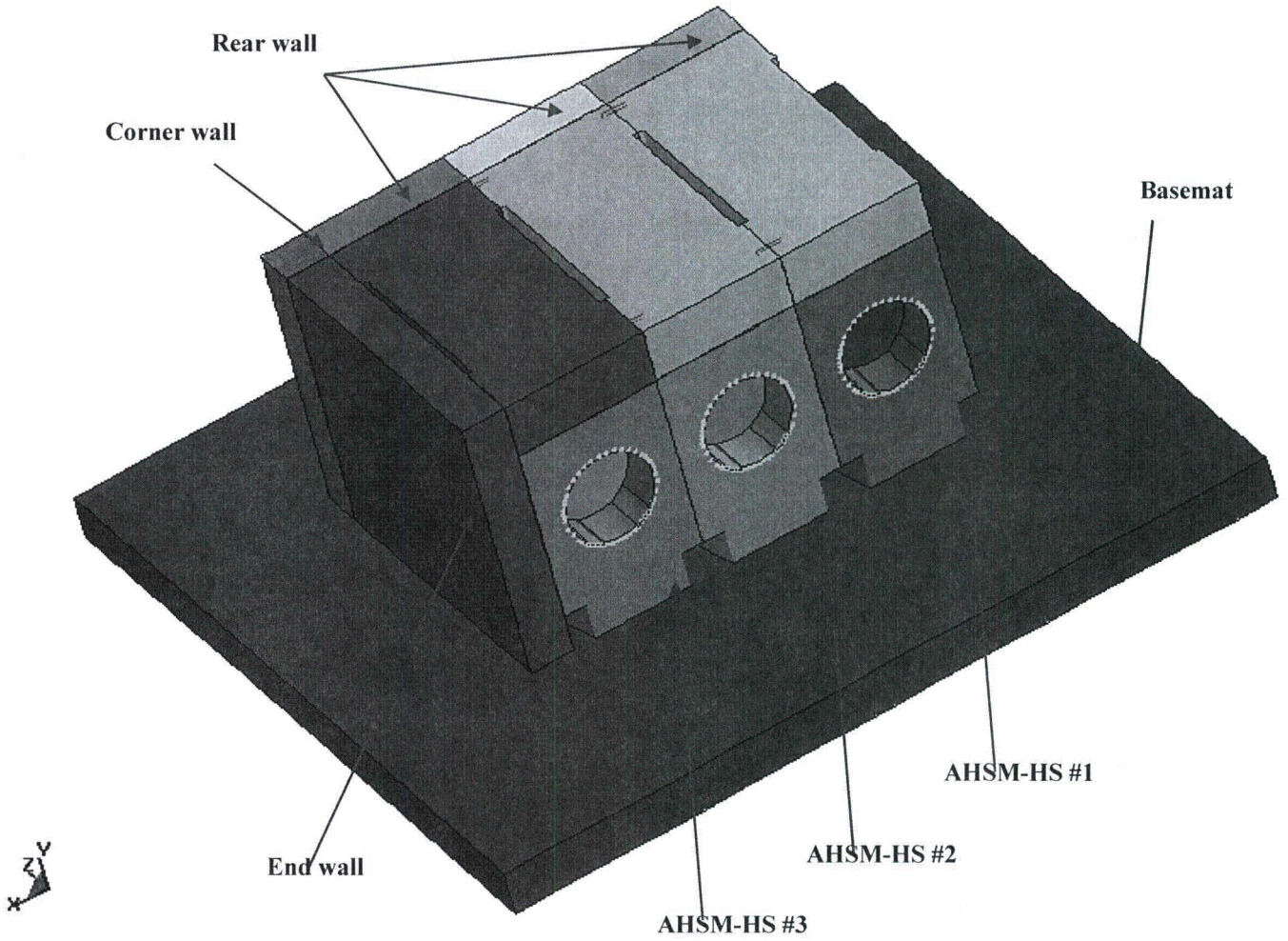

Figure B.11.2-1 LS-DYNA AHSM-HS Stability Analysis Model

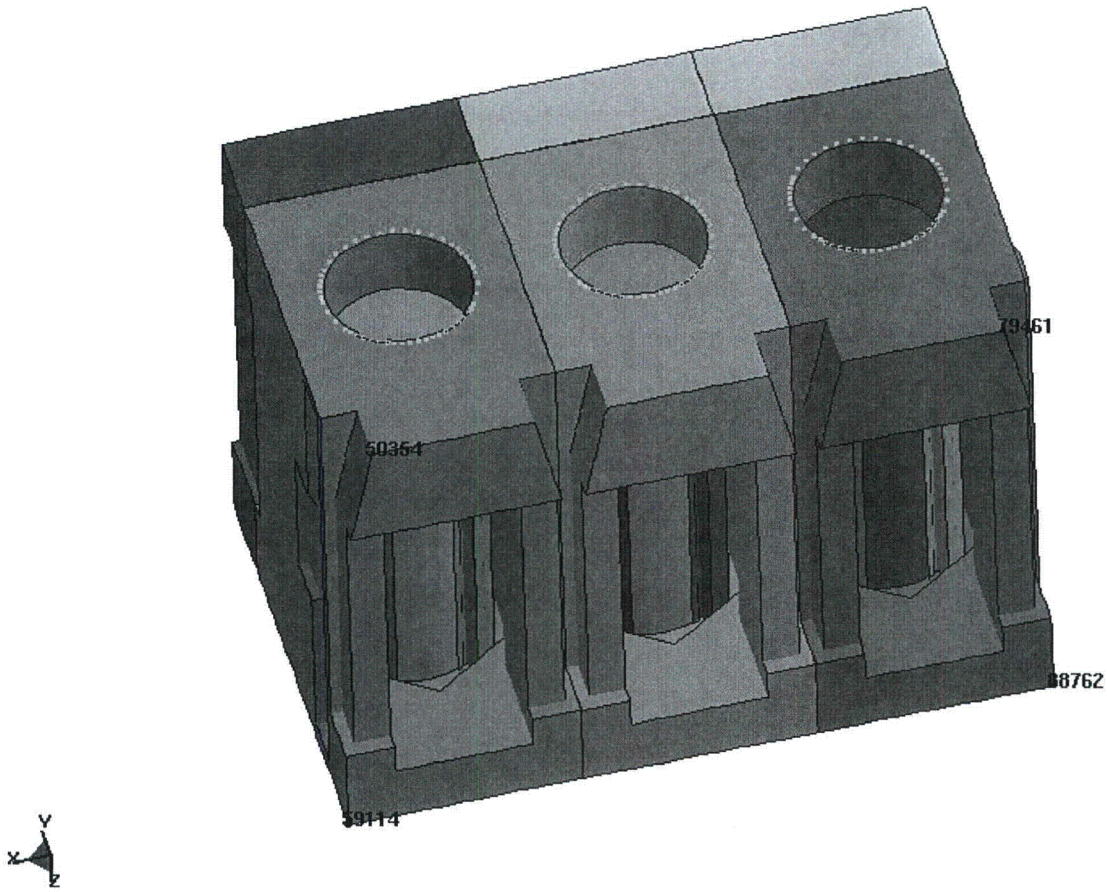

Figure B.11.2-2 LS DYNA Model –AHSM-HSs Loaded with 32PTH2 DSCs -View from Below

Proprietary information withheld pursuant to 10 CFR 2.390

Figure B.11.2-3 Horizontal X Sliding Displacement for Case TH1-2 (TH Set 1, 0.8)

Proprietary information withheld pursuant to 10 CFR 2.390

Figure B.11.2-4 Horizontal Z Sliding Displacement for Case TH1-2 (TH Set 1, 0.8)

Proprietary information withheld pursuant to 10 CFR 2.390

Figure B.11.2-5 Vertical Y Uplift Displacement for Case TH1-2 (TH Set 1, 0.8)

Proprietary information withheld pursuant to 10 CFR 2.390

Figure B.11.2-6 Horizontal X Sliding Displacement for Case TH2-1 (TH Set 2, 0.2)

Proprietary information withheld pursuant to 10 CFR 2.390

Figure B.11.2-7 Horizontal Z Sliding Displacement for Case TH2-1 (TH Set 2, 0.2)

Proprietary information withheld pursuant to 10 CFR 2.390

Figure B.11.2-8 Vertical Y Uplift Displacement for Case TH2-1 (TH Set 2, 0.2)

Proprietary information withheld pursuant to 10 CFR 2.390

Figure B.11.2-9 Horizontal X Sliding Displacement for Case TH2-5 (TH Set 2, 0.2, Gap=0.5)

Proprietary information withheld pursuant to 10 CFR 2.390

Figure B.11.2-10 Horizontal Z Sliding Displacement for Case TH2-5(TH Set 2, 0.2, Gap=0.5)

Proprietary information withheld pursuant to 10 CFR 2.390

Figure B.11.2-11 Vertical Y Sliding Displacement for Case TH2-5 (TH Set 2, 0.2, Gap=0.5)

Proprietary information withheld pursuant to 10 CFR 2.390

Figure B.11.2-12 AHSM-HS Configuration for Missile Impact Stability Analysis

B.11.3 Supplemental Information

B.11.3.1 References

[B11.1] American National Standards Institute, American Nuclear Society, ANSI/ANS-57.9-1984, Design Criteria for an Independent Spent Fuel Storage Installation (Dry Storage Type), 1984.

[B11.2] NRC Regulatory Guide 1.60, "Design Response Spectra for Seismic Design of Nuclear Power Plants," Revision 1, 1973.

[B11.3] LS-DYNA Version ls971sR27600.1224, Livermore Software Technology Corporation.

[B11.4] NRC NUREG-0800, Standard Review Plan for the Review of Safety Analysis Reports for Nuclear Power Plants, Revision 2, July 1981.

[B11.5] NRC Regulatory Guide 1.61, "Damping Values for Seismic Design of Nuclear Power Plants," October 1973.

[B11.6] Swanson Analysis Systems Inc., ANSYS Engineering Analysis System, Versions 10.0 and 10A1 5.3.

[B11.7] Transnuclear, Inc., Updated Final Safety Analysis Report for the Standardized NUHOMS® Horizontal Modular Storage System for Irradiated Nuclear Fuel, Revision 11, February 2010, US NRC Docket No. 72-1004.

[B11.8] NRC Regulatory Guide 1.76, Design Basis Tornado for Nuclear Power Plants, April 1974.

[B11.9] American Concrete Institute, Code Requirements for Nuclear Safety Related Concrete Structures and Commentary, ACI 349-06, American Concrete Institute, Detroit, MI.

[B11.10] J. Roark and W. C. Young, Formulas for Stress and Strain, Sixth Edition, McGraw-Hill, New York, N.Y., (1989).

[B11.11] "Fluid Mechanics," Raymond C. Binder, 4th Edition, Prentice-Hall, Inc.

[B11.12] NRC Regulatory Guide 1.92, "Combining Modal Responses and Spatial Components in Seismic Response Analysis," Revision 2, July 2006.

[B11.13] American Society of Civil Engineers, ASCE 7-05, Minimum Design Loads for Buildings and Other Structures.

[B11.14] American Society of Civil Engineers, ASCE Manual No. 58, Structural Analysis and Design of Nuclear Plant Facilities, 1980.

Listing of Computer Files Contained in Enclosure 10

Disk ID No. (size)	Discipline	System/ Component	File Series (topics)	Number of files
Enclosure 10 One Portable Hard Drive **Criticality Folder** (22.58 MB)	**Criticality**	**NUH32PTH2 Criticality Analysis Intact Fuel Analysis**	**Criticality - Folder**	
			001- Intact Fuel – **Folder** Input and output files for various sensitivity analyses and maximum enrichment requirements as a function of basket type. The folder supports Sections B.6.4.2.1 and B.6.4.2.2 of Appendix B.6	30
	Criticality	**NUH32PTH2 Criticality Analysis Damaged Fuel Analysis**	**Criticality - Folder**	
			002-Damaged Fuel – **Folder** Input and output files for damaged fuel models and maximum enrichment requirements as a function of basket type. The folder supports Sections B.6.4.2.3 and B.6.4.2.4 of Appendix B.6	44
	Criticality	**NUH32PTH2 Criticality Analysis**	**Criticality - Folder**	
			Spreadsheet describing each input and output file	1

Listing of Computer Files Contained in Enclosure 10

Disk ID No. (size)	Discipline	System/Component	File Series (topics)	Number of files
Enclosure 10 One Portable Hard Drive **Shielding Folder** (509 MB) (continued on next page)	**Shielding**	**NUH32PTH2 AHSM-HS Analysis**	001-Generic Array, 2 1x10, gamma files This folder supports Section B.10.2	3
			002-Generic Array, 2 1x10, neutron and secondary gamma files This folder supports Section B.10.2	3
			003-Generic Array, 2x10, gamma files This folder supports Section B.10.2	3
			004-Generic Array, 2x10, neutron and secondary gamma files This folder supports Section B.10.2	3
			005-Single AHSM-HS, gamma files This folder supports Sections B.5.3 and B.5.4	4
			006-Single AHSM-HS, neutron files This folder supports Sections B.5.3 and B.5.4	4
			007-Single AHSM-HS with dose reduction hardware, gamma files This folder supports Sections B.5.3 and B.5.4	4
			008-Single AHSM-HS with dose reduction hardware, neutron and secondary gamma files This folder supports Sections B.5.3 and B.5.4	4
		NUH32PTH2 OS200FC TC Analysis **(continued on next page)**	009-Accident configuration, gamma files This folder supports Sections B.5.3 and B.5.4	3
			010-Accident configuration, neutron and secondary gamma files This folder supports Sections B.5.3 and B.5.4	3
			011-Accident with fuel reconfiguration, gamma files This folder supports Sections B.5.3 and B.5.4	3
			012-Accident with fuel reconfiguration, neutron and secondary gamma files This folder supports Sections B.5.3 and B.5.4	3
			013-Decontamination configuration, gamma files This folder supports Sections B.5.3 and B.5.4	3
			014-Decontamination configuration, neutron and secondary gamma files This folder supports Sections B.5.3 and B.5.4	3
			015-Normal configuration, gamma files This folder supports Sections B.5.3 and B.5.4	3

Listing of Computer Files Contained in Enclosure 10

Disk ID No. (size)	Discipline	System/Component	File Series (topics)	Number of files
Enclosure 10 One Portable Hard Drive **Shielding Folder** (509 MB)	**Shielding**	**NUH32PTH2 OS200FC TC Analysis** **(continued)**	016-Normal configuration, neutron and secondary gamma files This folder supports Sections B.5.3 and B.5.4	3
			017-Normal configuration with control components in zone 2, gamma files This folder supports Sections B.5.3 and B.5.4	3
			018-Normal configuration with reconstitution with irradiated stainless steel rods in zone 2, gamma files This folder supports Sections B.5.3 and B.5.4	3
			019-Welding configuration, gamma files This folder supports Sections B.5.3 and B.5.4	3
			020-Welding configuration, neutron and secondary gamma files This folder supports Sections B.5.3 and B.5.4	3
		NUH32PTH2 Source Term Analysis	021-Control components This folder supports Section B.5.2.4	10
			022-Design basis, 31 GWd/MTU, 1.7 wt. % U-235 This folder supports Section B.5.2.6	8
			023-Design basis, 33 GWd/MTU, 1.7 wt. % U-235 This folder supports Section B.5.2.6	8
			024-Design basis, 35 GWd/MTU, 1.7 wt. % U-235 This folder supports Section B.5.2.6	8
			025-Design basis, 35 GWd/MTU, 1.8 wt. % U-235 This folder supports Section B.5.2.6	8
			026-Design basis, 57 GWd/MTU, 3.6 wt. % U-235 This folder supports Section B.5.2.6	8
			027-Design basis, 63 GWd/MTU, 4.3 wt. % U-235 This folder supports Section B.5.2.6	8
			028-Reconstituted with stainless steel rods This folder supports Section B.5.2.4	18
			029-Reconstituted with uranium This folder supports Section B.5.2.4	18
		NUH32PTH2 Shielding Analysis	Spreadsheet describing each input and output file	1

Listing of Computer Files Contained in Enclosure 10

Disk ID No. (size)	Discipline	System/ Component	File Series (topics)	Number of Files
Enclosure 10 One Portable Hard Drive **Structural Folder** (23.1 GB)	**Structural**	Basket	Basket Storage Loads ANSYS- Directory (B.3.6.1.2.5 B – input and output files for 32PTH2 Basket Seismic Load – ANSYS Evaluation)	5
		Basket	Basket Transfer Loads ANSYS- Directory (B.3.6.1.2.4 C – input and output files for 32PTH2 Basket Handling Load – ANSYS Evaluation)	5
		Basket	Basket Side Drop Accident LS-DYNA- Directory (B.3.6.1.2.6 A – input and output files for 32PTH2 Basket Accident 45° Side Drop – LS-DYNA Evaluation)	70
		Fuel Rod	CE_16x16 Fuel Side Drop Accident ANSYS- Directory (B.3.5.3.1 – input and output files for CE 16X16 PWR Fuel Side Drop – ANSYS Evaluation)	4
		Fuel Rod	CE_16x16 Fuel Corner Drop Accident LS-DYNA- Directory (B.3.5.3.2 – input and output files for CE 16X16 PWR Fuel Corner Drop – LS-DYNA Evaluation)	33
		Canister	Canister Level A&B 2D- Directory (B.3.6.1.1.2 iii – input and output files for 32PTH2 DSC 2D Axisymmetric Off-Normal Internal Pressure – ANSYS Evaluation) Note: Analysis load step number information: 2) 20 psig Internal pressure	7
		Canister	Canister Level D 2D- Directory (B.3.6.1.1.2 iii – input and output files for 32PTH2 DSC 2D Axisymmetric Accident Internal Pressure – ANSYS Evaluation) Note: Analysis load step number information: 3) 140 psi Internal Pressure	7
		Canister	Canister Level D 3D- Directory (B.3.6.1.1.7 A – input and output files for 32PTH2 DSC- 3D Accident Side Drop on Rails - ANSYS Evaluation)	8
		AHSM-HS	AHSM-HS Stability Evaluation/TH2-3_set2_f08_groupB- Directory (B.11.2.1.2.1– input and output files for 32PTH2 AHSM-HS Non Linear Seismic Stability (Uplift) – LS-DYNA Evaluation)	100
		AHSM-HS	AHSM-HS Stability Evaluation/TH2-5_gap_0.5_set3_f02- Directory (B.11.2.1.2.1– input and output files for 32PTH2 AHSM-HS Non Linear Seismic Stability (sliding) – LS-DYNA Evaluation)	96
		AHSM-HS	AHSM-HS Off normal Handling- Directory (B.3.6.2.2.7– input and output files for AHSM-HS Off Normal Handling (RA) – ANSYS Evaluation)	3
		AHSM-HS	AHSM-HS Transition Wall - Directory (B.3.6.2.4.6– input and output files for AHSM-HS Transition Wall– ANSYS Evaluation)	3

Listing of Computer Files Contained in Enclosure 10

Disk ID No. (size)	Discipline	System/Component	File Series (topics)	Number of files
Enclosure 10 One Portable Hard Drive **Thermal Folder** (48.0 GB) (continued on next page)	**Thermal**	NUHOMS® 32PTH2 Storage Conditions	001-Storage – **Directory**	
			1-AHSM-HS Geometry – **Folder** AHSM-H Model	4
			2-32PTH2 DSC Geometry – **Folder** 32PTH2 DSC Model	6
			3-ASHM-HS-S3 – **Folder** AHSM-HS, Off-Normal Hot, 37.2 kW, Load Case S3	23
			4-Map DSC Shell Temp – **Folder** Map Temperatures for DSC Shell	16
			5-32PTH2 DSC-S3 – **Folder** 32PTH2 DSC in AHSM-HS, Off-Normal Hot, 37.2 kW, Load Case S3	11
			6-ASHM-HS-S7 – **Folder** AHSM-HS Blocked Vents Accident, 37.2 kW, Load Case S7	43
			7-32PTH2 DSC-S7 – **Folder** 32PTH2 DSC in AHSM-HS Blocked Vents Accident, 37.2 kW, Load Case S7	25

Listing of Computer Files Contained in Enclosure 10

Disk ID No. (size)	Discipline	System/Component	File Series (topics)	Number of files
Enclosure 10 One Portable Hard Drive **Thermal Folder** (48.0 GB)	**Thermal**	NUHOMS® 32PTH2 Transfer Conditions	002-Transfer – **Directory**	
			1-OS200FC TC Geometry – **Folder** OS200FC TC Model	5
			2-OS200FC TC-T5A – **Folder** OS200FC TC, Normal, Hot, Vertical, Steady-State,31.2 kW, Load Case T5A	11
			3-Map DSC Shell Temp – **Folder** Map Temperatures for DSC Shell for Load case T5A	5
			4-32PTH2 DSC-T5A – **Folder** 32PTH2 DSC in OS200FC TC, Normal, Hot, Vertical, Steady-State,31.2 kW, Load Case T5A	9
			5-Initial TC Model Temp for T6 – **Folder** OS200FC TC initial model temperature for Normal, Hot, Vertical, Transient, 37.2 kW, Load Case T6	14
			6-OS200FC TC-T6 – **Folder** OS200FC TC, Normal, Hot, Vertical, Transient, 37.2 kW, Load Case T6	32
			7-Map DSC Shell Temp – **Folder** Map Temperatures for DSC Shell for Load Case T6	24
			8-Initial DSC Model Temp for T6, T7 – **Folder** 32PTH2 DSC initial temperature for load case T6, T7	10
			9-32PTH2 DSC-T6 – **Folder** 32PTH2 DSC in OS200FC TC, Normal, Hot, Vertical, Transient, 37.2 kW, Load Case T6	32
			10-Initial Model Temp for T7 – **Folder** OS200FC TC initial model temperature for Off-Normal, Hot, Horizontal, Transient, 37.2 kW, Load Case T7	14
			11-OS200FC TC-T7 – **Folder** OS200FC TC, Off-Normal, Hot, Horizontal, Transient, 37.2 kW, Load Case T7	31
			12-Map temp to DSC shell – **Folder** Map Temperatures for DSC Shell for Load Case T7	24
			13-32PTH2 DSC-T7 – **Folder** 32PTH2 DSC in OS200FC TC, Off-Normal, Hot, Horizontal, Transient, 37.2 kW, Load Case T7	32
			14-Flow rate – **Folder** Calculate OS200FC TC flow rate for load case T8	6
			15-OS200FC TC-T8 – **Folder** OS200FC TC, Off-Normal, Hot, Horizontal, Steady-State with Air Circulation, 37.2 kW, Load Case T8	13
			16-Map DSC Shell Temp – **Folder** Map Temperatures for DSC Shell for Load Case T8	5
			17-32PTH2 DSC-T8 – **Folder** 32PTH2 DSC in OS200FC TC, Off-Normal, Hot, Horizontal, Steady-State with Air Circulation, 37.2 kW, Load Case T8	8